UNIVERSITEIT VAN PRETORIA
UNIVERSITY OF PRETORIA
YUNIBESITHI YA PRETORIA

FUNDAMENTAL STUDIES OF THE ELECTROCHEMICAL AND FLOTATION BEHAVIOUR OF PYRRHOTITE

by

Nthabiseng Mphela

Submitted in partial fulfillment of the requirements for the degree

Master of Engineering (Metallurgical Engineering)

in the Faculty of Engineering, Built Environment and Information Technology

Supervisor: Dr. M.K.G. Vermaak

July 2010

ACKNOWLEDGEMENTS

I acknowledge with gratitude the assistance of the following:

- God for the strength, wisdom and ability to complete this project.
- My family and friends for their patience, support, prayers and encouragement; especially my mother Seane, my brother Tshepo, my sisters Sebueng and Mokotji, my grandmother Lydia Tshoke and my deceased father, Ramabele (may his soul rest in peace).
- Dr Thys Vermaak, my supervisor, for his expert advice, support, inspiration and guidance with the project.
- Prof. Chris Pistorius and Dr Dick Groot, for their invaluable input and the discussions on Electrochemistry.
- Prof. Johan de Villiers, for his invaluable input and discussions on pyrrhotite mineralogy and providing a pyrrhotite sample.
- The Department of Materials Science and Metallurgical Engineering at the University of Pretoria, for the use of its facilities.
- Mrs Sarah Havenga, Mrs Lillian Barlow, Mrs Louise Ackermann, Mr Markus Erwee, Mrs Elsie Snyman-Ferreira, Mr Joel Matea and the rest of the staff and post-graduate students (especially Miss Getrude Marape, Mr Robert Cromarty, Miss Mpilo Thethwayo and Mr Ogunniyi Iyiola Olatunji) from the Department, for their support.
- IMMRI staff, Prof. Tom Von Moltke, Mr Marius Biermann, Mr Carel Coetzee and Mrs Pheladi Mohlala for, their assistance with the analyses.
- The Department of Earth and Geological Sciences at the University of Pretoria, for the use of its facilities (Dr Sabine Verryn and Joseph Mogoru for XRD analyses and Mr Peter Graser for electron microprobe analyses).
- Prof. Jan D. Miller from the Department of Metallurgical Engineering at the University of Utah, for his input and support.
- MINTEK, for the financial assistance and Dr Mike Bryson for technical input.
- Mrs Megan Becker from UCT Department of Chemical Engineering, for the pyrrhotite samples.
- Mr Werner Jordaan from CSIR National Metrology Laboratory, for the use of the facilities (ToF-SIMS).

- Mr Braam Smit from Anglo American Research Centre, for the use of the facilities (Qemscan).

UNIVERSITEIT VAN PRETORIA
UNIVERSITY OF PRETORIA
YUNIBESITHI YA PRETORIA

FUNDAMENTAL STUDIES OF THE ELECTROCHEMICAL AND FLOTATION BEHAVIOUR OF PYRRHOTITE

by

Nthabiseng Mphela

Supervisor: Dr. M.K.G. Vermaak

Department of Materials Science and Metallurgical Engineering

Master of Engineering (Metallurgical Engineering)

ABSTRACT

Extensive research has shown that electrochemistry is one of the factors that govern the flotation of sulfide minerals. Flotation is often adversely affected by uncontrolled oxidation, which is also an electrochemical process. The interest in pyrrhotite recovery arose after observing that there is a substantial loss of PGM due to the depression of pyrrhotite and the subsequent loss of any PGMs associated with it.

The first part of this study focuses on the influence of chemical composition and crystal structure on the electrochemical behaviour of pyrrhotite in a 0.05 M $Na_2B_4O_7$ solution. Rest potential and polarisation resistance measurements, as well as anodic polarisation diagrams, showed that the magnetic 4C type pyrrhotite is anodically more reactive than the non-magnetic 6C type pyrrhotite. It was also shown in cathodic polarisation diagrams that the non-magnetic 6C type pyrrhotite is a better substrate for oxygen reduction and is less susceptible to oxidation. ToF-SIMS showed the formation of an oxide layer on the pyrrhotite surface after oxidation.

In the second part of this work, the influence of galvanic interactions on the electrochemical behaviour of pyrrhotite in contact with pentlandite was investigated. It was observed that,

under oxygen-saturated conditions, as the amount of pentlandite increases, the reactivity towards oxidation of the mixed mineral system is reduced. Impedance measurements showed a decrease in capacitance values, indicating the formation of a continuous oxide layer on the surface and an increase in oxide layer thickness with decreasing pentlandite content. Anodic polarisation diagrams showed that under oxygen-deficient conditions and in the low potential region, pentlandite behaves as an inert material and does not have an influence on the oxidation behaviour of pyrrhotite. Hence, the anodic activities of the different magnetic 4C type pyrrhotites from Sudbury Gertrude, Phoenix and Russia were compared. It was shown that the oxidation reactivity decreased in the following order: Sudbury Gertrude magnetic 4C pyrrhotite > Phoenix magnetic 4C pyrrhotite > Russian magnetic 4C pyrrhotite; it also varied according to location. In the transpassive region, higher anodic currents were observed on the mixed samples because both pentlandite and pyrrhotite reacts. The reactivity increased in the order: pure pyrrhotite (Russia) < medium-pentlandite (Sudbury Gertrude) < high-pentlandite (Phoenix).

In the presence of potassium ethyl xanthate, there was no change in the initial anodic reactivities of the different pyrrhotites. The anodic polarisation diagrams of the pure and mixed samples showed a reduction in the maximum anodic peak current, suggesting the presence of xanthate on the surface, which hinders oxidation of the mineral surface.

In addition, the influence of cleaning of oxidised pyrrhotite with gaseous carbon dioxide was studied, using electrochemical and microflotation measurements. Electrochemical measurements indicated that CO_2 treatment resulted in depassivation of the oxidised surfaces; this was supported by ToF-SIMS measurements that demonstrated a reduction in the oxide layer thickness after CO_2 treatment. Anodic polarisation diagrams showed a higher anodic peak current, indicating that the surface is more reactive. Gaseous carbon dioxide conditioning of oxidised pyrrhotite resulted in improved flotation response of pyrrhotite with the aid of copper activation and higher air flow rate.

Keywords: Pyrrhotite, PGE, electron microprobe analysis, rest potential, polarisation resistance, anodic polarisation diagrams, cathodic polarisation diagrams, capacitance, ethyl xanthate, galvanic interactions, carbon dioxide, ToF-SIMS, XRD, microflotation.

TABLE OF CONTENTS

LIST OF TABLES

LIST OF FIGURES

LIST OF ACRONYMS

A	Platreef Composite A
At	Atomic
ATR	Attenuated total reflectance
B	Platreef Composite B
BIC	Bushveld Igneous Complex
BSE	Back-scattered electron
C	Platreef Composite C
EDS	Energy dispersive spectrometer
EDTA	Ethylene diamine tetra-acetate
EDX	Energy dispersive X-ray
EIS	Electrochemical impedance spectroscopy
FTIR	Fourier transform infrared spectroscopy
IR	Infrared
KEX	Potassium ethyl xanthate
LMP	Lebowa Merensky
LUP	Lebowa UG-2
M	Metal
NaHS	Sodium hydrosulfide
NS	Non-sulfide mineral
PAX	Potassium amyl xanthate
PGE	Platinum-group element
PGM	Platinum-group mineral
Pn	Pentlandite
Po	Pyrrhotite
Rp	Polarisation resistance
Qemscan	Quantitative evaluation of minerals by scanning electron microscopy
QEM*SEM	Quantitative evaluation of minerals by scanning electron microscopy
SCE	Standard calomel electrode
SEM	Scanning electron microscopy
SHE	Standard hydrogen electrode
SIBX	Sodium isobutyl xanthate
SiC	Silicon carbide

Tof-SIMS	Time-of-flight secondary ion mass spectrometry
Wt	Weight
X	Xanthate
X_2	Dixanthogen
XPS	X-ray photoelectron spectroscopy
XRD	X-ray diffraction

1. INTRODUCTION

South Africa has the major (80 %) share of the world's platinum-group elements (PGEs) reserves and production, with Russia in second place and Canada third (Jones, 1999). South Africa's production centres on the Bushveld Igneous Complex (BIC), the platinum-group minerals (PGMs) bearing ores being mined primarily for the recovery of these metals. The precious metals are the most valuable products in South African platinum ores. In other countries, smaller quantities of platinum are produced as by-products or co-products, particularly of nickel, such as in the case of Norilsk in Canada where the PGEs are by-products of Ni-Cu mining, primarily from the Falconbridge and Inco deposits in the Sudbury area (Jones, 1999; Xiao and Laplante, 2004). Apart from South Africa's platinum mines, Stillwater Mine in Montana and Hartley Platinum in Zimbabwe are the only major primary producers of PGMs (Jones, 1999). Mimosa mine in Zimbabwe contains a significant amount of PGMs (Oberthür *et al.*, 2002). Mineralogical investigations performed on all effluent flotation streams of Mimosa mine indicate the presence of appreciable amounts of platinum-group minerals, which are not recovered due to the different modes of occurrence of the PGMs and base-metal sulfides (Van Wouw, 2003).

Pyrrhotite is the most abundant of the sulfide and oxide minerals in the Uitkomst complex of the Nkomati mine, namely: pentlandite, chalcopyrite, magnetite, ilmenite, chromite, digenite and pyrite (in a sequence of decreasing abundance) (Gauert *et al*., 1995). In many flotation plants, such as in the case of Cu-Ni ores and massive nickel ores, pyrrhotite is rejected to the flotation tailings as a waste product (Miller *et al.*, 2005). This practice has the desirable effect of removing a significant amount of sulfur prior to smelting so as to reduce the production of sulfur dioxide during smelting. This has become a particular concern, especially with the enactment of more stringent emission controls (Senior *et al.*, 1994). On the other hand, a strong interest in pyrrhotite recovery arises in certain instances, in particular, in terms of its importance in pyrrhotite flotation in the processing of PGE ores from the Bushveld Igneous Complex in South Africa (Miller *et al.*, 2005). This interest arose after observation of a substantial loss of PGE due to the depression of pyrrhotite and the subsequent loss of PGEs associated with it.

The flotation process for the Merensky and UG-2 ores is a bulk sulfides float that recovers the base-metal sulfides (Xiao and Laplante, 2004). Pyrrhotite is non-stoichiometric, having a variable composition and crystal structures varying from Fe_7S_8 to $Fe_{11}S_{12}$. Monoclinic pyrrhotite (Fe_7S_8) tends to be less Fe-rich and magnetic than the hexagonal variety (Fe_9S_{10}, $Fe_{11}S_{12}$). Various researchers have reported variations in pyrrhotite composition in different regions in the Bushveld Igneous Complex as well as other PGE deposits in the world (Kaiser and Specker, 1955; De Villiers *et al.*, 1980; Mostert, 1982; Merkle and Von Gruenewaldt, 1986; Penberthy, 2001; Becker, 2005; Godel *et al.*, 2007). Due to its variation in composition and crystal structure, each pyrrhotite sample may have a different nature. This is supported by studies done by Khan and Kelebek (2004) and Buswell and Nicol (2002) on the decomposition of pyrrhotite from Sudbury and South Africa. The compositions of the electrodes used were not provided. The pyrrhotite specimen used by Khan and Kelebek (2004) was a hexagonal type; the crystal structure of the pyrrhotite used by Buswell and Nicol (2002) was not provided. Khan and Kelebek (2004) reported that when potential is below -0.05 V (SHE), the initial rate of oxidation (anodic current density) is slow; Buswell and Nicol (2002) reported that when the potential exceeds -0.40 V (SHE), the initial rate of pyrrhotite oxidation becomes significant. These results suggest that pyrrhotite sourced from South Africa is much more reactive than the sample sourced from Sudbury.

Pyrrhotite is easily oxidised and this results in its slow and poor flotation (Miller *et al.*, 2005). Surface oxidation of sulfide minerals, such as that found in the regions of a sulfide ore body near the water table, can have a significant impact on flotation. Newell *et al.* (2005) reported the flotation response of surface oxidised sulfide minerals such as pyrrhotite, pentlandite and chalcopyrite, and the subsequent effect of three potential remedies. These remedies include: treatment in an ultrasonic bath, collector concentration and sulfidisation. It appeared, however, that the above-mentioned remedies have limitations, thus treatment of oxidised ores that will improve the recovery of all the valuable sulfide minerals is essential.

Miller and Misra (1987) developed a process for froth flotation of coal, using gaseous carbon dioxide and including a pre-conditioning treatment of the coal with gaseous carbon dioxide followed by froth flotation. The pre-treatment resulted in improved results: less reagent promoter and frother were required and the flotation time reduced. The process was deemed applicable to various grades and types of coal and may also be used for oxidised coal. The process proved to be particularly useful for producing “super” clean coal.

No process is known that uses gaseous carbon dioxide as a surface active reagent to improve the hydrophobic character of the oxidised sulfide minerals ore surface or clean the oxidised ore surface.

Extensive research has shown that electrochemistry is one of the factors that influence the flotation of sulfide minerals. Flotation is often adversely affected by uncontrolled oxidation, which is also an electrochemical process. Electrochemistry influences flotation in several ways, viz.:

- The surface composition of sulfide minerals is strongly dependent on the oxidation potential in the environment surrounding the mineral;
- The adsorption of thiol-type flotation collectors often occurs through an electrochemical mechanism;
- Precipitation of iron oxy/hydroxides from solution onto the mineral surfaces is affected by the oxidation potential.

The main focus of this study was to understand the electrochemical behaviour of pyrrhotite using electrochemical measurements on pyrrhotite electrodes as well as to determine whether variations in chemical composition and crystal structure of pyrrhotite affect its electrochemical behaviour (i.e. reactivity, oxidation) and flotation response. The aim was also to assess whether the poor flotation response of pyrrhotite could be related to its electrochemical behaviour. The electrochemical measurement techniques include the rest potential, polarisation resistance and electrochemical impedance measurements, as well as anodic and cathodic polarisation diagrams.

Another focus of this study was to investigate the influence of gaseous carbon dioxide conditioning on the electrochemical and flotation response of oxidised pyrrhotite using electrochemical measurements and microflotation tests. This was done to help address the slow flotatiom response of pyrrhotite due to its rapid oxidation during flotation. The aim was to establish whether gaseous carbon dioxide had the same cleaning effect on oxidised pyrrhotite as was reported by Miller and Misra (1987) with oxidised coal. Cleaning of oxidised pyrrhotite is expected to improve pyrrhotite's interaction with flotation reagents, particularly xanthate, and improve its flotation recovery.

The next section provides an overview of pyrrhotite and highlights the importance of studying the electrochemical behaviour of pyrrhotite.

2. LITERATURE REVIEW

2.1. Mineralogy

2.1.1. Sulfide minerals and PGE association and distribution

The PGEs, which may occur as discrete PGMs, most commonly occur in association with the base-metal sulfide minerals; these minerals contribute approximately 1 % (by volume) to the PGE ore within the Merensky and UG-2 reefs. Pentlandite [$(Fe,Ni)_9S_8$], chalcopyrite ($CuFeS_2$) and pyrrhotite [$Fe_{(1-x)}S$] are the most commonly occurring sulfides within the PGE ore, which also has small amounts of pyrite (FeS_2). The PGE may also occur in solid solution within the sulfide minerals (Buswell and Nicol, 2002; Miller *et al.*, 2005). Sulfides are a major repository of PGEs and PGMs (Vermaak, 2005). The interest in pyrrhotite recovery arose after observing that there is a substantial loss of PGM due to the depression of pyrrhotite and the subsequent loss of any PGMs associated with it (Miller *et al.*, 2005).

PGE ores are generally grouped into the following three classes: PGE dominant (such as at the Bushveld Igneous Complex, Stillwater Complex, Lac des Iles and Great Dyke), Ni-Cu dominant (such as at Nkomati, Sudbury, Norilsk and Tati mine) and miscellaneous ores. Both the PGE dominant and Ni-Cu ores formed part of the focus of this project and some are discussed below, with the aim of comparing the relative abundance of base-metal sulfides in these ore bodies, specifically pyrrhotite and PGEs.

2.1.2. PGE dominant ores

These ores are exploited primarily for their PGE content; other associated metals, such as Ni, Cu and Co, are produced as by-products, having major economic value. The following are the types of PGE dominant ore deposits:

2.1.2.1. Bushveld Igneous Complex

The BIC extends for 400 kilometres in the Limpopo Province of South Africa. It contains the world's largest known deposits of PGEs such as platinum, palladium, rhodium, ruthenium, iridium and osmium; together with gold and silver, these are considered 'precious' metals. This complex is made up of two major reefs, namely the Merensky and UG-2 reef. The Platreef is found in the northern extension of the BIC.

Although the platinum-palladium ratio in the Merensky and UG-2 reefs is close to three to one, the two metals are found in equal measure in the Platreef deposits (http://www.bullion.org.za). The Platreef can be considered as metallurgically similar to Merensky ore, although somewhat enriched in palladium (Jones, 1999).

Merensky reef ore contains up to 3 % (by mass) base-metal sulfide minerals with the following composition: pyrrhotite (45 %), pentlandite (32 %), chalcopyrite (16 %) and pyrite (2-4 %) (Jones, 1999). These values are in agreement with those reported by Vermaak and Hendriks (1976), which are as follows: pyrrhotite (45 %), pentlandite
(34.8 %), chalcopyrite (15.5 %) and pyrite (3.7 %). The majority of the PGMs in the Merensky ore are associated with pentlandite, occurring either in pentlandite grains or at the pentlandite-gangue grain boundaries. UG-2 ore has the same principal sulfides as the Merensky ore but with less millerite. The sulfide grains of the UG-2 ore are generally finer than those of the Merensky ore (Jones, 1999). The grain size of the base-metal sulfides in the Merensky ore (from the Western limb of the Bushveld Igneous Complex) is about 40 to 50 µm (Dunne, 2007). Clusters of base-metal sulfides, in which PGMs in the Merensky reef (from the Amandebult section of Rustenburg Platinum mine) are generally contained, are relatively large (> 1 mm) (Viljoen *et al.*, 1986).

A modal analysis of the heavy minerals was made from borehole ML34 of the Merensky reef and the percentages of pyrite, chalcopyrite, pentlandite, pyrrhotite and the oxide minerals (mainly chromite and rutile) are presented in *Figure 1* and *Table 1*.

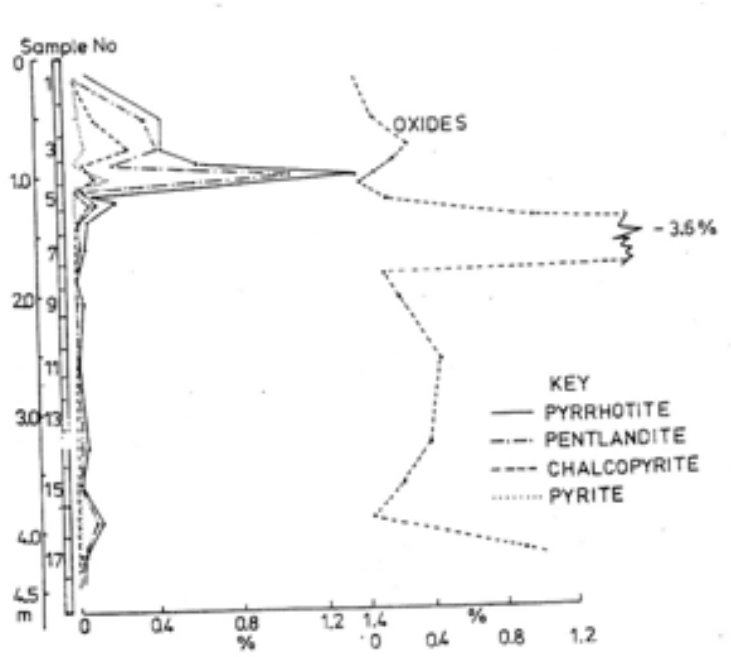

Figure 1: Section of the Merensky Reef in borehole ML34 showing the vertical variation of the major sulfide and oxide minerals (Brynard *et al.*, 1976).

Figure 1 shows the depth from which the samples were obtained.

Table 1: Relative amounts (wt %) of the major sulfide minerals and oxides in Borehole ML34 Merensky Reef at the Western Platinum mine (Brynard *et al.*, 1976).

Sample no.	Pyrrhotite	Pentlandite	Chalcopyrite	Pyrite	Oxides	BMS*
1	0.15	0.04	0.02	0.00	0.01	0.21
2	0.55	0.40	0.13	0.04	0.09	1.12
3	0.52	0.49	0.32	0.09	0.29	1.42
4A	0.73	0.23	0.07	0.00	0.22	1.03
4B	1.40	1.25	0.13	0.21	0.11	2.99
5A	0.12	0.05	0.01	0.00	0.03	0.18
5B	0.34	0.17	0.10	0.01	0.16	0.62
6	0.08	0.03	0.01	0.02	0.97	0.14
7	0.07	0.04	0.03	0.02	3.60	0.16
8	0.01	0.00	0.01	0.00	0.14	0.02
9	0.04	0.03	0.01	0.00	0.24	0.08
11	0.03	0.02	0.01	0.00	0.45	0.06
14	0.05	0.02	0.01	0.00	0.39	0.08
15	0.01	0.01	0.00	0.01	0.26	0.03
16	0.14	0.12	0.03	0.01	0.06	0.30
17	0.03	0.02	0.01	0.01	1.02	0.07
Average	**0.27**	**0.18**	**0.06**	**0.03**	**0.50**	**0.53**

* BMS: Base-metal sulfides

The above table and *Figure 1* show variation in sulfide mineral content with depth in the Merensky reef. Pyrrhotite was found to be the dominant sulfide mineral in all samples, followed by pentlandite, chalcopyrite and pyrite. These results are in agreement with the results reported by Jones (1999) and Vermaak and Hendriks (1976). On average, base-metal sulfides have a slightly higher content than do oxides.

Brynard *et al*. (1976) reported the PGE content of both the non-magnetic and magnetic pyrrhotites from the Western Platinum mine (*Table 2*). *Table 2* highlights the importance of recovering pyrrhotite and the variation in the PGE content of different types of pyrrhotite.

Table 2: PGEs and Au in pyrrhotite from the Western Platinum Mine of the Merensky Reef (Brynard *et al.*, 1976).

Mineral	PGEs (ppm)					
	Pt	**Pd**	**Ru**	**Rh**	**Ir**	**Au**
Non-magnetic pyrrhotite	16.0	8.8	11.0	1.3	4.2	1.2
Magnetic pyrrhotite	29.0	18.0	12.0	6.6	10.0	2.8

As can be seen, the magnetic pyrrhotite contains a larger amount of PGEs than the non-magnetic pyrrhotite.

The relative proportions of sulfide minerals from the UG-2 reef were reported by Penberthy (2001). The bulk modal analysis of the base-metal sulfide measured by image analysis and the modal amounts of the different base-metal sulfides in the samples are reported in *Table 3.* Samples were collected underground on the Lonrho Mining property in the Marikana Brits area.

Table 3: Sulfide modal composition in mass %, calculated from bulk modal analysis measured by image analysis and relative proportions of sulfide minerals (volume %) (Penberthy, 2001).

Sample locality	**An fw**	**Nor fw**	**Peg fw**		**Pothole**		**RPeg fw**	**Faulted**	**Faulted**	**Pothole**	**Nor fw**	**Faulted**	**Peg fw**	**An fw**
	A2	**B2**	**A1**	**B1**	**A3**	**B3**	**A4**	**B4**	**A5**	**C1**	**C2**	**C3**	**C4**	**C5**
BMS	0.10 ±0.03	0.11 ±0.05	0.13 ±0.02	0.17 ±0.04	0.11 ±0.02	0.15 ±0.08	0.18 ±0.04	0.15 ±0.02	0.09 ±0.08	0.03 ±0.01	0.07 ±0.03	0.04 ±0.01	0.04 ±0.01	0.04 ±0.02
Chalcopyrite	0.02 ±0.01	0.03 ±0.02	0.03 ±0.01	0.04 ±0.01	0.03 ±0.01	0.02 ±0.02	0.04 ±0.02	0.02 ±0.00	0.01 ±0.01	0.01 ±0.00	0.01 ±0.01	0.02 ±0.01	0.01 ±0.00	0.01 ±0.01
Pentlandite	0.05 ±0.02	0.05 ±0.02	0.07 ±0.02	0.08 ±0.02	0.05 ±0.01	0.07 ±0.05	0.09 ±0.02	0.07 ±0.01	0.07 ±0.03	0.00 ±0.00	0.00 ±0.00	0.00 ±0.00	0.00 ±0.00	0.00 ±0.00
Pyrrhotite	0.01 ±0.01	0.00 ±0.00	0.02 ±0.01	0.04 ±0.02	0.01 ±0.00	0.04 ±0.03	0.04 ±0.01	0.05 ±0.01	0.00 ±0.00	0.00 ±0.00	0.00 ±0.00	0.00 ±0.00	0.00 ±0.00	0.00 ±0.00
Pyrite	0.01 ±0.00	0.02 ±0.01	0.02 ±0.00	0.01 ±0.00	0.01 ±0.01	0.00 ±0.00	0.00 ±0.00	0.01 ±0.00	0.00 ±0.00	0.00 ±0.00	0.03 ±0.02	0.00 ±0.00	0.01 ±0.00	0.02 ±0.02
Millerite	0.00 ±0.00	0.00 ±0.00	0.00 ±0.00	0.00 ±0.00	0.00 ±0.00	0.00 ±0.00	0.00 ±0.00	0.00 ±0.00	0.00 ±0.00	0.01 ±0.01	0.02 ±0.01	0.01 ±0.00	0.02 ±0.01	0.01 ±0.00

BMS: Base-metal sulfides; An fw: Anorthosite footwall; Nor fw: Norite footwall; Peg fw: Pegmatoid footwall; Pothole: Pothole edge; RPeg fw: Replacement pegmatoid footwall; Faulted: Faulted UG-2

Average base-metal sulfide content (mass %) and individual sulfides (volume %).

BMS	0.094
Chalcopyrite	0.021
Pentlandite	0.067
Pyrrhotite	0.030
Pyrite	0.016
Millerite	0.014

BMS: Base-metal sulfides

Table 3 shows the average base-metal sulfide content was determined to be 0.094 wt %. Pentlandite was the dominant sulfide, then pyrrhotite, chalcopyrite, pyrite and millerite. It is evident from *Tables 1* and *3* that the Merensky ore has a higher sulfide content than the UG-2 ore (0.53 vs 0.094 wt %).

The PGE content in the Merensky reef ranges between 4-10 g/t, whereas in the UG-2 reef PGE content ranges from 3.5 to 19.16 ppm, 3.6 ppm Pt, 3.81 ppm Pd, 0.33 ppm Ru and others 2.26 ppm (Gain, 1984). Minerals in the Merensky ore are found in a silicate substrate, while UG-2 ore has a chromite matrix.

The platreef is a platinum-group element (PGE) and base-metal enriched mafic/ultramafic layer situated along the base of the northern (Potgietersrus) limb of the Bushveld Igneous Complex (Mostert, 1982). Wagner (1929) described three distinct layers, which Buchanan (1979) later referred to as the A, B and C units (or reefs), ordered from the base to the top, based on texture and mineral mode. Modal mineral abundance studies in the three Platreef horizons (three pyroxenite/gabbronite units separated by hornfels interlayers on the farm Townlands: Lower, Middle and Upper zones) showed that sulfides are most abundant in the Middle Platreef and less so in the Upper Platreef; whereas the Lower Platreef is relatively sulfide-poor, with the Lower Platreef containing 1-2 wt %, Middle Platreef 0-10 wt % (with massive veins up to 3 cm in width) and Upper Platreef 0-3 wt %. The sulfide assemblage in all three layers consists predominantly of pyrrhotite and chalcopyrite, with minor pentlandite and pyrite occurrences. The sulfide minerals average 2-5 wt % in abundance in three layers. The mineral and whole rock data, including the S-isotopic data, show distinct compositional variations (breaks) between the different Platreef layers (Manyeruke, 2003).

Mostert (1982) worked on the Platreef on Drenthe 778 LR, which lies at the base of the Rustenburg Layered Suite of the Potgietersrus limb of the Bushveld Igneous Complex. Mostert (1982) reported that the distribution of sulfide minerals throughout the Platreef is not homogeneous, that the position of sulfide enrichment differs from borehole to borehole and that correlation along strike is difficult. The Ni:Cu ratio fluctuates both laterally and vertically and has a tendency to decrease with depth (*Figure 2*).

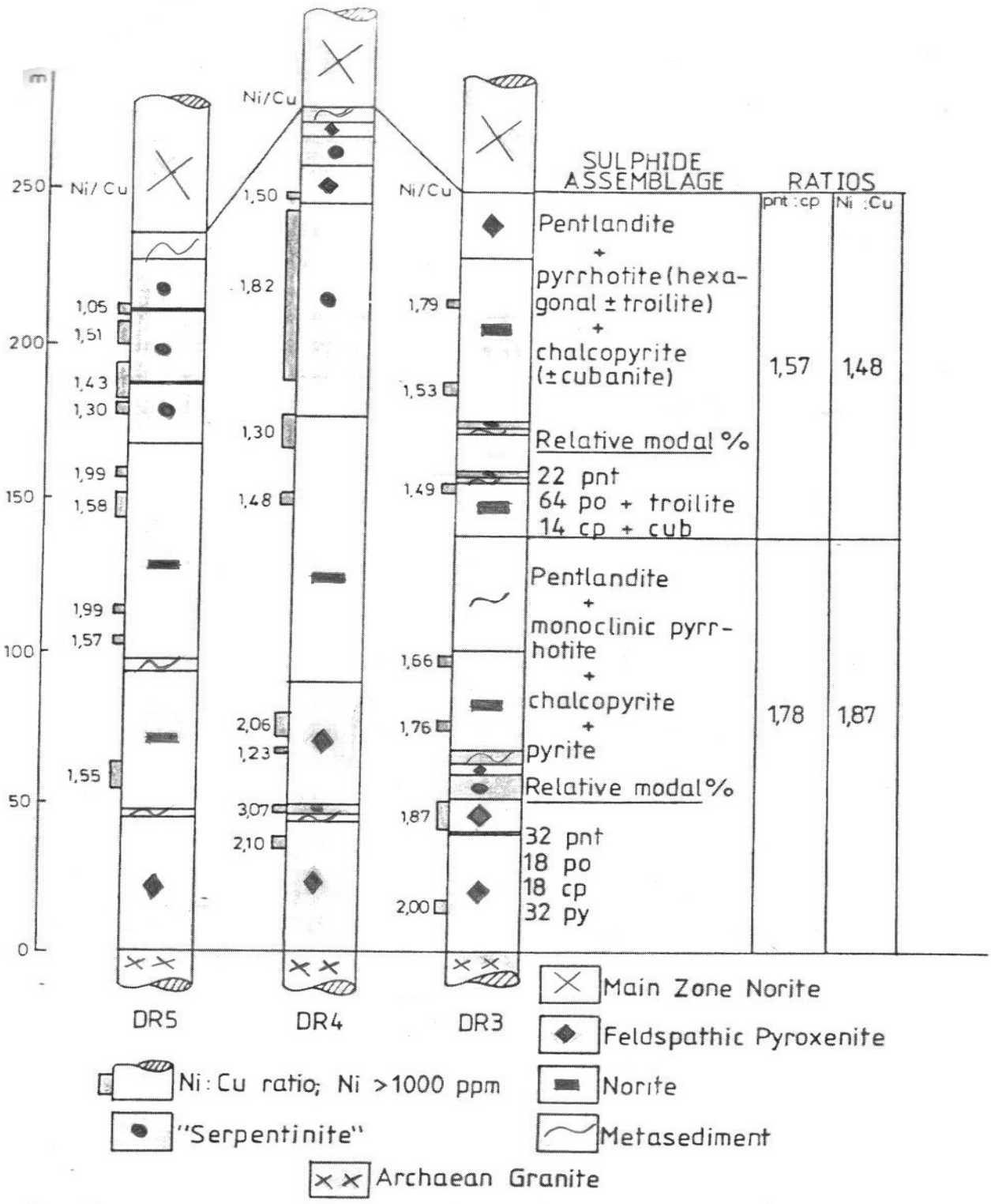

Figure 2: Borehole profiles of the Platreef with Ni:Cu ratios where Ni concentration > 1000 ppm. Sulfide assemblages are also shown (Mostert, 1982).

Pt, Pd and Rh make up a constant 95 % of the value of all the precious elements in the Merensky, Platreef and UG-2 ores. The Merensky ore has an average PGE minerals grain size of 45 µm, which is larger than that of UG-2 ore at 15 µm (Jones, 1999).

Pyrrhotite is the most abundant of all three common sulfides in the Bushveld Igneous Complex reefs (Miller *et al.*, 2005). Cabri (1988) reported the following quantities of PGE in solid solution in pyrrhotite at elevated temperatures: 11 % Pd, 1.3 % Ru, 10.5 % Rh and 2.2 % Pt, but it should be noted that upon cooling most of these PGMs are expelled. A higher Fe content in pyrrhotite is detrimental to the solubility of PGMs in the mineral. Cabri (1988) found pyrrhotite to contain PGEs very close to the detection limit, which he reported to be of the order of 10 ppmw for many PGMs. These findings were supported by Oberthür *et al.* (1997), who reported that pyrrhotite usually contains PGEs at concentrations close to or lower than the detection limit.

2.1.3. Ni-Cu dominant ores

In these ore types, PGEs are recovered as by-products and occur as discrete PGMs in solid solution with metal sulfides and to a lesser extent with gangue minerals (Xiao and Laplante, 2004).

2.1.3.1. Nkomati

2.1.3.1.1. Uitkomst Complex of South Africa

The ore extracted at the Nkomati mine is derived from the Uitkomst Complex of South Africa. Several lenses of the massive sulfides (2.9 Mt at 2.04 % Ni, 1.13 % Cu, and 6 ppm total PGE) are situated in the immediate floor of the intrusion (Maier *et al.*, 2003).

The massive sulfide body was reported by Theart and De Nooy (2001) to have the following composition: 70 wt % pyrrhotite, 9 wt % pentlandite, 6.3 wt % chalcopyrite, 3.8 wt % pyrite and 10.5 wt % magnetite. Nkomati massive sulfide samples are dominated by coarse-grained (up to 1000 µm) pyrrhotite (Becker, 2005), which accounts for about 65 % on a mass basis.

The following table shows the sulfide minerals composition within the Nkomati ore deposit obtained by Newell *et al.* (2005).

Table 4: Nkomati Sample Mineral Composition (Newell *et al.*, 2005).

Mineral	**Percent**	**Mass**
	EDS[*a]	**Chemical**[*b]
Pyrrhotite	66.3	66.7
Pentlandite	8.4	9.0
Chalcopyrite	5.4	6.1
Pyrite	3.2	3.5
Iron Oxides	15.2	13.6
Silicates	1.5	1.3

EDS: Energy dispersive spectrometer

*[a] Average of three QEM*SEM samples

*[b] Reconciliation based on all test work samples

These sulfide minerals concentrations are similar to the ones reported by Theart and De Nooy (2001), with pyrrhotite being the dominant sulfide.

2.1.3.2. Sudbury, Thomson and Shebandowan mine

INCO has three sulfide producing regions, which deal with somewhat different ores and mineral compositions. These regions are the Sudbury basin, Thomson (Manitoba) and Shebandowan mine (located in north western Ontario). An approximate average composition of ore treated is given in *Table 5*, which shows that pyrrhotite content is higher than those of other sulfides (chalcopyrite and pentlandite) in all ore bodies.

Table 5: Approximate ore compositions (mass %) (Agar, 1991).

	Sudbury	Thompson	Shebandowan
Pentlandite	3	7.1	5
Chalcopyrite	3.7	0.5	2.3
Pyrrhotite	20	23	20
Quartz	16	28	6
Feldspar	14	24	7
Chlorite	21	-	25
Biotite	11	7	-
Amphibole	10	6	<5
Carbonates	2	<5	10
Tremolite	-	-	15
Talc	-	-	4

2.1.3.3. Tati mine near Francistown, Botswana

The Tati mine, located 30 km east of Francistown in Botswana, exploits two sulfide deposits, namely the Phoenix and Selkirk deposits. The Phoenix deposit is relatively small and occurs within mafic (Mg-Fe rich) intrusive rocks of Archean (http://www.miningweekly.com). Mineralogically, the sulfide ore comprises on average 70 % pyrrhotite, 20 % pentlandite and 10 % chalcopyrite. The tenor of the massive sulfides can be as high as 8 % nickel (http://www.miningweekly.com). The mineralisation hosts significant platinum-group elements.

The Selkirk massive sulfide body, located 15 km south of Phoenix, is a shallow plunging zone of massive sulfide mineralisation, approximately 200 m long, 100 m wide and up to 20 m thick. Mineralogically, the massive sulfide deposit is comprised of about 77 % pyrrhotite, 10 % pentlandite, 10 % magnetite and 3 % chalcopyrite; it is graded at approximately 2.6 % nickel and 1.6 % copper (http://www.miningweekly.com).

Pyrrhotite is the most abundant sulfide followed by pentlandite, pyrite and chalcopyrite. Minor sphalerite is also present (Johnson, 1986).

Properties of pyrrhotite are discussed next, so as to highlight the complexities surrounding its behaviour in flotation.

2.2. Pyrrhotite properties

2.2.1. Chemical composition and crystal structure

Pyrrhotite, $Fe_{(1-x)}S$, is non-stoichiometric and of a variable composition, with a density varying from 4.58 to 4.65 (Miller *et al.*, 2005). The x value varies from 0 to 0.2, i.e. the amount of sulfur varies from 50 to 55 atoms per 50 atoms of iron. The non-stoichiometry is due to a system of ordered vacancies within the Fe lattice (Vaughan and Craig, 1978; Pofsai and Dodonay, 1990; Thomas *et al.*, 2000; Thomas *et al.*, 2001). The formula can also be expressed as $Fe_{n-1}S_n$ with $n \geq 8$ to give structures from Fe_7S_8 to $Fe_{11}S_{12}$. The Fe-S distance is in the range of 0.237-0.272 nm (Vaughan and Craig, 1978). There are two commonly occurring crystallographic types of pyrrhotite, namely monoclinic and hexagonal; the monoclinic pyrrhotite tends to be less Fe-rich (Fe_7S_8) than the hexagonal variety (Fe_9S_{10}, $Fe_{11}S_{12}$) (refer to *Figure 3*) (Klein and Hurlburt, 1993).

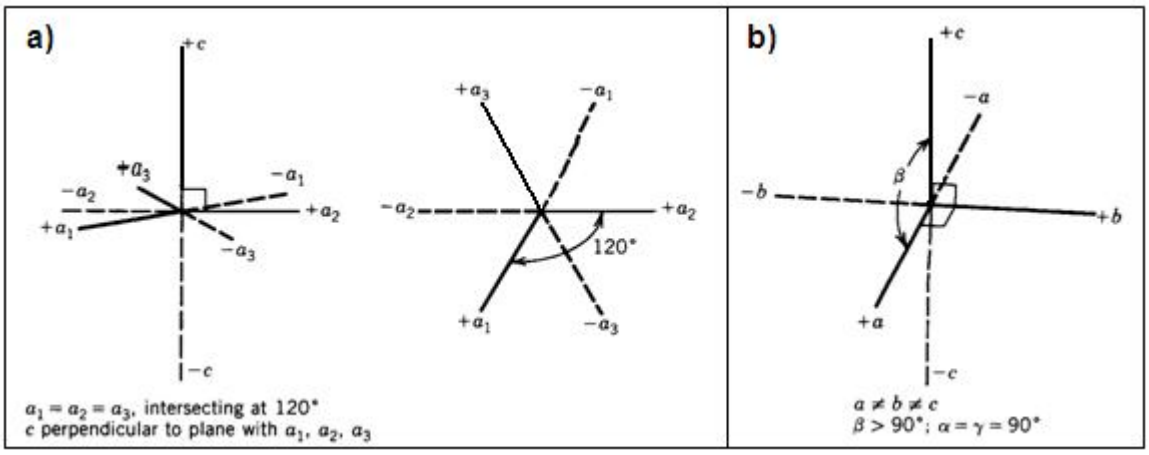

Figure 3: Diagrammatic illustration of the hexagonal (a) and monoclinic crystal (b) systems. Lower case letters indicate crystallographic axes whereas Greek letters correspond to the angles between axes (Klein and Hurlburt, 1993).

Table 6 shows the different pyrrhotite common names, ideal chemical compositions and crystal structures.

Table 6: Pyrrhotite common names, ideal chemical compositions and crystal structures (Nakazawa and Morimoto, 1971; Morimoto *et al.*, 1975).

Common name	Crystal structure	Atomic Fe:S	Chemical composition	Type (xC)
Magnetic	Monoclinic	0.875	Fe_7S_8	4C
Non-magnetic	Hexagonal	0.900	Fe_9S_{10}	5C
Non-magnetic	Hexagonal	0.917	$Fe_{11}S_{12}$	6C
Non-magnetic	Troilite	1.000	FeS	2C

In monoclinic pyrrhotite, the iron content ranges between 46.5 and 46.8 % in Fe on a mole (atomic %) basis; in hexagonal pyrrhotite, it ranges between 47.4 and 48.3 %. Monoclinic pyrrhotite is well known for its magnetic properties, which may be exploited during mineral processing. Miller *et al.* (2005) reported monoclinic pyrrhotite to have a magnetic susceptibility of about 13.1 e.m.u./g.; compare this to the 10^{-5} e.m.u./g of hexagonal pyrrhotite.

Most pyrrhotite occurrences tend to contain variable combinations of these two phases. From the 82 terrestrial pyrrhotite samples analysed by Arnold (1967), 73 % of the pyrrhotites investigated were mixtures of hexagonal and monoclinic forms, 10 % contained hexagonal

pyrrhotite only and 9 % contained hexagonal and monoclinic pyrrhotite. In the remaining samples, 8 % contained troilite, stoichiometric FeS (when x = 0). Hexagonal pyrrhotite may also be associated with the mineral troilite (FeS; e.g. Bushveld Complex [Liebenberg, 1970]), whereas primary monoclinic pyrrhotite is never associated with troilite.

Nkomati pyrrhotite is a mixture of hexagonal and monoclinic types; although monoclinic pyrrhotite appears to predominate. Pyrrhotite also occurs in clusters associated with gangue minerals, which may show variation from interlocking pyrrhotite and gangue crystals to elongated stringers of pyrrhotite hosted by silicate minerals/gangue (*Figure 4*).

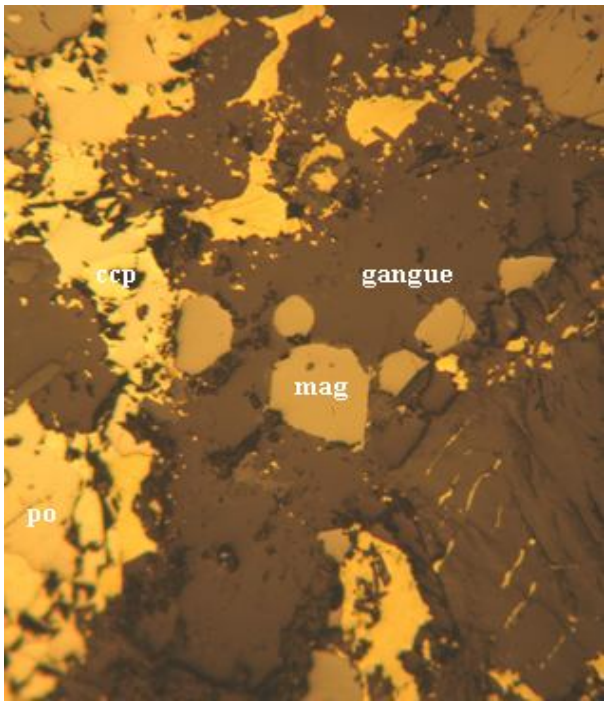

Figure 4: Back-scattered electron image showing intergrown pyrrhotite and gangue. Note the magnetite grains within the gangue and pyrrhotite. Samples viewed in polarised reflected light (mag: magnetite, ccp: chalcopyrite, po: pyrrhotite) (Becker, 2005).

The base-metal sulfides from the Tati samples tend to occur in variable settings, predominantly as disseminated sulfides scattered throughout the silicate/gangue minerals, but also as massive sulfide domains (Becker, 2005).

De Villiers *et al.* (1980) conducted an electron-microprobe analysis of selected grains of pyrrhotite from the Merensky ore and the results are presented in *Table 7*. Brynard *et al.* (1976) reported similar values and showed the total metal and trace element content of the major sulfide minerals in the Merensky Reef at the Western Platinum mine.

Table 7: Electron-microprobe analyses of pyrrhotite (wt %) (De Villiers *et al.*, 1980).

Sample	**Fe (%)**	**Ni (%)**	**Co (%)**	**S (%)**	**Total**	**Fe:Ni (mass ratio)**	**Fe:S (molar ratio)**
Hexagonal pyrrhotite	61.40	0.61	0.33	39.10	101.44	100.66	0.90
	62.76	0.52	0.33	38.47	102.08	120.69	0.93
	61.96	0.50	0.33	38.95	101.75	123.92	0.91
	61.28	0.55	0.32	39.20	101.35	111.42	0.89
Average	**60.84**	**0.54**	**0.32**	**38.30**	**100**	**114.17**	0.91
Monoclinic pyrrhotite	60.40	0.60	0.34	40.07	101.43	100.67	0.86
	60.61	0.54	0.35	40.03	101.53	112.24	0.87
Average	**58.63**	**0.56**	**0.34**	**38.47**	**100**	**106.45**	0.87

Table 7 indicates that the chemical composition of pyrrhotite varies per sample. Monoclinic pyrrhotite has less Fe content than hexagonal pyrrhotite, hence the large Fe:S molar ratios and Fe:Ni mass ratios of hexagonal pyrrhotite. On average, the sulfur, nickel and cobalt content for both pyrrhotite varieties are similar. Ni content is higher than Co.

Godel *et al.* (2007) studied a slab of normal 'narrow' Merensky Reef from Frank Shaft, Rustenburg Platinum mine in detail (*Figure 5*). The Merensky Reef sample is composed, from bottom to top, of five layers: a basal anorthosite overlain by a 0.7-1 cm chromitite, which undulates on a centimetre scale; a coarse-grained melanorite of ~10 cm thickness; second layer of chromitite of ~1 cm thickness; and finally, a melanorite.

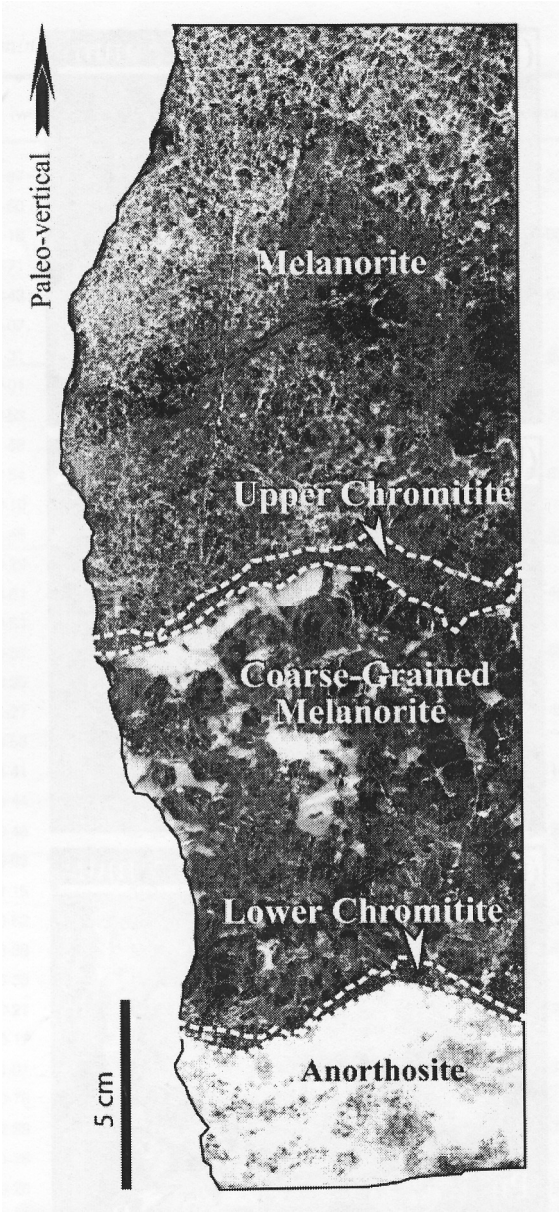

Figure 5: Photograph of the sample of the Merensky Reef (Godel *et al*., 2007).

Results of the microprobe analyses are presented in *Table 8*.

Table 8: Average composition (wt %) of major elements of pyrrhotite as a function of stratigraphy (Godel *et al.*, 2007).

Rock type	n	S (%)	Fe (%)	Cu (%)	Ni (%)	Co (%)	Total	Fe:S (molar ratio)
AN	3	38.99	59.97	<0.01	0.42	<0.01	99.39	0.88
LC & CGM	2	37.99	61.13	<0.01	0.30	<0.01	99.60	0.92
CGM	4	37.26	61.45	<0.01	0.12	<0.01	98.83	0.94
UC	3	38.03	61.27	<0.01	0.16	<0.01	99.45	0.92
M	4	37.73	61.15	<0.01	0.17	<0.01	99.05	0.93
M	5	37.33	61.01	<0.01	<0.01	<0.01	98.34	0.93
M	4	37.95	60.58	<0.01	0.51	<0.01	99.04	0.91
M	4	38.02	60.48	<0.01	0.44	<0.01	98.94	0.91
Average		**37.91**	**60.88**	**<0.01**	**0.30**	**<0.01**	**99.08**	0.92

n: number of different analyses; AN: anorthosite; LC: lower chromitite; CGM: coarse-grained melanorite; UC: upper chromitite; M: melanorite.

In *Table 8*, pyrrhotite composition varies with depth. Fe:S content varies as well. Fe:S content is lower at the anorthosite layer and higher at the coarse-grained melanorite layer. Within the melanorite layer, there are variations in composition as well. Cu and Co content is very low (< 0.01 wt %) and lower than Ni.

The uppermost 1200 m of the upper zone of the western Bushveld Complex at Bierkraal was investigated by whole-rock geochemistry and mineral chemistry of olivine and sulfides. Electron-microprobe analyses were carried out and the calculated reproducibilities (1 sigma) are given in brackets after the approximate range on which calculations are based (all values in atomic %). Reproducibility for pyrrhotite was as follows, S: 50 to 53.3 % (0.097); Fe: 46.7 to 50 % (0.095); Co: 0.04 to 0.09 % (0.005 to 0.008); and Ni: 0.02 to 0.03 % (0.004). Compositions of some of the pyrrhotites analysed is presented in *Table 9* (Merkle and Von Gruenewaldt, 1986).

Table 9: Selected compositions (wt %) of pyrrhotite co-existing with pentlandite at a depth of 1009.6 m (Merkle and Von Gruenewaldt, 1986).

Samples	S (%)	Fe (%)	Ni (%)	Co (%)	Total	Fe:S (molar ratio)
1	38.89	60.60	0.064	0.122	99.68	0.89
2	38.90	60.98	0.058	0.109	100.05	0.90
3	38.53	61.12	0.066	0.106	99.82	0.91
4	38.37	61.60	0.064	0.108	100.14	0.92
5	37.84	62.21	0.059	0.081	100.19	0.94
6	37.84	62.36	0.047	0.101	100.35	0.94
7	36.73	62.81	0.004*	0.114	99.66	0.98
8	36.38	63.09	0.005*	0.080	99.56	0.99
9	36.78	63.39	0.031	0.076	100.28	0.98
10	36.74	63.63	0.000*	0.091	100.46	0.99

* below detection limit

Table 9 illustrates that chemical composition of pyrrhotite varies within the same ore deposit, with the Fe content and Fe:S molar ratio increasing and sulfur decreasing from sample 1 to 10. The cobalt content is higher than the nickel content.

Compositions of pyrrhotite from samples collected underground on the Lonrho Mining property in the Marikana Brits area taken from the work of Penberthy (2001) are presented in *Tables 10* to *12*. Pyrrhotite analyses were obtained in two samples, viz. A1 and B4. These analyses indicated that the average composition of pyrrhotite from samples A1 and B4 is $Fe_{0.99}S_{1.00}$ (close to that of troilite) and $Fe_{0.90}S_{1.00}$ respectively (Penberthy, 2001).

Table 10: Analytical reproducibility of S, Fe, Ni, Co and Cu (wt %) in pyrrhotite calculated at the 95% confidence level from duplicate analyses (Kaiser and Specker, 1955).

N	**42**
S	38.10 ± 0.58
Fe	61.41 ± 0.96
Ni	0.10 ± 0.39
Co	0.07 ± 0.05
Cu	0.02 ± 0.04
Fe:S	**1.61**

N = number of grains on which calculations were based

Table 11: Detection limits of Pt, Rh, Pd and Ru in ppm in pyrrhotite calculated at the 99 % confidence level (Penberthy, 2001).

	Pyrrhotite	**X-ray line**
Pt	295	M_{α}
Rh	225	L_{α}
Pd	285	L_{β}
Ru	210	L_{α}

Table 12: Average compositions (wt %) of pyrrhotite from samples A1 and B4 determined by electron-microprobe analysis. The 90 % confidence interval was calculated using the Student t-distribution (Penberthy, 2001).

	Sample no.	
	A1	**B4**
Element	**(n=18)**	**(n=27)**
	36.53 ± 0.16	38.80 ± 0.15
Fe	62.87 ± 0.17	60.57 ± 0.16
Ni	0.05 ± 0.03	0.13 ± 0.06
Co	0.07 ± 0.01	0.06 ± 0.01
Cu	0.02 ± 0.01	0.03 ± 0.01
Rh	b.d.l	b.d.l
Pd	b.d.l	b.d.l
Pt	b.d.l	b.d.l
Ru	b.d.l	b.d.l
Fe:S (mass ratio)	**1.72**	**1.56**

b.d.l. = below detection limit n=number of grains analysed

According to Penberthy (2001) pyrrhotite appeared not to host significant amounts of PGEs in solid solution (*Table 12*) or as discrete grains, therefore this line of investigation was not pursued any further. Contrarily, Brynard *et al.* (1976) reported the PGE content of both the non-magnetic and magnetic pyrrhotites (*Table 2*), highlighting the importance of recovering pyrrhotite as an important carrier of PGEs. Penberthy (2001) showed that the pyrrhotite composition within the UG-2 ore deposit varies.

In a mineralogical and petrological study, Mostert (1982) observed three modifications of pyrrhotite, i.e. troilite (stoichiometric pyrrhotite), hexagonal and monoclinic pyrrhotite. Mostert (1982) reported that monoclinic pyrrhotite may occur together with the hexagonal modification but not with troilite, which is in accordance with the work of Desborough and Carpenter (1965) and Liebenberg (1970). The iron content of the pyrrhotites generally seems to increase with height above the floor; a trend which is also borne out (to some extent) by analyses of pyrrhotites from different stratigraphic positions in the Platreef (*Table 13* and *Figure 6*). The pyrrhotites were analysed by means of an energy dispersive X-ray analytical system coupled to an electron microscope.

Table 13: Energy dispersive X-ray analysis of pyrrhotite from the Platreef (Mostert, 1982).

Sample no.	**4/2**	**4/31**	**4/14**	**5/19**	**4/20**	**5/17**
Fe (wt %)	59.73	59.79	61.17	60.42	60.36	62.88
S (wt %)	39.28	39.34	39.79	38.67	38.16	36.22
Total	**99.01**	**99.13**	**100.96**	**99.09**	**98.52**	**99.1**
Fe:S (molar ratio)	**0.87**	**0.87**	**0.88**	**0.89**	**0.90**	**0.99**

Height above the floor increases from left to right (height shown in Figure 6) →

Ni could not be analysed for, however qualitative investigation showed that pyrrhotite contains very little Ni (Mostert, 1982). Pyrrhotites analysed by De Villiers *et al.* (1980) and Penberthy (2001) also contained little amounts of Ni.

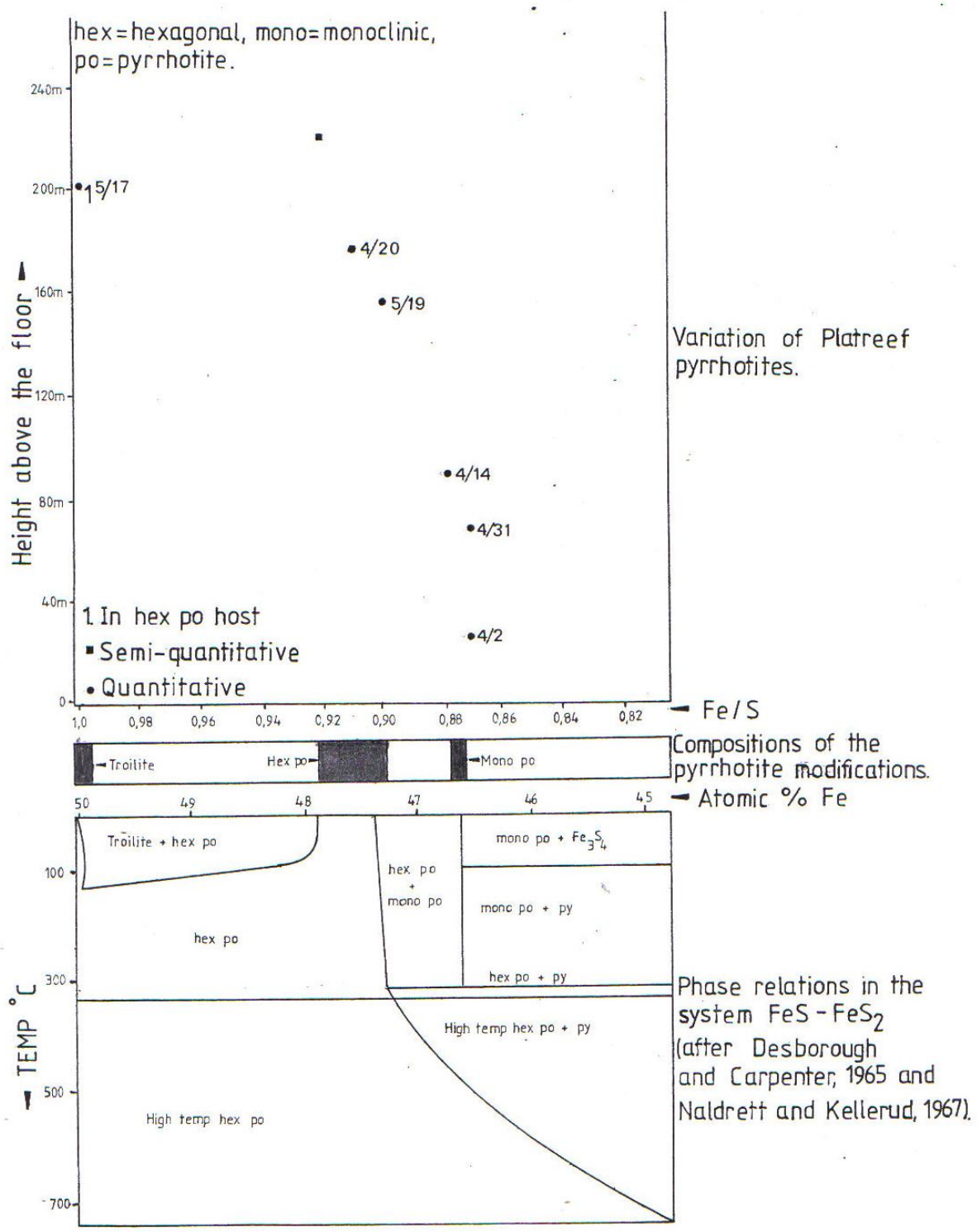

Figure 6: Variation of the composition of pyrrhotite with stratigraphic height and the phase relations in the system FeS - FeS_2 (Mostert, 1982).

These results indicate that pyrrhotite chemical compositions from the Merensky, UG-2 and Platreef, as well as compositions of pyrrhotite within the same ore deposit, vary.

Becker (2005) also conducted an electron-microprobe analysis on selected grains of pyrrhotite from the Nkomati and Tati ore; these results are presented in *Tables 14* and *15*.

Table 14: Mineralogical analyses of Nkomati pyrrhotite obtained using the electron microprobe. Concentrations are given as weight percent and atomic percent (Becker, 2005).

Samples	S (wt %)	Fe (wt %)	Ni (wt %)	Total (wt %)	Fe:Ni (mass ratio)	Fe:S (molar ratio)	At. metal %
1	39.71	60.28	0.75	100.75	80.37	0.87	46.82
2	39.38	60.29	0.68	100.35	88.66	0.87	47.00
3	39.46	60.41	0.71	100.58	85.08	0.87	47.02
4	39.74	60.25	0.71	100.70	84.86	0.87	46.77
5	39.94	60.06	0.72	100.72	83.42	0.86	46.58
6	39.70	60.68	0.41	100.80	148.00	0.87	46.86
7	38.49	61.11	0.91	100.50	67.15	0.91	48.00
8	39.88	60.06	0.56	100.49	107.25	0.86	46.55
9	40.32	59.91	0.46	100.68	130.24	0.85	46.18
10	39.75	60.09	0.40	100.24	150.23	0.86	46.58
11	38.82	60.65	0.82	100.28	73.96	0.89	47.56
12	39.33	60.99	0.68	100.99	89.69	0.89	47.32
13	39.30	60.87	0.76	100.93	80.09	0.89	47.33
14	39.40	60.04	0.78	100.22	76.97	0.87	46.93
15	38.62	60.33	0.72	99.67	83.79	0.89	47.52
16	38.82	60.86	0.55	100.23	110.65	0.90	47.55
17	39.88	60.50	0.28	100.66	216.07	0.87	46.63
18	39.20	60.51	0.37	100.08	163.54	0.88	47.09
19	40.03	60.51	0.20	100.73	302.55	0.86	46.50
20	38.96	61.25	0.59	100.80	103.81	0.90	47.62
21	39.56	60.31	0.66	100.54	91.38	0.87	46.89
22	38.98	60.30	0.75	100.03	80.40	0.88	47.29
23	40.26	59.72	0.44	100.42	135.73	0.85	46.13
24	39.62	60.47	0.76	100.86	79.57	0.87	46.96
25	39.63	60.82	0.40	100.85	152.05	0.88	46.96
26	39.17	60.40	0.71	100.28	85.07	0.88	47.20
27	39.08	60.83	0.72	100.62	84.49	0.89	47.43
28	40.23	59.55	0.78	100.56	76.35	0.85	46.21
29	40.50	60.04	0.39	100.94	153.95	0.85	46.09
30	38.29	61.16	1.02	100.47	59.96	0.91	48.19
Average	**39.47**	**60.44**	**0.62**	**100.53**	**110.84**	**0.88**	**46.99**

Table 15: Mineralogical analyses of Tati pyrrhotite obtained using the electron microprobe. Concentrations are given as weight percent and atomic percent (Becker, 2005).

Samples	S (wt %)	Fe (wt %)	Ni (wt %)	Total (wt %)	Fe:Ni (mass ratio)	Fe:S (molar ratio)	At. metal %
1	38.58	58.78	1.79	99.15	32.84	0.87	47.33
2	38.71	59.62	0.92	99.24	64.80	0.88	47.26
3	39.16	59.34	1.13	99.63	52.51	0.87	46.93
4	39.53	58.79	1.02	99.35	57.64	0.85	46.43
5	39.76	58.95	1.06	99.77	55.61	0.85	46.36
6	39.99	59.42	0.94	100.35	63.21	0.85	46.37
7	39.94	59.73	1.02	100.69	58.56	0.85	46.56
8	39.55	59.02	1.38	99.96	42.77	0.85	46.65
9	40.75	59.75	0.51	101.01	117.16	0.84	45.87
10	40.07	59.69	0.47	100.23	127.00	0.85	46.25
11	40.27	59.44	0.68	100.40	87.41	0.84	46.10
12	41.12	58.77	0.98	100.87	59.97	0.82	45.42
13	42.28	56.53	1.64	100.45	34.47	0.76	44.06
14	40.05	58.20	1.91	100.16	30.47	0.83	46.21
15	39.79	59.42	0.79	100.00	75.22	0.85	46.43
16	39.97	59.19	0.94	100.10	62.97	0.85	46.29
17	39.89	59.28	1.00	100.16	59.28	0.85	46.40
18	40.03	58.78	1.60	100.41	36.74	0.84	46.34
19	40.20	58.97	1.12	100.29	52.65	0.84	46.12
20	40.14	59.40	0.57	100.11	104.21	0.85	46.12
21	39.69	59.64	1.21	100.54	49.29	0.86	46.75
22	40.73	56.73	2.98	100.44	19.04	0.80	45.60
23	39.83	59.50	0.87	100.20	68.39	0.85	46.47
24	39.37	58.88	1.68	99.93	35.05	0.85	46.83
25	40.28	59.34	0.98	100.60	60.55	0.84	46.17
26	40.16	58.92	1.43	100.51	41.20	0.84	46.25
27	40.36	59.40	1.21	100.96	49.09	0.84	46.24
28	40.66	59.55	0.46	100.67	129.46	0.84	45.82
29	40.73	59.40	0.66	100.78	90.00	0.83	45.80
30	39.96	58.85	1.16	99.96	50.73	0.84	46.24
31	40.92	59.06	1.11	101.08	53.21	0.82	45.72
32	40.72	58.54	1.35	100.61	43.36	0.82	45.71
33	40.20	58.86	1.11	100.17	53.03	0.84	46.08
34	39.64	58.73	0.98	99.35	59.93	0.85	46.32
35	39.85	58.73	1.42	100.00	41.36	0.84	46.36
Average	**40.08**	**59.01**	**1.15**	**100.23**	**60.55**	**0.84**	**46.22**

Table 14 shows that pyrrhotite from Nkomati has between 46.09 and 48.19 atomic percent metal and is compositionally similar to pyrrhotite analysed by Van Zyl (1996), where the atomic percent metal includes the substitution of Ni and Cu cations for Fe. The atomic metal content of the Tati pyrrhotite tends to be lower however, at 44.06 – 47.33 atomic % *(Table 15)*. In contrast, the Ni concentration of the Tati pyrrhotite is considerably higher (1.22 ±0.65

wt % Ni) than that of Nkomati (0.62± 0.19 wt % Ni). The Fe:S ratio of Nkomati (at 0.88) is slightly higher than that of Tati (at 0.84).

In *Table 7*, the variation in the Fe content of both the hexagonal and monoclinic pyrrhotites is shown, with monoclinic pyrrhotite having less Fe content than the hexagonal pyrrhotite. This supports the earlier statement that monoclinic pyrrhotite is indeed less Fe rich.

When the monoclinic and hexagonal content of the Merensky ore were combined, the average Fe:Ni mass ratio was found to be 111.60. For the Tati and Nkomati ores, the averages were calculated to be 60.55 and 110.84, respectively. The Fe:S molar ratio of the Bushveld Igneous Complex ore deposits was higher than the Nkomati and Tati ore deposits. Electron microprobe analyses indicated that pyrrhotites from BIC are a mixture of both the magnetic and non-magentic pyrrhotites. Majority of the Nkomati and Tati samples are magnetic pyrrhotites.

These results indicate the compositional variation of pyrrhotite in various ore bodies from different locations. This variation in composition is expected to impact the surface chemistry and hence the flotation characteristics and electrochemical behaviour of pyrrhotite, which could potentially affect the recovery of PGEs.

Following is the flotation behaviour of pyrrhotite in terms of its interaction with flotation reagents and other sulfide minerals, including under different pulp conditions.

2.2.2. Pyrrhotite flotation

2.2.2.1. Natural or collectorless flotation

The natural floatability of pyrrhotite was attributed to the following reasons:

- A stable intermediate surface state, $Fe(OH)S_2$, formed in an acidic solution for short conditioning times and at a low oxidation potential of 0-200 mV (SHE), accounting for the natural hydrophobicity observed under certain conditions (Hodgson and Agar, 1984).

- Elemental sulfur formation at the mineral surface, since sulfur is strongly hydrophobic and may remain stable for a long time, even in alkaline solutions (Peters, 1977).
- The formation of iron-deficient/sulfur-rich metastable intermediates at relatively low pH and mild oxidation potentials (Hamilton and Woods, 1981; Hamilton and Woods, 1983; Heyes and Trahar, 1984; Buckley and Woods, 1985; Jones *et al.*, 1992), whose formation may be described by the following reactions:

$$Fe_{1-x}S + 3yOH^- = Fe_{1-(x+y)}S + yFe(OH)_3 + 3ye^- \qquad \textbf{\textit{Eq. 1}}$$

and

$$Fe_{1-x}S + 3(1-x)H_2O = (1-x)Fe(OH)_3 + S + 3(1-x)H^+ + 3(1-x)e^- \qquad \textbf{\textit{Eq. 2}}$$

Pyrrhotite is reactive, thus it is rapidly oxidised in the presence of air. Long exposure to air results in the formation of iron(III)hydroxide on the surface (Heyes and Trahar, 1984; Buckley and Woods, 1985; Smart *et al.*, 2003). This is represented by the following equation:

$$Fe_{1-x}S + (7-3x)H_2O = (1-x)Fe(OH)_3 + SO_4^{2-} + (11-3x)H^+ + (9+3x)e^- \qquad \textbf{\textit{Eq. 3}}$$

It is under these conditions that the natural flotation of pyrrhotite does not occur.

2.2.2.2. Factors affecting pyrrhotite floatability

2.2.2.2.1. Flotation with thiocarbonate or xanthate collectors

Collectors are flotation reagents that render the valuable mineral hydrophobic. They are made up of a polar hydrophilic portion and a non-polar hydrophobic portion, through which they attach to the mineral and to the bubble, respectively. The hydrophobic tail is usually a hydrocarbon (Lovell, 1982). It has been found that PGM recovery in bulk flotation is limited, in some instances, by the poor flotation response of pyrrhotite (Miller *et al.*, 2005). The presence of oxygen, in conjunction with short-chain sulfydryl collectors, results in the effective flotation of metal sulfides. This is due to the following phenomena:

- The large size of the sulfide ion on the collector, which exhibits little tendency to form hydrogen bonds.
- The formation of insoluble salts between heavy metal ions and short-chain sulfydryl collectors at a relatively low concentration. In addition to this, certain sulfydryl collectors undergo oxidation to dimers, such as dixanthogen and dithiophosphatogen.

Ralston (1991) reported that on a heterogeneous surface such as pyrrhotite, “patches” of dixanthogen multi-layers form, while the rest of the surface is left almost bare. As this occurs, increasing xanthate concentration does not improve recovery. It was suggested that the excess xanthate is adsorbed into these patches of multi-layers without imparting further hydrophobicity to the particle. This results in inefficient collector distribution.

2.2.2.2.2. Addition of copper sulfate and collector

As mentioned earlier, the Bushveld Igneous Complex typically has a combined sulfide grade of less than 1 % (by volume) making efficient beneficiation of the ore to a flotation concentrate a prerequisite. Amongst the major sulfide minerals in the deposit, pyrrhotite is recognised as the most difficult to efficiently float, especially as fine particles, and is generally termed ‘slow floating’. Penberthy (2001) found that after copper activation, the overall recovery rate for sulfides appeared to be as follows: pyrite > chalcopyrite ≈ millerite ≈ pentlandite >> pyrrhotite. The coarsest base-metal sulfide grains were recovered to the fastest floating concentrates, with progressively finer grains being recovered with time. In a study by Bradshaw *et al*. (2006), the flotation performance (i.e. grade and recovery) of iron sulfides was improved following $CuSO_4$ addition. During copper activation, copper ions are added so as to promote xanthate adsorption onto some minerals, such as pyrrhotite and sphalerite. The nature and extent of the surface oxidation plays an important role in understanding the subsequent reaction with reagents (Buswell and Nicol, 2002). The activation process is such that copper ions are added to the flotation system to allow the adsorption of copper ions on the sulfide mineral surface; collector is then added, which reacts with the adsorbed copper ions to form a hydrophobic species - this results in flotation. It has been proposed that the following reactions are likely to occur at the mineral surface (Fuerstenau, 1982; Wesseldijk *et al.*, 1999):

$$Cu^{2+} + 2X^{-} \rightarrow CuX_2 \qquad \textit{Eq. 4}$$

followed by the rapid decomposition

$$2CuX_2 \rightarrow 2CuX + X_2 \qquad \textit{Eq. 5}$$

Any Cu(I) at the surface will immediately form CuX, but the majority of the added copper at these alkaline pH values, will be in the form of $Cu(OH)_2$ and will react to form CuX_2. The activation process will also depend on the ratio of the added collector to the amount of copper present. This is important since, in some operations, the collector is added to the mill before the addition of the copper sulfate.

In a study done by Wiese *et al.* (2005), it was shown that the only condition that led to a strong activation of pyrrhotite being present in the ore was the addition of the SIBX/DTP (sodium isobutyl xanthate/dithiophosphate) collector combination to the mill in conjunction with $CuSO_4$. This improved recovery is due to the interaction of activator and collector with fresh created surfaces in the mill before any major oxidation occurs. The addition of the collector combination to the cell did not yield any greater pyrrhotite recovery than that found in the absence of $CuSO_4$ addition. These results support the addition of flotation reagents to the mill practiced at some of the concentrators.

Significant copper activation of pyrrhotite has been observed in acidic solutions (Chang *et al.*, 1954; Buswell and Nicol, 2002; Miller *et al.*, 2005). In contrast, the role and effectiveness of copper ions for the activation of pyrrhotite in alkaline solutions is not fully understood and the conclusions are controversial. Some researchers (Nicol, 1984; Miller *et al.*, 2005) argue that copper activation is not possible in alkaline solutions, since copper ions are present in the form of insoluble metal hydroxide as soon as copper sulfate is added and are thus not available for reaction with the pyrrhotite surface. Furthermore, pyrrhotite particles are likely to be well oxidised and covered with ferric hydroxide/oxide, which may inhibit any activation reaction with the underlying mineral surface. Other studies have shown that pyrrhotite flotation recovery is significantly improved with the addition of copper sulfate in alkaline solutions (Leppinen, 1990; Senior *et al.*, 1995; Kelebek *et al.*, 1996) and that copper has been detected on concentrate particles from actual flotation circuits (Yoon *et al.*, 1995). In some

studies, it was suggested that the mechanism of activation in this pH range may be via the reaction of the collector with copper hydroxide precipitates (Ralston and Healy, 1980; Laskowski *et al.*, 1997). Weisener and Gerson (2000) studied the copper adsorption mechanism on pyrite, using various surface techniques; the study showed that the activation occurred even in the alkaline range via the reaction of Cu^{2+} with surface sulfur sites to the reduced form Cu^{+} together with an over-layer of colloidal $Cu(OH)_2$.

2.2.2.2.3. Other chemical factors

Pulp potential and pH

The pulp or mineral/solution interface potential is the controlling factor for the electrochemical mechanism; it is an important parameter for controlling the recovery and selectivity of sulfide minerals. Senior *et al.* (1994) reported pyrrhotite as displaying a sharp flotation edge in the recovery-potential curve in the region of 0.12 to 0.18 V (SHE); this potential is close to that required for the oxidation of xanthate to dixanthogen. Yuehua *et al.* (2005) studied the influence of pulp potential and pH on pyrrhotite recovery in the presence of 1×10^{-4} M KEX (see *Figure 7*). Results showed that pyrrhotite floated well from pH 2 to pH 11; recoveries exceeded 80 % when the pH was between 4 and 8. At pHs higher than 12, pyrrhotite recovery declined significantly. As the mineral is conditioned for various times and pH values, as well as under different atmospheres, the zeta potential–pH characteristics change dramatically as the nature and quantity of surface species change (Ralston, 1991). H^{+} and OH^{-} ions determine the potential of the sulfide-solution interface. OH^{-} ions reduce the zeta potential, whereas H^{+} ions increase the zeta potential. *Figure 7* shows the pulp potential decreased with increasing pH, because in highly alkaline solutions ferric hydroxides are easily formed and the presence of large quantities of OH^{-} ions in the solution results in the reduction of the pulp potential.

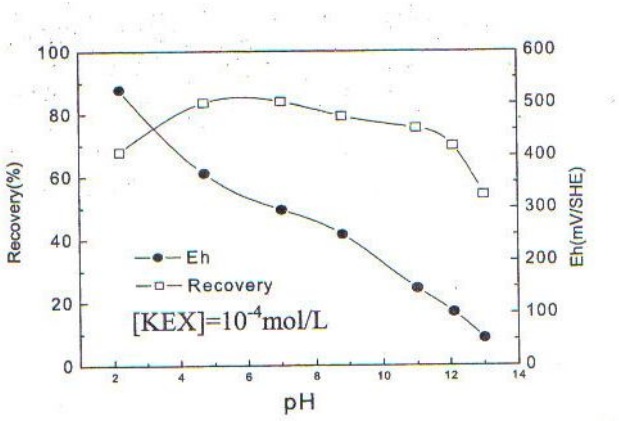

Figure 7: Flotation recovery of pyrrhotite as a function of pH and pulp potential (Yuehua *et al.*, 2005).

In the plant milled pulp: acid conditioning improved pyrrhotite recovery and the electrode potential; the magnitude of change in the electrode potential of pyrrhotite increased significantly upon addition of the collector after acid conditioning. The decrease in the electrode potential of acid cleaned pyrrhotite, after interaction with xanthate, was substantially higher than without acid cleaning, showing higher xanthate adsorption. This was thought to be due to the dissolution of hydrophilic iron oxy/sulfoxy species from the pyrrhotite surface (Buswell *et al.*, 2002; Rao, 2004).

2.2.2.2.4. Physical (operation) factors

Pyrrhotite flotation rate improves with the addition of solids until a critical solids concentration is reached. Particle size has an effect on pyrrhotite floatability. Coarse particles float better than fine particles due to the particle-bubble effect: very fine particles result in low recoveries, which are due to the low probability of particle-bubble collisions. Fine particles follow water more easily, have less collision energy for attachment and higher intensity of entrainment. On the other hand, poor mineral recoveries of very coarse particles are due to a high probability of particle detachment from the bubble surface (Nguyen and Schulze, 2004).

2.2.2.2.5. Flotation of pyrrhotite in the presence of other sulfide minerals

The sulfide minerals association influences their behaviour during flotation, resulting in what is termed galvanic interactions. Rest potentials of sulfide minerals in distilled water at pH 4 are shown in *Table 16*.

Table 16: Rest potentials for sulfide minerals in water at pH 4 (Ralston, 1991).

Mineral	Rest potential (V vs. SHE)
Molybdenite	0.11
Stibnite	0.12
Argentite	0.28
Galena	0.40
Bornite	0.42
Covellite	0.45
Sphalerite	0.46
Chalcopyrite	0.56*
Marcasite	0.63
Pyrite	0.66

*anomalous

Table 16 shows that pyrite has the more cathodic or reducing potential than other sulfides, i.e. it is the most electrochemically noble sulfide mineral. Rand (1977) also reported pyrite as the best catalyst for oxygen reduction among the sulfide minerals.

In *Table 17*, the rest potentials of the sulfide minerals are compared in the presence of three different alkyl dithiolates (regarded as flotation collectors) so as to show whether or not a thiol is converted to dithiolate at the surface of a particular mineral.

Table 17: Rest potentials of minerals in 100 ppm thiol solutions at 25°C (Finkelstein and Poling, 1977).

	DTP	DTC	MBT
Reduction potential (volts), 100 ppm soln.	0.448	0.081	0.144
Rest potential (volts) of 100 ppm soln. with			
Pyrite	+0.545	+0.475	+0.380
Pyrrhotite	+0.350	+0.130	+0.205
Arsenopyrite	+0.259	+0.145	+0.145
Galena	+0.238	-0.035	+0.060
Molybdenite	+0.355	+0.045	+0.085
Covellite	+0.290	+0.115	+0.165
Chalcopyrite	+0.251	+0.095	+0.095
Chalcocite	+0.225	-0.155	+0.195
Bornite	+0.085	-0.045	+0.035
Sphalerite	-0.015	-0.035	+0.039
Stibnite	-0.115	-0.155	-0.025
Antimonite	-0.215	-0.215	-0.035
Orpiment	+0.161	-0.270	-0.160
Realgar	+0.169	-0.220	-0.145

The rest potential of a mineral is regarded an indicator of whether or not dithiolate is formed on the mineral surface under particular conditions. The reduction potential represents the equilibrium potential at which the conversion of thiol to dithiolate is expected. In the presence of three different collectors, the most cathodic mineral (i.e. pyrite) is regarded as a better substrate for dithiolate formation. This is because pyrite does not readily oxidise and form hydrophilic oxides on the surface which hinders collector-mineral interaction.

When a galvanic couple is formed, the compound with a more negative potential is an anode and the compound with a more positive potential is a cathode. Particles in pulp must be long enough in contact for charge transfer to take place. In the presence of xanthate, oxidation of xanthate to dixanthogen is expected to take place on the anode, and oxygen reduction on the cathode.

Understanding the behaviour of pyrrhotite is of importance due to its association with other sulfides during its recovery, especially its association with pentlandite. Pentlandite usually occurs as exsolved flames or blebs in pyrrhotite. These flames are usually small (<50 µm)

and are most likely to remain locked in pyrrhotite, unless ultra-fine grinding is incorporated into the flotation circuit (Becker, 2006). This will have an impact on the recovery of PGMs.

Pyrrhotite-pyrite system

In terms of the pyrrhotite-pyrite interaction, pyrrhotite recovery is improved during flotation. This has been attributed to a shift of oxygen reduction from sites on pyrrhotite to pyrite; this reduces iron hydroxide formation on pyrrhotite and promotes its flotation (Nakazawa and Iwasaki, 1985). Floatability of pyrrhotite is improved because, in the presence of xanthate, oxidation of xanthate (i.e. dixanthogen formation) is favoured on pyrrhotite, rendering pyrrhotite hydrophobic. As shown in *Table 16*, oxidation of xanthate is expected to occur on pyrrhotite and oxygen reduction on pyrite.

Pyrrhotite-chalcopyrite system

With respect to pyrrhotite-chalcopyrite association, chalcopyrite was reported to speed up the oxidation reaction of xanthate on pyrrhotite (i.e. effective collector adsorption), which enhances pyrrhotite floatability. This is due to the cathodic and anodic actions of both chalcopyrite and pyrrhotite, respectively. A lower floatability of chalcopyrite was observed and was attributable to either the formation of iron hydroxide on its surface or the shift of xanthate adsorption to pyrrhotite (Cheng and Iwasaki, 1992).

Pyrrhotite-pentlandite system in nickel ores

Nickel has been extracted from pentlandite in ores containing both pentlandite and pyrrhotite. In earlier years, pyrrhotite rejection was not considered important. It was considered to be beneficial to recover pyrrhotite as it contains nickel in solid solution, which improves nickel recovery. However, as mentioned earlier, it was found during smelting that large quantities of sulfur dioxide are produced by pyrrhotite with little nickel. As a result, it was decided that most of the pyrrhotite had to be rejected in order to reduce the SO_2 emissions and obtain high grade nickel concentrates.

No cost effective procedure resulting in high pentlandite recoveries and sufficient selective rejection of pyrrhotite was found, as some of the tested procedures were too difficult or expensive to implement.

To address the problem of separating pyrrhotite from pentlandite, Senior *et al.* (1994) investigated the floatability of pentlandite and pyrrhotite and examined aspects of the behaviour of these sulfides that might be used to improve their separation. Khan and Kelebek (2004) used sodium *n*-butyl xanthate (1 x 10^{-4} M) to investigate the flotation selectivity between pyrrhotite and pentlandite at pH 9.0 to 9.5 under potential control. The results are presented in *Figure 8*. The samples employed in these tests originated from process streams consisting mainly of pyrrhotite-pentlandite middlings processed in the Ni-Cu plant in the Sudbury region of Canada.

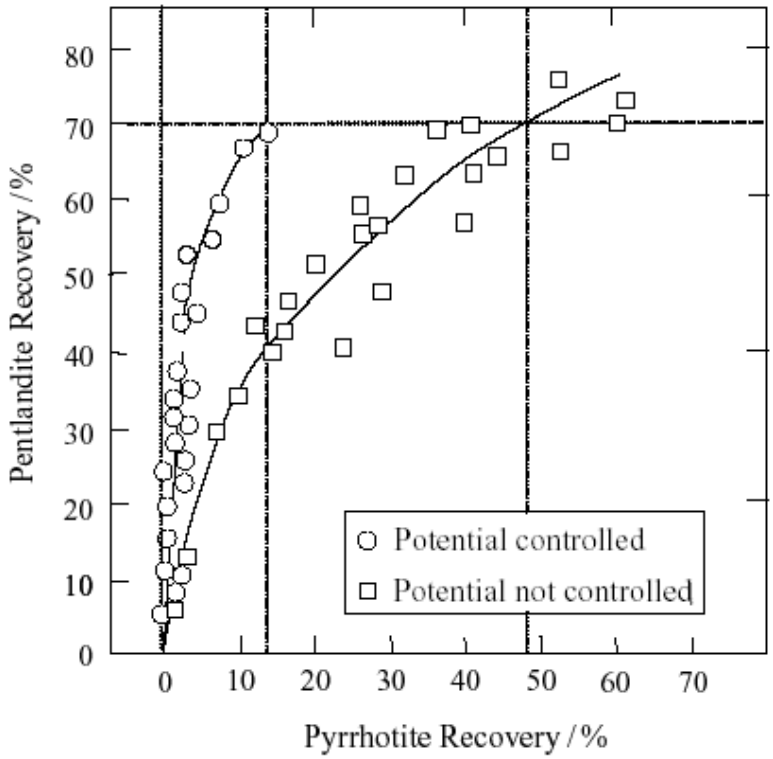

Figure 8: Flotation selectivity between pentlandite and pyrrhotite at pH 9.0 to 9.5; potential controlled: -0.095 to -0.005 V (SHE), potential uncontrolled: 0.25-0.30 V (SHE); sodium *n*-butyl xanthate (1 x 10^{-4} mol/l) (Khan and Kelebek, 2004).

It is evident in *Figure 8* that much better selectivity of pentlandite from pyrrhotite was observed under potential control. With uncontrolled potential, less flotation selectivity was observed. These results suggest that pyrrhotite flotation in the system studied is favoured at a relatively high potential (open to air during conditioning). In support of these findings, cyclic voltammetric studies by Hodgson and Agar (1989) showed that aeration is required at low potentials [i.e. -0.005 to -0.055 V (SHE)] to induce hydrophobicity on pyrrhotite after xanthate was added. This result implies that dixanthogen, formed by the oxidation of xanthate, is necessary to render pyrrhotite hydrophobic. In support of this finding, various authors (Finkelstein and Poling, 1985; Fornasiero *et al.*, 1995; Yuehua *et al.*, 2005) found dixanthogen to be the principal product on pyrrhotite. In similar cyclic voltammetric studies of pentlandite, Hodgson and Agar (1989) showed a distinct anodic reaction attributable to xanthate chemisorption at -0.055 V (SHE) and peaking at -0.095 V (SHE) in the pH range 6–10; the position of this peak was independent of pH. The anodic peak was attributed to the formation of nickel xanthate, where the collector directly chemisorbed onto the nickel site according to the following reaction:

$$Ni + X^- = NiX + e^- \qquad \textbf{\textit{Eq. 6}}$$

The reaction indicates that pentlandite hydrophobicity is induced at lower (i.e. more cathodic) potentials than pyrrhotite and that dixanthogen is not required to induce hydrophobicity. However, aeration was found to promote hydrophobicity on pentlandite by the oxidation of xanthate to dixanthogen, according to the reaction:

$$NiX + X^- = Ni(X_2) = NiX_2 + e^- \qquad \textbf{\textit{Eq. 7}}$$

Pyrrhotite-pentlandite-quartz system

When milling these three minerals together at pH 9, it was found that pyrrhotite floatability increased and resulted in some loss of selectivity. Recovery-size results showed that the presence of pentlandite improved the intermediate and coarse pyrrhotite particles' floatability, however the presence of pyrrhotite resulted in the depression of coarse pentlandite particles. Overall, there was little change as a result of mixing these minerals (Senior *et al.*, 1994).

Overall, the recovery of intermediate sized pentlandite particles was similar when collector or copper sulfate was added. Almost complete recovery of these particles is likely in any separation of pentlandite from pyrrhotite.

The major findings from the work of Senior *et al.* (1994) that are of interest, in terms of separating pentlandite from pyrrhotite, are that:

- Pentlandite can be floated selectively from pyrrhotite, provided the pH of the pulp is adjusted to about 9 and the collector addition is maintained at a moderate level.
- There seems little prospect of separating pentlandite from pyrrhotite by controlling the pulp potential of flotation at pH 7 or by exploiting the self-induced floatability of these minerals.

In contrast to these results, Hodgson and Agar (1989) and Khan and Kelebek (2004) showed that: pulp potential control is necessary to improve the selective separation between pentlandite and pyrrhotite; adjusting the pH to 9 and maintaining a moderate collector level will not improve selectivity. The potential and pH ranges used by Senior *et al.* (1994) and Khan and Kelebek (2004) are different and these affect the oxygen reduction kinetics on pyrrhotite and pentlandite as they behave differently under different pulp conditions.

In the study done by Bozkurt *et al.* (1998), when pentlandite shared the same solution with pyrrhotite, dixanthogen formation on pentlandite was promoted, whereas the opposite occurred for pyrrhotite. This result was more pronounced when the minerals were in direct contact.

This is in contrast to the behaviour of pyrrhotite-pyrite and pyrrhotite-chalcopyrite systems. According to Rand (1977), pentlandite has a higher mixed potential than pyrrhotite, suggesting that it is a better surface for oxygen reduction. In the presence of xanthate, the anodic reaction involves the oxidation of xanthate to dixanthogen, which renders the mineral hydrophobic. Dixanthogen formation should be favoured on pyrrhotite, therefore improving its recovery. However, according to Bozkurt *et al.* (1998), the order was reversed in the presence of xanthate, making pyrrhotite a better surface for oxygen reduction and favouring the oxidation of xanthate on pentlandite. This could be due to different pyrrhotite samples obtained from different locations having different chemical compositions.

Pyrrhotite-nickel arsenide system

Nickel arsenide, which has a lower open circuit potential than pyrrhotite, acted as an anode. In the presence of pyrrhotite, nickel and arsenic concentrations were found to be higher than in the absence of pyrrhotite. Pyrrhotite floatability was decreased due to the formation of iron hydroxide on its surface (Nakazawa and Iwasaki, 1986).

Pyrrhotite-grinding media

There has been considerable interest regarding the role of galvanic interactions between sulfide minerals and the milling media, and in complex sulfide ores between the various minerals themselves (Adam *et al.,* 1984; Rao and Finch, 1988; Ahn and Gebhardt, 1991). The grade of the sulfide minerals and degree of liberation has a major effect on the relevance of galvanic interactions. In platinum-group mineral (PGM) bearing sulfide ores from the Bushveld Igneous Complex, the combined sulfide grade is typically less than one percent by volume. With such ores, it is unlikely that sufficient physical contact could occur between fully liberated individual particles. Using QEM*SEM (quantitative evaluation of mineral composition by scanning electron microscopy) analysis, Buswell *et al.* (1988) indicated that with these PGM ores there is a high degree of liberation at current grinding levels. There may be galvanic interaction between the milling media and the sulfide minerals in the ore.

The most obvious difference between the milling media is the nature of the milling media in terms of its propensity for corrosion and abrasion (Ahn and Gebhardt, 1991). For example, mild steel is more reactive than stainless steel; it will tend to impart a reducing environment on the pulp through the depletion of oxygen, which is due to the iron/ferrous/ferric couples that will be set up in the solutions. Abraded fine particles may coat sulfide particles, particularly magnetic minerals such as pyrrhotite, making galvanic coupling an important consideration (Iwasaki, 1988).

2.2.3. Reactivities

2.2.3.1. Oxidation of pyrrhotite and oxidation products

Oxygen is the ultimate oxidant of sulfide minerals in natural surface waters and the direct oxidant at pH > 4, while ferric iron oxidises sulfides at pH < 4 (Nordstrom and Alpers, 1999). These two oxidants are the most important for pyrrhotite (Lowson, 1982; Bierens de Haan, 1991; Belzile *et al.,* 1997a). According to Nicholson and Scharer (1994), when O_2 is the primary oxidant, the oxidation reaction proceeds as follows:

$$Fe_{1-x}S + (2-0.5x)O_2 + xH_2O \Rightarrow (1-x)Fe^{2+} + SO_4^{2-} + 2xH^+ \qquad \textbf{\textit{Eq. 8}}$$

If pH is not too low, the oxidation of ferrous iron produces ferric ions that can precipitate out of the solution to form ferric hydroxide.

Fe^{2+} is oxidised and precipitated as ferric oxyhydroxides, mainly ferrihydrite and goethite, as follows:

$$Fe^{2+} + 1/4O_2 + 2H^+ \Rightarrow Fe^{3+} + 1/2H_2O \qquad \textbf{\textit{Eq. 9}}$$

$$Fe^{3+} + 3H_2O \Rightarrow Fe(OH)_{3(s)} + 3H^+ \qquad \textbf{\textit{Eq. 10}}$$

Ferric iron can, in turn, oxidise more pyrrhotite and generate more acidity in the system, according to the following reaction:

$$Fe_{1-x}S + (8-2x)\ Fe^{3+} + 4H_2O \Rightarrow (9-3x)Fe^{2+} + SO_4^{2-} + 8H^+ \qquad \textbf{\textit{Eq. 11}}$$

If *reaction 9* occurs under acidic conditions, a significant quantity of Fe^{3+} will remain in the solution and maintain a cyclic reaction with *reaction 11*, where ferric iron is the oxidant.
Authors Steger (1982), Jambor (1986) and Ahonen and Tuovinen (1994), observed (from field and laboratory studies) that the oxidation may not be complete and instead generates sulfur according to the following acid-consuming reaction:

$$Fe_{1-x}S + 1/2(1-x)O_2 + 2(1-x)H^+ \Rightarrow (1-x)Fe^{2+} + S^0 + (1-x)\,H_2O \qquad \textbf{\textit{Eq. 12}}$$

$$Fe_{1-x}S + (2-2x)\,Fe^{3+} \Rightarrow (3-3x)Fe^{2+} + S^0 \qquad \textbf{\textit{Eq. 13}}$$

Major oxidation products of pyrrhotite are goethite and elemental sulfur (which are in agreement with *reactions 10, 12* and *13)* as well as smaller amounts of ferric sulfate and various sulfooxyanions (Steger and Desjardins, 1978).

According to Hamilton and Woods (1981), pyrrhotite oxidises to both sulfur and sulfate, with the former being the major product of the pyrrhotite oxidation reaction. Pyrrhotite oxidation is strongly inhibited by the iron oxide produced on the surface in alkaline solution.

Using XPS, Buckley and Woods (1985a) showed that exposure of pyrrhotite to air leads to the consecutive formation of iron (II) oxide, an iron (III) hydroxy-oxide or hydrated iron (III) oxide.

The presence of elemental sulfur, together with sulfate and iron-deficient sulfide, were detected by Buckley and Woods (1985b) when a hydrogen peroxide solution was used as an oxidant. They proposed that the oxidation of pyrrhotite proceeds via a series of iron deficient sulfides (and possibly polysulfides) through to elemental sulfur - these steps being acid-consuming.

Metastable intermediates of sulfate, including thiosulfate (Steger and Desjardins, 1977; Steger and Desjardins, 1978), polythionate and $S_4O_6^{2-}$ are also reported (Plysunin *et al.*, 1990; Mikhlin *et al.*, 2002); the presence of these intermediates is likely to be related to oxidation conditions.

2.2.3.2. Factors affecting oxidation

Reactions 8 to *13* suggest that several factors affect and determine the rate of pyrrhotite oxidation. Some of the factors that can play a determining role in the nature of the oxidation products are presented below.

2.2.3.2.1. Crystal Structure

Pratt *et al.* (1996) reported that the modification of mineral structures due to the pressures and stresses associated with the milling of ore can increase the reactivity of pyrrhotite in mine tailings as well as its susceptibility to oxidation processes. In comparison to pyrite, the 20-100 times faster oxidation rate of pyrrhotite can also be related to lower crystal symmetry, which is due to the vacancy of iron atoms in the crystal structure (Nicholson and Scharer, 1994). Despite the suggestion by Yakhontova *et al.* (1983) and Orlova *et al.* (1989) that the crystal structure of pyrrhotite can affect its oxidation rate, Janzen *et al.* (2000) reported no apparent correlation between pyrrhotite oxidation by oxygen or ferric iron and crystal structure.

2.2.3.2.2. Oxygen and moisture

Reaction 8 shows the required presence of water when pyrrhotite is oxidised by oxygen (air). Steger (1982) reported a direct increase in the oxidation rate with increasing relative humidity. Using XPS, Knipe *et al.* (1995) confirmed that oxygen is the primary oxidant: no evidence of oxidation could be shown when pyrrhotite was exposed to de-oxygenated water. There are no systematic studies relating the effect of oxygen content to pyrrhotite oxidation, but the oxidation rate is expected to be related to the concentration or partial pressure of O_2.

2.2.3.2.3. Ferric iron

Oxidation rates are significantly increased by the presence of Fe^{3+} (Janzen, 1996; Janzen *et al.*, 2000). The pyrrhotite oxidation rate by ferric iron varies with the presence and absence of oxygen, ranging from zero order for de-oxygenated to half order under oxygen-saturated conditions (Kwong, 1995).

2.2.3.2.4. pH

The influence of pH on oxidation of pyrrhotite by ferric iron shows inconsistent results and suggests a competing effect of the proton with Fe^{3+} and possibly Fe^{2+} for adsorption sites on the surface (Janzen, 1996).

2.2.3.2.5. Temperature

Temperature has been reported to have a more significant effect than pH, with the reaction rate: doubling between 25 and 35 °C (Kwong, 1995); increasing by 3 to 5 times for a 20°C increase with oxygen as oxidant and by 2 to 11 times for a 30 °C increase with ferric iron as the oxidant (Janzen, 1996). In both studies, the oxidation process follows Arrhenius behaviour. In a study done by Majima and Peters (1996) on the oxidation of sulfide minerals, at a high temperature of 120 °C and high oxygen pressure of 855 kPa, pyrrhotite was observed to oxidise much more rapidly (at pH 2.7) than all the other sulfides. The same study showed that the oxidation of pyrrhotite is significantly reduced at neutral and alkaline pH values.

2.2.3.2.6. Trace Metal Element

Kwong (1995) and Janzen *et al.* (2000) noticed a trend of decreasing reaction rates with increasing trace metal content, but no statistically significant effect on the oxidation rate could be established for individual trace metals (Co, Cu, Mn, Ni) or total trace metal content. Belzile *et al.* (2004) reported that more research needs to be done to clarify the effect of trace metals on pyrrhotite oxidation. This also forms part of the focus of this study.

Information on the oxidation mechanism has been obtained using X-ray techniques such as: X-ray photoelectron spectroscopy (XPS); Auger electron spectroscopy (AES) X-ray powder diffraction (XRD); Mössbauer spectroscopy and secondary electron microscopy (SEM).

Taking into account the variable nature of pyrrhotite compounds and the various experimental designs, it was not surprising to find variable results for oxidation rates and products. In recent years, the combination of X-ray (e.g. XRD) and spectroscopic (e.g. XPS, FTIR) techniques has been particularly useful in improving understanding of the oxidation mechanism at the molecular level and the chemical bonds formed at the surface of oxidised pyrrhotite. More systematic studies are required to better understand and control the oxidation of this reactive mineral so as to improve both mineral extraction and environmental protection (Belzile *et al.*, 2004).

2.2.3.3. Oxygen reduction activity

Oxygen reduction on the mineral surface is an important step in xanthate adsorption. Rand (1977) studied the cathodic reduction of oxygen at rotated electrodes of the sulfide minerals, namely: arsenopyrite (FeAsS), bornite (Cu_5FeS_4), chalcocite (Cu_2S), chalcopyrite ($CuFeS_2$), covellite (CuS), galena (PbS), pentlandite ($(Fe,Ni)_9S_8$), pyrite (FeS_2) and pyrrhotite ($Fe_{1-x}S$) in both acid and alkaline solutions. *Figure 9* shows a comparison of the oxidation reduction activities of mineral sulfides with those of platinum and gold by plotting current densities obtained at various potentials in the Tafel region of each electrode.

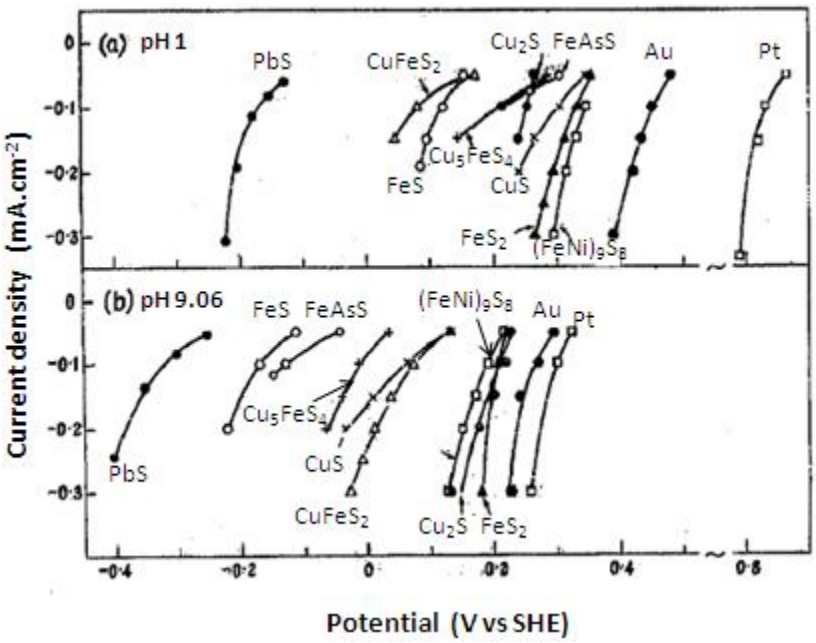

Figure 9: Activation-controlled currents at the foot of the O_2 reduction wave on various sulfide minerals and noble metal electrodes in O_2-saturated (A) 0.1 M $HClO_4$ and (B) 0.05 M $Na_2B_4O_7$ (Rand, 1977).

It is evident from *Figure 9* that pyrite is the best catalyst for oxygen reduction among the sulfide minerals and that its oxygen reduction activity is closer to that of gold when compared to other sulfide minerals. In *Figure 9*, the order of oxygen reduction activity at pH 9.06 decreased in the order pyrite > chalcopyrite > arsenopyrite > pyrrhotite > galena. These results correlate well with the findings by Plaskin and Bessonov (1957), who showed that, in a neutral solution, the oxygen requirement increased in the order: galena < pyrite <

chalcopyrite < pyrrhotite < arsenopyrite. However, galena behaved differently to the others: it was the poorest catalyst, yet required the least amount of oxygen for flotation.

Rand (1977) suggested that this might be due to the difference in nature of the hydrophobic surface of galena compared to that of other sulfide minerals. In the galena-xanthate(X^-) system, the thiolate produced under typical flotation conditions would be PbX_2, with the concomitant formation of either elemental sulfur (Buckley *et al.*, 2003):

$$PbS + 2X^- \rightarrow Pb(X_2) + S + 2e^- \qquad \textbf{\textit{Eq. 14}}$$

or a metal-deficient lead sulfide:

$$PbS + 2yX^- \rightarrow yPbX_2 + Pb_{1-y}S + 2ye^- \qquad \textbf{\textit{Eq. 15}}$$

Reaction 15 would be favoured in the initial stages at low rates, with *reaction 14* occurring when the composition of the sulfidic product phase has a sulfur content above the stable, or metastable, stoichiometry range (Buckley *et al.*, 2003).

Buckley and Woods (1997) showed that significant flotation of galena occurs at solution potentials at which surface coverage by collector is low, i.e.: 50 % recovery at a surface coverage of < 0.2 and 0 V (SHE); 90 % recovery corresponding to about 0.5 coverage and 0.1 V (SHE). Chemisorption of xanthate results in the formation of a Pb-X in the first layer of adsorbate and in multi-layers of co-adsorbed dixanthogen if this species is present in sufficient excess relative to the available surface area of galena. While it is generally accepted that the co-adsorption of lead xanthate and dixanthogen increases the degree of hydrophobicity, Buckley and Woods (1997) reported galena to acquire enough hydrophobicity to cause flotation, even by chemisorbed xanthate alone.

On the anodic portion of the galena cyclic voltammograms, there is a “pre-wave”, indicating the chemisorption of xanthate; on other sulfide minerals (such as pyrite, pyrrhotite, chalcopyrite) there is no “pre-wave”, indicating that chemisorption takes place at the same potential as where xanthate is oxidised (Buckley and Woods, 1997). On the other hand, Hodgson and Agar (1989) reported a “pre-wave” in the case of pentlandite, indicating the chemisorption of xant4hate; however, Khan and Kelebek (2004) did not observe any “pre-

wave" on the pentlandite cyclic voltammograms. The differences could be attributed to the differences in the sample location, chemical compositions and impurities present on the surfaces. Pentlandite samples used in the studies by Hodgson and Agar (1989) and Khan and Kelebek (2004) were sourced from Sudbury, Ontario Division and Manitoba mining region of Canada, respectively. Chemical compositions and impurities were not provided.

With pyrite, chalcopyrite, pyrrhotite and arsenopyrite, the order for oxygen requirement in flotation resembles that for their oxygen activity, with only pyrrhotite and arsenopyrite being reversed. Rand (1977) also mentioned that a comparison of flotation data with electrochemical measurements suggested that differences in the rate of flotation (i.e. xanthate formation) are determined by differences in activity with oxygen reduction.

2.2.4. Electrochemistry

Electrochemical potential is considered an important parameter for controlling the recovery and selectivity of sulfide minerals during flotation (Buswell *et al.*, 2002).

The adsorption of xanthate collectors onto sulfide minerals, such as chalcopyrite, pentlandite, pyrrhotite and pyrite occur via an electrochemical mechanism that involves the anodic oxidation of xanthate coupled to the reduction of oxygen (Woods, 1984). Dixanthogen is the hydrophobic species formed on all three minerals, i.e. chalcopyrite, pentlandite and pyrrhotite (Allison *et al.*, 1972; Persson, 1993). The mineral/solution interface potential is known to be the controlling factor for this electrochemical mechanism.

Oxidation constitutes a central part of the electrochemical reactivity of sulfide minerals in flotation systems. Oxidation products on sulfide minerals include hydroxides, oxides, oxy-sulfides and poly-sulfides (Hamilton and Woods, 1981; Hodgson and Agar, 1989; Khan and Kelebek, 2004). A sulfur-rich surface covered with ferric hydroxide was considered to be the oxidation product of pyrrhotite in alkaline media (Hamilton and Woods, 1981; Hodgson and Agar, 1989). It was difficult to identify the exact form of sulfur on the surface of the oxidised mineral. However, in acidic conditions, the formation of sulfate is less favoured than in alkaline conditions; the result is that surfaces are likely to become more sulfur-rich under acidic conditions (Buswell and Nicol, 2002). Although reports by various researchers state

that a certain degree of oxidation is necessary for xanthate adsorption, it is clear that heavily oxidised particles are not readily floated due to the hydrophilic nature of the iron oxide surfaces (Buswell and Nicol, 2002; Rao, 2004).

Many researchers (Hamilton and Woods, 1981; Bozkurt *et al.*, 1998; Cheng *et al.*, 1999; Buswell and Nicol, 2002) have used electrochemical methods, as they provide useful information on the oxidising/reducing characteristics of sulfide minerals (Khan and Kelebek, 2004). A discussion of results obtained by various researchers on electrochemical measurements, oxidation of pyrrhotite, xanthate adsorption and the effect of galvanic interactions on the recovery of pyrrhotite follows.

Using cyclic voltammetry and rest potential measurements, Khan and Kelebek (2004) investigated the electrochemical characteristics of pyrrhotite and pentlandite and their interaction with the xanthate in the presence and absence of dissolved oxygen. The sample was sourced from the Sudbury mining region of Canada.

Buswell and Nicol's (2002) study was aimed at developing an understanding of the flotation of pyrrhotite by using electrochemical techniques to investigate surface compositions and reactions. Buswell and Nicol (2002) studied the reactions of dissolved copper sulfate and sodium isobutyl xanthate with the mineral because of their specific industrial use in the platinum industry for the flotation of sulfides. The massive samples were sourced from Ward's Natural Science and from the South African Mineral Dealer. X-ray diffraction analysis showed the presence of peaks in the pyrrhotite sourced from South Africa, which could only be attributed to hexagonal pyrrhotite.

2.2.4.1. Rest potentials and galvanic interactions

The standard equilibrium potential for xanthate/dixanthogen couple was calculated by Buswell and Nicol (2002) as -0.128 V (SHE) from their data using the Nernst equation, which is similar to the one obtained by Winter and Woods (1973) and Buswell *et al.* (2002).

Khan and Kelebek (2004) carried out rest potential measurements under similar conditions to the voltammetric studies. The rest potential variation of pyrrhotite under various conditions as a function of time is presented in *Figure 10.*

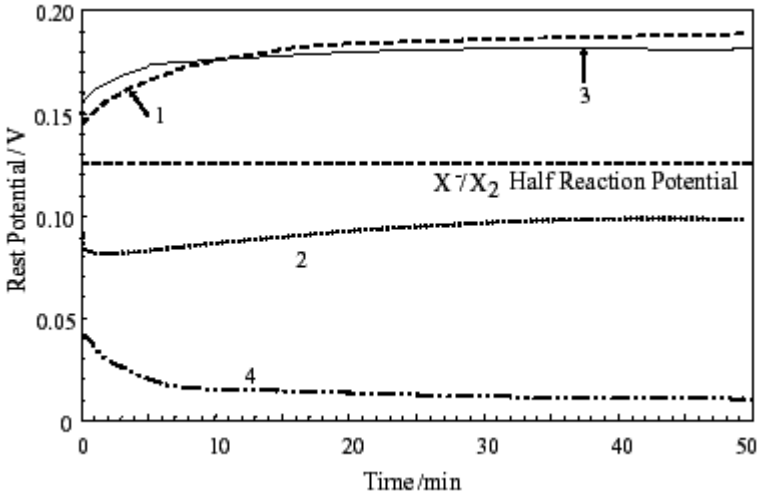

Figure 10: Rest potential variation of pyrrhotite electrode under various conditions (pH 9.2). (Numbers indicate concentrations of dissolved oxygen (DO) and sodium n-butyl xanthate (X): (1) DO = 8.15 mg/l, X = 0 mol/m^3; (2) DO = 0.1 mg/l, X = 0 mol/m^3; (3) DO = 8.15 mg/l, X = 0.1 mol/m^3; (4) DO = 0.1 mg/l, X = 0.1 mol/m^3; V/SHE) (Khan and Kelebek, 2004).

Pyrrhotite exhibits the same rest potential profile in the presence and absence of xanthate under oxygen-saturated conditions (curves 1 and 3 in *Figure 10*), the only significant difference being the magnitude of the potential change. The straight line represents the equilibrium potential for the transformation of xanthate to dixanthogen, which is around 0.125 V (SHE) for *n*-butyl xanthate under the experimental conditions used (10^{-4} M xanthate). This value falls within the range at which the development of appreciable hydrophobicity on pyrrhotite surfaces was observed by Yoon *et al.* (1995). The standard equilibrium potential for a xanthate/dixanthogen couple was reported as being -0.128 V (SHE); correcting for a concentration of xanthate of 10^{-4} M, this resulted in an equilibrium potential of 0.108 V (SHE) (Winter and Woods, 1973). When the electrolyte has a low dissolved oxygen concentration, the rest potential of pyrrhotite in the presence of xanthate is significantly below the potential required for X^-/X_2 transformation. This indicates that the formation of dixanthogen is not possible under oxygen-deficient conditions. When there is a

negligible amount of oxygen in the solution, the xanthate-dixanthogen reaction is not supported since pyrrhotite, as reported by Rand (1977), is a poor catalyst for oxygen reduction.

Bozkurt *et al.* (1998) used the rest potential technique and proposed the formation of dixanthogen on pentlandite and retardation of its formation on pyrrhotite in a mixed mineral system. Open circuit measurement results obtained by Bozkurt *et al.* (1998) are shown in *Figure 11*.

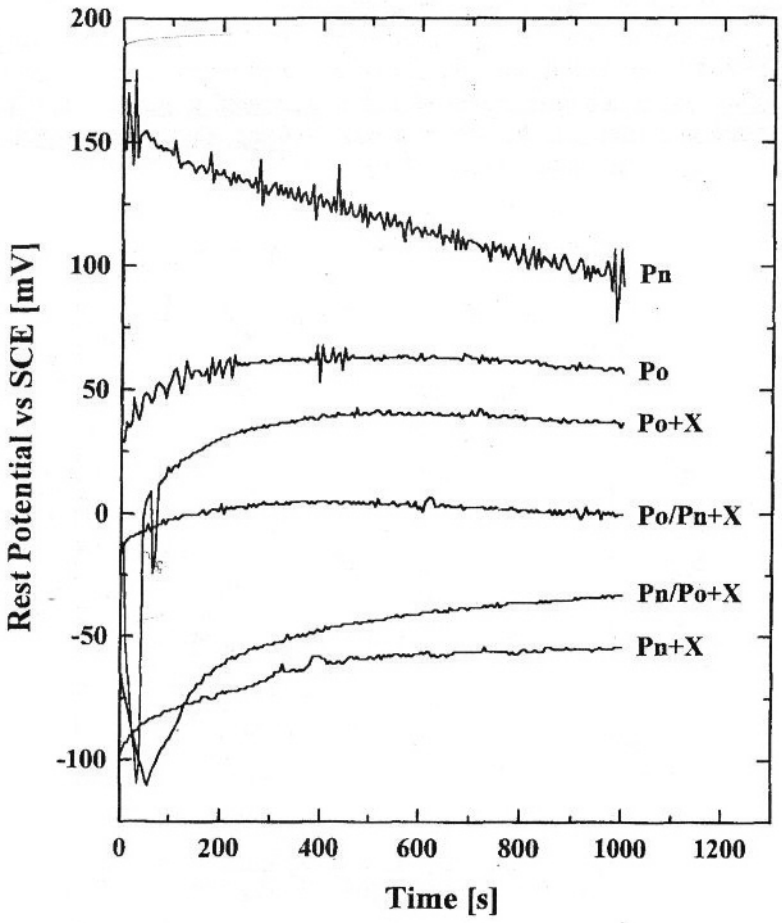

Figure 11: Open circuit potentials of: pentlandite in contact with pentlandite powder (Pn) and in the presence of xanthate (Pn + X); pyrrhotite in contact with pyrrhotite powder (Po) and in the presence of xanthate (Po + X); pentlandite in contact with pyrrhotite powder in the presence of xanthate (Pn/Po + X); pyrrhotite in contact with pentlandite powder in the presence of xanthate (Po/Pn + X). Xanthate concentration in each case is $2x10^{-3}$ M (Bozkurt *et al.*, 1998).

It is evident that the potential changed with time for all cases of pyrrhotite that reached a constant (equilibrium) value after about 10 minutes. The rest potential of pure pentlandite alone continued decreasing and did not stabilise after 10 minutes. With regards to pentlandite in contact with pyrrhotite powder in the presence of xanthate: the rest potential seemed to continue to increase after ten minutes. For both minerals: in the presence of xanthate, the equilibrium potentials are reduced, since xanthate acts as a reducing agent in these systems (Woods, 1976). This reduction in potential is greater for pentlandite than for pyrrhotite, indicating that xanthate uptake is preferential on pentlandite, as confirmed by the spectroscopic studies (which will be discussed later). In contrast, at a higher dissolved oxygen concentration, Khan and Kelebek (2004) did not observe a similar reducing action of xanthate on the rest potentials of both pyrrhotite and pentlandite. The rest potential of pyrrhotite only dropped by about 0.008 V (SHE); for pentlandite there was no reduction in the rest potential.

In the study done by Khan and Kelebek (2004), pentlandite exhibited higher rest potentials than did pyrrhotite under all conditions studied. Ruonala *et al.* (1997) studied the influence of a grinding medium (iron vs non-iron [Al_2O_3] balls) on the rest potentials of pentlandite and pyrrhotite electrodes during grinding and flotation tests, as well as during separate flotation tests using air as a process gas. Pentlandite showed a higher rest potential than pyrrhotite. According to a number of authors, pentlandite has a higher rest potential than pyrrhotite (McIntosh and Groat, 1997; Lu *et al.*, 2000; Mason and Rice, 2002; Cruz *et al.*, 2005; Santos *et al.*, 2006; Lin-lin *et al.*, 2009). These authors reported that as pentlandite usually has high rest potentials, while pyrrhotite shows lower values, in those ores where there is an electronic contact between both minerals, the rest potential indicates that pyrrhotite dissolves faster than pentlandite, given a certain set of conditions. While pyrrhotite grains are being oxidised, any pentlandite in electrical contact with them would be galvanically protected due to its higher open circuit potential. Thus, pyrrhotite oxidation will preferentially provide electrons for the reduction of the oxidant, i.e. any reduction reaction occurring on the surface of pentlandite would consume electrons produced by pyrrhotite dissolution (McIntosh and Groat, 1997; Lu *et al.*, 2000; Mason and Rice, 2002; Cruz *et al.*, 2005; Santos *et al.*, 2006; Lin-lin *et al.*, 2009). As pentlandite has a large oxidation potential, it would be necessary to have high potentials in the leaching system for its complete dissolution (Santos *et al.*, 2006). This suggests that when pentlandite is in contact with pyrrhotite, the mixed potential is oxidising

to pyrrhotite and reducing to pentlandite. Thus, in the flotation system, higher potentials are required to oxidise pentlandite.

Bozkurt *et al.* (1998) reported a lower rest potential for pentlandite in the presence of xanthate than for pyrrhotite. This was not expected, since pentlandite is more noble than pyrrhotite and would, therefore, be expected to have a higher rest potential. Rand (1977) summarised the oxygen reduction rates and corresponding potentials at pH 1 and 9.06 for various minerals (*Figure 9*). At pH 9.06 and cathodic current densities of -0.05 and -0.2 mA/cm^2, pyrrhotite had corresponding reduction potentials of -0.11 and -0.22 V (SHE), whilst for pentlandite it was 0.2 and 0.15 V (SHE). The reduction curves of pyrrhotite and pentlandite are far apart and distinct, indicating the large differences in the rest potentials of these sulfide minerals. Thus, the possibility of pyrrhotite having a higher rest potential than pentlandite is ruled out.

Pentlandite in contact with pyrrhotite powder in the presence of xanthate showed a higher rest potential than pentlandite with xanthate alone; which was not expected. Furthermore, pyrrhotite in contact with pentlandite powder in the presence of xanthate, showed a rest potential lower than that of pyrrhotite in the presence of xanthate alone, which is also in contrast to what was expected. Bozkurt *et al.* (1998) have not shown any repeats in the rest potential measurements and the fact that the rest potentials have not stabilised makes it difficult to compare these results with the results of other authors.

The preferred formation of dixanthogen on pentlandite, rather than on pyrrhotite, in the study done by Bozkurt *et al.* (1998), using the mixed potential model, was based on the rest potential measurements results of single minerals (i.e. pyrrhotite and pentlandite) in the presence of xanthate; these are not in agreement with what was expected, as shown in *Figure 12*.

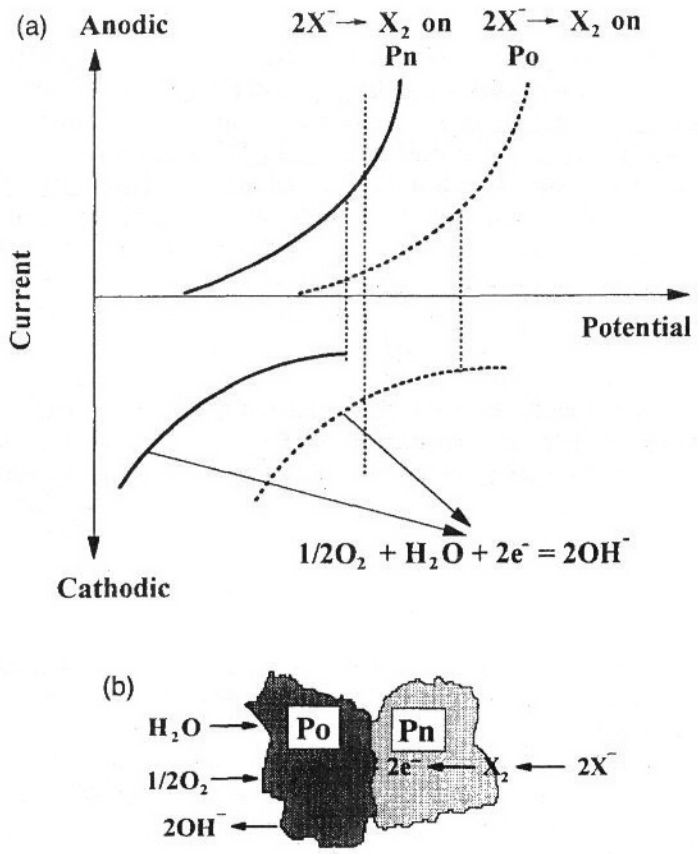

Figure 12: (a) Schematically constructed current (I) vs potential (V) diagram using open circuit potentials. (b) Schematic representation of galvanic interaction between pentlandite and pyrrhotite in the presence of xanthate (Bozkurt *et al.*, 1998).

A mixed potential model presented in *Figure 13* is used to help interpret the observations by other authors (Hodgson and Agar, 1989; Senior *et al.*, 1994; Khan and Kelebek, 2004) *Figure 13* illustrates that whether a system is oxidising or reducing depends on the redox couple being considered: for couple 1, the system is oxidising; for couple 2, the system is reducing. It is also shown that an equivalent way of looking at the system is to consider an average anodic current (i.e. the average of the two anodic currents) and an average cathodic current with the measured potential being when these two are equal. Mixed potentials arise whenever there is more than one redox couple in the system. *Figure 13* is an example of the two redox couples: the potential measured now is that when the anodic current of redox couple 1 equals the cathodic current of redox couple 2 (Rao, 2004).

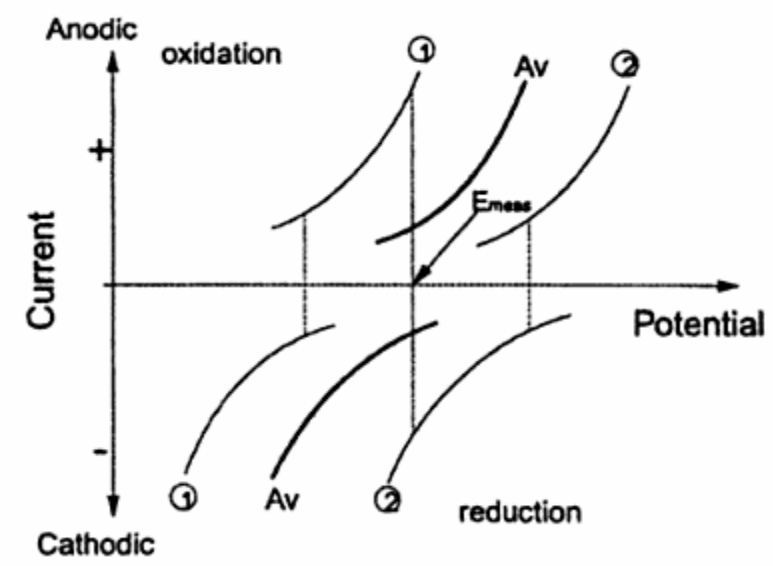

Figure 13: Mixed potential concept of anodic and cathodic currents extended to system with two redox couples. Potential measured (Emeas) occurs when anodic current 1 equals cathodic current 2, or when the average (Av) of anodic currents 1 and 2 equals the average (Av) of cathodic currents 1 and 2 (Rao, 2004).

In this discussion, couple 1 and couple 2 refer to oxidation-reduction reactions on pyrrhotite and pentlandite, respectively, since pyrrhotite has a lower rest potential than pentlandite in the presence of xanthate, as shown by Rand (1977), Ruonala *et al.* (1997), and Khan and Kelebek (2004). The anodic reaction is the oxidation of xanthate to dixanthogen and the cathodic reaction is the reduction of oxygen. When the minerals are in direct contact, the system exhibits a mixed potential E_{meas} somewhere between the two individual potentials. This again represents an equivalence of anodic and cathodic currents, but now the anodic reaction is $2X^- \rightarrow X_2$ on pyrrhotite and the cathodic reaction is oxygen reduction on pentlandite.

According to Rand (1977) and the mixed potential theory, when looking at the rest potential results of Bozkurt *et al.* (1998): pyrrhotite powder is supposed to reduce the rest potential of pentlandite in contact with pyrrhotite powder in the presence of xanthate; and pentlandite powder is supposed to increase the rest potential of pyrrhotite in contact with pentlandite powder in the presence of xanthate. This is expected to happen because when galvanic interactions are present, the galvanic potential is in between the individual potentials of pyrrhotite and pentlandite (which is more noble); this results in an increase in the potential on

pyrrhotite and a decrease in the potential on pentlandite. Bozkurt *et al.* (1998) have not shown any reproducibility of measurements and the fact that some of the rest potential measurements did not stabilise raise questions regarding the results.

The mixed potential theory supports the work of Hodgson and Agar (1989), Senior *et al.* (1994) and Khan and Kelebek (2004). These authors showed that under oxygen-saturated conditions, the selectivity in pentlandite and pyrrhotite separation is lost, promoting the flotation of pyrrhotite. These results suggest that dixanthogen formation is favoured on pyrrhotite and oxygen reduction on pentlandite. The recovery of intermediate sized pentlandite particles was similar when collector or copper sulfate was added and almost complete recovery of these particles is likely in any separation of pentlandite from pyrrhotite (Senior *et al.*, 2004). Pentlandite floatability is not significantly affected, since it is likely that chemisorption of xanthate on pentlandite takes place and renders pentlandite hydrophobic, given that it does not need dixanthogen to induce hydrophobicity. Pentlandite can develop nickel sites, which can support chemisorption of xanthate and which may be well enough for its flotation (Hodgson and Agar, 1989; Khan and Kelebek, 2004). Recovery-size results showed that the presence of pentlandite improved the intermediate and coarse pyrrhotite particles' floatability; however the presence of pyrrhotite resulted in the depression of coarse pentlandite particles (Senior *et al.*, 1994).

In the study done by Bozkurt *et al.* (1998), xanthate adsorption on pyrrhotite and pentlandite singly and in either indirect or direct physical contact was examined using FTIR-ATR spectroscopy. Bozkurt *et al.* (1998) examined the IR spectra of pyrrhotite with isobutyl xanthate adsorption at $5x10^{-5}$ M SIBX and pH 9.2 (this is shown in *Figure 14*). Well defined bands were observed at 1265, 1048, ad 1026 cm^{-1}, which are characteristic of coupled S-C-S and C-O-C stretching vibrations in dixanthogen. These results are similar to those reported by Leppinen *et al.* (1989), Leppinen (1990) and Valli and Persson (1994).

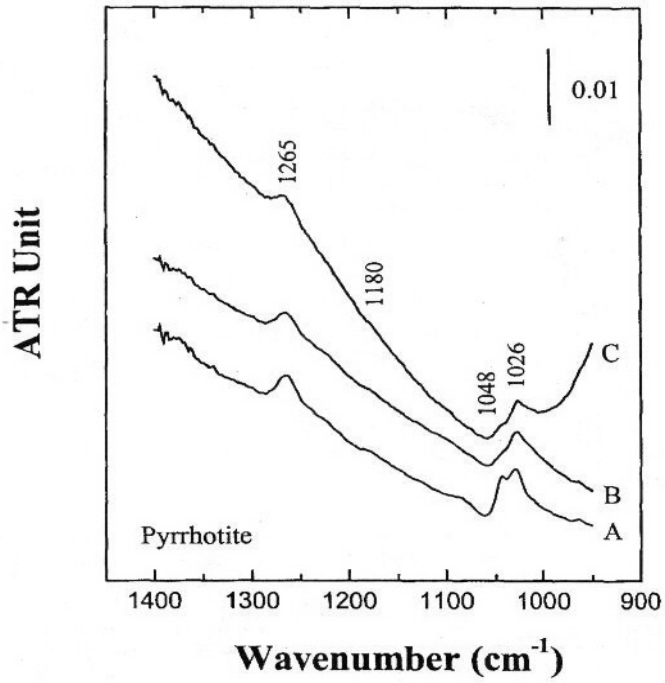

Figure 14: FTIR-ATR spectrum of pyrrhotite in the case of: single minerals (method A); mixed minerals in solution contact (method B, with pentlandite); and mixed minerals in direct contact (method C, with pentlandite). Xanthate concentration is $5x10^{-5}$ M and pH 9.2 (Bozkurt *et al.*, 1998).

It can be seen from *Figure 14* that the adsorption density of dixanthogen at the pyrrhotite surface was a little greater for pyrrhotite alone (A) than for the pyrrhotite in direct contact with pentlandite (C). This indicates that contact between pentlandite and pyrrhotite enhances the difference in dixanthogen formation between the two minerals in favour of the pentlandite, as shown by the open circuit potential measurements in the similar work.

FTIR has found many applications relating to the adsorption of xanthates on sulfide mineral surfaces (Rao, 2004). Various authors (Jones and Woodcock, 1986; Yoon *et al.*, 1995; Yuehua *et al.*, 2005) applied the internal reflection spectroscopy to determine the adsorption density of xanthate at the mineral surface. If the refractive index of the mineral, incident angle and wavelength of light are known, the adsorption process can be quantified (Rao, 2004). Yoon *et al.* (1995) and Yuehua *et al.* (2005) showed that the intensity of IR signals can be correlated to the adsorption density of dixanthogen on the pyrrhotite surface. It was also demonstrated that the intensity of IR signals was dependent on potential. The IR signals of the characteristic dixanthogen peaks and hence dixanthogen adsorption on pyrrhotite

decreased with decreasing potential from 0.40 to -0.30 V (SHE). This correlated well with the contact angle and flotation results. At around pH 9, flotation recovery, contact angle and dixanthogen adsorption on pyrrhotite were reduced with a decrease in pulp potential.

According to the mixed potential theory, mixed potential on pentlandite is reduced, but increases on pyrrhotite when in contact in the presence of xanthate. The intensity of the IR signals of the characteristics dixanthogen peaks on pyrrhotite in the study done by Bozkurt *et al.* (1998), were supposed to increase due to the expected higher potential and higher xanthate oxidation rate on pyrrhotite when in contact with pentlandite. Bozkurt *et al.* (1998) reported a decreasing rest potential of pentlandite that did not stabilise after 10 minutes, suggesting that the rest potential could have been lower than that of pyrrhotite after a longer period of time. This suggests that pentlandite might have been less noble than pyrrhotite, hence supporting the favourable dixanthogen formation on pentlandite.

For minerals sharing the same xanthate solution, the amount of dixanthogen on pentlandite increased compared to pentlandite alone (Bozkurt *et al.*, 1998). This could be because the rest potential in the presence of pyrrhotite increased, favouring a higher dixanthogen absorption density. The rest potential measurements of single pyrrhotite and pentlandite in the presence of xanthate do not support the FTIR adsorption measurements of Bozkurt *et al.* (1998): pentlandite was reported to have a higher dixanthogen absorption density than pyrrhotite when its rest potential was lower than that of pyrrhotite. If it had a higher dixanthogen absorption density, its rest potential would be more anodic than pyrrhotite, thus showing agreement with the mixed potential theory (i.e. that pentlandite is more noble than pyrrhotite). As a result, it can be said that the rest potential measurements reported by Bozkurt *et al.* (1998), which do not agree with the findings of other authors and spectroscopic studies, were used in the mixed potential model and led to the conclusion that dixanthogen formation is favoured on pentlandite rather than on pyrrhotite when the two minerals are in contact.

2.2.4.2. Cyclic voltammetry of pyrrhotite

The cyclic voltammograms of pyrrhotite in the study done by Khan and Kelebek (2004) are presented in *Figure 15*. The working electrode was subjected to four different conditions (i.e. the presence and absence of dissolved oxygen and xanthate).

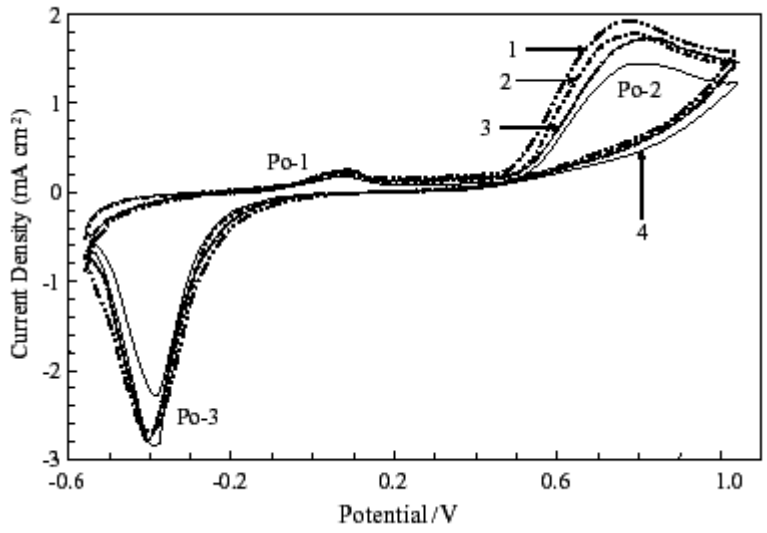

Figure 15: Cyclic voltammograms of pyrrhotite electrode under various conditions (pH 9.2), with a scan rate of 10 mV/s (numbers indicate concentrations of dissolved oxygen (DO) and sodium n-butyl xanthate (X); (1) DO = 8.15 mg/l, X = 0 mol/m^3; (2) DO = 0.1 mg/l, X = 0 mol/m^3; (3) DO = 8.15 mg/l, X = 0.1 mol/m^3; (4) DO = 0.1 mg/l, X = 0.1 mol/m^3 (Khan and Kelebek, 2004).

Potential measurements of pyrrhotite electrodes carried out in plant slurries showed that the mineral is exposed to potentials in the region of 0.2 to 0.3 V (SHE) prior to flotation (Ralston, 1991; Buswell and Nicol, 2002).

In *Figure 15*, peak Po-1 was observed in the potential range -0.05 – 0.11 V (SHE) and was attributed to the following electrochemical reaction:

$$Po[Fe_{1-x}S] + 3yOH^- = Po[Fe_{1-(x+y)}S + (y-z)Fe(OH)_3] + zFe(OH)_3 + 3ye^- \quad \textbf{\textit{Eq. 16}}$$

where $Fe_{1-x}S$ is depicted as an iron deficient surface of pyrrhotite, with x typically increasing to 0.2. Pyrrhotite reacts with an alkaline solution and forms a surface product with even

greater iron-deficiency and ferric hydroxide. Excess sulfur has been considered to be in the form of elemental sulfur (Hamilton and Woods, 1981) and polysulfide (Hodgson and Agar, 1984).

In a study done by Buswell and Nicol (2002), the oxidation of pyrrhotite in the absence of a collector or activator was investigated in an attempt to establish the nature of the mineral surface prior to reaction with flotation reagents. The cyclic voltammogram of a pyrrhotite electrode in a de-aerated borate solution is presented in *Figure 16*.

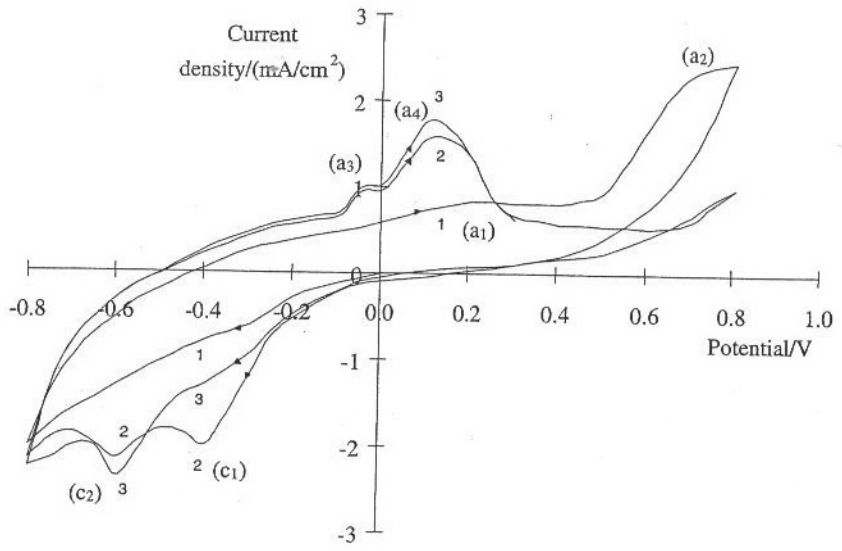

Figure 16: Cyclic voltammogram for a stationary pyrrhotite electrode in de-oxygenated 0.05 M $Na_2B_4O_7$ (pH 9.3) with a sweep rate of 20 mV/s. (Numbers represent sweep number and letters in parenthesis identify reactions) (Buswell and Nicol, 2002).

Buswell and Nicol (2002) also reported pyrrhotite voltammograms (*Figure 16*) but did not indicate a peak in this region (-0.05 – 0.11 V [SHE]) in their first scan in the anodic direction. There was only a fairly small anodic current plateau, from 0.20 to 0.50 V (SHE), even though subsequent anodic scans produced two peaks in the same potential range. Khan and Kelebek (2004) reported a new current peak at (Po-2) at 0.50 V (SHE), which reached its maximum current density at 0.75 V (SHE). This anodic process was considered to involve oxidation of the sulfide part of pyrrhotite, in addition to the formation of ferric hydroxide (Hamilton and

Woods, 1981; Ribbe, 1984). The following is the overall reaction leading to sulfate formation:

$$Po[FeS_{1.13}] + 4.52H_2O = Po[Fe(OH)_3] + 1.13SO_4^{2-} + 9.04H^+ + 9.78e^- \qquad \textbf{\textit{Eq. 17}}$$

Pyrrhotite dissolution studies under differing conditions have been carried out by electrochemical and spectroscopic techniques (Hamilton and Woods, 1981; Buckley and Woods, 1985a; Buckley and Woods, 1985b; Hodgson and Agar, 1989; Mikhlin, 2000; Buswell and Nicol, 2002; Khan and Kelebek, 2004; Cruz *et al*., 2005). The results of the electrochemical behaviour of pyrrhotite suggest that its alteration involves the formation of three surface layers: (1) in immediate contact with pyrrhotite corresponding to a metal-deficient sulfide; (2) an intermediate layer corresponding to elemental S, and; (3) the external layer, consisting of precipitates of Fe-oxyhydroxides, like goethite.

In most of these studies, the formation of a non-stoichiometric, non-equilibrium or metastable layer ($Fe_{1-x-y}S$, subsequently referred as NL) has been proposed as a result of preferential dissolution of Fe relative to S, such as indicated in *reaction 16*. Iron precipitates have been identified as Fe-oxyhydroxides covering the NL. The composition and characteristics of the NL are extremely widespread and depend on the conditions under which the alteration takes place (Cruz *et al*., 2005).

On the basis of the data reported by various authors (Hamilton and Woods, 1981; Buckley and Woods, 1985a; Buckley and Woods, 1985b; Hodgson and Agar, 1989; Mikhlin, 2000; Buswell and Nicol, 2002; Khan and Kelebek, 2004; Cruz *et al*., 2005) it can be suggested that the electrochemical oxidation process of pyrrhotite takes place in three stages. The first stage, depicted by anodic peaks at lower potentials on the voltammograms (see *Figures 15* and *16*), may be related to the formation of metal-deficient sulfide. Secondly, the continuous loss of metal results in the formation of elemental S (S^0) on the mineral surface. The amount of S^0 increases until it forms a passivating layer. This is indicated by low anodic currents after the first anodic peaks in *Figures 15* and *16*. The released Fe^{2+} will oxidise to form ferric hydroxides. The last stage of the pyrrhotite electrochemical oxidation consists of the rupture of the elemental S passivating layer at potentials over 0.50 V (SHE), which occurs due to the S^0 oxidation in the formation of sulfate (see *equation 17*).

According to Hamilton and Woods (1981), the quantity of pyrrhotite oxidised to sulfur and sulfate is a function of the potential limit of the sweep. Sulfur is the major oxidation product and initially accounts for all the pyrrhotite oxidised. The amount of sulfate produced increases as the sweep is taken to higher potentials and it is also a function of time. However, part of the current at the higher potentials still goes to produce sulfur, with the sulfur yield continually increasing with potential. Sulfate is the dominant product on sweeps taken to much higher potentials (Hamilton and Woods, 1981; Hodgson and Agar, 1989).

Oxidation of pyrrhotite is inhibited significantly in an alkaline solution, suggesting that iron oxide on the surface retards further reaction (Hamilton and Woods, 1981). The pyrrhotite reactivity seems to be controlled by the formation of oxidation product layers that coat and passivate the pyrrhotite surface. The formation of the passivating S layer affects the reactivity of pyrrhotite more significantly than the diffusion barrier of the FeOOH layer (Cruz *et al*., 2005).

No significant effect of the presence of xanthate was observed on the starting potential of the peak, but the maximum peak potential shifted to 0.80 V (SHE) and the maximum current density was reduced (see *Figure 15*). It was observed that in the presence of xanthate, the current flow corresponding to the oxidation of pyrrhotite surface is somewhat inhibited for both levels of oxygen in the electrolyte, hence the low current densities in the presence of xanthate even at higher oxygen levels. No anodic peak for xanthate adsorption was observed for pyrrhotite, which agrees with the results produced by Hodgson and Agar (1989) and Buswell and Nicol (2002).

Due to oxidation, some ferrous species may be released from pyrrhotite, interact in solution and are transformed into other species, depending on the solution chemistry, to form positive surface sites in favourable areas of pyrrhotite by readsorption. Initial xanthate adsorption proceeds at these specific sites as a result of electrostatic interaction via the following reactions, as shown by Khan and Kelebek (2004):

$$Po[Fe(OH)]^{+} + X^{-} \rightarrow Po[Fe(OH)]^{+}.\ X^{-} \rightarrow Po[Fe(OH)X] \qquad \textbf{\textit{Eq. 18}}$$

More stable forms of ferric counterparts can follow through the transformation steps as, for example:

$$Po[Fe(OH)X] + OH^- \rightarrow Po[Fe(OH)_2X] + e^- \quad \textit{Eq. 19}$$

Further xanthate adsorption can lead to dixanthogen formation:

$$Po[Fe(OH)_2X] + X^- \rightarrow Po[Fe(OH)_2X\text{-}X] + e^- \quad \textit{Eq. 20}$$

$$Po[Fe(OH)_2X\text{-}X] + X^- \rightarrow Po[Fe(OH)_2X\text{-}X_2] + e^- \quad \textit{Eq. 21}$$

Similarly, Hodgson and Agar (1989) found no chemisorption of xanthate on pyrrhotite and reported that xanthate was adsorbed on the pyrrhotite surface and formed an Fe(OH)[S]X product. Unlike chemisorption, no electron transfer is considered to arise through the adsorption of xanthate on the surface, the collector being adsorbed through coulombic attraction with the cationic iron(III) site generated by oxidation of the mineral surface, according to the following reactions:

$$FeS + 2H_2O = Fe(OH)[S]^+ + 2H^+ + 2e^- \quad \textit{Eq. 22}$$

$$Fe(OH)[S]^+X^- = Fe(OH)[S]X \quad \textit{Eq. 23}$$

Xanthate then oxidises to dixanthogen through the reduction of oxygen at the pyrrhotite surface. As no additional peak was detected on the cyclic voltammogram, which could be ascribed to dixanthogen, dixanthogen formation was considered to take place adjacent to the oxidised pyrrhotite surface and to be physisorbed via the alkyl groups of the Fe(OH)[S]X complex.

Development of appreciable hydrophobicity on pyrrhotite surfaces is observed in the potential range of 0.10 – 0.125 V (SHE) [Yoon *et al.*, 1995], which is in agreement with the current peak position reported by Buswell and Nicol (2002).

The cathodic current peak (Po-3) (in *Figure 15*) is relatively broad, starting between -0.20 and 0 V (SHE) and reaching a maximum current density of around -0.40 V (SHE). It is known that xanthate adsorbs on pyrrhotite in this initial potential range (in anodic direction), which then requires a hydrophobic character (Yoon *et al.*, 1995). However, in this case, the cathodic sweeps obtained in the presence and absence of xanthate are similar, indicating that

there was no xanthate desorption under reducing conditions. On the whole, this potential range is attributable to reduction of the ferric species (i.e. ferric hydroxide and some residual xanthate derivatives of ferric hydroxide) formed during anodic scans. Another relevant aspect to note here is the reversal of another surface reaction involving sulfur oxidation. It is also evident in *Figure 15* that the reduction current density is relatively higher than the anodic current densities, suggesting that the electrode surface has been altered by oxidation to a greater degree than indicated by the summation of anodic current densities.

2.2.4.3. Reagents addition

In addition to results obtained by Buswell *et al.* (2002), Buswell and Nicol (2002) also reported the following result on the reaction of the minerals and copper ions: exposure to copper ions did not have a significant effect on the kinetics of oxygen reduction. One of the problems associated with studying the reaction of pyrrhotite with xanthate is that pyrrhotite oxidises at the potentials where the anodic adsorption of xanthate is expected. Prior exposure to copper ions improved the anodic currents in the presence of xanthate. The activation process and mechanism in which xanthate interacts with the mineral surface is changed (this was discussed earlier in *Section 2.2.2.2.2*).

As mentioned earlier, anodic reactions representing chemisorption of xanthate were not detected, thus supporting the view that the initial adsorption of xanthate occurs via physisorption (Hodgson and Agar, 1989; Buswell and Nicol, 2002). At higher potentials, the oxidation of the mineral involves the formation of sulfur and sulfate, in addition to ferric hydroxide (Hamilton and Woods, 1981; Buswell and Nicol, 2002, Khan and Kelebek, 2004). In acidic solutions, the reaction between pyrrhotite and copper ions results in CuS, which enhances xanthate adsorption (Chang *et al.*, 1954; Buswell and Nicol, 2002). Under alkaline conditions, no CuS was detected, thus suggesting that pyrrhotite flotation activation may occur via a different mechanism, which might involve a copper hydroxide species and which may be favourable for xanthate adsorption (Fuerstenau, 1982; Wesseldijk *et al.*, 1999; Buswell and Nicol, 2002). The anodic reaction of xanthate and pyrrhotite was observed and this reaction was partly inhibited by the oxidation of the mineral surface.

Pyrrhotite flotation may be improved by minimising the effects of oxidation through the rapid addition of collector reagents and/or by imposing reducing conditions on the pulps until reagent addition. As shown by Wiese *et al.* (2005), adding reagents (collectors and copper sulfate) to the mill improved pyrrhotite floatability more than additions to the cell. Reagents interact with fresh surfaces in the mill before any major oxidation of sulfides occurs and any negative impact caused by the grinding media is also reduced.

In terms of controlling the pulp potential, Newmont Mining Company has developed the N_2-TEC process in which grinding and flotation are under nitrogen atmosphere instead of the conventional flotation condition (open to air). The process operates in the potential range -0.1 to 0.5 V versus Ag/AgCl and potassium amyl xanthate (PAX) is used as the collector (Simmons *et al.*, 2003). PAX is used mainly because of its low rest potential of -0.159 V (SHE) when compared to short carbon chain length xanthates, as it is easily oxidised to dixanthogen under the reducing conditions prevailing in the N_2-TEC process. PAX is again used because selectivity in the N_2-TEC is not a problem. PAX is less selective when compared to short carbon chain length xanthates, because the longer collector chain length can cover hydrophilic sites and render the mineral surface hydrophobic. N_2-TEC is used to treat many gold-bearing sulfide ores. *Figure 17* compares gold recovery under nitrogen and air atmospheres.

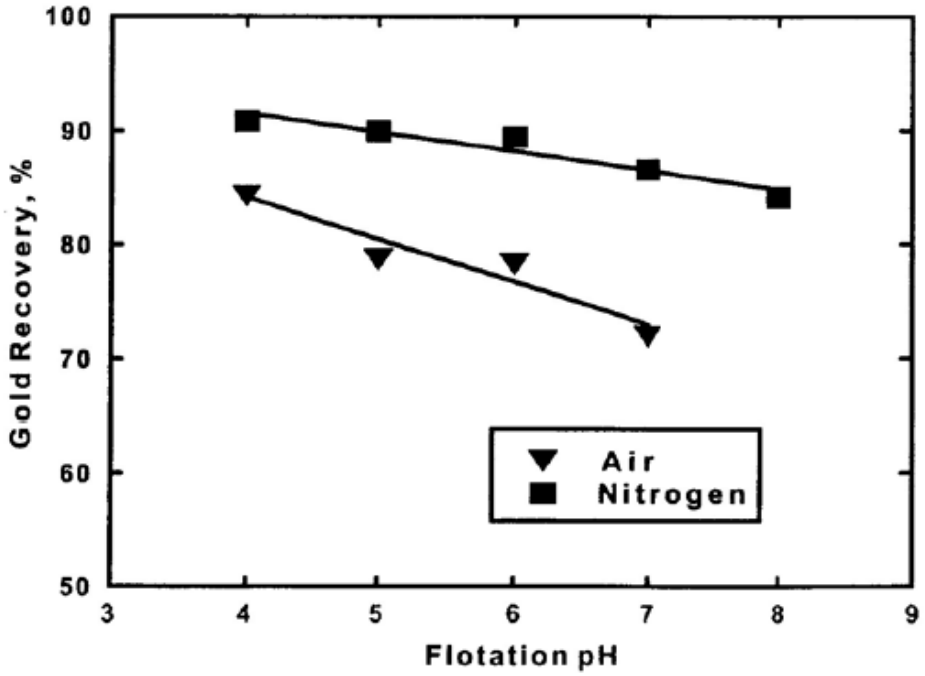

Figure 17: Gold recovery obtained in bench-scale flotation experiments of Lone Tree ore as a function of pH for air and nitrogen (Miller *et al*., 2002).

Miller *et al.* (2002) reported a notable difference between flotation with nitrogen and conventional air flotation. These results indicate that for flotation under nitrogen, oxidation of auriferous pyrite is limited and collector adsorption occurs at low Eh values. Thus the hydrophobicity and recovery of sulfide minerals is improved, resulting in improved recovery of valuable minerals such as gold. The N_2-TEC can also be used to treat platinum and palladium ores, however, in South African PGE ores, it has not been used due to the low sulfide content and the expensive production of nitrogen (Miller *et al*., 2002).

Galvanic interactions in the study done by Buswell and Nicol (2002) were ruled out due to the low grade of the sulfide minerals. Base-metal sulfide minerals contribute approximately one percent by volume to the PGE ore within the Merensky and UG-2 reefs. The interaction between the sulfides must be long enough for electron transfer to take place. When comparing the sulfide minerals results or behaviour from different researchers, there is a concern regarding the origin of the mineral samples in that their electrochemical behaviour often differs considerably, depending on the origin of the sample. These differences can be associated with impurity levels and crystallographic effects (Abramov and Avdohin, 1997).

Buswell *et al.* (2002) suggested that minerals samples should be obtained from the ore body in question where possible.

As mentioned earlier, pyrrhotite is non-stoichiometric, having a variable composition and crystal structures. Miller *et al.* (2005) highlighted the effect of these characteristics by evaluating the results obtained by other researchers (Buswell and Nicol, 2002; Khan and Kelebek, 2004). Due to its variation in composition and crystal structure, each pyrrhotite sample may have a different nature, which is supported by the results indicated below.

Khan and Kelebek (2004) and Buswell and Nicol (2002) examined the kinetics of pyrrhotite decomposition by electrochemical measurements using cyclic voltammetry. *Figure 15* shows the results obtained by Khan and Kelebek (2004), which indicates that when the potential is below -0.05 V (SHE) the initial rate of pyrrhotite oxidation (anodic current density) is quite slow, even though there is a peak for the oxidation in the potential region from -0.05 to 0.18 V (SHE). The maximum current density for this peak is 0.20 mA/cm^2 at pH 9.2 and an oxygen concentration of 0.1 mg/l in the absence of collector (curve 2). In contrast, Buswell and Nicol (2002) showed that at pH 9.3 and 0.05 M $Na_2B_4O_7$, pyrrhotite from a South African Mineral Dealer is more active than the Sudbury pyrrhotite sample used by Khan and Kelebek (2004) (see *Figure 16)*.

These results suggest that when the potential exceeds -0.40 V (SHE), the initial rate of pyrrhotite oxidation (anodic current density) becomes significant. The anodic current density varies from 1.0 to 2.0 mA/cm^2 at a potential of 0 to 0.20 V (SHE) (Miller *et al.*, 2005). These results show that the electrochemical behaviour of pyrrhotite from different locations is different. As shown earlier, pyrrhotite particles from the PGE-reefs in the Bushveld Igneous Complex have varying chemical compositions. This variation in chemical composition is expected to have an effect on the electrochemical behaviour of pyrrhotite.

It was also shown that pyrrhotite is easily oxidised and this results in slow and poor flotation of pyrrhotite (Miller *et al.*, 2005). Following is the discussion of techniques used to remedy the excessive oxidation on valuable sulfide minerals, with the aim of improving the interaction between the sulfide surfaces and xanthate so as to enhance flotation.

2.3. Techniques to treat heavily oxidised surfaces

Surface oxidation of sulfide minerals, such as that found in the regions of a sulfide ore body near the water table, can have a significant impact upon flotation (Newell *et al.*, 2005). The vital role of oxygen in the interaction of xanthate at sulfide minerals has been well recognised. However, it has been well established that excessive oxidation of sulfide minerals results in the deterioration of the sulfide's floatability by xanthate type collectors (Rao, 2004). The two possible causes for the adverse effect of excessive oxidation are: (1) the failure of the surfactant employed to adsorb; and (2) the failure to make the adsorbed layer hydrophobic. Pyrrhotite is easily oxidised and this results in slow, poor flotation of pyrrhotite and loss of PGMs associated with it (Miller *et al.*, 2005).

In this section, various methods that could be employed to remove oxidation products on the oxidised pyrrhotite surface (so as to improve pyrrhotite interaction with xanthate and restore pyrrhotite floatability) are discussed. Oxidation products from the mineral can be removed by various mechanical and chemical methods (Clarke *et al.*, 1995), some of which are discussed below.

2.3.1. Dissolution by lowering the pH

As mentioned earlier (*Section 2.2.2.2.3.*), in the plant milled pulp, acid conditioning improved pyrrhotite recovery and the electrode potential and the magnitude of change in the electrode potential of pyrrhotite increased significantly upon addition of collector after acid conditioning. The decrease in the electrode potential of acid cleaned pyrrhotite after interaction with xanthate was substantially higher than without acid cleaning, showing a higher xanthate adsorption. This was thought to be due to the dissolution of hydrophilic iron oxy/sulfoxy species from the pyrrhotite surface (Buswell *et al.*, 2002; Rao, 2004).

2.3.2. Cupric ion activation

Moignard *et al.* (1977) established that zinc hydroxide is present on the sphalerite surface, as indicated by its low collectorless flotation and its zeta potential (iep [isoelectric point]

moving from 1.6, for a non-oxidised sphalerite, to 8.5 for a fully oxidised sphalerite surface or for zinc oxide). XPS and EDTA extraction studies by Clarke (1995) revealed that the oxidation products, in particular zinc hydroxide, are removed from the sphalerite surface on Cu(II) addition, therefore exposing a more hydrophobic "virgin" surface. Cu(II) exchanges with Zn(II) ions in the sphalerite lattice, with a subsequent reduction to Cu(I) (Finkelstein and Allison, 1976; Fuerstenau, 1982; Wang *et al.*, 1989). Ralston and Healy (1980a), Ralston *et al.* (1981) and Wang *et al.* (1989) showed this reduction of copper to be associated with the oxidation of sulfide to elemental sulfur or polysulfide at the mineral surface. Both the removal of zinc hydroxide and the oxidation of sulfide to elemental sulfur or polysulfide may explain the increase in sphalerite flotation on addition of Cu(II) [Clarke *et al.*, 1995].

2.3.3. Milling

Milling involves the following main breakage mechanisms: surface chipping and abrasion, low-energy impact fracture, and high-energy impact and compression fracture.

Grinding is expected to weaken the physical integrity of oxidation layers on sulfides to allow more favourable sites for collector action, thus improving liberation as well as potentially minimising the fraction of coarse particles where greater flotation losses are observed (Nanthakumar *et al.*, 2007). Industrially, wet grinding is preferred to dry grinding, owing to downstream processing requirements, as well as the higher energy efficiency associated with wet grinding (amongst others) (Feng and Aldrich, 2000). Feng and Aldrich (2000) investigated the effect of dry and wet grinding on the flotation of complex sulfide ores from the Merensky Reef in South Africa. The advantages and disadvantages of both the wet and dry grinding environments were compared, with the following being observed:

- Wet grinding proceeds with the preferential formation of new surfaces and little bulk deformation of particles.
- Wet grinding can favour chemical surface reaction products.
- The wet ground sample showed higher concentrate grades and slightly higher recoveries.
- The wet ground sample’s surfaces were cleaner, resulting in higher flotation selectivity.
- In the denser wet grinding media (90 % solids compared to 66 % solids), some of the energy was also converted into particle surface energy. Moreover, the particle

surfaces were completely clean, leading to an improvement in both the flotation kinetics and concentrate grade.

- Wet milling rapidly enlarged the surface area, while dry milling resulted in the activation of the ground sample. The dry ground samples had comparatively rough particle surfaces, compared to the wet ground samples, which had smooth surfaces.
- When the same new surface formed, dry grinding consumed more energy than wet grinding.
- In dry milling, some of the energy was stored in the form of crystal defects. These defects serve as active centres for speeding up particle dissolution and reagent adsorption.
- The dry ground samples showed more stable, highly loaded froths, faster flotation kinetics and lower flotation selectivity. The fast flotation kinetics could be attributed to the activation of particle surfaces in dry milling, while the low flotation selectivity could be attributed to non-selective adsorption of fines onto the activated particle surfaces. In contrast, the wet ground sample exhibited higher flotation selectivity and slower flotation kinetics.
- In the dense wet milling (90 % solids in the pulp phase), the particle surfaces had some defects and the ground samples appeared to have faster flotation kinetics than the less dense, diluted milling process (66 % solids in the pulp phase). The combination of wet and dry milling could improve flotation. The dry milling process was used to increase the enthalpy of the ground sample; wet milling was used to depress the non-selective aggregates resulting from dry milling.
- Although dry milling can greatly improve flotation kinetics, it is difficult to apply to practical sulfide flotation systems, owing to the tendency of fine sulfides to oxidise in air. This is obviously not a problem as far as oxide ores are concerned.

2.3.4. Sonication

Clarke *et al.* (1995) investigated the effect of sonication on the flotation of chalcopyrite and galena. The flotation rate and recovery increased with an increase in the power of sonication of the mineral pulp. Complementary analyses (XPS, EDTA extraction) have revealed that the amount of iron and lead hydroxide on the surface of chalcopyrite and galena, respectively, is reduced on sonication, exposing a more hydrophobic surface (Fornasiero *et al.*, 1994;

Fairthorne, 1995). Importantly, the oxidation products removed by sonication from the mineral surface are readsorbed if they are not removed from the solution or if flotation is not performed immediately (Clarke *et al.*, 1995).

2.3.5. Attritioning with quartz

The action of quartz present in an ore on the flotation of the other minerals is well known (Clarke *et al.*, 1995). Chander (1991) found that when the proportion of quartz particles contained in a chalcopyrite or pyrite quartz mixture is increased, the flotation of chalcopyrite and pyrite is improved. This behaviour was attributed to the preferential adsorption or precipitation on the quartz surface, rather than on the sulfide surface, of the metal hydroxides formed in solution following their dissolution from the corresponding metal sulfide mineral. Apart from this increase in flotation recovery, a corresponding decrease of the zeta potential of quartz was observed, implying that some positively charged species, probably metal hydroxides, have adsorbed on the quartz surface (Chander, 1991). A similar trend was observed in the flotation recovery of sphalerite in the presence of quartz, together with a decrease of the quartz zeta potential by Clarke *et al.* (1995). Chander (1991) reported that the removal by quartz of oxidation products from an oxidised mineral surface seems to indicate that attritioning is the mode of surface cleaning by quartz.

2.3.6. Sodium hydrosulfide

Freeman *et al.* (2000) reported that at Nothparks Mine, gold ore is processed using flotation with sodium hydrosulfide (NaHS) as a sulfidiser. The ore surface was resulfidised. Orwe *et al*. (1997, 1998) investigated the use of NaHS in the flotation of the two Ok Tedi ores. It was learnt that the main influence of the hydrosulfide ion on the copper ores is to resulfidise the oxidised chalcocite/digenite/bornite (bornite is a secondary copper mineral known to oxidise readily) (Buckley *et al.*, 1985). The addition of this reagent, however, also increased the flotation characteristics of an ore containing predominantly chalcopyrite, which is much less susceptible to oxidation. The increase in recovery after addition of NaHS was most apparent for the fine sizes, since these were more oxidised than the coarser particles. Conditioning with NaHS restored the oxidised chalcocite to its original form. Sulfidisation usually results

in a strongly hydrophobic surface in the presence of collector. As such, it is likely that sulfidisation minimises the collector consumption during flotation by precipitating metal hydroxides as insoluble metal sulfides.

Newell *et al.* (2005) studied the flotation response of surface oxidised sulfide minerals, such as pyrrhotite, pentlandite and chalcopyrite, and the subsequent effect of three potential remedies, including treatment in an ultrasonic bath, collector concentration and sulfidisation, as well as selected combinations of these techniques. Nkomati massive sulfide ores were selected for the study as they contain the same base-metal sulfide minerals as the Merensky ores. Their findings are presented below:

- Heavily surface oxidised Merensky type sulfide minerals prepared by thermal oxidation form depleted surface layers covered by non-porous surface oxidation products; the flotation response of these oxidised sulfide minerals deteriorates with time.
- Some improvement in the flotation response of less oxidised samples was achieved at higher collector concentrations as well as ultrasonic cleaning; however for the heavily oxidised sulfide minerals, these techniques were not effective.
- The combination of ultrasonic cleaning, followed by sulfidisation and decantation, restored the flotation response of heavily oxidised Merensky type sulfide minerals.
- The sulfidisation and collector requirements for the three sulfide minerals appeared to be different, particularly for oxidised pentlandite.
- Flotation recoveries of oxidised pyrrhotite and pentlandite deteriorated under longer sulfidisation conditioning times, due to the oxidation of the freshly formed sulfide surfaces.

Thus, it appeared likely that in a mineral processing operation treating oxidised Merensky type ores, two stages of sulfidisation employing different conditions would be required.

In sulfidisation, the sulfoxyl species like sulfite or sulfate can be removed and the surface reconverted to sulfide by treating the surface with a soluble sulfide like sodium sulfide (Rao, 2004).

2.3.7. Interaction of gaseous carbon dioxide with oxides

Baltrusaitis and Grassian (2005) studied the CO_2 and iron hydroxides interaction mechanism, which involved the surface reactions of carbon dioxide at the adsorbed water-iron oxide interface using FTIR spectroscopy. The surface chemistry of CO_2 on Fe_2O_3 nanoparticles (≈ 30 nm diameter) under ambient conditions of temperature and relative humidity was studied.

One mechanism that can explain the observed results is shown in *Figure 18*. It involves the direct reaction of H_2O and CO_2 to yield carbonic acid, which deprotonates into bicarbonate. Bicarbonate then goes on to displace OH on the surface, followed by deprotonation of adsorbed bicarbonate.

It was determined from quantitative analysis of gas-phase CO_2 that considerably more CO_2 is adsorbed in the presence of adsorbed water. At 40 % relative humidity (RH), it is determined that the coverage of adsorbed CO_2 on the surface increases by a factor of 5 when compared to dry conditions. Thus, adsorbed water enhances the adsorption of CO_2 on iron oxide. In the case of sulfide minerals, particles are dispersed in water. As a result, the adsorbed water layer (shown in *Figure 18*) is present on the mineral surfaces and is expected to enhance the adsorption of CO_2 on the hydroxide/oxide layers that have formed on the mineral surface.

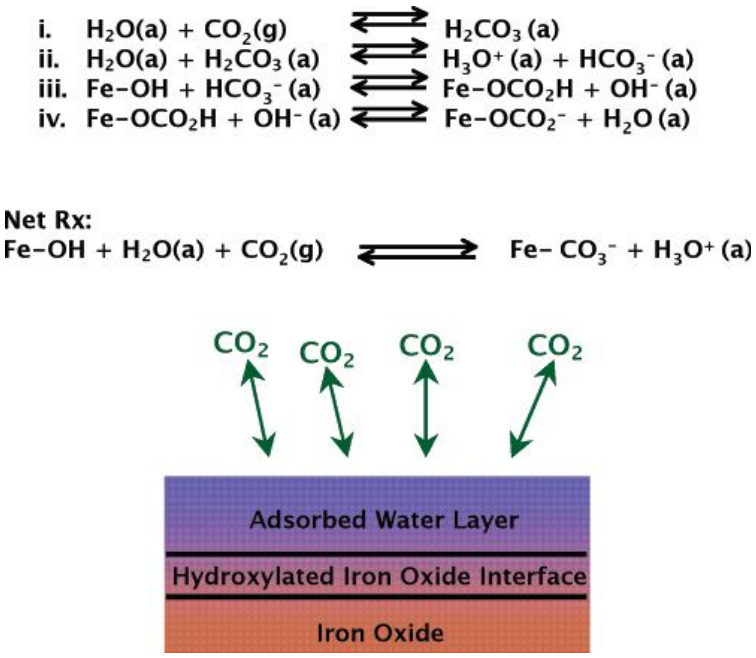

Figure 18: Surface reactions of CO_2 and H_2O on Fe_2O_3 (Baltrusaitis and Grassian, 2005).

Linter and Burstein (1999) studied the reactions of pipeline steels in carbon dioxide solutions. It was observed that the dissolved gas reacts with the iron component of these steels in such a way as to contribute to the depassivation of steel. The mechanism proposed is that of complexing with Fe(II) within the hydroxide film to give both ferrous carbonate and a dissolved complex. This agrees with results by Baltrusaitis and Grassian (2005).

Because of the possibility that the observed effect of dissolved CO_2 could, in principle, be attributed to small changes in pH that may occur when the buffered solutions are saturated with CO_2, the effects of small changes in pH were examined. *Figure 19* shows the anodic branches of the polarisation curves at pH 3.4, 3.7 and 4.0 in the absence of CO_2.

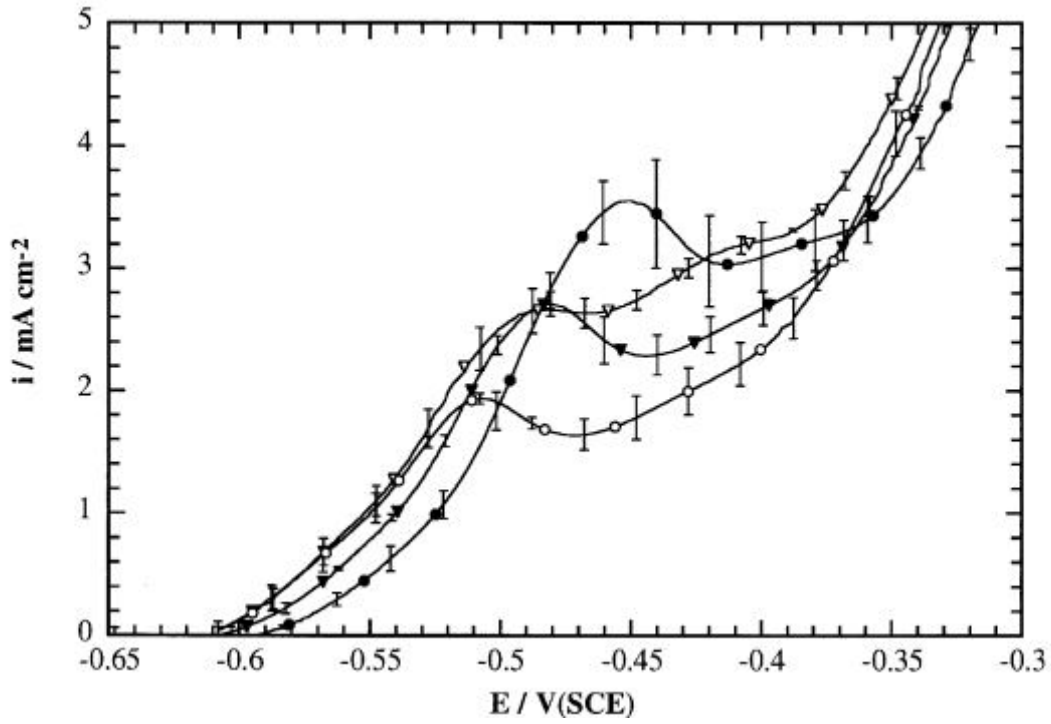

Figure 19: Anodic polarisation of 0.5 Cr steel in 0.5 M NaCl, 0.05 M potassium hydrogen phthalate, showing that the effect of CO_2 saturation cannot be related simply to a variation in pH. ●: pH 3.4, Ar purged. ▼: pH 3.7, Ar purged. ○: pH 4.0, Ar purged. ▽: pH 4.0, CO_2 purged. The electrode was rotated at 20 Hz. Scatter bands represent the standard deviations of three runs (Linter and Burstein, 1999).

As the solution is made more acidic, the current density at the anodic peak increases, as does the potential at which this occurs. In addition, the trough in current that succeeds the anodic peak is also more anodically reactive. This trough shows an attempt by the metal surface to establish passivity; however, the anodic current then rises further and no passivity ensues. It should be noted that, effectively, the whole anodic curve is moved to a more anodic potential with a decrease in pH.

The data from the pH 4.0 solution saturated with CO_2 are also shown in *Figure 19*. The presence of CO_2 causes a rise in the peak current density and a continuing rise in the region that succeeds it. The peak current density from this CO_2 solution of pH 4.0 is the same as that in the pH 3.7 solution in the absence of CO_2; the current trough immediately past the peak is still accelerated by CO_2. The effect is clearly quite different from that of the pH and therefore the role of CO_2 cannot be simply to decrease the pH. This is further evident from the fact that

the current in the active rise, prior to the peak, is the same for both pH 4.0 solutions with and without CO_2. The dissolved gas enhances the anodic dissolution of Fe in the potential regime around and above that of the anodic current peak. It was deduced that this acceleration must arise from the effect of CO_2 on a surface film.

Miller and Misra (1987) developed a process for froth flotation of coal using gaseous carbon dioxide, including conditioning treatment of the coal with gaseous carbon dioxide followed by froth flotation. The treatment resulted in improved results in that less reagent promoter and frother were required and the flotation time reduced. The process was deemed applicable to various grades and types of coal and may also be used for oxidised coal. The process proved to be particularly useful for producing “super” clean coal.

It can be said that most of the oxidised ores cleaning methods that have been used in practice have limitations. It is also known that the ore is usually oxidised under the plant milling conditions (such as oxygen-saturated conditions), thus forming surface oxidation products that inhibit the efficient interaction between the freshly created mineral surface and the surfactants (Healy, 1984; Rao, 2004). Newell *et al.* (2005) showed that the sulfidisation and collector requirements for the three sulfide minerals (pyrrhotite, pentlandite and chalcopyrite) appeared to be different, particularly for oxidised pentlandite.

No process is known that uses gaseous carbon dioxide as a surface active reagent to improve the hydrophobic character of the oxidised sulfide minerals’ ore surface or clean the oxidised ore surface. Therefore, it was also the aim of this study to investigate the influence of gaseous carbon dioxide on the electrochemical and flotation response of oxidised pyrrhotite using electrochemical measurements and microflotation tests.

3. RESEARCH PROBLEM AND OBJECTIVES

Literature was reviewed (in *Section 2*) to give an overview of pyrrhotite, including: the mineralogy of PGE containing ores, characteristics of pyrrhotite and factors affecting its floatability, as well as electrochemical measurements on pyrrhotite. It was found that the PGE dominant and Cu-Ni dominant ore bodies have a different sulfide content. There are variations in the chemical composition of pyrrhotite from various ore bodies and within the same ore deposit. Most of the work by various authors (Buswell and Nicol. 2002; Khan and Kelebek, 2004) has been done on natural sulfide mineral samples of high purity sourced from mineral dealers or locations where specimens in massive form are available.

Unfortunately, relatively pure, massive samples cannot be obtained from the Bushveld Igneous Complex mining operations and no electrochemical work has been done on the Bushveld Igneous Complex ore deposits. The effect of compositional variation and crystal structure of natural pyrrhotite on its electrochemical behaviour has not yet been investigated. Studies by Khan and Kelebek (2004) and Buswell and Nicol (2002) on the decomposition of pyrrhotite showed that pyrrhotite sourced from South Africa is much more reactive than the sample sourced from the Sudbury region in Canada. The chemical composition of the pyrrhotite samples studied was not provided.

This project was aimed at understanding the electrochemical behaviour of pyrrhotite from various ore deposits, using electrochemical measurements such as rest potential and polarisation resistance measurements, as well as anodic and cathodic polarisation diagrams on pyrrhotite electrodes. It was also the aim of this project to determine whether variations in chemical composition and crystal structure of pyrrhotite affect its electrochemical behaviour (i.e. reactivity, oxidation) and flotation response.

Pyrrhotite is easily oxidised and this results in its slow and poor flotation. Surface oxidation of sulfide minerals, such as that found in the regions of a sulfide ore body near the water table, can have a significant impact upon flotation.
There are various chemical and mechanical methods that can be used to remove the surface oxidation products. Chemical methods include: dissolution, by lowering the pH; cupric ion activation; treatment with ethylene diamine tetra-acetate (EDTA); and sulfidisation.

Mechanical methods include: milling; sonication; and attritioning with quartz. These methods have proved to achieve some success in removing the surface oxidation products on minerals; however they have been shown to have limitations. Gaseous carbon dioxide conditioning of coal, prior to coal flotation, has been reported by Miller and Misra (1987) to produce “super” clean coal and the process was deemed applicable to various grades and types of coal.

No process is known that uses gaseous carbon dioxide as a surface active reagent to improve the hydrophobic character of the PGE oxidised ore surface or to clean the PGE oxidised ore surface.

Another focus of this study was to investigate the influence of gaseous carbon dioxide conditioning on the electrochemical behaviour and flotation response of oxidised pyrrhotite, using the above-mentioned electrochemical techniques and microflotation tests.

4. EXPERIMENTAL PROCEDURE

Brief descriptions of the experimental methods used to meet the objectives of the present study are presented in this section. Electrochemical measurements were employed to determine the effect of compositional and crystal structure variations of pyrrhotite, electrical contact with pentlandite and gaseous carbon dioxide conditioning on its electrochemical behaviour in the absence and presence of reduced oxygen and xanthate. Micro-electrodes and massive pyrrhotite electrode samples used in the electrochemical studies were sourced from various locations within the Bushveld Igneous Complex and Mponeng mine in South Africa and Russia. Microflotation measurements were used to study the influence of gaseous carbon dioxide conditioning on the flotation response of oxidised pyrrhotite. The sample used in the microflotation tests was sourced from Russia.

4.1. Sample preparation

4.1.1. Micro-electrodes

One of the aims of this study was to investigate the influence of chemical composition, crystal structure and source of pyrrhotite on its electrochemical behaviour and the extent to which these factors affect pyrrhotite electrochemical response. It was also the aim of this study to determine whether the information obtained could be used in order to predict the processing behaviour of pyrrhotite from a new ore deposit or area of the mine in the Bushveld Igneous Complex. It was decided, therefore that pyrrhotites sourced from different reefs in the Bushveld Igneous Complex would be compared. Samples sourced from various reefs within the Bushveld Igneous Complex were selected, so as to ensure a variation in chemical composition and crystal structure. It has been reported that ores from different areas of the same mine can have quite different characteristics (http://www.bullion.org.za). By understanding the electrochemical behaviour of pyrrhotite it would be possible to predict the flotation response of pyrrhotite from the Bushveld Igneous Complex. This would enable the process to be manipulated so as to improve pyrrhotite flotation.

Unfortunately, relatively pure, massive samples cannot be obtained from the Bushveld mining operations. The grain size of the base-metal sulfides in the Merensky ore (from the Western limb of the Bushveld Igneous Complex) is about 40 to 50 µm (Dunne, 2007). Clusters of base-metal sulfides in which PGMs in the Merensky reef (from the Amandebult section of Rustenburg Platinum mine) are generally contained, are relatively large (> 1 mm) (Viljoen *et al.*, 1986). As a result, concentrates from the various reefs in the Bushveld Igneous Complex were used in this study. Concentrate samples of the Bushveld Igneous Complex deposits chosen for this study were obtained from:

- Lebowa Merensky Reef
- Lebowa UG-2
- Platreef: three composites (composites A, B and C) from different levels were chosen since it has been reported that pyrrhotite composition varies with depth (Mostert, 1982)

Lebowa samples were considered an easier option of getting sulfides. It has been reported that cumulative amount of sulfides in the Merensky reef of the eastern Bushveld Complex is a factor of 5 to 10 times greater than that encountered in the more common reef types (http://arkisto.gtk.fi/ej/ej49_backups/ej49_pages_258_260.pdf).

Concentrates were sieved with 150, 106, 90, 75 and 63 µm sieves. The +106 µm size fraction was chosen for the electrochemical measurements; the coarser the particles the easier and better the chances of picking pyrrhotite particles because finer particles are easily broken and aggregate onto the glass rod used to pick particles. Using the sheets of paper, the particles were placed onto a microscope glass and examined with an optical microscope. Particles (i.e. shiny, yellow and bronze particles) were hand-picked and attached to carbon tape under an optical microscope. Scanning electron microscopy (Jeol JSM 6300), coupled with energy-dispersive X-ray analysis (EDX) (Noran System), was employed as an aid to pyrrhotite identification. Quantitative EDX analysis was carried out on the particles; the elements analysed were Fe and S. Particles with a molar Fe to S ratio close to 1 were identified as pyrrhotite. Impurities such as Ni, Co and Cu were not taken into account due to their small quantities and because quantitative EDX analysis gives a rough estimation of composition. Electron microprobe analysis was employed to obtain accurate chemical compositions.

Particles in the concentrates are fine (micron size), therefore micro-electrodes were prepared and employed in studying the influence of compositional variations of pyrrhotite from the Bushveld Igneous Complex on pyrrhotite reactivity.

Electrical contact with a pyrrhotite particle was achieved using a 50 µm tungsten wire cemented to a 0.5 mm copper wire. It should be noted that the diameter of the tungsten wire is dependent on the bottom size limit of the sulfide particles; smaller particles require thinner wires. The two wires were cemented using silver dag (Acheson Electrodag 1415M, silver in Methyl Isobutyl Ketone) and the wire assembly was left to dry overnight.

Following drying, conductive silver epoxy was used to create an electrical contact between the tungsten wire and the pyrrhotite particle. The tip of the small wire was dipped in conductive silver epoxy by using a micromanipulator (shown in *Figure 20*) fitted to an optical microscope. After dipping the tip, the small tungsten wire was brought into contact with the sulfide particle using a micromanipulator.

Figure 20: Micromanipulator (http://products.narishige-group.com).

Particles were carefully cemented at the bottom-end, along the longest axis, to ensure good exposure during polishing, without running the risk of exposing the wire and silver epoxy. The wire assembly containing the particle was left to cure overnight and was then cured at 40 °C for 10 minutes in an oven to achieve maximum conductivity and adhesion. The particle-wire assembly was embedded in a mounting epoxy (Epofix resin and hardener at 15 parts of resin: 2 parts of hardener by volume) using 30 mm outside diameter and 20 mm inside diameter "Plexiglas" Acrylic tubes, with the copper-end of the wire arrangement protruding from the tube. The resin and hardener mixture was first heated at 40 °C in an oven to remove any bubbles, prior to mounting to prevent bubbles forming around the particles. If bubbles had formed around the particle after polishing, the exposed area would not have been easy to measure and the wire and silver epoxy might have been exposed, which would have contributed to the current readings obtained, resulting in erroneous measurement. The particle might easily have broken off of the wire during polishing if bubbles had formed around the particle. The resin was left to cure overnight.

The resin was then polished away using silicon carbide (SiC) papers to expose the particle and an optical microscope was employed to investigate the surface for exposure of the particle. P-1200 grit SiC paper was used to expose the particle. The moment a very small area (measuring a few microns in diameter) was exposed, a 2400 grit SiC paper was used to slowly expose the mineral surface further and to obtain a flat surface. Very slow polishing is required to ensure that the epoxy does not break away from the edges of the particle. An optical microscope was continuously employed to monitor the progress during polishing. Scanning electron microscopy (Jeol JSM 6300), coupled with energy-dispersive X-ray analysis (EDX) (Noran System), was employed as an aid to pyrrhotite identification. Quantitative EDX analyses was carried out on the exposed particle surface and the elements analysed for were Fe and S. Particles with a molar Fe:S ratio close to 1 (one) were identified as pyrrhotite. Analytical conditions were: 15 keV accelerating voltage; a beam current of 3 nA; a working distance of 20 mm; and counting time of 100 seconds. A $\phi(\rho Z)$ matrix correction procedure was applied to the raw data.

To obtain a flat and smooth surface (as shown in *Figure 21*) for electron microprobe analysis and electrochemical measurement, final polishing was done on the Struers Rotopol-11 polishing machine, obtained from IMP Scientific Precision Company, using a Daran cloth (with a 6 µm diamond suspension), followed by the MDNap polishing cloth (using a 1 µm

diamond suspension). The Daran and MDNap polishing cloths were supplied by Advanced Laboratory Solutions and IMP Scientific Precision Company, respectively.

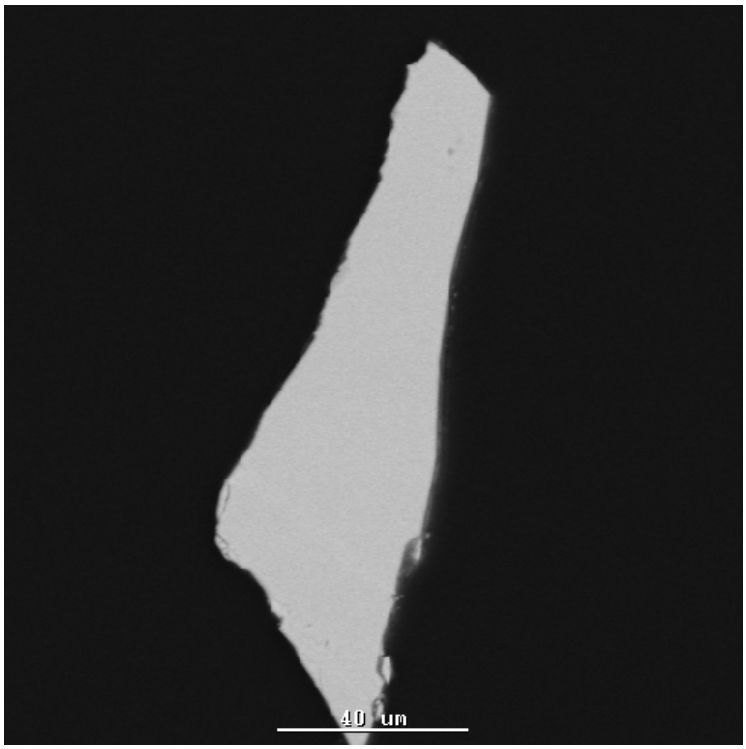

Figure 21: Back-scattered electron image of a polished pure pyrrhotite micro-electrode at an accelerating voltage of 15 keV.

4.1.2. Massive electrodes

Pure massive pyrrhotite samples were sourced from other locations so as to compare the electrochemical behaviour of these pyrrhotites to pyrrhotite from the Bushveld Igneous Complex. The massive samples used in the test work were sourced from:

- Mponeng mine, South Africa
- Two pyrrhotites, sourced from Russia, were purchased from Ward's Natural Science Establishment. One was obtained from Dalnegorsk and the exact area from which the other sample was obtained could not be determined.
- Sudbury ore deposit in Canada, from the Gertrude mine
- Pyrrhotite from Tati Nickel mine in Botswana was sourced from the Phoenix deposit.

The Sudbury and Phoenix samples were obtained from the University of Cape Town. The Mponeng and Russian samples are pure and were used to investigate the influence of chemical composition and crystal structure on the electrochemical response of pyrrhotite. The Sudbury and Phoenix samples are not pure (i.e. pyrrhotite mixed with other sulfide and non-sulfide minerals) and were employed in the investigation of the influence of galvanic interactions of the electrochemical behaviour of pyrrhotite.

A dremel tool was used to drill out the pyrrhotite grains from massive sample rocks. The SiC papers were used to grind away any of the visible phases, such as oxides and other sulfide minerals. A similar procedure to that of micro-electrode preparation was followed. In the case of massive samples, electrical contact between a pyrrhotite particle and a 0.5 mm copper wire was achieved using conductive silver epoxy. The massive particles did not require a micromanipulator and tungsten wire.

Figure 22 shows images of the pure and mixed massive pyrrhotites after polishing. In this document, pyrrhotite from the unknown mine deposit in Russia will be referred to as Russia_1; the sample from Dalnegorsk will be referred to as Russia_2.

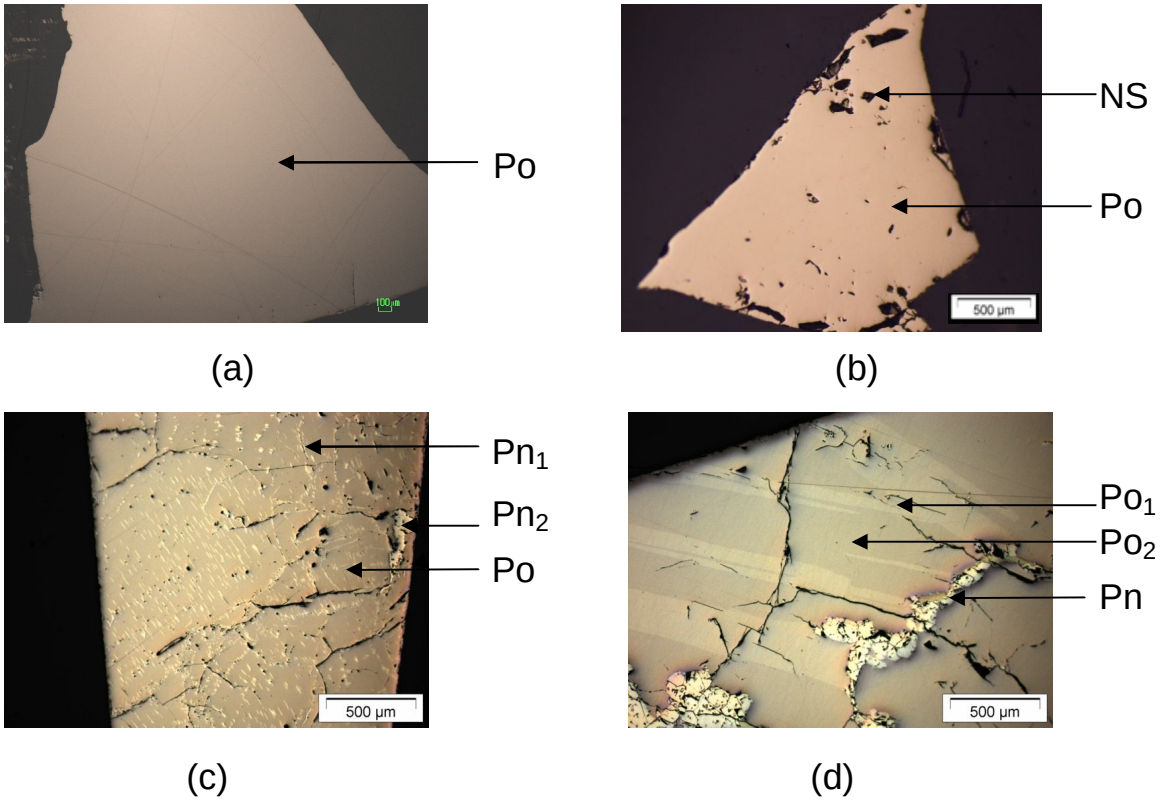

Figure 22: Back-scattered electron images of massive pyrrhotite electrodes after polishing from: (a) Russia_1 (Po: pure pyrrhotite); (b) Russia_2 (NS: non-sulfide mineral, Po: pyrrhotite); (c) Phoenix deposit (Pn_1: flame pentlandite lamellae, Pn_2: granular pentlandite, Po: pyrrhotite); (d) Sudbury Gertrude mine (Pn: granular pentlandite, Po_1 and Po_2: twinning in pyrrhotite).

It is evident in *Figure 22* that: the Russia_1 sample was pure; the Russia_2 sample had non-sulfide minerals embedded into the pyrrhotite. Both the Phoenix and Sudbury Gertrude samples had pentlandite in contact with pyrrhotite and cracks. It was difficult to obtain a pure pyrrhotite sample from these deposits. The Sudbury Gertrude sample had larger pentlandite grains than the Phoenix sample; the volume fraction of pentlandite in contact with pyrrhotite was lower in the Sudbury Gertrude sample.

4.3. Electron microprobe analysis

The exact chemical composition of all the pyrrhotite grains was determined using electron microprobe analysis. Electron microprobe analyses were carried out with a Cameca SX-100

electron microprobe at the Geology Department of the University of Pretoria. Pyrrhotite grains were analysed for Fe, S, Ni, Co and Cu. The standards used were the following: troilite for S and Fe; nickel oxide for Ni; cobalt metal for Co; and chalcopyrite for Cu. The electron microprobe was operated at an acceleration potential of 20 kV with a beam current of 20 μA. Counting times for Fe, Ni, Co and Cu were 20 seconds and 10 seconds for S. The number of spots analysed on each pyrrhotite particle was limited by the particle size. Three spot-analyses were performed on each pyrrhotite particle. To minimise any analytical error in the analyses, all pyrrhotite particles were analysed employing the same electron microprobe calibration.

4.4. X-ray diffraction (XRD) analysis

Powder XRD (X-ray diffraction) analysis, is the most widely used X-ray technique for characterising materials. It is used to characterise the crystallographic structure, crystallite size and preferred orientation in polycrystalline or powdered solid samples. Powder diffraction is commonly used to identify unknown substances, by comparing diffraction data against a database maintained by the International Centre for Diffraction Data. It may also be used to characterise heterogeneous solid mixtures to determine relative abundance of crystalline compounds and, when coupled with lattice refinement techniques, such as Rietveld refinement, can provide structural information on unknown materials. The XRD pattern is a direct representation of the structure, both of which are unique.

The mineralogy of the massive pyrrhotite samples, mentioned earlier in *Section 4.1,* was determined using powder X-ray diffraction. This was done to identify the crystalline phases, the amount of minerals present and crystal structures of pyrrhotite grains used in this study. The samples were prepared for XRD analysis using a universal sample holder. The samples were analysed with a PANalytical X'Pert PRO powder diffractometer with X'Celerator detector and variable divergence and receiving slits with Fe filtered Co-Kα radiation. The machine was operated at 35 kV, 50 mA and 25 °C. Pyrrhotite grains were analysed at the Geology Department of the University of Pretoria. The phases were identified using the PANalytical Highscore Plus software (incorporated into the PANalytical X'Pert PRO powder diffractometer). Mineral quantification was done using the Autoquan software (BGMN® program), which uses the fundamental parameters approach for the quantification of phases

using few parameters. The experimental XRD pattern is compared to the calculated one. The Rwp factor is an indication of the correspondence between the experimental and the calculated XRD patterns. In addition to the XRD spectrum, the difference plot (between the experimental and the calculated XRD patterns) is also obtained, as it helps in the following ways:

- To detect the presence of unexpected phases
- To detect errors in zero error, lattice parameters
- To discover errors in structure parameters
- To detect refinements where crystallite size is unreasonably small, usually with minor phases, and
- To identify preferred orientation.

Electron microprobe analyses indicated that the Mponeng pyrrhotite is a 6C type pyrrhotite. A comparison of the calculated powder diffraction patterns of the 5C and 6C structures showed that the diffraction patterns are almost the same suggesting that conventional X-ray powder diffraction methods cannot be employed for distinction and quantification of the two NC pyrrhotites. As a result, a single-crystal X-ray method was employed to characterise the crystal structure of the Mponeng pyrrhotite. A detailed procedure for characterisation of the Mponeng pyrrhotite has been reported by De Villiers and Liles (2010). A summary of how the Mponeng pyrrhotite was characterised is as follows: The unit cell was determined and diffraction data were collected using the *Fd* setting suggested by Koto *et al.* (1975) to retain the metrically orthorhombic setting. The cell symmetry is monoclinic with dimensions a = 6.897(2), b = 11.954(3), c = 34.521(7), and with β = 90.003(4)°. The structure has been refined with anisotropic displacement parameters to R = 0.029 using 1493 observable reflections with $I > 2\sigma(I)$ and R = 0.034 for all 1800 reflections. The internal R_{int} is 0.023 for the symmetrically equivalent reflection data. The crystal structure resembles that of the 5C pyrrhotite in that the atomic positions of the Fe and S atoms are arranged in a very similar fashion, the only real difference being the arrangement of partially occupied iron sites. The coordination of the iron atoms is octahedral and short Fe-Fe distances along the *c*-axis are also encountered in this structure.

The vacancy distribution is similar to that postulated by Koto *et al.* (1975) and is characterised by the stacking of two approximately half-occupied sites, followed by an essentially fully occupied layer. This is however a simplification and results in a composition

that is too metal-rich. Two other slightly defect sites with occupancies of 0.90 and 0.87 are also present in the structure, and all layers contain both fully occupied and partially occupied sites. Refinement of the occupancies of all these sites gives rise to an atomic distribution that resembles the measured composition most closely, and is refined as $Fe_{10.99}S_{12}$.

4.5. Qemscan

Qemscan uses a combination of back-scattered electron (BSE) contrast and EDS (energy dispersive spectroscopy) analysis to identify the minerals present in a sample and a particle/phase size and surface area. Pyrrhotite and impurities such as pentlandite on the exposed mineral surfaces were quantified using Qemscan (QEMSCAN E230 Evo) from Anglo American Research.

The SEM part of the instrument is made by Zeiss. It is fitted with Bruker detectors and the software was developed by Intellection. The samples were analysed at 25 kV using a BMA (Bulk modal analysis) measurement mode, which is a line scan method. The Qemscan line scan technique uses X-ray point analysis on a grid system. Each mineral phase gives off unique elemental intensities. It is these elemental intensities that are used to classify a particular mineral. Therefore an X-ray is collected for a point, which gives elemental intensities. The intensities are then compared to a previously established database and a mineral is classified.

4.6. Electrochemical measurements

As mentioned earlier in *Section 2.2.3.1*, oxygen is the ultimate oxidant of sulfide minerals in natural surface waters and the direct oxidant at pH > 4, while ferric iron oxidises sulfides at pH < 4 (Nordstrom and Alpers, 1999). These two oxidants are the most important for pyrrhotite (Lowson, 1982; Bierens de Haan, 1991; Belzile *et al.*, 1997a).

In this study, the oxidation of the sulfide mineral (i.e. pyrrhotite) is treated as the anodic reaction, with oxygen as the main oxidant. The reduction of oxygen is the cathodic reaction.

According to Nicholson and Scharer (1994), when O_2 is the primary oxidant, the oxidation reaction can proceed as follows:

$$Fe_{1-x}S + (2-0.5x)O_2 + xH_2O \Rightarrow (1-x)Fe^{2+} + SO_4^{2-} + 2xH^+ \qquad \textbf{\textit{Eq. 24}}$$

If pH is not too low, the oxidation of ferrous iron produces ferric ions that can precipitate out of the solution to form ferric hydroxide.

Fe^{2+} is oxidised and precipitated as ferric oxyhydroxides, mainly ferrihydrite and goethite, as follows:

$$Fe^{2+} + 1/4O_2 + 2H^+ \Rightarrow Fe^{3+} + 1/2H_2O \qquad \textbf{\textit{Eq.25}}$$

$$Fe^{3+} + 3H_2O \Rightarrow Fe(OH)_{3(s)} + 3H^+ \qquad \textbf{\textit{Eq. 26}}$$

The cathodic reduction reaction (i.e. reduction of oxygen) is shown in the following reaction:

$$0.5O_{2(abs)} + H_2O + 2e^- = 2OH^- \qquad \textbf{\textit{Eq. 27}}$$

In the presence of xanthate, the oxidation reaction that takes place is the oxidation of xanthate to dixanthogen:

$$2X^- = X_2 + 2e^- \qquad \textbf{\textit{Eq. 28}}$$

Possible reactions taking place at the pyrrhotite surface were shown previously (*Section 2.2.4.*).

The main experimental advantage of the electrochemical nature of the reactions is that the reactions can be tracked by electrochemical techniques such as potentiodynamic measurements and impedance measurements (Vermaak *et al.* 2004). As a result, potentiodynamic measurements were undertaken with the aim of determining the possible interactions between oxygen, xanthate and pyrrhotite electrodes.

4.6.1. Rest potential and polarisation resistance (Rp) measurements

These electrochemical measurement techniques were employed in studying the oxidation and reduction characteristics of pyrrhotite. The Rp values represent the resistance of the surface layer to the flow of electrical current (i.e. it indicates the ease or difficulty with which the different pyrrhotites can oxidise and form non-conductive layers of oxides and hydroxides). A higher Rp indicates that the mineral is more reactive (i.e. easily oxidised) and has a thick surface product layer.

4.6.1.1. Rest potential

This is the potential which an electrochemical system will naturally approach if no external voltage is applied. A mineral with a lower rest potential is more anodically reactive than a mineral with a higher rest potential.

4.6.1.2. Polarisation resistance

The polarisation resistance technique is mainly used in corrosion applications. Polarisation methods to measure corrosion rates have inherent advantages. Usually only a few minutes are required to determine the rate of corrosion by polarisation resistance. The methods are highly sensitive and accelerating factors, such as elevated temperature, to increase rates in the laboratory, are usually unnecessary (Jones, 1999). Polarisation measurements are non-destructive and may be repeated numerous times to measure consecutive corrosion rates on the same electrode (Jones, 1999).

Polarisation resistance, defined as the slope of the polarisation curve at the origin, is independent of the degree of linearity.

$$Rp = [dE/d_{i_{app}}]_{E\rightarrow 0} = [\Delta E/\Delta i_{app}]_{E\rightarrow 0} \qquad \textit{Eq. 29}$$

Where E = potential (V)

i_{app} = current (A)

The slope $[dE/di_{app}]_{E\rightarrow 0}$, is inversely proportional to the corrosion rate. If a potentiodynamic scan is applied, the necessary current, i_{app}, follows the controlled voltage and the polarisation resistance curve can be plotted automatically. *Figure 23* shows a typical polarisation resistance curve obtained potentiodynamically.

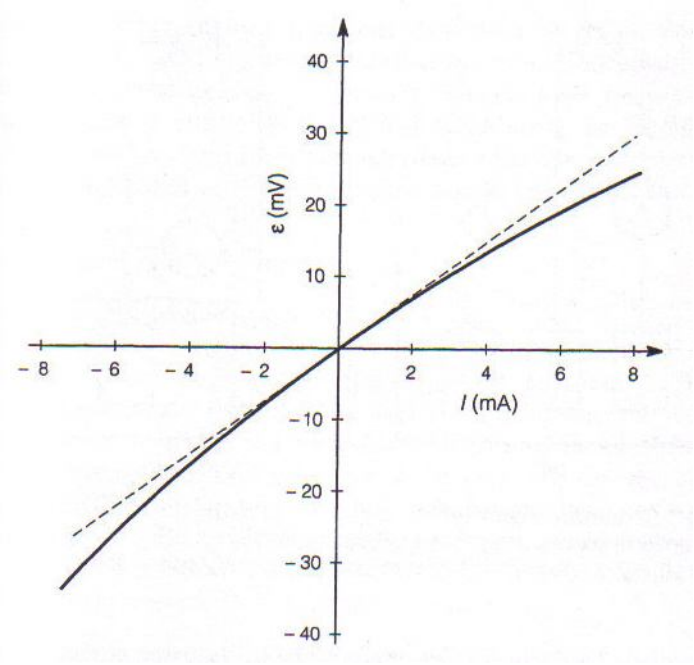

Figure 23: Polarisation resistance curve generated potentiodynamically (Jones, 1996).

The Rp_time program (timed polarisation resistances) was used to obtain Rp measurements in this study. The program works in such a way that if a potentiodynamic scan is applied, current versus potential data is obtained and a polarisation resistance curve can be plotted. As a result, Rp and rest potential measurements are simultaneously obtained as a function of time instead of a single Rp value. The polarisation resistance and rest potential were obtained by scanning at 10 mV/s positive and negative voltage direction from rest potential. Total duration was 40 minutes. Current versus rest potential data was obtained and this current was then converted to current density by dividing by the area of the pyrrhotite particle, which is estimated by using the imaging software (Image Tool™). A typical current density versus rest potential curve is shown in *Figure 24*. Polarisation resistance was determined using the equation:

$$Rp = [\Delta E/\Delta i_{app}] \qquad \textbf{\textit{Eq. 30}}$$

Three slopes (Δi/Δpotential) were obtained, two from the top two horizontal lines and one from the bottom horizontal line. An inverse of the average of the three slopes was taken as the Rp for that specific time. The rest potential was obtained by averaging the potentials where the current density is zero on either side of the curve.

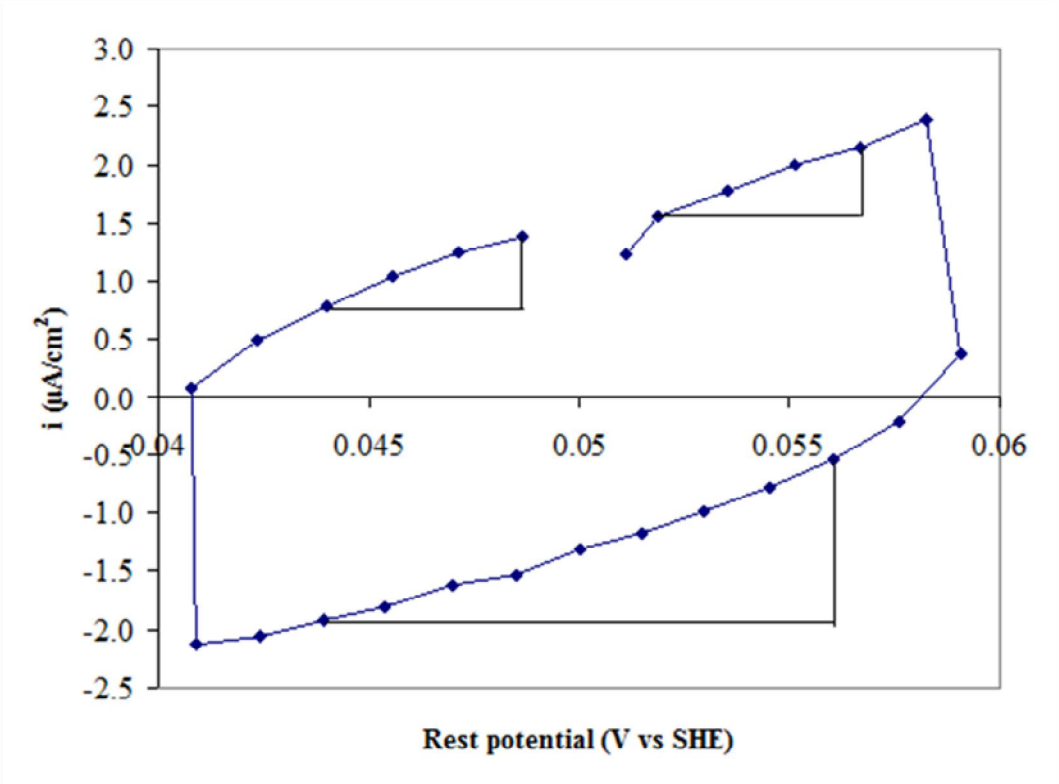

Figure 24: Polarisation resistance curve generated potentiodynamically in an oxygen-saturated 0.05 M borate solution at a pH of 9.3 with a scan rate of 10 mV/s. Slope = $\Delta y/\Delta x = \Delta i/\Delta E$ = change in current density/change in rest potential = Rp (polarisation resistance).

In this study, the Rp value is related to the oxidation of the mineral. An increase in Rp indicates the formation of a layer on the surface and that the mineral is reactive (i.e. easily oxidised). The change in Rp on the mineral surface is given as a function of time.

The electrochemical set-up employed involved: a standard three-electrode cell using a pyrrhotite electrode as the working electrode, two inert platinum counter electrodes and Ag/AgCl electrode as the reference electrode. In all experiments, the working electrode was

in suspension and kept stationary. A schematic diagram of the experimental set-up that was used for electrochemical measurement studies is shown in *Figure 25.*

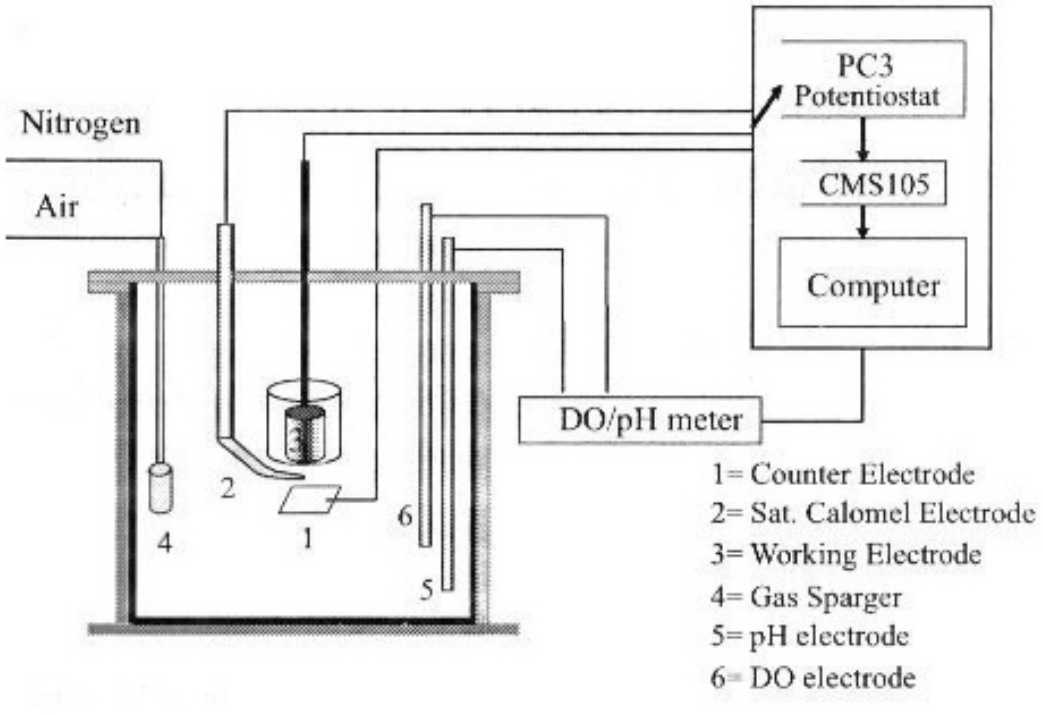

Figure 25: A schematic diagram of the experimental set-up for cyclic voltammetry and rest potential experiments (Khan and Kelebek, 2004).

Potentials were measured against an Ag/AgCl reference electrode filled with saturated KCl, which has a potential of +0.20 V on the standard hydrogen electrode (SHE) scale. Two platinum electrodes fitted in glass tubes, which were closed with porous glass discs at the ends, were placed at equal distances from the working electrode for better current distribution. Experiments were conducted at 25 °C (± 1 °C) in a 0.05 M sodium tetraborate ($Na_2B_4O_7.H_2O$) solution, which was used to buffer the solution at a pH of 9.3. The borate solution is often used for electrochemical measurements because of its high conductivity and its pH-buffering capacity. Solutions were prepared using distilled water with a final resistivity of 18 MΩ.cm. The scans were recorded with a Schlumberger 1287 potentiostat.

For each experimental run, the pyrrhotite surface was wet-ground using 2400 grit SiC paper and 0.05 µm Micropolish Alumina-B suspension. This was followed by wet-polishing with an MDNap polishing cloth and 0.05 µm Micropolish Alumina-B suspension. Distilled water was used to rinse the surface. Measurements were recorded after the open-circuit potential

was allowed to stabilise for two minutes. To de-aerate the solution, nitrogen gas (99.99 %) was used. The solution was replaced between runs to avoid contamination. Purified potassium ethyl xanthate (KEX) (at 10^{-3} M) was the collector of choice for the electrochemical measurements because it is most frequently used in fundamental studies involving functional groups and surfaces (Vermaak, 2005).

The potential and scan rate were set on the potentiostat and the response of current to the potential was measured and recorded by a potentiostat. Current flowed from the potentiostat to the working electrode. It was then carried from the electrolyte by counter electrodes (i.e. inert platinum electrodes) back to the potentiostat to complete the circuit. This current was then converted to current density by dividing by the area of the pyrrhotite particle. The area estimations were performed by taking digital images and using imaging software (Image Tool^{TM}) on the images.

An oxygen probe was employed to measure the amount of dissolved oxygen before taking electrochemical measurements. For the Rp measurements, a scan rate of 10 mV/s was used.

4.6.2. Electrochemical impedance spectroscopy (EIS)

This technique was used to complement the polarisation resistance technique. According to Craig (1991), the capacitance is given by:

$$C = 1/(2\pi Rpf) \qquad \textit{Eq. 31}$$

The thickness of such a film can then be calculated by the relation:

$$t = A\varepsilon/C \qquad \textit{Eq. 32}$$

where C = capacitance (F)
Rp = polarisation resistance (Ω)
f = frequency (Hz)
t = surface film thickness (m)
A = electrode area (m^2)
ε = dielectric constant ($F.m^{-1}$)

These equations show that capacitance is inversely proportional to polarisation resistance and the film thickness, implying that the formation of a surface film will be indicated by low capacitance and high Rp values. In this study, the oxidation of pyrrhotite is treated as the corrosion reaction (i.e. anodic reaction) in the absence of xanthate. The reduction of oxygen is the cathodic reaction. Impedance measurements are based on the modelling of an electrode in solution as an electronic circuit containing resistors, capacitors and inductors. A simplified circuit is shown in *Figure 26*, with a resistor in series and with a parallel circuit containing a capacitor and resistor.

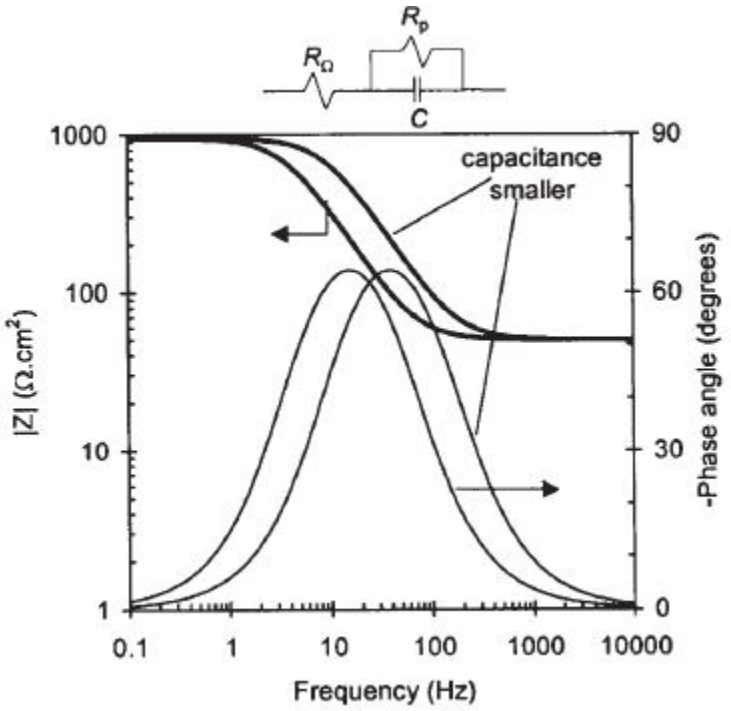

Figure 26: Equivalent circuit of a metallic electrode in a solution showing the different components. Also added is a Bode plot of the impedance as a function of the frequency. The effect of a decrease in capacitance is shown in the Bode plot drawn for: R_Ω = 50 Ω.cm^2, Rp = 900 Ω.cm^2 and C = 50 µF/cm^2 or 20 µF/cm^2; Z = impedance. (Vermaak *et al.*, 2004)

The same electrochemical set-up, involving a standard three-electrode cell, used for the polarisation resistance measurements and operating conditions (as described in *Section 4.6.1*) was also employed for the EIS measurements. The measurements were carried out at a frequency of 120 Hz and a potential of 0.20 V (SHE). The oxygen-saturated 0.05 M tetraborate solution was used in all the experiments. Prior to transferring the electrode to the

electrochemical cell, the electrodes were polished using the method described earlier in *Section 4.6.1*. The electrodes were then rinsed thoroughly with distilled water and immediately transferred to the cell to minimise air oxidation. The measurements were done in triplicate and the results were reproducible.

4.6.3. Anodic polarisation diagrams

Anodic scans were used to investigate the oxidation behaviour of different pyrrhotites in the absence and presence of xanthate. Anodic scans were recorded in a de-oxygenated 0.05 M sodium tetraborate solution buffered at pH 9.3. The solution was de-aerated with nitrogen prior to measurements being taken by sparging nitrogen gas (with 99.99 % purity) in solution for an hour to a dissolved oxygen concentration of about 0.05 ppm. In the absence of xanthate, immediately after deoxygenating the solution and polishing the electrode (as described earlier), the electrode was transferred to the cell in order to minimise surface oxidation. Measurements were recorded after the open-circuit potential was allowed to stabilise for two minutes. Anodic scans were recorded by changing the potential from 50 mV negative of the mineral's rest potential to oxidising potentials (i.e. positive potentials). The maximum potential chosen for this study was 0.60 V (SHE) and a scan rate of 10 mV/s.

Purified potassium ethyl xanthate was used in all the experiments at a constant concentration of 10^{-3} M. KEX was purified by dissolving it in acetone, filtering the solids and evaporation of the acetone in a vacuum (De Wet *et al.*, 1997). After sparging nitrogen for an hour into the solution, the desired amount of xanthate was added into the cell and nitrogen sparging continued for another five minutes to allow efficient mixing of the collector with the solution. The reactivity of pyrrhotites can be compared and reactions which take place on the surface and on subsequent products can be deduced from the type and position of peaks on the anodic scans. Reproducible measurements of the anodic scans were obtained.

4.6.4. Current density-time transients

To verify the reactivity results obtained via polarisation resistance measurements and anodic scans, current density-time transients' response to a step in electrode potential from rest

potential to 0.25 V (SHE) in a de-oxygenated 0.05 M sodium tetraborate solution buffered at pH 9.3 were recorded for 10 minutes. This was done under similar conditions as the anodic scans in the absence of xanthate. Reproducible measurements of the current density-time curves were obtained.

4.6.5. Cathodic polarisation diagrams

Cathodic scans were used to study the oxygen reduction characteristics/activity of pyrrhotite. Oxygen reduction on the mineral surface is an important step in xanthate adsorption. The knowledge of the electro-catalytic activity for oxygen reduction is helpful in understanding differences in flotation rates between different minerals and ultimately in improving flotation performance (Rand, 1977). To obtain cathodic scans, an oxygen-saturated 0.05 M sodium tetraborate solution buffered at pH 9.3 was used. The dissolved oxygen concentration of the solution (with no bubbling of gas) was measured at around 5.5 ppm with a dissolved oxygen probe at 25 °C. The presence of oxygen is a requirement in obtaining cathodic scans. The electrodes were polished (as described earlier) before being transferred to the cell. Scanning started from 50 mV positive of the mineral's rest potential to reducing potentials (i.e. negative potentials). The minimum potential selected for this study was - 0.40 V (SHE) and a scan rate of 1 mV/s.

Results from the electrochemical measurements will help in: understanding the electrochemical behaviour of pyrrhotite in terms of its chemical composition, crystal structure and electrical contact with pentlandite; predicting its processing behaviour.

4.7. ToF-SIMS

Time-of-flight secondary ion mass spectrometry (ToF-SIMS) is one of the most surface sensitive and the most versatile of the surface analysis techniques. It provides a powerful combination of capabilities for molecular detection of organic films and contaminants, trace element determination, imaging and microanalysis and shallow depth profiling (http://serc.carleton.edu/research_education/geochemsheets/techniques/ToFSIMS.html).
During shallow sputter depth profiling, an ion gun is operated in the DC mode during the

sputtering phase in order to remove material, and the same ion gun or a second ion gun is operated in the pulsed mode for acquisition phase. Depth profiling by TOF-SIMS allows monitoring of all species of interest simultaneously, and with high mass resolution. (http://www.phi.com/surface-analysis-techniques/TOFSIMS.html).

This technique complements the polarisation resistance and capacitance measurements in the sense that it can show (confirm) the presence of a surface film; a depth profile of the surface film can be obtained, which indicates the thickness of the surface film. ToF-SIMS was used to examine the mineral surface and the surface oxidation by obtaining a depth profile and images of a polished, oxidised and CO_2 treated pyrrhotite surface. IONTOF ToF-SIMS at the National Metrology Laboratory (NML) at the CSIR was used to analyse the samples. The oxidised and CO_2 treated pyrrhotite surfaces were removed from the solution and dried before mounting in the spectrometer. Approximately 3minutes exposure to air occurred before evacuation in the fore-vacuum of the instrument. A high vacuum of 10^{-9} to 10^{-10} torr was used. TOF-SIMS was used in static negative ion mode with the pulsed bismuth beam at currents between 70 and 100 nA and an energy of 25 keV into a 300 x 300 μm^2 area at an angle of 45°. The secondary ions were accelerated using an extraction potential of 2 keV. The negative secondary ion mass spectrum was determined.

ToF-SIMS assisted in showing the formation of an oxide layer on the surface. It should be noted that ToF-SIMS results cannot be directly compared to the electrochemical measurements; because during electrochemical measurements, the electrodes are kept in the solution throughout the measurements and taken out of the solution after the tests have been completed. Prior to transferring the samples to the ToF-SIMS equipment, samples are taken out of the solution and dried. This causes the samples to react with oxygen in the atmosphere, which affects the surface. As pointed out by Debnath and Anderson (1982), many *ex situ* investigations of passive layers suffer from the disadvantage that loss of water and film restructuring occur under high vacuum conditions, the situation being further exacerbated by ion beam heating.

4.8. Gaseous carbon dioxide cleaning of oxidised pyrrhotite

Pyrrhotite is easily oxidised and this results in a poor flotation response and subsequent loss of valuable minerals associated with it. Various chemical and mechanical methods have previously proved successful in removing the oxidation products on the different sulfide minerals from various ore bodies. Gaseous carbon dioxide conditioning of coal for froth flotation was reported by Miller and Misra (1987) to result in less reagent promoter and frother requirements; this reduced flotation time and the process produced “super” clean coal. The use of gaseous carbon dioxide conditioning on oxidised PGE ores has not been done before, thus it was the aim of this study to investigate the effectiveness of this process on cleaning oxidised pyrrhotite, which is known to oxidise easily and form surface hydroxides. The experimental programme presented below was used to investigate the influence of CO_2 conditioning on the electrochemical and flotation behaviour of heavily oxidised pyrrhotite.

4.8.1. Sample

The massive pyrrhotite electrodes from Russia and Mponeng ore deposits were used in the CO_2 test work. These samples were found to have different chemical compositions and crystal structures by means of electron microprobe analysis and XRD analysis. The samples were used with the aim of determining how each of the samples would behave following treatment with gaseous carbon dioxide.

4.8.2. Electrochemical measurements

Electrochemical measurements, such as the rest potential, polarisation resistance measurements as well as anodic scans, were used to investigate the influence of gaseous carbon dioxide conditioning on the flotation response of heavily oxidised pyrrhotite. The electrodes were oxidised for an hour in an air-saturated tetraborate solution buffered at pH 9.3 and a dissolved oxygen concentration of 5.5 ppm in order to make sure the electrode surfaces were completely oxidised. Then CO_2 was sparged into the solution for an hour and the pH dropped to values between 6.60 and 6.80. The effect of CO_2 was investigated by monitoring the rest potential and polarisation resistance measurements as well as anodic

scans of the pyrrhotite surface. The polarisation resistance of the freshly polished surface, after oxidation and one hour of CO_2 treatment, was measured at a scan rate of 10 mV/s. The measurements were performed in a pH 9.3 buffered air-saturated tetraborate solution.

Before recording of the anodic scans, the electrode was oxidised and treated with gaseous carbon dioxide in a separate solution, then transferred into a cell with freshly de-oxygenated tetraborate solution buffered at pH 9.3. Anodic scans were recorded by changing the potential linearly from 50 mV negative of the mineral's rest potential to a maximum potential of 0.60 V (SHE) at a scan rate of 10 mV/s. The rest potential of the CO_2 treated electrode was taken as the rest potential prior to the recording of anodic scans. The polarisation resistance and rest potential measurements were taken two minutes after the potential had stabilised.

The depth profiles of the pure, oxidised and CO_2 treated surfaces were obtained using ToF-SIMS. This was done to show whether or not the oxidation products were removed after CO_2 treatment and, if so, to what extent.

Any changes in the rest potential and polarisation resistance measurements would indicate the influence of dissolved CO_2 on the surface oxidation of the minerals. If CO_2 is to have the same cleaning influence as it has in the case of coal (Miller and Misra, 1987), both the Rp and rest potential values were expected to decrease, indicating that the surface oxidation products were being removed.

4.8.3. Microflotation

The microflotation measurements on pyrrhotite were conducted to investigate the influence of gaseous carbon dioxide conditioning on the flotation response of oxidised pyrrhotite.

4.8.3.1. Sample

Pure natural pyrrhotite grains obtained from Ward's Natural Science were used in the experiments. This was the only pure magnetic (i.e. monoclinic) pyrrhotite sample that could be sourced in large quantities. It was difficult to find a large amount of a non-magnetic (i.e.

hexagonal) pyrrhotite sample to compare to the flotation behaviour of the magnetic pyrrhotite. XRD and electron microprobe analyses on the sample were performed. XRD analysis confirmed the phase composition of the pyrrhotite sample and identified the monoclinic crystal structure of pyrrhotite (see *Sections 5.1* for XRD spectra and *5.2.2* for electron microprobe analysis results). The sample was ground in an agate mortar and sieved with 106, 75, 53 and 38 µm sieves. A particle size distribution of -106 + 38 µm was produced and used for microflotation experiments.

4.8.3.2. Reagents and water

Synthetic plant water used in the microflotation tests was prepared by modifying distilled water with the addition of various chemical salts (see *Table 18*). The synthetic water contained major ions found in concentrator plant process water, although concentrations may vary. The pH was adjusted to pH 9 using sodium hydroxide.

Table 18: Chemical salts used in the preparation of synthetic plant water.

Chemical salts	**g/l**
$MgSO_4.7H_2O$	0.615
$Mg(NO_3)_2.6H_2O$	0.107
$Ca(NO_3)_2.4H_2O$	0.236
$CaCl_2$	0.111
NaCl	0.356
Na_2CO_3	0.030

Purified sodium isobutyl xanthate (SIBX) obtained from SENMIN was used in all the tests, instead of potassium ethyl xanthate, because SIBX is the xanthate commonly used in industry. SIBX was purified by dissolving it in acetone, filtering the solids and evaporation of the acetone in a vacuum (De Wet *et al.*, 1997). Analytical grade $CuSO_4$ was used as an activator. Frother was not added to the microflotation cell because the influence of froth characteristics and cell dynamics were not investigated - the interactions in the pulp were.

4.8.3.3. Microflotation procedure

All microflotation tests were conducted in a 250 ml microflotation cell to investigate the flotation response of pyrrhotite. This equipment was developed to measure bubble loading, which, it has been suggested, is a measure of mineral floatability (Bradshaw and O'Connor, 1995). The microflotation cell is similar in operation to conventional flotation cells, except that it is designed to provide total recovery of a mineral in a hypothetical froth phase and minimal entrainment of mineral particles. The aim of the microflotation experiments was to keep as many variables as possible as close as possible to plant conditions in order to establish the true flotation response of pyrrhotite. Since the purpose of the microflotation tests was to determine the effect of gaseous carbon dioxide conditioning on the flotation behaviour of oxidised pyrrhotite, all other factors affecting flotation response (such as equipment, operating factors and reagents) were kept constant throughout.

A full description of all the flotation conditions studied is provided in *Table 19*.

Table 19: Description of flotation conditions.

Test no.	Sample	Collector	$CuSO_4$	CO_2 treatment time
1	Freshly ground	✓	-	-
2	Freshly ground	✓	✓	-
3	Water oxidised	✓	✓	-
4	Water oxidised	✓	✓	30 minutes
5	Water oxidised	✓	✓	45 minutes

The freshly ground sample refers to the pyrrhotite sample that was ground prior to each experiment. The water oxidised sample refers to a sample that was oxidised in distilled water for 24 hours to determine the influence of carbon dioxide conditioning on oxidised pyrrhotite.

Synthetic water was added to the cell and a peristaltic pump, which was used to circulate the pulp, was set at 90 rpm in order to remove air bubbles. The 2g pyrrhotite sample was added to the cell and conditioned for 1 minute in synthetic water. It was initially decided not to use an activator so as to determine the effect of CO_2 conditioning on pyrrhotite flotation response without activation. However, poor flotation results were observed. Therefore, $CuSO_4$ (at a

concentration of 0.4 x 10^{-5} M) was added to the cell and the sample was conditioned further for 5 minutes. This was followed by the addition of SIBX at a concentration of 5 x 10^{-5} M and a further conditioning of 3 minutes. The cell was then carefully topped up with the synthetic water and the cone was placed at the top of the cell. Air flow rate was initially calibrated at 6 ml/min. The pyrrhotite flotation response observed was poor. Air was then introduced through a needle valve at the base of the cell at a higher flow rate of 58 ml/min. Mineral-loaded bubbles rose through the cell, deflected off the cone and ultimately reported to the launder. After 3, 6, 10 and 20 minutes, the cone was removed, the concentrate collected and the cell topped up with the make-up solution. The concentrates and tailings were then filtered, dried and weighed. The reproducibility of the flotation measurements was not successfully confirmed because of insufficient pyrrhotite samples needed to perform the measurements. This is a problem because reproducibility is important in establishing the reliability and variance of the results.

5. RESULTS AND DISCUSSION

5.1. Electron microprobe analysis

The chemical compositions of the selected pyrrhotite grains are reported in terms of major elements (Fe and S) and trace elements (Ni, Co and Cu).

Table 20 shows the different pyrrhotite common names, ideal chemical compositions and crystal structures.

Table 20: Pyrrhotite common names, ideal chemical compositions and crystal structure (Nakazawa and Morimoto, 1971; Morimoto *et al.*, 1975).

Common name	Crystal structure	Fe:S (molar ratio)	Chemical composition	Type (xC)
Magnetic	Monoclinic	0.875	Fe_7S_8	4C
Non-magnetic	Hexagonal	0.900	Fe_9S_{10}	5C
Non-magnetic	Hexagonal	0.917	$Fe_{11}S_{12}$	6C
Non-magnetic	Troilite	1.000	FeS	2C

Information in *Table 20* helped to classify crystal structures from the microprobe analyses results and helped to compare these with the XRD data in *Section 5.2*.

The chemical compositions of the micro-electrodes and massive electrodes are provided below.

5.1.1. Micro-electrodes

Electron microprobe analyses were conducted to determine the chemical compositions of both the pyrrhotite micro-electrodes and massive pyrrhotite specimens. The chemical compositions of the micro-electrodes are presented to show the variation in pyrrhotite chemical composition within the Bushveld Igneous Complex. The results are shown in *Table 21*. Letters A, B and C designate the different composites in the Platreef ore deposit. These

were explained earlier in *Section 4.1*. Wagner (1929) described three distinct layers seen from the base to the top, which Buchanan (1979) later referred to as the A, B and C units (or reefs), and which are based on texture and mineral mode. The three Platreef horizons (three pyroxenite/gabbronite units separated by hornfels interlayers on the farm Townlands) represent the lower, middle and upper zones (i.e. composites A, B and C). The label A13, represents a pyrrhotite electrode from composite A, sample number 13. Numbers were chosen randomly before analysis and have no other relevance.

Table 21: Compositions (at. %) of micro-electrode pyrrhotites from the Bushveld Igneous Complex determined by electron-microprobe analysis. A: Composite A, B: Composite B, C: Composite C, LMP: Lebowa Merensky Reef, LUP: Lebowa UG-2.

Samples	S	Fe	Co	Ni	Cu	Atomic M:S ratio	Average	Formula	xC
Platreef	52.30	47.44	0.00	0.25	0.00	0.912			5C
(A13)	52.48	47.27	0.00	0.23	0.02	0.905			5C
	52.68	47.03	0.00	0.28	0.00	0.898	0.905	$Fe_{0.91}S$	5C
Platreef	52.53	47.13	0.00	0.33	0.00	0.904			5C
(A14)	52.50	47.21	0.00	0.29	0.00	0.905			5C
	52.44	47.23	0.00	0.33	0.00	0.907	0.905	$Fe_{0.91}S$	5C
Platreef	52.87	46.84	0.00	0.30	0.00	0.892			5C
(A17)	52.64	47.05	0.00	0.31	0.00	0.900			5C
	52.65	46.98	0.00	0.38	0.00	0.899	0.897	$Fe_{0.90}S$	5C
Platreef	50.12	49.86	0.00	0.01	0.02	0.995			2C
(B20)	50.29	49.70	0.00	0.00	0.01	0.988			2C
	50.50	49.49	0.00	0.02	0.00	0.980	0.988	$Fe_{0.99}S$	2C
Platreef	52.15	47.67	0.00	0.16	0.02	0.917			6C
(C11)	51.91	48.01	0.00	0.08	0.00	0.926	0.922	$Fe_{0.92}S$	6C
	50.35	49.59	0.00	0.04	0.02	0.986	0.986	$Fe_{0.99}S$	2C
Platreef	52.05	47.91	0.00	0.04	0.00	0.921	0.921		6C
(C12)	52.29	47.62	0.00	0.09	0.00	0.912	0.912		5C
	51.95	47.95	0.00	0.10	0.00	0.925	0.925	$Fe_{0.92}S$	6C
Platreef	52.42	47.29	0.00	0.29	0.00	0.908			5C
(C13)	52.42	47.29	0.00	0.26	0.02	0.908			5C
	52.53	47.24	0.00	0.23	0.01	0.904	0.906	$Fe_{0.91}S$	5C
Merensky	53.27	46.46	0.00	0.27	0.00	0.877			4C
(LMP3)	53.58	46.10	0.00	0.32	0.00	0.866			4C
	53.32	46.48	0.00	0.20	0.00	0.875	0.873	$Fe_{0.87}S$	4C
Merensky	53.55	46.05	0.00	0.40	0.00	0.867			4C
(LMP17)	53.14	46.42	0.00	0.42	0.02	0.882			4C
	53.51	46.10	0.00	0.37	0.02	0.869	0.873	$Fe_{0.87}S$	4C
UG-2	53.39	46.38	0.00	0.23	0.00	0.873			4C
(LUP6)	53.53	46.23	0.01	0.22	0.01	0.868			4C
	53.16	46.61	0.00	0.23	0.00	0.881	0.874	$Fe_{0.87}S$	4C

M:S : Metal to sulfur ratio.

The atomic percent metal (in M:S ratio) includes the substitution of Ni and Cu cations for Fe. The chemical composition of each electrode was determined based on the average atomic percentage of total metal to sulfur ratio (i.e. the average of the three analyses per grain). Of the trace metals present in the samples, Ni is the most abundant trace metal, then copper; cobalt was found to be negligible in the various deposits. Ni content within the various ore

bodies varied and was also found to vary within the same ore deposit. Within the Platreef, the Ni content increased in the order: composite B < composite C < composite A. The exception was the C13 electrode, which had a Ni content similar to that of composite A. S increased in the same order as the Ni content and Fe decreased in the order: composite B > composite C > composite A.

LMP (Lebowa Merensky) and LUP (Lebowa UG-2) samples contained large amounts of Ni and S, and small amounts of Fe compared to the Platreef. From the chemical compositions, crystal structures were established based on *Table 20* shown earlier. The four modifications of pyrrhotite were observed in the various deposits from which the micro-electrode pyrrhotite particles were sourced. These results show that there are variations in the chemical composition and crystal structure of pyrrhotite within the various ore bodies in the Bushveld Igneous Complex. In sample C11, both the 2C (i.e. troilite) and 6C (i.e. hexagonal pyrrhotite) modifications were observed. This agrees with the results obtained by Mostert (1982), i.e. that troilite is developed either as lamellae in a hexagonal host or as host to hexagonal lamellae. The analysed pyrrhotite particles in other deposits, such as composites A and B of the Platreef and Lebowa Merensky Reef show similar crystal structures (5C and 4C, respectively). This does not mean these crystal structures are the only types that could be found in those deposits, because only a few pure pyrrhotite particles (labelled A13, A14, A17 from the Platreef, and LMP3 and LMP17 from the Lebowa Merensky Reef in *Table 21*) were analysed.

5.1.2. Massive samples

The chemical composition of pure massive pyrrhotite samples selected from various ore deposits is presented in *Table 22* below.

Table 22: Compositions (at. %) of pure massive pyrrhotite samples determined by electron-microprobe analysis.

Samples	S	Fe	Co	Ni	Cu	Atomic M:S ratio	Average	Formula	xC
Russia_1	53.23	46.76	0.00	0.01	0.00	0.879			4C
	53.48	46.52	0.00	0.00	0.00	0.870			4C
	53.29	46.69	0.00	0.02	0.00	0.877	0.875	$Fe_{0.88}S$	4C
Russia_2	53.62	46.38	0.00	0.00	0.00	0.865			4C
	53.38	46.58	0.00	0.01	0.02	0.873			4C
	53.51	46.45	0.00	0.03	0.01	0.869	0.869	$Fe_{0.87}S$	4C
Mponeng	52.18	47.57	0.01	0.24	0.00	0.916			6C
	51.76	47.99	0.00	0.25	0.00	0.932			6C
	52.28	47.51	0.00	0.20	0.01	0.913	0.920	$Fe_{0.92}S$	6C

Ni was found to be the most abundant trace metal, then copper. Cobalt was found to be negligible in all the samples. The Russia_1 and Russia_2 pyrrhotites contain less Ni, less Fe and more sulfur than the Mponeng pyrrhotite. Pure massive pyrrhotite grains (with no other sulfide minerals visible on the surface) were selected to prepare electrodes. Chemical compositions reported in *Table 22* are of the pure pyrrhotite electrode surfaces. Both the Russia_1 and Russia_2 samples have the same crystal structure (4C type) with only slight variations in their metal to sulfur ratios. The Mponeng sample is a hexagonal and a 6C type pyrrhotite.

Table 23 shows the composition of mixed (i.e. pyrrhotite and other sulfide minerals) massive pyrrhotite samples. Images of these samples were shown earlier in *Section 4.2*.

Table 23: Compositions (at. %) of pyrrhotite co-existing with pentlandite determined by electron microprobe analysis.

Samples	S	Fe	Co	Ni	Cu	Atomic M:S ratio	Average	Formula	xC
Gertrude	53.44	46.02	0.01	0.54	0.00	0.871			4C
	53.48	45.99	0.00	0.53	0.00	0.870			4C
	53.51	45.92	0.00	0.55	0.02	0.869	0.870	$Fe_{0.87}S$	4C
Phoenix	53.30	45.26	0.04	1.39	0.00	0.876			4C
	53.29	45.27	0.03	1.37	0.03	0.876			4C
	53.77	44.90	0.07	1.24	0.01	0.860	0.871	$Fe_{0.87}S$	4C

Pyrrhotite occurs in association with other sulfide minerals. The most predominant is usually pentlandite (Vermaak and Hendriks, 1976; Brynard *et al.*, 1976; Johnson, 1986; Agar, 1991; Jones, 1999; Newell *et al.*, 2005) and this was also found to be the case in the mixed samples used in this study. The differences observed were in the trace metal content and the major differences were in the Ni content. The Gertrude and Phoenix pyrrhotite specimens were found to contain Cu in higher quantities than was found in the pure and micro-electrode samples. Unlike the micro-electrode and pure massive samples, the Phoenix pyrrhotite had a measurable quantity of Co. These mixed samples have the same crystal structure and chemical composition (i.e. the mixed samples are both magnetic 4C type pyrrhotites).

Figure 27 compares the number of analyses with the atomic Fe:S ratio of the pyrrhotite grains for the micro-electrodes, pure and massive samples. Three spot-analyses were performed on each sample. The metal to sulfur ratio of the pyrrhotite grains was referred to as the Fe:S ratio.

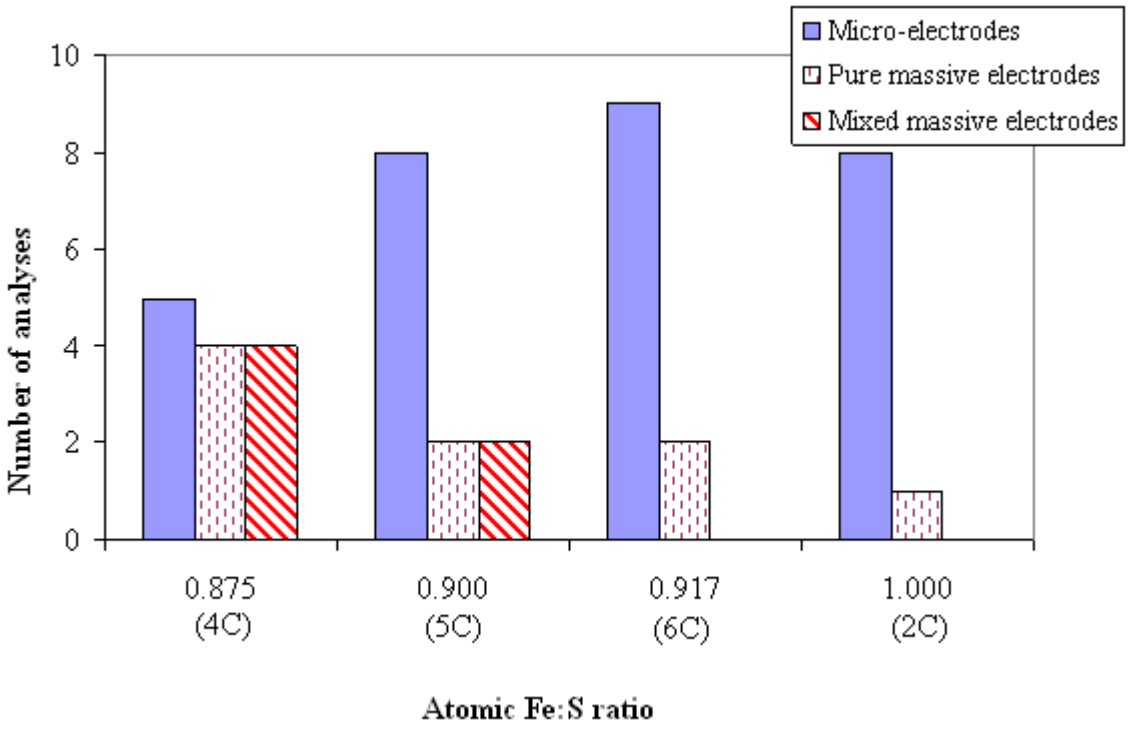

Figure 27: Frequency distribution curve of the atomic Fe:S ratio of the pyrrhotite grains.

The normal distribution of the micro-electrodes shows most of the analyses fall within the non-magnetic 6C pyrrhotite range, then equal proportions of non-magnetic 5C and 2C pyrrhotites, then magnetic 4C pyrrhotite. The pure massive samples had a large proportion of the magnetic 4C pyrrhotite, then smaller, equal proportions of the non-magnetic 5C pyrrhotite and non-magnetic 6C pyrrhotite, and even smaller proportions of the 2C type pyrrhotite. The mixed samples contain a large proportion of magnetic 4C pyrrhotite, then the non-magnetic 5C pyrrhotite. *Figures 28* to *31* show the Fe to Ni (atomic %) content of the micro and massive pyrrhotites in terms of the different crystal structures (i.e. 2C, 4C, 5C and 6C types) from various locations within and outside South Africa.

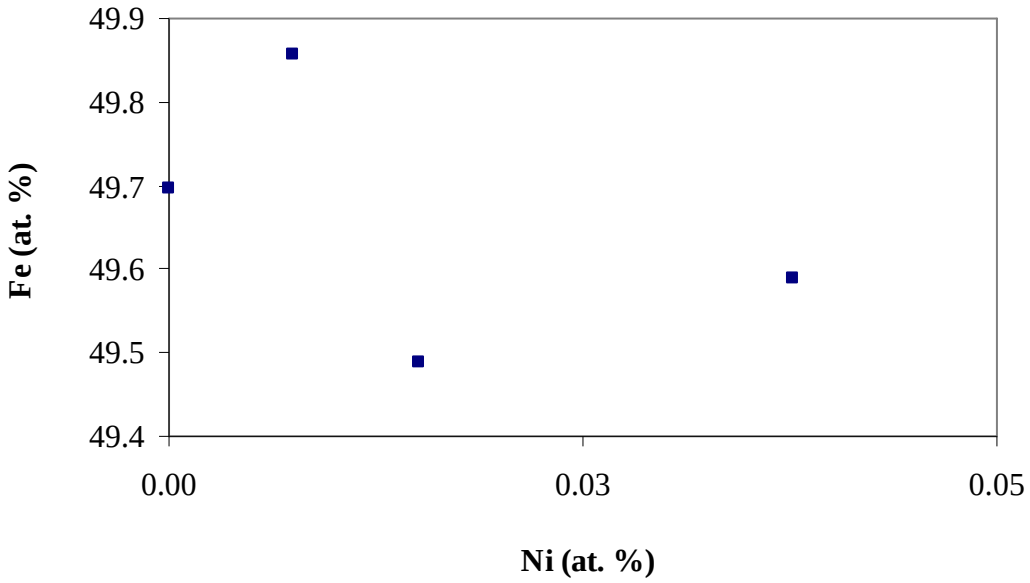

Figure 28: Atomic Fe and Ni content of the 2C type pyrrhotites from the pure micro-electrodes and the pure and mixed massive pyrrhotite samples.

For the 2C type pyrrhotite, there is no definite relationship between the Fe and Ni content.

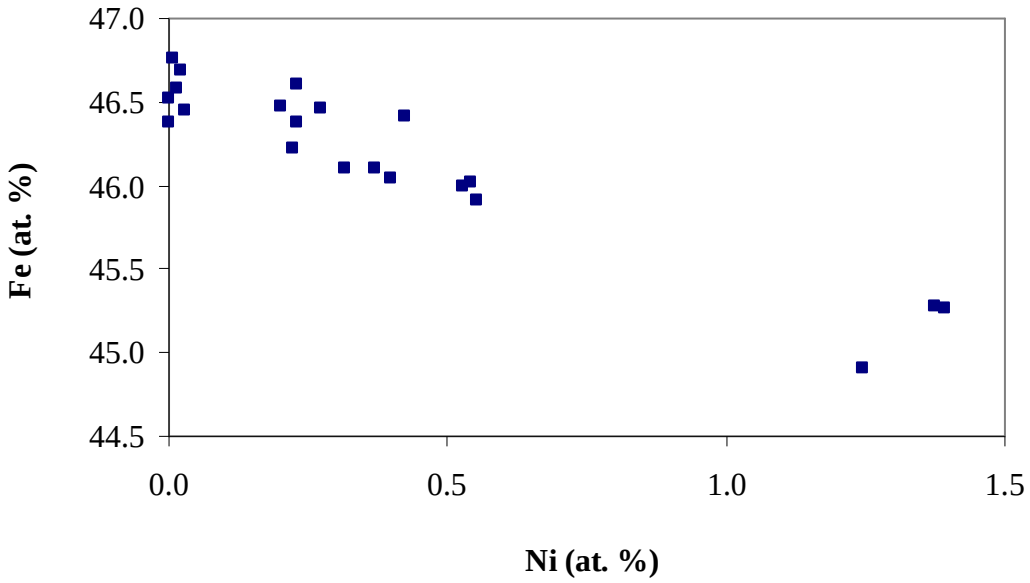

Figure 29: Atomic Fe and Ni content of the 4C type pyrrhotites from the pure micro-electrodes and the pure and mixed massive pyrrhotite samples.

The Fe and Ni content of the 4C type pyrrhotite are inversely related.

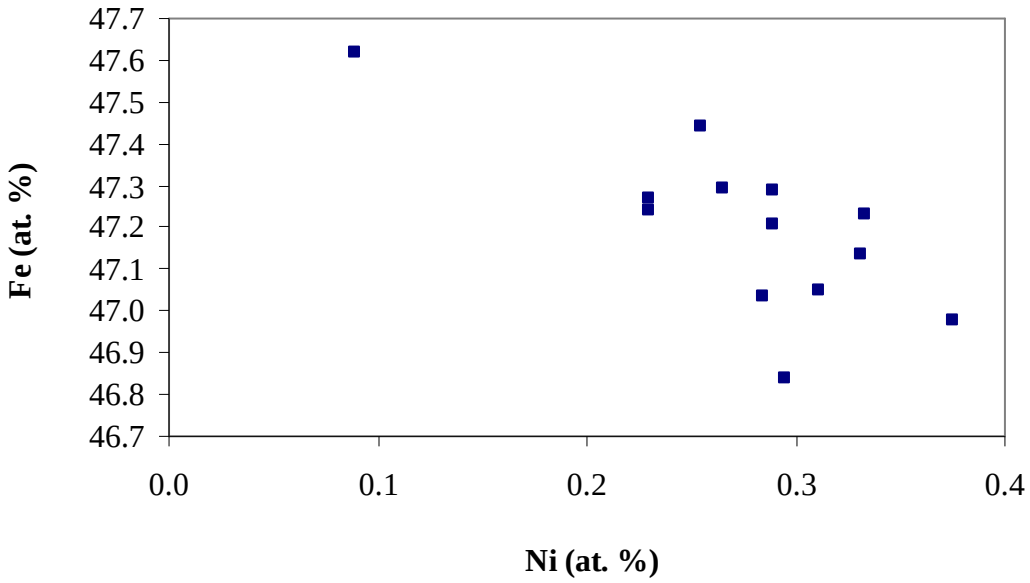

Figure 30: Atomic Fe and Ni content of the 5C type pyrrhotites from the pure micro-electrodes and the pure and mixed massive pyrrhotite samples.

The 5C type pyrrhotite showed that the relationship between Fe and Ni content is not strong.

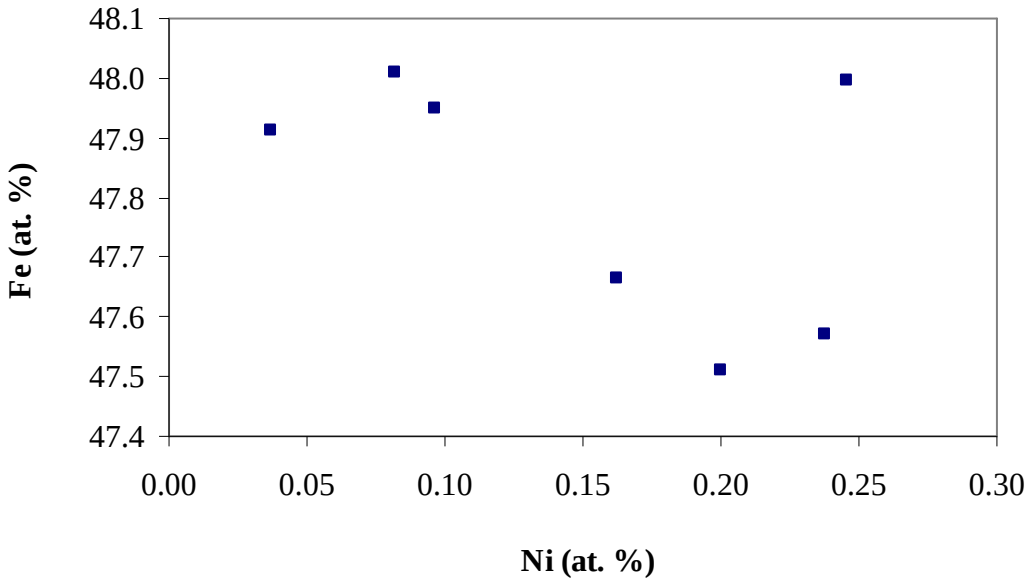

Figure 31: Atomic Fe and Ni content of the 6C type pyrrhotites from the pure micro-electrodes and the pure and mixed massive pyrrhotite samples.

Figure 31 shows that the Fe and Ni in the 6C pyrrhotite have a weak relationship.

According to *Figures 28* to *31*, the Fe content increases in the following order, as expected: 4C < 5C < 6C < 2C type pyrrhotite (i.e. iron increases from iron-deficient magnetic pyrrhotite to iron-rich troilite). The Ni content is inversely related to Fe content in the 4C pyrrhotite. The Fe and Ni in the 2C, 5C and 6C do not have a strong relationship. Overall, the Ni content increases from troilite to magnetic pyrrhotite. It is evident that the magnetic pyrrhotite is richer in Ni than the non-magnetic pyrrhotite.

These results indicate the compositional variation of pyrrhotite within the same ore body and between various ore bodies from different locations. For further characterisation of the pyrrhotite samples, crystal structures were determined using XRD analysis and this is discussed in the following section.

5.2. X-ray diffraction (XRD) analysis

Crystals of pyrrhotite (see *Section 4.1*) sourced from regions with different geological conditions were studied by powder X-ray diffraction. Samples from different regions were used with the aim of obtaining samples with variations in mineralogical composition. The results showed two different modifications of pyrrhotite (i.e. monoclinic and hexagonal structures). Various researchers described three different kinds of pyrrhotite as stable phases at low temperatures (based on natural specimens). These pyrrhotites are superstructures of the NiAs-type structure, which has the following cell dimensions: A, about 3.45 Å, C about 5.8 Å.

The three pyrrhotite types are: monoclinic pyrrhotite (Fe_7S_8) with the supercell of $2\sqrt{3}A$, 2A, 4C; hexagonal or intermediate pyrrhotite (Fe_9S_{10}) of 2A, 5C; and troilite (FeS) of 2A, 2C (where A and C are the equivalent *a* and *c* parameters of the simple NiAs-type sub-cell). The pyrrhotite types are conventionally labelled as the 4C, 5C and 2C types, respectively. A fourth, stable, low temperature phase with a hexagonal supercell of 2A, 6C was described by Fleet and MacRae (1969). It was then named a 6C type with a stoichiometric composition $Fe_{11}S_{12}$ (Morimoto *et al.*, 1975).

XRD characterisation was carried out on the massive pyrrhotite samples only. Only two types (i.e. 4C and 6C) were observed in the crystals selected for this study. The Autoquan program was used to refine a database diffraction pattern against the measured diffraction pattern involving only unit cell and peak shape parameters. The patterns are fitted onto the standard patterns in the database. *Figures 32* to *36* below demonstrate the various pyrrhotites' diffraction patterns, together with the differences between the pyrrhotite standard pattern and the pattern of the minerals used. The difference plot (showing the difference between the calculated and observed intensities) is an indication of how good the fit between the calculated and observed XRD pattern is and it should be a featureless, horizontal line.

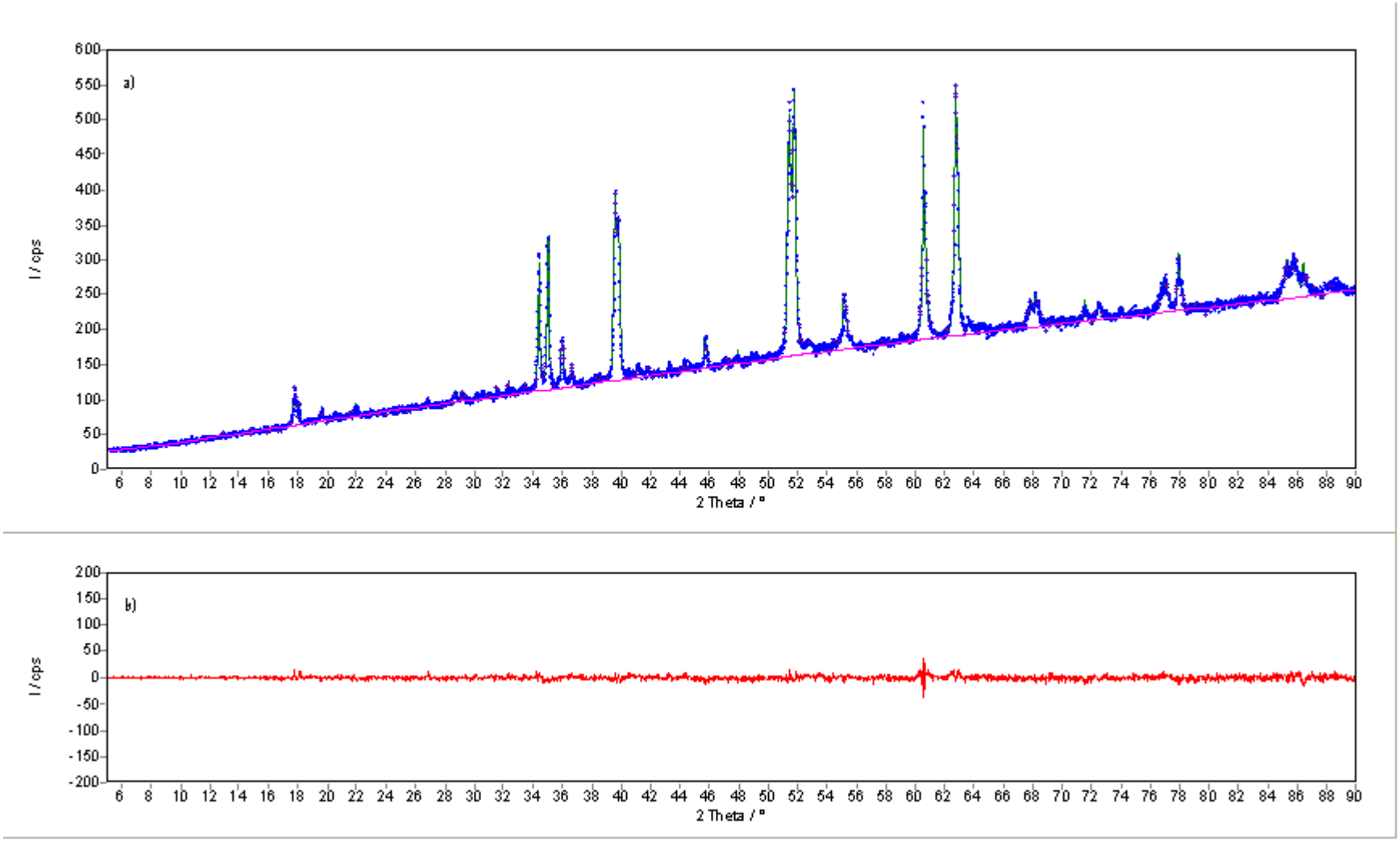

Figure 32: a) XRD powder pattern of the Phoenix pyrrhotite; b) the difference plot (showing the difference between the calculated and observed intensities). I/cps = Intensity/counts per second.

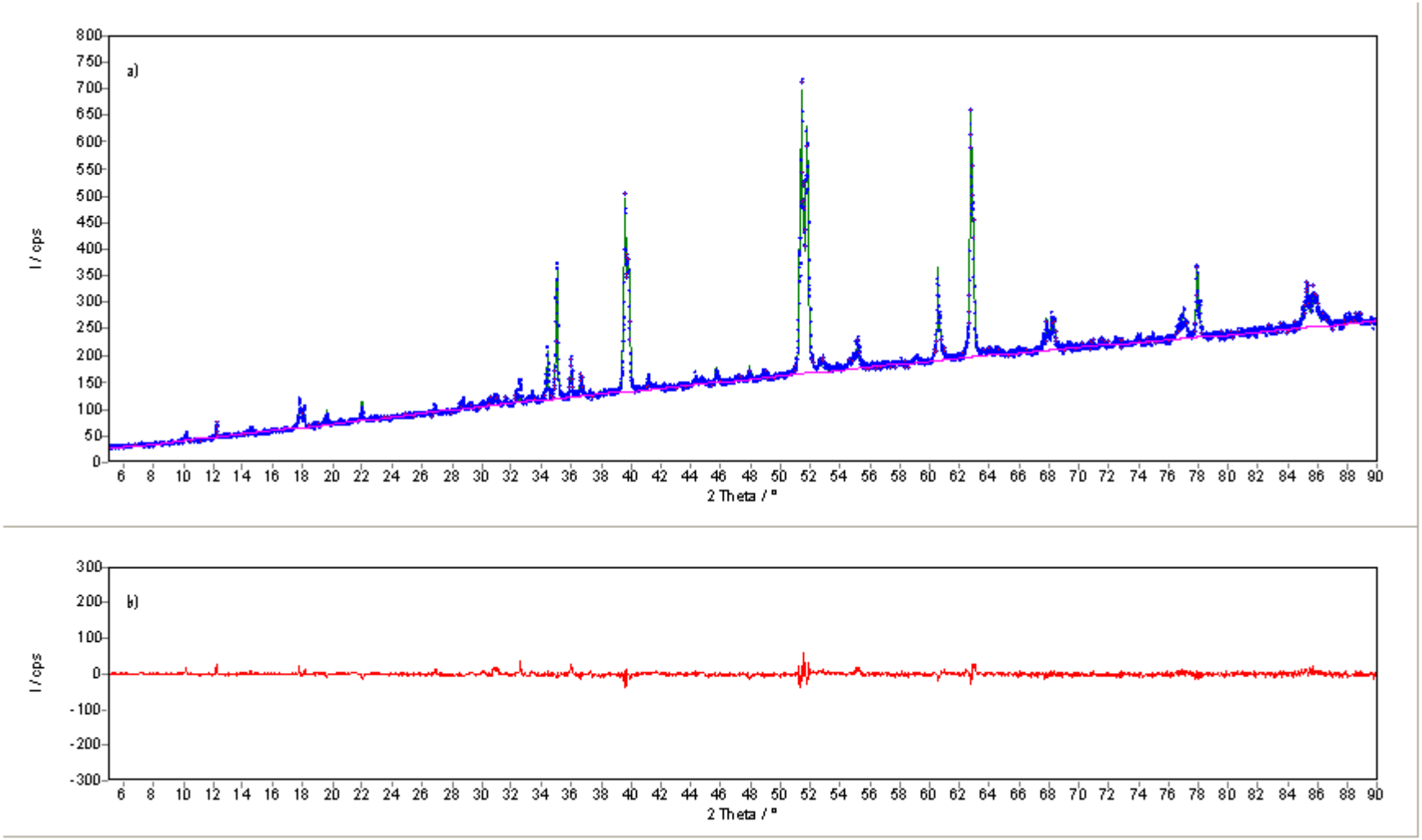

Figure 33: a) XRD powder pattern and; b) difference plot of the Sudbury Gertrude pyrrhotite.

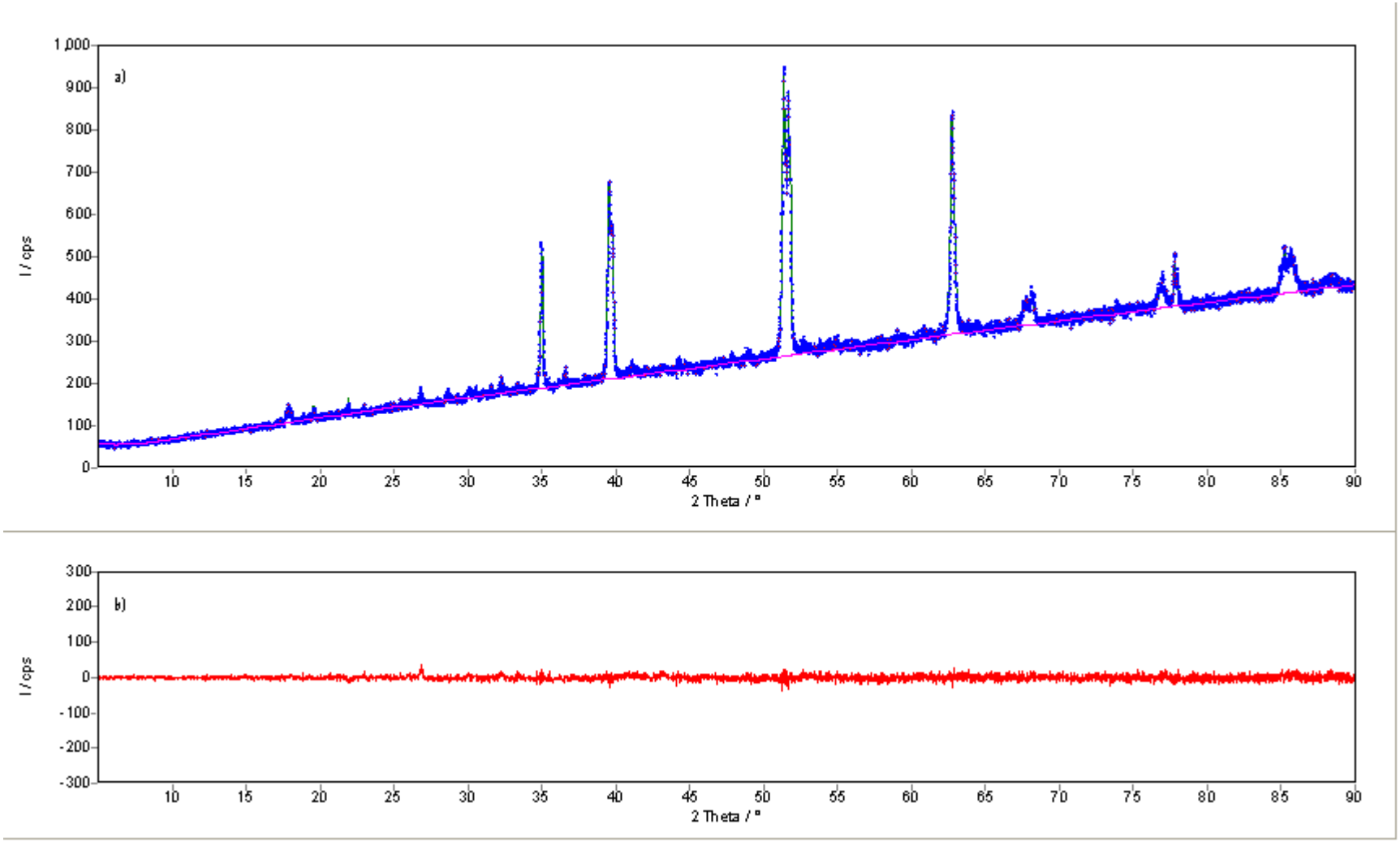

Figure 34: a) XRD powder pattern and; b) difference plot of the Russia_1 pyrrhotite.

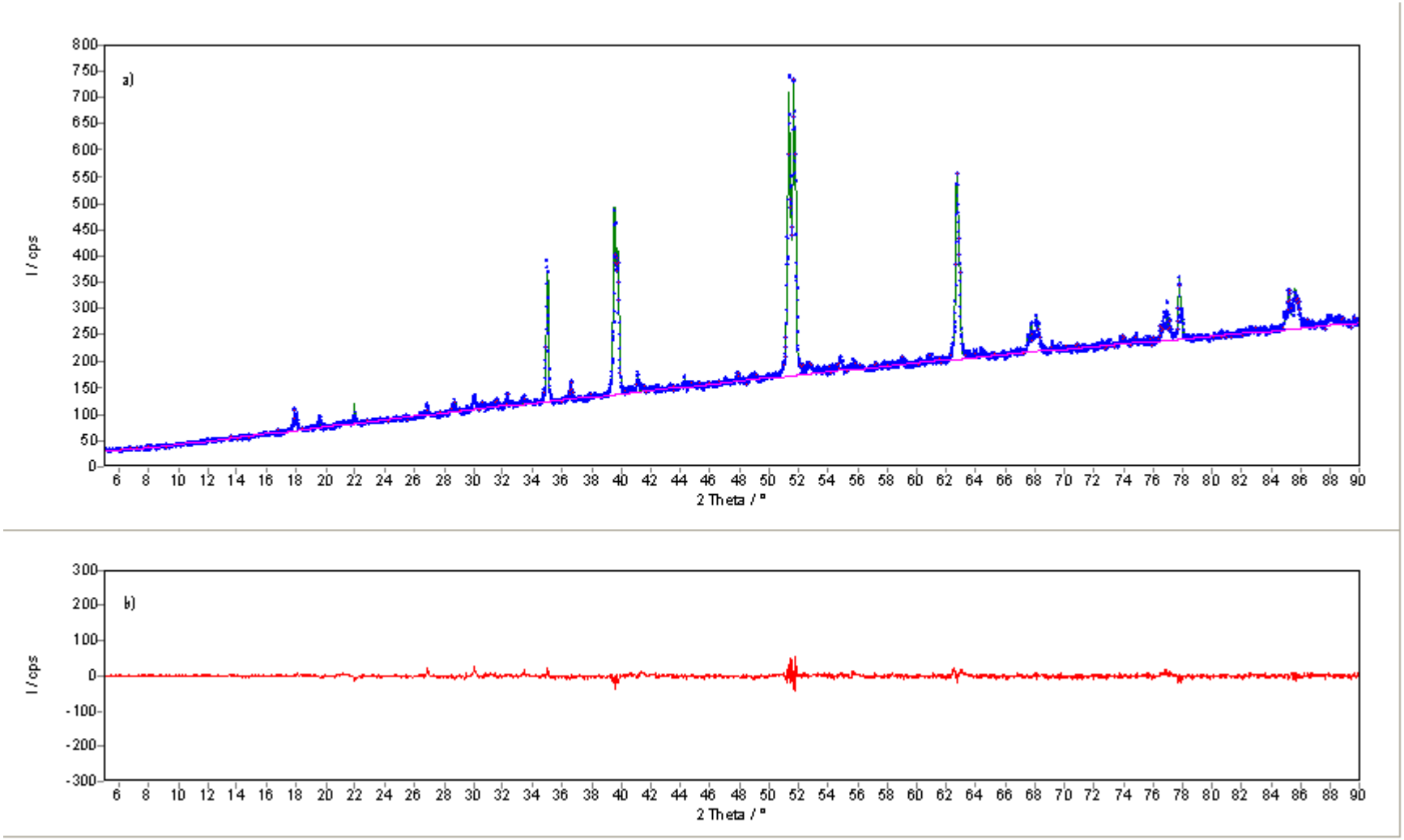

Figure 35: a) XRD powder pattern and; b) difference plot of the Russia_2 pyrrhotite.

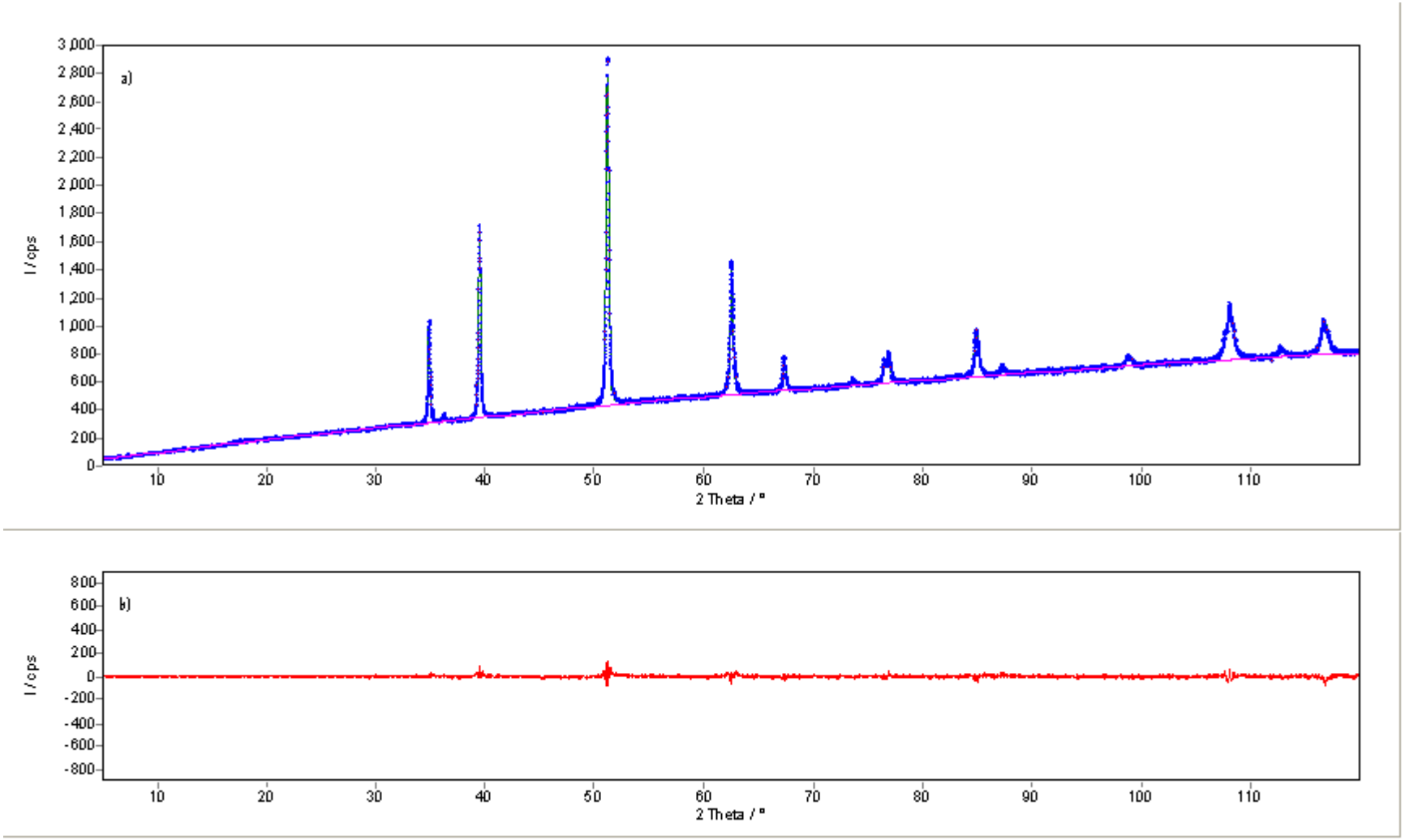

Figure 36: a) XRD powder pattern and; b) difference plot of the Mponeng pyrrhotite.

According to the XRD data, both the Russian pyrrhotites had the same XRD pattern. X-ray diffraction analysis showed the presence of peaks that could only be attributed to monoclinic pyrrhotite. Thus these samples were considered to be pure 4C type pyrrhotites. The Phoenix and Sudbury Gertrude samples also showed peaks attributable to monoclinic pyrrhotite as well as extra peaks that are due to other phases or impurities present in the samples. The Mponeng pyrrhotite had a different pattern, its X-ray diffraction analysis showed the presence of peaks which could only be attributed to a "hexagonal" pyrrhotite and it was characterised as a 6C type pyrrhotite by employing a single-crystal X-ray method. Microprobe analysis (discussed in the previous section) also assisted with the characterisation of samples, especially the Mponeng 6C type pyrrhotite because its spectrum is similar to that of a 5C type pyrrhotite. In all samples, the difference plot shows that the difference between the pyrrhotite XRD and calculated patterns is minimal, confirming the accuracy of the phase quantification.

The main sulfide minerals present in each of the samples were quantified so as to determine the purity of the samples, with the error given at 3 sigma level (*Table 24*).

Table 24: X-ray powder diffraction analysis of selected pyrrhotite crystals.

Sample	**Phoenix (4C)**		**Sudbury Gertrude (4C)**		**Russia_1 (4C)**		**Russia_2 (4C)**		**Mponeng (6C)**	
Phase	**wt.%**	**3σ**	**wt.%**	**3σ**	**wt.%**	**3σ**	**wt.%**	**3σ**	**wt.%**	**3σ**
Chalcopyrite	0.1	0.2	0.2	0.2	0.0	0.0	0.1	0.2	0.0	0.0
Pentlandite	18.0	0.7	8.1	0.5	0.0	0.0	0.0	0.0	0.0	0.1
Pyrite	0.7	0.6	0.0	0.0	0.0	0.0	0.3	0.4	0.0	0.0
Pyrrhotite	81.2	0.8	91.7	0.5	100.0	0.0	99.6	0.5	100.0	0.1

Analysis of the XRD spectra showed that chalcopyrite, pentlandite, pyrite and pyrrhotite were the dominant sulfides present in the samples. It is evident that only one type of pyrrhotite was found in each specimen. XRD data indicate that the pyrrhotite from Russia_1 contains no measurable impurities. The Russia_2 pyrrhotite contains minute amounts of both chalcopyrite (0.1 wt %) and pyrite (0.3 wt %); the Mponeng pyrrhotite contains insignificant amounts of pentlandite. Therefore, the Russia_1, Russia_2 and Mponeng samples were considered to be pure pyrrhotites. However, both the Sudbury Gertrude and Phoenix samples are contaminated with varying large amounts of pentlandite and small amounts of other sulfide minerals. The

Phoenix sample has more pentlandite than the Sudbury Gertrude sample: 18.0 wt % and 8.1 wt %, respectively. The Sudbury Gertrude contains no pyrite and low chalcopyrite (0.2 wt %), whereas the Phoenix sample contains pyrite (0.7 wt %) and chalcopyrite (0.1 wt %). The pyrrhotite content of the Sudbury Gertrude sample is higher than that of the Phoenix sample; 91.7 wt % and 81.2 wt %, respectively.

Crystal structures that were determined using the XRD data are supported by the chemical compositions (*Section 5.1*) that were determined based on the total metal to sulfur ratios. The XRD results shown in *Table 24* were obtained from grinding a piece of pyrrhotite sample and XRD analysis was employed to identify all the phases present in the sample. The only sample considered to be pure was the Russia_1; the Russia_2 and Mponeng samples contained minor impurities (other sulfide minerals).

In this study, it was possible to characterise massive pyrrhotite samples using XRD analysis and electron microprobe analysis to determine variations in pyrrhotite chemical composition and crystal structure.

5.3. Qemscan quantification

The Phoenix and Gertrude samples were chosen to investigate the influence of galvanic interactions on the electrochemical response of pyrrhotite in contact with pentlandite and other sulfide minerals. These samples have the same crystal structure and slight variations in chemical composition. Qemscan was employed to determine the concentration of pentlandite and other sulfides on the exposed mineral surfaces of the mixed samples. Relative amounts of the various sulfides and gangue are presented in *Table 25*.

Table 25: Summary of the concentration (wt %) of various sulfides in the mixed massive sulfide electrodes.

	Phoenix	**Gertrude**
Pentlandite	17.63	5.66
Pyrrhotite	80.44	87.21
Other sulfides	1.15	0.75
Gangue	0.77	6.38
Total	100.00	100.00

Everything except sulfide minerals was referred to as gangue (see *Table 2A* in *Appendix 2A*). *Figure 37* shows the relative proportions of the sulfide minerals.

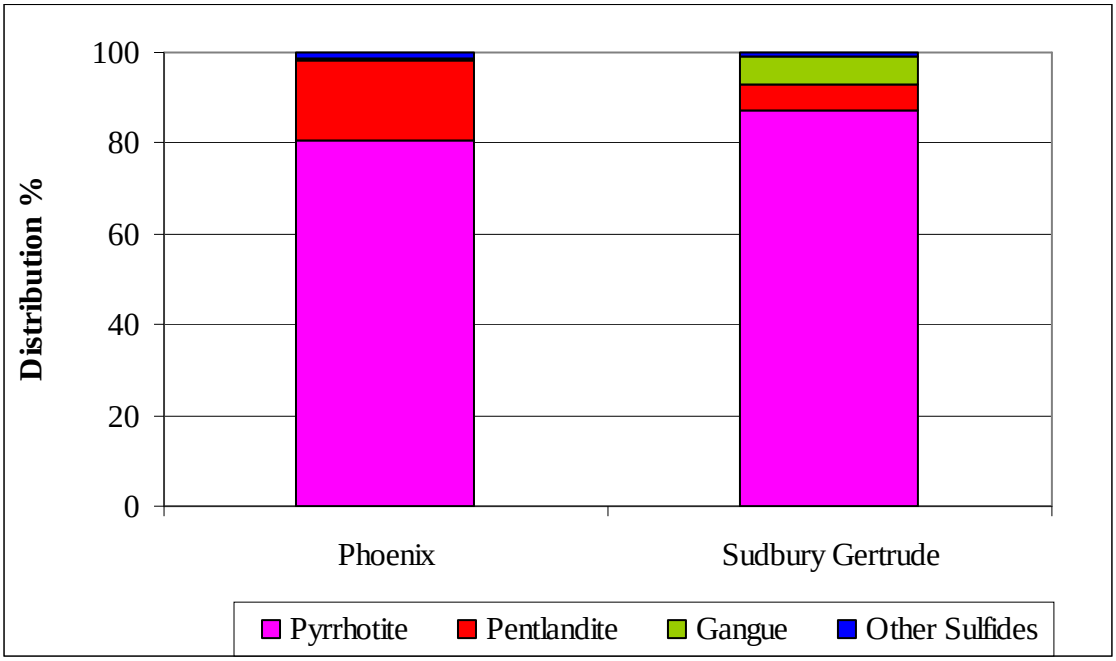

Figure 37: Mixed pyrrhotite samples showing a relative abundance of sulfides and gangue.

The Phoenix sample contained a large amount of pentlandite (17.63 wt % vs 5.66 wt % in the Sudbury Getrude sample) and other sulfides, with a lower pyrrhotite and gangue content compared to the Sudbury Gertrude sample. These results are in agreement with the XRD data shown earlier in *Section 5.2*. The occurrence of pentlandite and other sulfides are known to influence the behaviour of pyrrhotite. This phenomenon is termed galvanic interactions and will be discussed later.

5.4. Electrochemical measurements

Electrochemical techniques, such as polarisation resistance, rest potential, cathodic and anodic polarisation diagrams, were used to investigate the influence of chemical composition, crystal structure and galvanic interactions on pyrrhotite reactivity.

5.4.1. The influence of chemical composition and crystal structure on pyrrhotite reactivity

The electrochemical response of micro-electrodes was not satisfactory. The measured currents were small and not stable, making it impossible to obtain any reliable data. This was attributed to the porous, brittle nature of the micro-electrodes. Currents in electrochemical experiments at the micrometer scale are no longer in the range of µA (10^{-6}) and nA (10^{-9}), but rather in the range of pA (10^{-12}) and fA (10^{-15}) (Suter *et al.*, 1995). To detect such extremely low currents, good shielding against electromagnetic interference is necessary. Consequently, the electrochemical equipment was set up within a Faraday cage made of copper plates 3 mm thick. All cables were specially shielded and kept as short as possible. The Faraday cage did not help with the detection of currents for pyrrhotite grains in the +106 µm range (micro-electrodes). Therefore, only the massive pyrrhotite samples mentioned in *Section 4.1* were used to study the electrochemical behaviour of pyrrhotite. Unfortunately, relatively pure massive pyrrhotite samples cannot be obtained from the Bushveld Igneous Complex, hence the use, in all the electrochemical measurements, of massive pyrrhotite samples sourced from Mponeng mine in South Africa and various deposits outside South Africa.

Pure massive pyrrhotite samples from Russia and Mponeng mine in South Africa were characterised and used to study the effect of chemical composition and crystal structure variations on the electrochemical behavior of pyrrhotite. Unless otherwise stated, in this section: 4C type pyrrhotite refers to both the Russia_1 and Russia_2 magnetic pyrrhotites; 6C type pyrrhotite refers to the Mponeng non-magnetic pyrrhotite.

5.4.1.1. Rest potential measurements

The Rp_time program (timed polarisation resistance) was employed to obtain Rp and rest potential measurements as a function of time at a scan rate of 10 mV/s around the mixed potential. The program works in such a way that the rest potential is obtained at the same time as the polarisation resistance. The repeatability of the rest potential measurements is shown in *Appendix 1A*. All potentials are reported in terms of a standard hydrogen electrode (SHE). The rest potentials of pure massive pyrrhotite electrodes as a function of time are shown in *Figure 38*. The rest potential (open circuit potential) refers to the mixed potential between the pyrrhotite oxidation and oxygen reduction at the pyrrhotite surface.

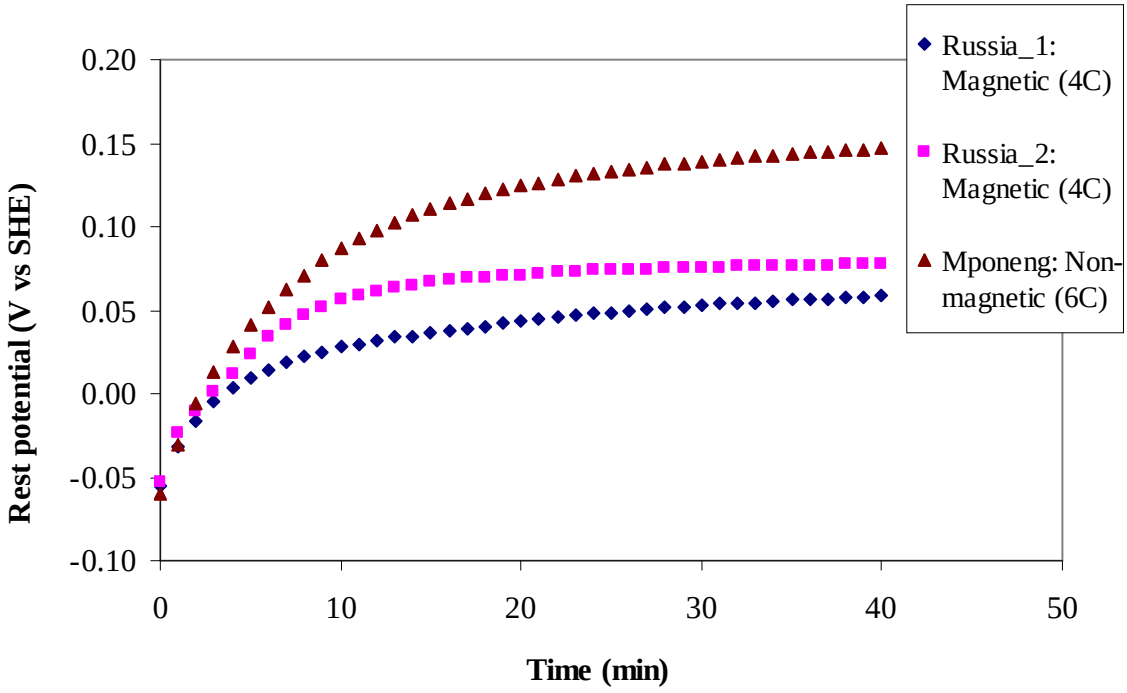

Figure 38: Rest potentials of pure massive pyrrhotites in an oxygen-saturated 0.05 M borate solution at a pH of 9.3. Potential sweeps were carried out at 10 mV/s.

The non-magnetic (6C type) pyrrhotite had a higher rest potential than the magnetic (4C type) pyrrhotite. The magnetic pyrrhotites had different rest potentials: the Russia_2 pyrrhotite had a slightly higher rest potential than the Russia_1 pyrrhotite. According to Rand (1977), minerals with lower rest potentials are more reactive and are susceptible to oxidation. Tolley *et al.* (1996) reported that a decrease in open circuit rest potentials (as a function of mineral

type) indicates increased reactivity of the mineral toward the solution. As a result, the order in the anodic reactivity of the pure pyrrhotite minerals used in this study was expected to decrease as follows: Russia_1 (magnetic 4C) > Russia_2 (magnetic 4C) > Mponeng (non-magnetic 6C).

5.4.1.2. Cathodic polarisation diagrams

Cathodic scans were recorded by changing the potential linearly with time from 50 mV positive of the mineral's rest potential of each pyrrhotite to -0.40 V (SHE) at a scanning rate of 1 mV/s in an oxygen-saturated 0.05 M $Na_2B_4O_7$ solution at a pH of 9.3 to study the oxygen reduction activity of the selected pyrrhotite grains (*Figure 39*). The repeatability of data is shown in *Appendix 1B*. Measured current was converted to current density by dividing by the area of the pyrrhotite particle. The area estimations were performed by taking digital images and using imaging software (Image Tool^{TM}).

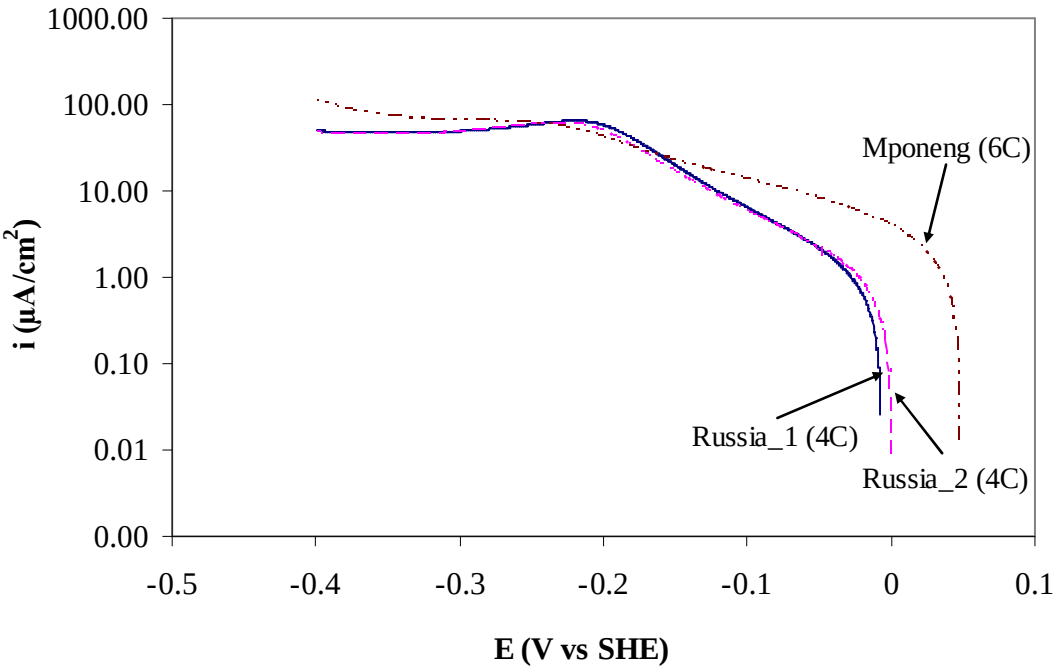

Figure 39: The cathodic polarisation diagrams of pure massive pyrrhotite samples in an oxygen-saturated 0.05 M borate solution at a pH of 9.3. Potential sweeps were carried out at 1 mV/s.

In the cathodic curves shown in *Figure 39*, the total cathodic polarisation is the sum of activation and concentration polarisation. At low cathodic polarisation, the reduction process is activation controlled; at high polarisation, it is diffusion or concentration controlled. When the reduction current density approaches its limiting current density (i.e. the measure of a maximum reaction rate that cannot be exceeded because of a limited diffusion rate of oxygen to the surface), concentration polarisation takes over from activation polarisation and the corrosion rate becomes limited by the diffusion of the oxidiser (oxygen) from the bulk solution (Jones, 1996).

Rand (1977) reported the minerals with high rest potentials to be better surfaces for oxygen reduction. Mponeng 6C pyrrhotite shows higher cathodic currents in the region of activation control than do the rest of the other samples, suggesting that it is a better surface for oxygen reduction compared to the Russian 4C pyrrhotites. The oxygen reduction activity of the Russian pyrrhotites was the same. These results are in agreement with the previously shown order in reactivity rates of these pyrrhotites. From these results, it can be said that the more noble the surface (i.e. less reactive towards oxidation), the higher the oxygen reduction current. Current densities of both minerals are similar in the region of diffusion control. In this region, catalytic activity plays no role, because oxygen is reduced at its diffusion limited rate due to its low concentration and ease of reduction.

In heavily oxidising environments, a more reactive surface is prone to oxidation, hence it becomes a poor substrate for xanthate adsorption. Excessive surface oxidation results in the formation of hydroxides on the surface, preventing the interaction of xanthate with the mineral surface (Buswell and Nicol, 2002; Rao, 2004). On the other hand, it has been reported that a certain degree of oxidation is necessary for xanthate adsorption (Hodgson and Agar, 1989; Khan and Kelebek, 2004).

5.4.1.3. Polarisation resistance measurements

The Rp_time program (timed polarisation resistance) was used to obtain Rp measurements in this study. The polarisation resistance was obtained by scanning at 10 mV/s positive and negative voltage direction from the rest potential. Total duration was 40 minutes. Current versus potential data was obtained and this current was then converted to current density by

dividing by the area of the pyrrhotite particle (estimated by using the imaging software [Image Tool^{TM}]). Three slopes were obtained from the current versus potential curve (see *Figure 24* in *Section 4.6.1.2*): two from the top two horizontal lines and one from the bottom horizontal line. An inverse of the average of the three slopes was taken as the Rp for that specific time.

The polarisation resistance (Rp) results of the pure pyrrhotite samples as a function of time are presented in *Figure 40*. The polarisation resistance increased with time. The repeatability of the rest potential measurements is shown in *Appendix 1C*.

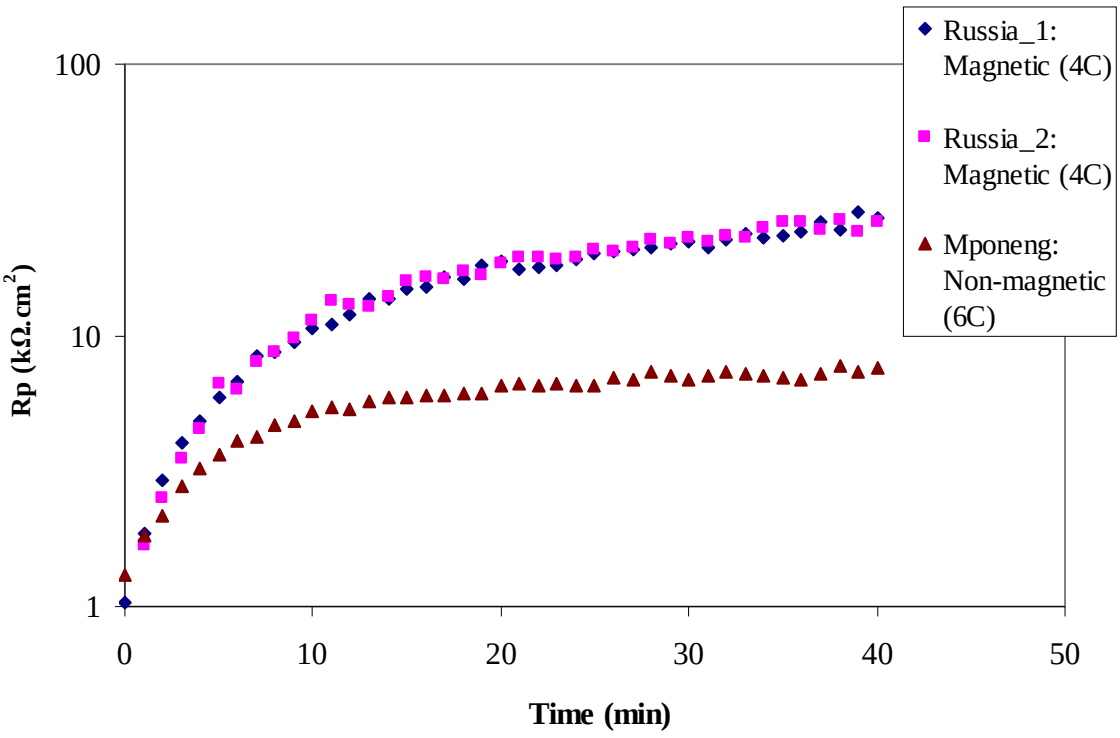

Figure 40: Comparison of the polarisation resistance of pure massive pyrrhotites in an oxygen-saturated 0.05 M borate solution at a pH of 9.3. Potential sweeps were carried out at 10 mV/s.

A steep slope in the Rp-relationship with time indicates that Rp changes faster and is also an indication of quick formation of a layer on the mineral surface, suggesting that the mineral is initially more reactive. An increase in the resistance to electrical current flowing through the surface is attributed to the oxidation of the mineral. This indicates that a passivation layer, caused by increasing amounts of iron hydroxides on the surface, is formed on the surface

during oxidation; the resistance of this layer is increased with an increased oxidation period. The higher final Rp value indicates the extent of passivation. The final Rp of the Russian 4C type pyrrhotites was about 71 % higher than that of the Mponeng 6C type pyrrhotite.

The initial change in Rp was taken for the first five minutes in order to investigate the reactivity towards oxidation of pure massive pyrrhotites (*Figure 41*). The initial change in Rp with time (dRp/dt) was used to compare the initial relative reaction rates of the polished minerals on contact with the solution.

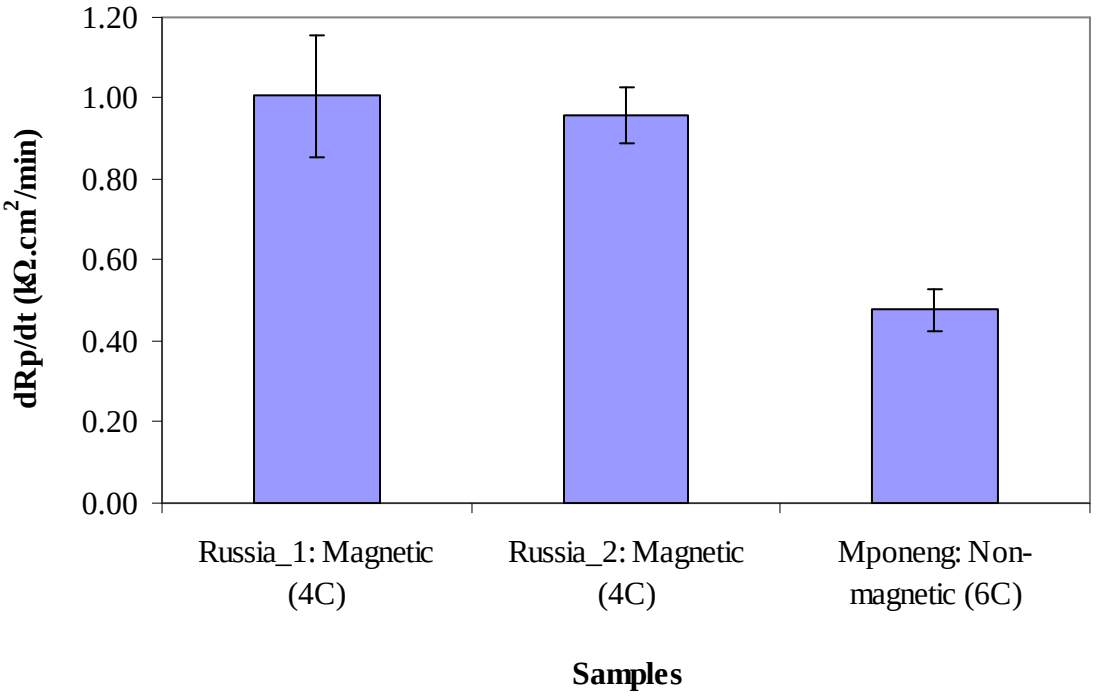

Figure 41: Comparison of the initial change in Rp of pure pyrrhotite samples in an oxygen-saturated 0.05 M borate solution at a pH of 9.3. Potential sweeps were carried out at 10 mV/s.

Both the Russian 4C type pyrrhotites showed the same change in the initial slope and Rp measurements, indicating the same reactivity. These results (*Figures 40 and 41)* show that the 4C pyrrhotite's Rp changed more rapidly, demonstrating that it has the highest reactivity. The change in the Rp of the 6C type pyrrhotite was more gradual. The same decreasing order (i.e. dRp/dt [magnetic 4C pyrrhotite] > dRp/dt [non-magnetic 6C pyrrhotite]), observed for

the initial change in Rp, was also observed in the Rp measurements, indicating a similar reactivity trend towards oxidation.

In the work by Tolley *et al.* (1996), a decrease in open circuit rest potential (as a function of mineral type) correlated with an increase in polarisation resistance, suggesting that an increase in polarisation resistance indicates an increase in reactivity of the mineral toward the solution. As a result, the magnetic (4C type) pyrrhotite demonstrates a higher reactivity than the non-magnetic (6C type) pyrrhotite. These results are in close agreement with the work of Lehmann *et al.* (2000), who demonstrated that the rate of dissolution of the monoclinic (i.e. magnetic) pyrrhotite under the variety of conditions was found to be greater than that of the hexagonal (i.e. non-magnetic) pyrrhotite. In another study, done by Dunn *et al.* (1995), it was shown that the rate of dissolution increased linearly as the pyrrhotite composition changed from $Fe_{0.97}S$ to $Fe_{0.86}S$ (i.e. non-magnetic to magnetic). Alekseeva (1965) also reported that the oxidation rate grows with an increase in the atomic ratios of sulfur to iron (1.00 to 1.14; FeS to Fe_7S_8).

Both the rest potential and polarisation resistance measurements showed the same trend in the reactivities of the pure pyrrhotites (i.e. 4C pyrrhotite is more reactive towards oxidation than 6C pyrrhotite). The cathodic scans also showed that the mineral that is less reactive towards oxidation is a good substrate (catalyst) for oxygen reduction and it is less susceptible to oxidation.

5.4.1.4. Anodic polarisation diagrams in the absence of xanthate

Pyrrhotite oxidation in the absence of flotation reagents (such as xanthate and activator) was investigated; the aim was to establish the nature and behavior of the mineral surface prior to reaction with flotation reagents. The anodic scans were recorded by changing the potential linearly with time from 50 mV negative of the mineral's rest potential to 0.60 V (SHE). The repeatability of measurements is presented in *Appendix 1D. Figure 42* shows the different anodic behaviour of different pure pyrrhotites in a de-oxygenated 0.05 M tetraborate solution.

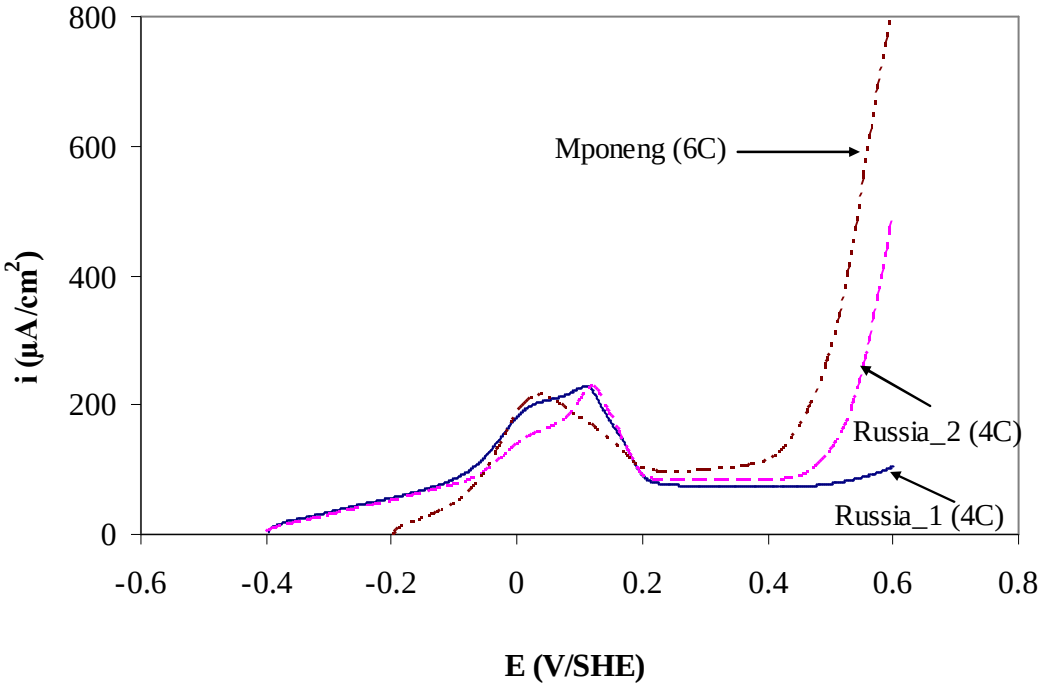

Figure 42: Anodic behaviour of pure pyrrhotite samples in a de-oxygenated 0.05 M $Na_2B_4O_7$ solution at pH 9.3. Potential sweeps were carried out at 10 mV/s.

Under oxygen-deficient conditions, the rest potentials of the pyrrhotites are very low. When the potential exceeds -0.40 V (SHE), the initial rate of pyrrhotite oxidation becomes significant for both the 4C type pyrrhotites; with the 6C type pyrrhotite, oxidation only starts at potentials greater than -0.20 V (SHE). These results show that the 4C pyrrhotites are initially more reactive than the 6C type pyrrhotite at potentials less than -0.10 V (SHE). Peaks are observed in the potential range -0.10 to 0.25 V (SHE). This region is within the potential region where flotation normally takes place (Yoon *et al.*, 1995). The peaks represent the oxidation products on the surface. Khan and Kelebek (2004) reported an anodic peak in the potential range -0.05 to 0.11 V (SHE). Buswell and Nicol (2002) also reported a fairly small anodic current plateau from 0.20 to 0.50 V (SHE), although even though subsequent anodic scans produced two peaks in the same potential range.

On the basis of the data reported by various authors (Hamilton and Woods, 1981; Buckley and Woods, 1985a; Buckley and Woods, 1985b; Hodgson and Agar, 1989; Mikhlin, 2000; Buswell and Nicol, 2002; Khan and Kelebek, 2004; Cruz *et al.*, 2005), the anodic peaks in

the potential range -0.10 to 0.25 V (SHE) shown in *Figure 42* are attributed to the following: (1) the formation of metal-deficient sulfide due to the preferential dissolution of Fe relative to S; (2) the formation of elemental S (S^0) on the mineral surface; and (3) oxidation of released Fe^{2+} to ferric hydroxide. Anodic peaks of the Russian (4C) pyrrhotites are slightly different. The differences might be due to slight variations in trace metal content and atomic Fe:S ratios.

As in the studies done by Buswell and Nicol (2002) and Khan and Kelebek (2004), no additional current peaks were observed when the scanning potential in the intermediate range was increased. This can be attributed to the increasing amount of oxidation products that form a passivating layer at intermediate potentials (Cruz *et al.*, 2005). In the passive region at potentials between 0.25 and 0.40 V (SHE), current densities of the Mponeng 6C pyrrhotite are slightly higher, suggesting that it is slightly less passivated than the Russian 4C type pyrrhotites. This result agrees with the Rp measurements shown earlier, where the Rp of the Russian 4C type pyrrhotites was higher than that of the Mponeng 6C type pyrrhotite. The variation in the percentage difference could be attributed to the different conditions (i.e. presence and absence of oxygen) under which the electrodes were treated and to the different techniques used.

An increase in anodic currents was only observed when the potential reached about 0.40 V (SHE). This increase in current was attributed to the formation of sulfates by the rupturing of the elemental S passivating layer (Cruz *et al.*, 2005) in addition to the formation of ferric hydroxide (Hamilton and Woods, 1981; Ribbe, 1984). Part of the current at higher potentials still goes to produce sulfur and sulfate; however sulfate is the dominant product on sweeps taken to much higher potentials (Hamilton and Woods, 1981; Hodgson and Agar, 1989). The anodic processes take place according to *reactions 16* and *17* shown earlier in *Section 2.2.4.2*.

The increase in current at potentials higher than 0.40 V (SHE) started earlier for the 6C pyrrhotite; with for the 4C pyrrhotites, the anodic currents increased at a potential of about 0.45 V (SHE). The Mponeng 6C type pyrrhotite showed higher anodic currents than the Russian 4C type pyrrhotites; the Russia_2 pyrrhotite showed higher currents than the Russia_1 pyrrhotite. As for the Russian_1 4C pyrrhotite, the formation of sulfates appears to be inhibited and this can be attributed to the extent of passivation of the mineral and the integrity of the surface oxidation layer. The pyrrhotite reactivity seems to be controlled by the

formation of oxidation product layers that coat and passivate the pyrrhotite surface. Therefore, it could be said that the low anodic currents observed for the Russian_1 4C pyrrhotite could be due to the passivating oxidation product layer. Surface characterisation tests of the different pyrrhotites would have been useful to determine the integrity, properties and composition of the surface oxidation product layer in order to explain the differences in the behaviour of the pyrrhotites.

5.4.1.5. Current density-time transients

Potentiostatic current versus time transient experiments were used to investigate the oxidation rates of the selected pure massive pyrrhotite samples. The reproducibility of measurements is demonstrated in *Appendix 1E*. *Figure 43* presents a set of current density–time transients in response to a step in electrode potential from rest potential to 0.25 V (SHE) in a de-oxygenated 0.05 M $Na_2B_4O_7$ solution at a pH value of 9.3. The Russia_2 pyrrhotite was the 4C type pyrrhotite chosen for this test, since there were no significant electrochemical differences observed between the Russian 4C type pyrrhotites at the selected potential of 0.25 V (SHE).

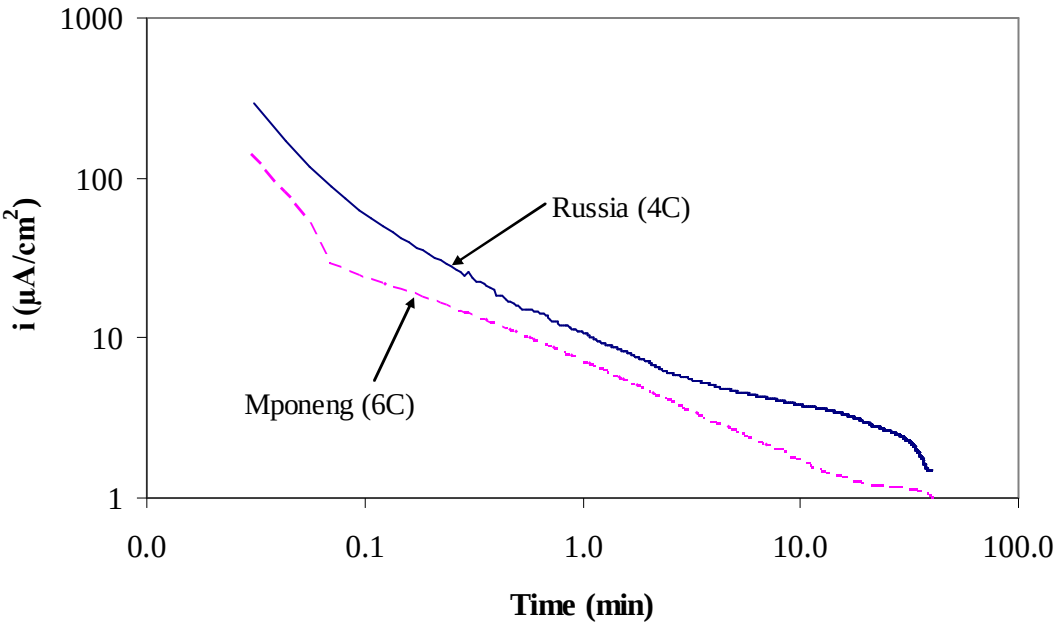

Figure 43: Current density-time transients in response to a step in electrode potential from rest potential to 0.25 V (SHE) in a 0.05 M $Na_2B_4O_7$ solution at pH 9.3.

Initially, when the electrodes were immersed in the solution, there was no dissolved Fe in solution in close proximity to the electrode surface. With time, Fe dissolved into the solution in the form of Fe^{2+}. As a result, there was a concentration gradient that formed close to the surface, with the Fe^{2+} concentration decreasing away from the surface into the bulk solution. Results in *Figure 43* show that when oxidised potentiostatically, the oxidation rate of the Russia_2 (4C) pyrrhotite was higher than that of the Mponeng (6C) pyrrhotite. Although the faster oxidation of the 4C type pyrrhotite is expected to lead to thicker passive layers, the oxidation rates remained in the order: 4C pyrrhotite > 6C pyrrhotite during the whole oxidation process, implying that the passivation of the 4C pyrrhotite was less extreme than that of the 6C pyrrhotite.

Lehmann *et al.* (2000) reported the dissolution rate of the monoclinic (i.e. magnetic) pyrrhotite, under the variety of conditions, to be greater than that of the hexagonal (i.e. non-magnetic) pyrrhotite. Hexagonal pyrrhotite has a higher iron content and would be expected to afford a denser iron-oxy-hydroxide coating than the monoclinic form (Lehmann *et al.*, 2000). In relation to the present study, this could suggest that the greater the density of the

coating, the greater the propensity for it to inhibit the diffusion of Fe to the film-solution interface or of anions to the metal-film interface. If a coating is formed, which then sloughs off once it reaches a certain mass and some of the pyrrhotite is taken with it, then the available surface area may increase rapidly and begin a new phase of the reaction (Lehmann *et al.*, 2000). This occurred in monoclinic pyrrhotite and not hexagonal pyrrhotite because in part, as pointed out earlier, hexagonal pyrrhotite contains more iron than monoclinic pyrrhotite and so affords a more consistent adhering iron oxy/hydroxy coating which prevents the break-up of the surface (Lehmann *et al.*, 2000).

The current continued decreasing during the oxidation process, indicating that both pyrrhotites continued reacting. This suggests that a porous oxidation layer, rather than a compact layer was formed on the pyrrhotite surface. Linge (1995) reported the formation of a porous layer, rather than a compact layer on the pyrrhotite surface during oxidation and this layer becomes a greater barrier to diffusion with time. A porous thickening and protective iron-oxy-hydroxide layer starts to form and control the oxidation reaction. These results suggest that the solid-state ionic transport (i.e. diffusion and migration) of Fe may be the rate-determining step in the oxidation, once the Fe surface sites have been oxidised (Vaughan *et al.*, 1995).

These results are in agreement with the Rp measurements and anodic scans, which showed that the 4C type pyrrhotite is anodically more reactive than the 6C type pyrrhotite. However, in terms of surface passivation, the results are contradictory. The Rp measurements (see *Figure 40*) showed that passivation of the 4C pyrrhotite is greater than the 6C pyrrhotite. The differences might be attributed to the different operating conditions, specifically, the presence of oxygen in solution, which might affect the rate-determining step in the oxidation process and the integrity of the passivation layers.

Anodic films present a barrier to further reaction, however, several mechanisms do exist whereby further oxidation, either dissolution or film growth may continue (Ritchie *et al.*, 1999). If the film has an appreciable solubility, a steady state can ensue, especially under hydrodynamically controlled conditions, where the rate of formation is balanced by the rate of dissolution. If the film is porous, especially when the dissolution precipitation mechanism operates, the film may grow thicker as material deposits at a location remote to the site of corrosion. A coherent film may still grow thicker under such conditions that it allows ionic

conduction of metal ions to the film-solution interface or of anions to the metal-film interface. Finally, a protective film would prevent further oxidation or current flow, resulting in passivation (Ritchie *et al.*, 1999).

Solution composition has a significant influence on the nature of the products of pyrite oxidation in alkaline media (Caldeira *et al.*, 2003). It is thus expected that the absence and presence of oxygen in the solution could have an influence on the nature of the oxidation product layers on the 4C and 6C type pyrrhotites. The differences in the dissolution profile and the extent of dissolution, suggests that the crystal structure of the pyrrhotite significantly affects the mechanism by which each type dissolves (Lehmann *et al.*, 2000). Therefore, in the present study, in terms of passivation of the 4C and 6C type pyrrhotites, it should be stressed that conclusive evidence is hard to come by. Surface characterisation would have been ideal in determining the microstructure, morphology, nature and properties of the oxidation product layers such as the porosity, grain size and thickness.

5.4.1.6. ToF-SIMS

ToF-SIMS was used to investigate the changes on the surface of the polished pyrrhotite surface in an oxygen-saturated 0.05 M borate solution after an hour, for both the Russian (4C type) and Mponeng (6C type) pyrrhotites. Images of polished and oxidised surfaces are shown in *Figures 44* and *45*, respectively.

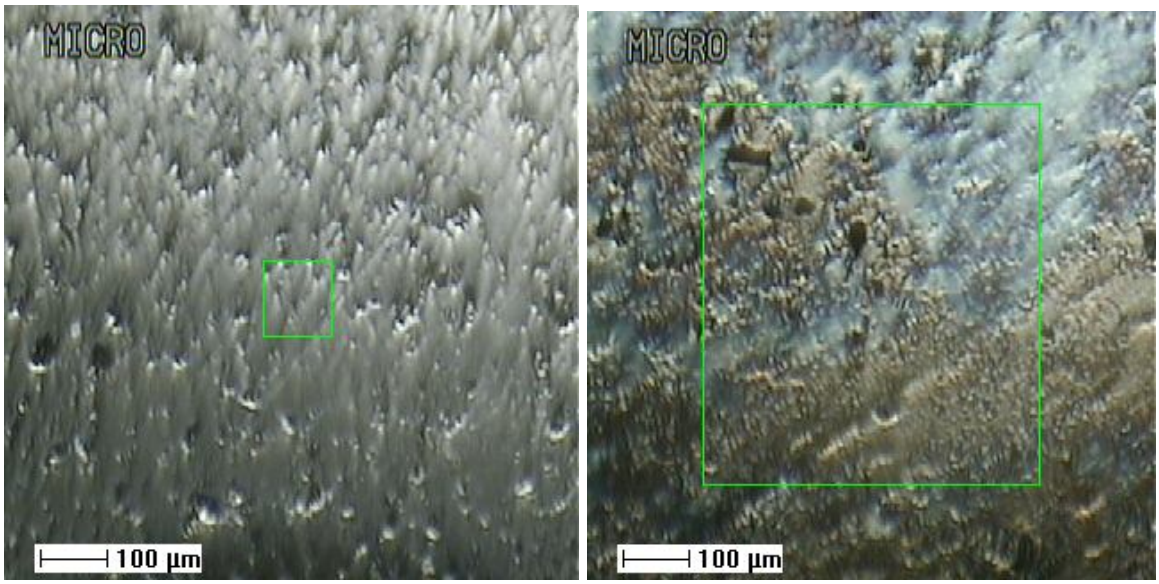

(a) (b)

Figure 44: The ToF-SIMS images of the Russian pyrrhotite (a) polished surface and; (b) 1 hour oxidised surface in an oxygen-saturated 0.05 M borate solution at pH 9.3.

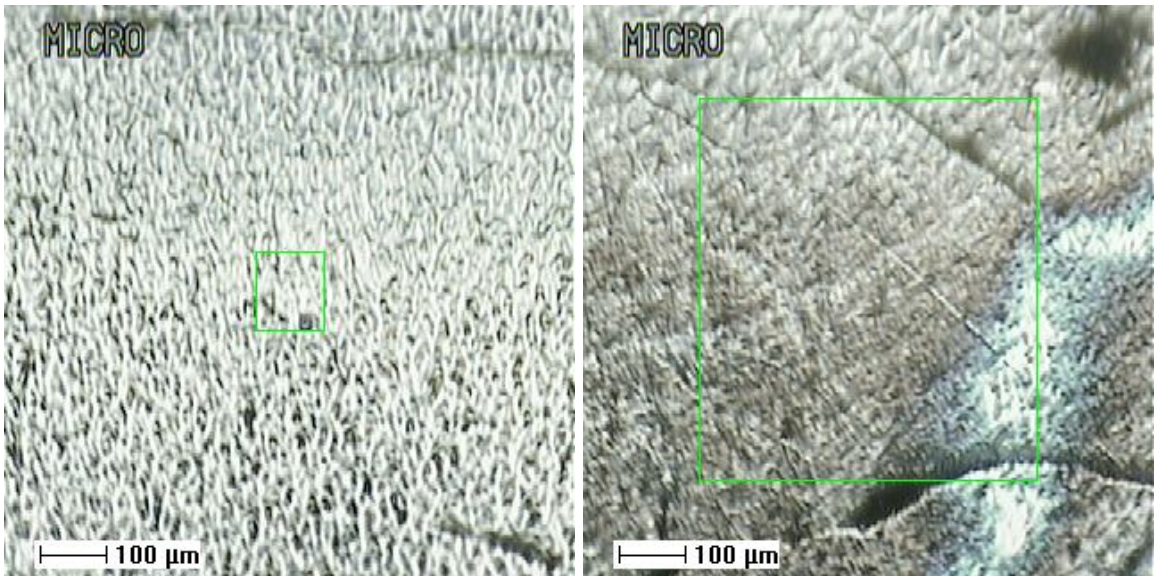

(a) (b)

Figure 45: The ToF-SIMS images of the Mponeng pyrrhotite (a) polished surface and; (b) 1 hr oxidised surface in an oxygen-saturated 0.05 M borate solution at pH 9.3.

It is evident from the images in *Figure 44 (a)* and *(b)* and *Figure 45 (a)* and *(b)* that there is a change between the freshly polished surface and the oxidised surface: surface texture changed, indicating the formation of a surface layer.

Depth profiles (*Figures 46* and *47*) of the above-mentioned surfaces show that oxygen containing species were formed on the surface after oxidation. Pratt *et al.* (1994) who studied the oxidation of pyrrhotite and the XPS iron and oxygen data, suggested a Fe(III)-oxyhydroxide to be the species forming and attributed this to the vacancies inherent to non-stoichiometric pyrrhotite; these were proposed to promote diffusion of iron to the surface, resulting in the formation of iron oxyhydroxide species. Buckley and Woods (1985a) reported the formation of oxide coatings on pyrrhotite surfaces after only a few minutes of exposure to air.

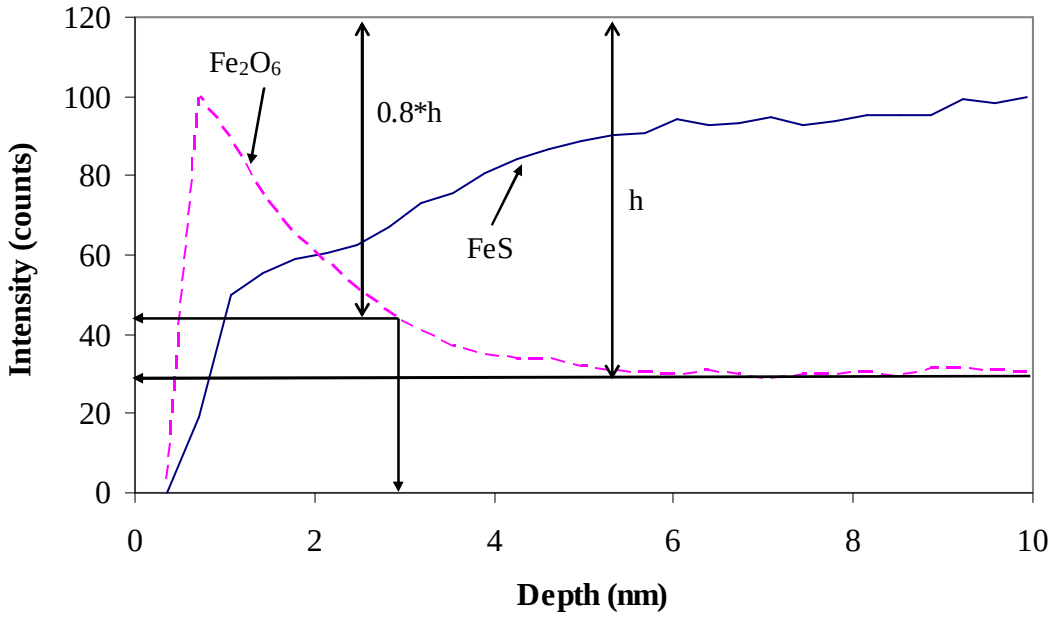

Figure 46: ToF-SIMS depth profile of polished 4C type pyrrhotite.

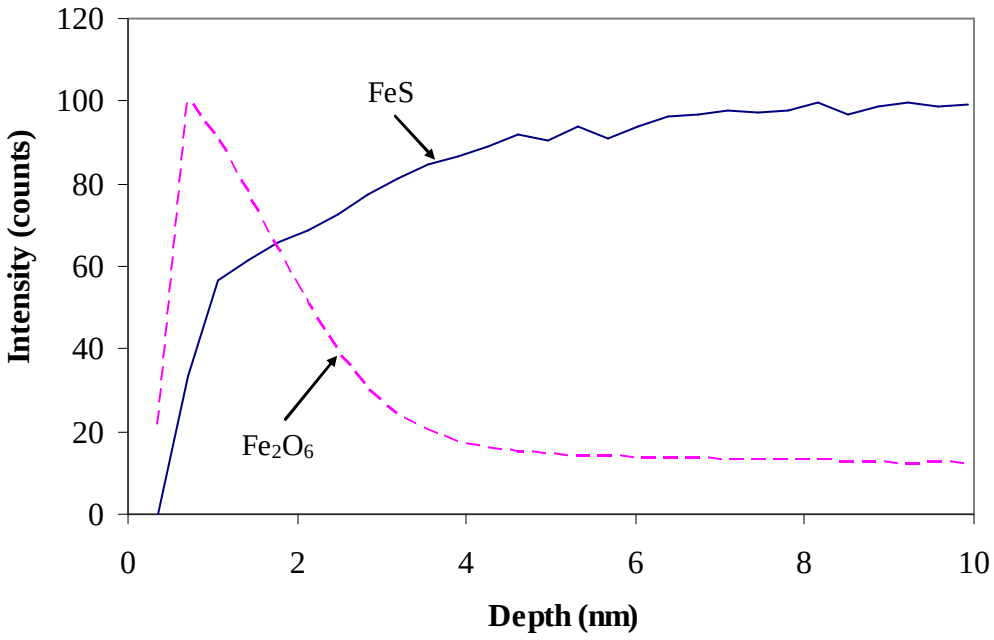

Figure 47: ToF-SIMS depth profile of polished 6C type pyrrhotite.

On the depth profile graph, FeS and Fe_2O_6 refer to the pyrrhotite surface and oxidation product, respectively. The point where the two curves intersect does not indicate the thickness of the oxide layer on the surface. When determining the oxide layer thickness, a 20 % error has to be taken into account because of uneven sputtering. As indicated in *Figures 44* and *45*, the surfaces are not flat, therefore uneven sputtering is expected. If there was no error, the thickness would be taken as the depth corresponding to where height 'h' starts becoming constant (see *Figure 46*). Taking into account the 20 % error, on the oxide depth profile, the thickness is the depth corresponding to 80 % of height 'h'.

In this study, it appeared that after wet polishing, the surface reacted with oxygen in the atmosphere and the oxide layer thickness for both the polished 4C and 6C pyrrhotites was 2.89 and 3.06 nm, respectively. The differences in the thickness could be attributed to the interaction of the different mineral surfaces with the adsorbed water (during polishing) and oxygen in the atmosphere.

Comparison of the two profiles for oxidised 4C and 6C pyrrhotites, in *Figures 48* and *49* respectively, demonstrates progressive oxidation of the surface.

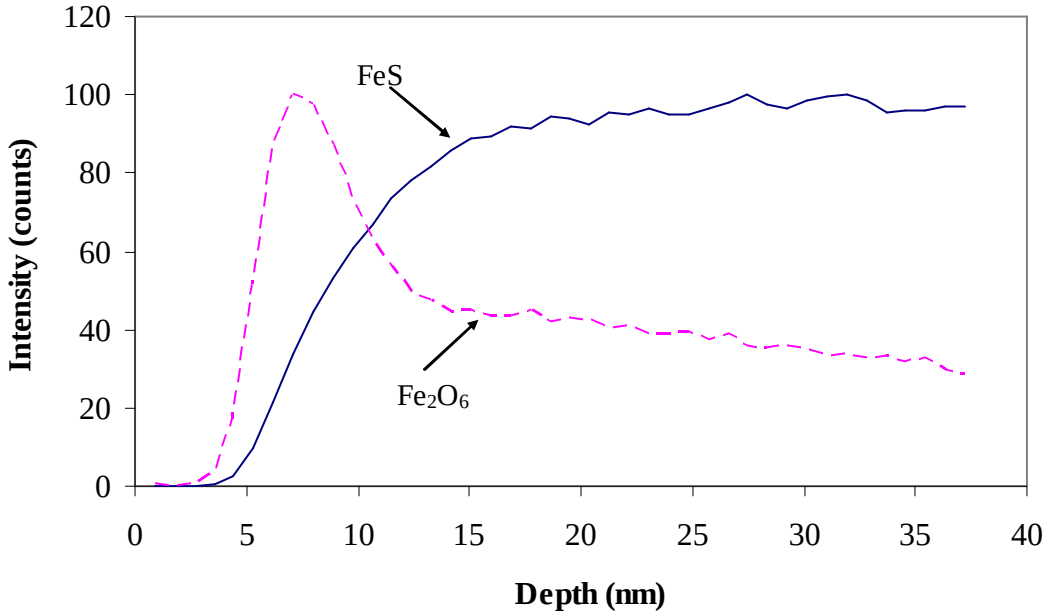

Figure 48: ToF-SIMS depth profile of an oxidised 4C type pyrrhotite in an oxygen-saturated 0.05 M borate solution at pH 9.3.

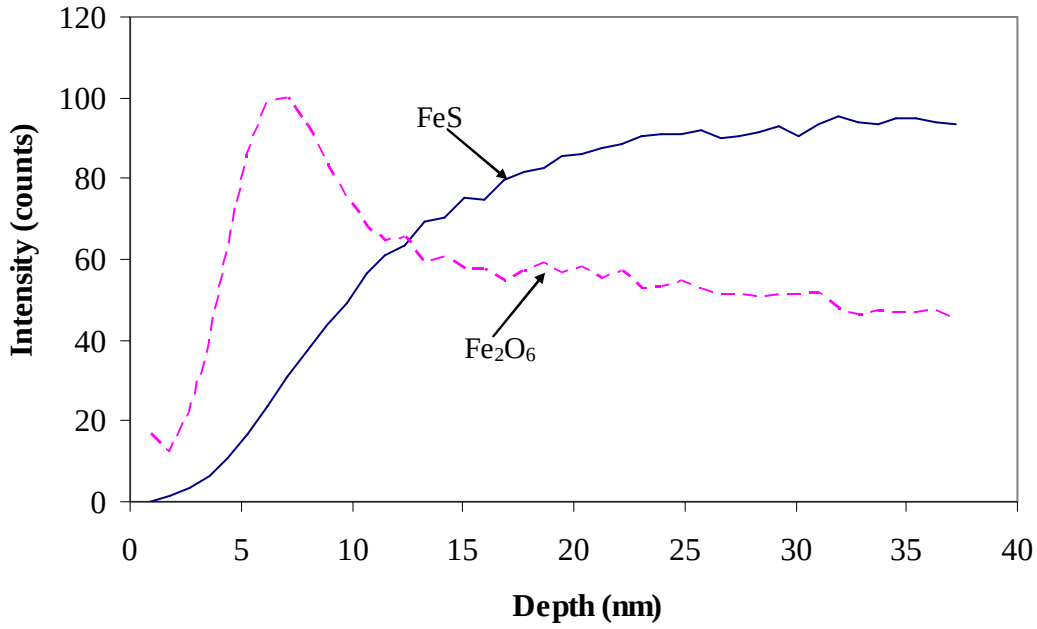

Figure 49: ToF-SIMS depth profile of an oxidised 6C type pyrrhotite in an oxygen-saturated 0.05 M borate solution at pH 9.3.

As can be seen in *Figures 48* and *49*, the oxide profile did not stabilise: it continued decreasing. Height 'h' was determined at the point of inflection, where the rate of the reduction in intensity starts slowing. After one hour of oxidation in O_2-rich solution, the oxide layer thickness increased by 8.67 nm to 11.56, and by 7.40 nm to 10.46 nm for the 4C and 6C pyrrhotites, respectively. The oxide layer thickness of the 4C pyrrhotite was slightly higher than that of the 6C pyrrhotite by 1.10 nm. These results are in agreement with the Rp measurements shown earlier in *Figure 40*, as well as the passivation region in the anodic scans in *Figure 42* (showing that the 4C pyrrhotite is more passivated than the 6C pyrrhotite). These results suggest that the 4C pyrrhotite is more reactive and forms a thicker oxide layer than the 6C pyrrhotite. Thus, ToF-SIMS assisted in showing the formation of an oxide layer on the surface, however, it does not provide information on the integrity (i.e. its porosity) of the oxide layer. However, care should be taken when comparing the ToF-SIMS results to the electrochemical measurements; this because during electrochemical measurements, the electrodes are kept in the solution throughout the measurements and taken out of the solution after the tests have been completed. Prior to transferring the samples to the ToF-SIMS equipment, samples are taken out of the solution and dried. This causes the samples to react with oxygen in the atmosphere, which affects the surface. As pointed out by Debnath and Anderson (1982), many *ex situ* investigations of passive layers suffer from the disadvantage that loss of water and film restructuring occur under high vacuum conditions, the situation being further exacerbated by ion beam heating.

5.4.1.7. Anodic polarisation diagrams in the presence of xanthate

The oxidation behaviour of pyrrhotite was investigated in an attempt to establish the influence of chemical composition and crystal structure on pyrrhotite response in the presence of xanthate. The anodic polarisation diagrams of the pure massive pyrrhotite samples were constructed by changing the potential from 50 mV negative of the mineral's rest potential to 0.60 V (SHE) in a de-aerated 0.05 M borate solution in the presence of a 1.0 x 10^{-3} M potassium ethyl xanthate (KEX). The repeatability of the measurements is shown in *Appendix 1F*. *Figures 50* to *52* indicate the influence of xanthate on the anodic current densities of the pure pyrrhotites.

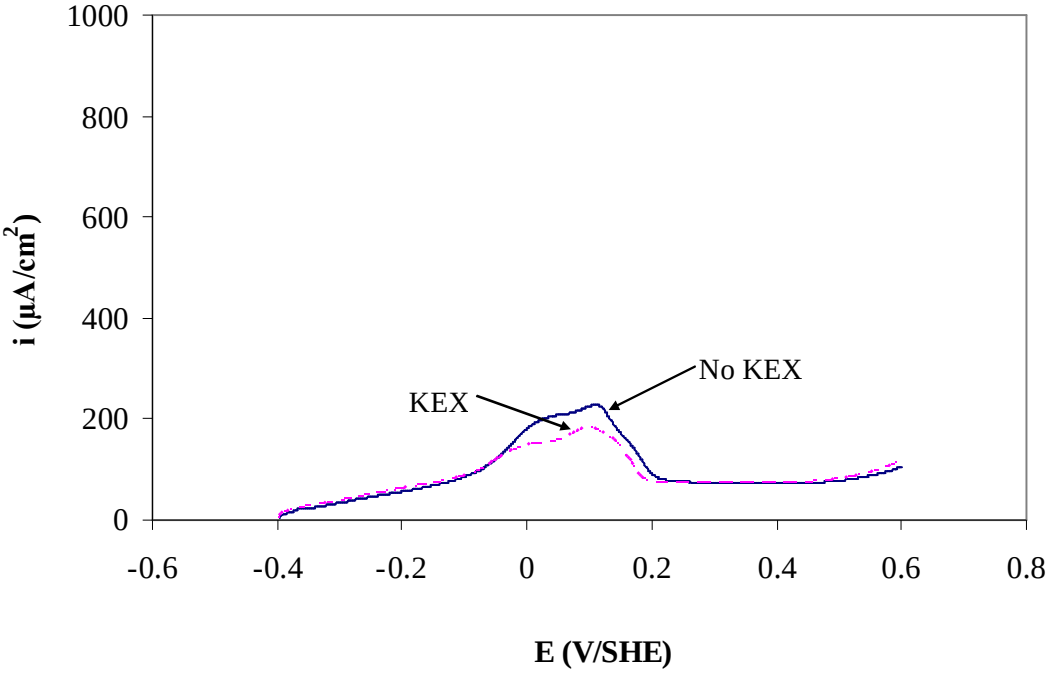

Figure 50: The anodic polarisation diagram of the Russian_1 4C pyrrhotite in a 0.05 M borate solution at pH 9.3 in the absence and presence (1.0×10^{-3} M) of potassium ethyl xanthate (KEX). Potential sweeps were carried out at 10 mV/s.

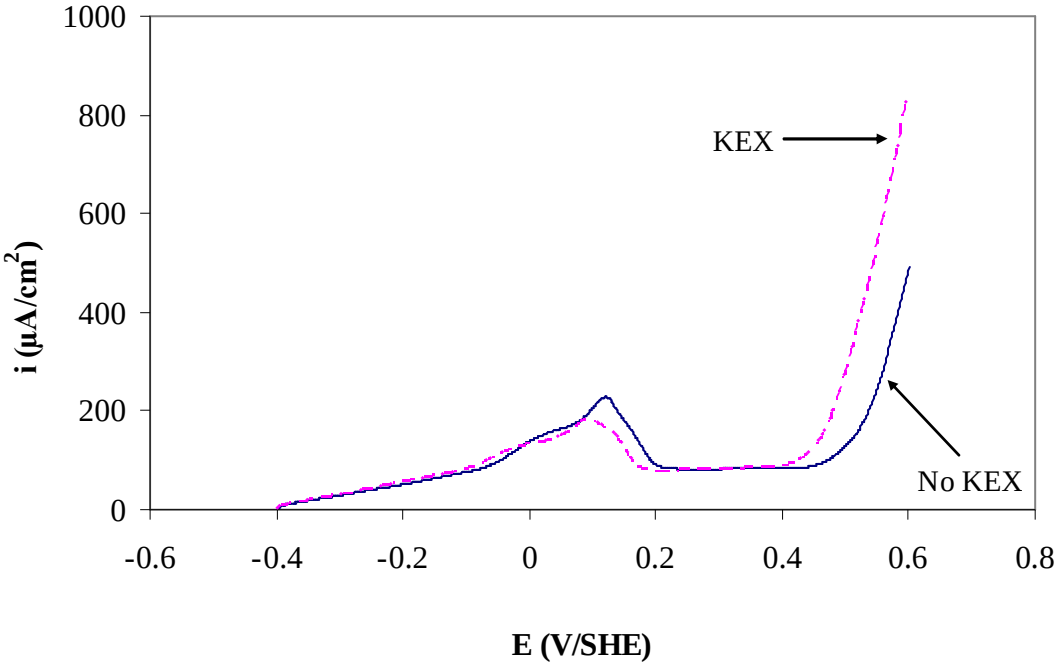

Figure 51: The anodic polarisation diagram of the Russia_2 4C pyrrhotite in a 0.05 M borate solution at pH 9.3 in the absence and presence (1.0 x 10^{-3} M) of potassium ethyl xanthate (KEX). Potential sweeps were carried out at 10 mV/s.

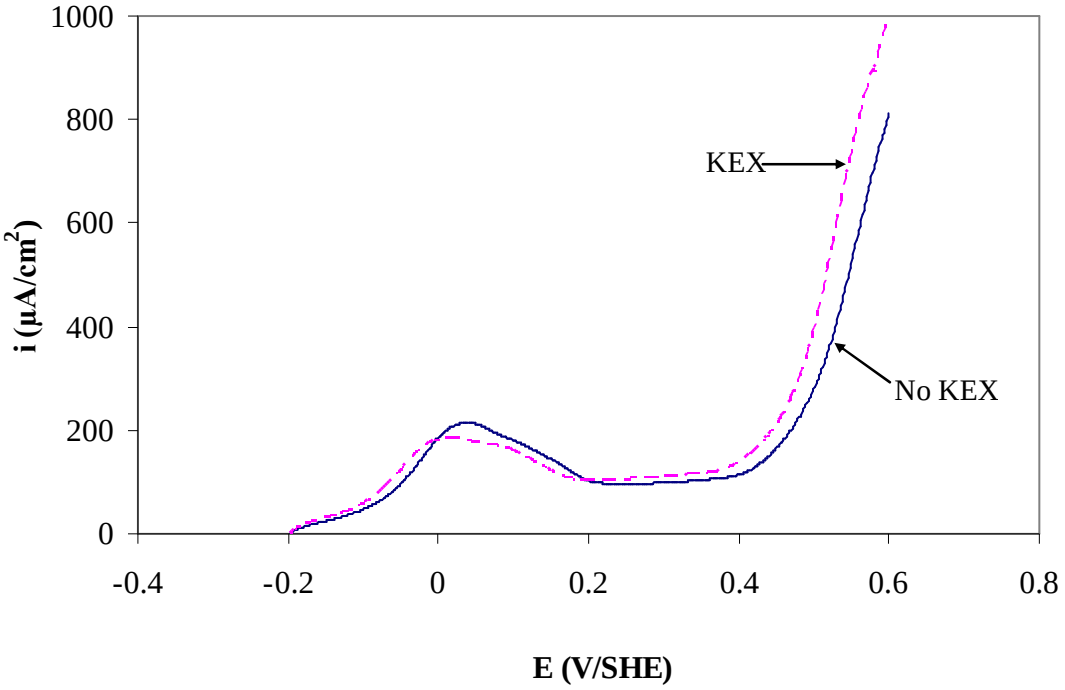

Figure 52: The anodic polarisation diagram of the Mponeng 6C pyrrhotite in a 0.05 M borate solution at pH 9.3 in the absence and presence (1.0 x 10^{-3} M) of potassium ethyl xanthate (KEX). Potential sweeps were carried out at 10 mV/s.

Figures 50 to *52* show that the starting potentials of the minerals did not change with the addition of KEX for the Russian and Mponeng pyrrhotites. The same behaviour was observed by Khan and Kelebek (2004). These figures show slightly enhanced anodic activity at negative potentials up to 0 V (SHE) and above 0.40 V (SHE) in the presence of xanthate. However, above 0.40 V (SHE), the anodic activity of the Russia_1 pyrrhotite was still low (similar to the results obtained in absence of xanthate). The increase in anodic current on xanthate addition is attributed to the anodic reaction of the xanthate with the pyrrhotite surface (Buswell and Nicol, 2002). There was no "pre-wave" observed on the anodic scans because adsorption and oxidation of xanthate on pyrrhotite take place in the same region (Buswell and Nicol, 2002). The oxidation currents at potentials between -0.10 and 0.25 V (SHE), where the surface oxidation products are expected to form, are reduced due to the adsorption of xanthate on the surface (Tolley *et al.*, 1996; Buswell and Nicol, 2002; Khan and Kelebek, 2004). The low oxidation currents in this potential range suggest that the oxidation of the mineral continues more slowly when the mineral is protected by a layer of xanthate,

which impedes current flow between the mineral and the solution. The following Nernst equation was used to determine the potential needed for xanthate to dixanthogen transformation for the system used in the present work:

$$E_h = E_h° - 0.0592\log[X^-] \qquad \textit{Eq. 33}$$

where E_h = redox potential,
$E_h°$ = standard redox potential, which equals -0.06 V (SHE) for KEX (Allison *et al.*, 1972),
$[X^-]$ = concentration of thiol collector.

Thus, at a KEX concentration of 1.0 x 10^{-3} M, the potential needed for the xanthate to dixanthogen formation was determined to be 0.118 V (SHE). Khan and Kelebek (2004) reported the transformation of xanthate to dixanthogen at 0.125 V (SHE) for *n*-butyl xanthate at 10^{-4} M. The development of appreciable hydrophobicity on pyrrhotite surfaces is observed in the potential range of 0.10 – 0.125 V (SHE) (Yoon *et al.*, 1995). The potential, i.e. 0.118 V (SHE), at which the xanthate to dixanthogen transformation is expected falls within the -0.10 to 0.25 V (SHE) potential range where the anodic current peaks occur, suggesting that the adsorption of xanthate and the formation of dixanthogen on the surface are in the same region where mineral oxidation takes place. In anodic scans, the potentiostat drives the reaction to form dixanthogen since there is no oxygen to oxidise xanthate to dixanthogen.

In spectroscopic studies using ethyl xanthate on hexagonal pyrrhotite, Fornasiero *et al.* (1995) found: that for the highest xanthate concentration (5.21 x 10^{-4} M) the infrared spectra were dominated by the dixanthogen formation; and dixanthogen was the only xanthate species present on the surface of pyrrhotite, its concentration increasing with conditioning time. Yuehua *et al.* (2005) also showed in the FTIR reflection spectra that at pH 8.8, which is close to pH 9.3 in this study, the xanthate species with a higher adsorption density on pyrrhotite is dixanthogen. In addition it was shown that the dixanthogen adsorption is independent of potential in the range 140 to 250 mV (SHE) due to the occurrence of almost the same dixanthogen characteristic bands. Nevertheless, the IR signals of the characteristic dixanthogen peaks, and hence dixanthogen adsorption on pyrrhotite, increased with increasing potential from 140 to 250 mV (SHE).

Figure 53 compares the anodic behaviour of pure pyrrhotites in the presence of potassium ethyl xanthate.

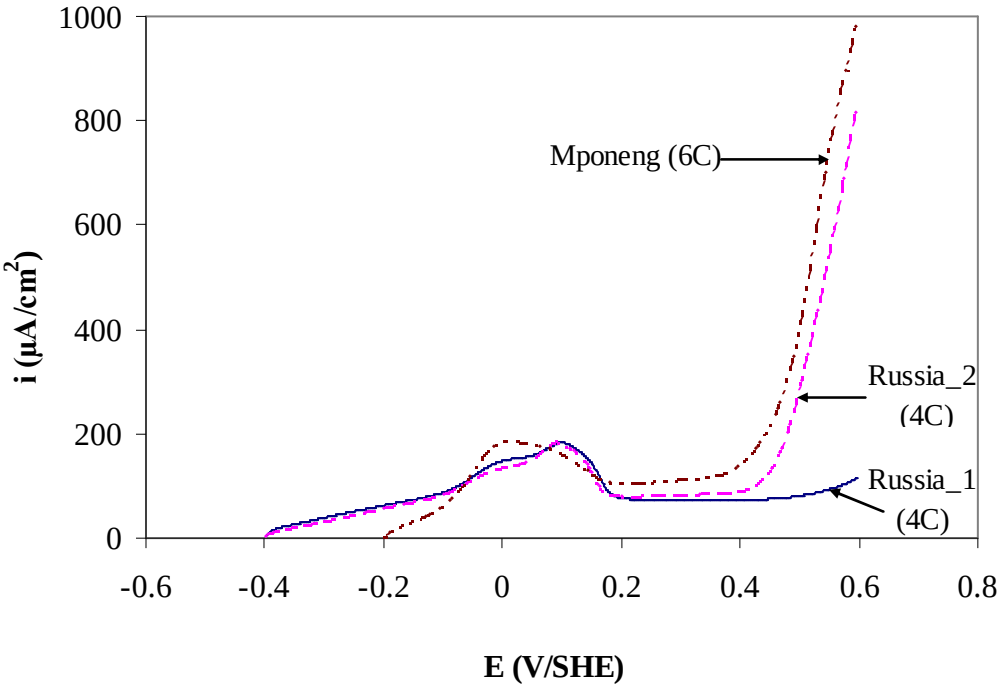

Figure 53: Comparison of the anodic behaviour of pure pyrrhotite samples in a de-oxygenated 0.05 M $Na_2B_4O_7$ solution in the presence (1.0×10^{-3} M) of potassium ethyl xanthate (KEX). Potential sweeps were carried out at 10 mV/s.

Similar to what was seen in the previous anodic polarisation diagram (see *Figure 42*), in the absence of xanthate, the Russian 4C pyrrhotites had lower starting potentials than the Mponeng 6C pyrrhotite. This shows that the presence of xanthate does not alter the order of the reactivity of the minerals (i.e. 4C type pyrrhotite is more reactive than the 6C type pyrrhotite). The anodic peaks of the Russian 4C pyrrhotites are similar. In the potential range of 0.10 – 0.125 V (SHE), where the development of appreciable hydrophobicity on pyrrhotite surfaces was observed by Yoon *et al.* (1995), the Mponeng anodic currents are slightly lower. However, at more positive potentials above 0.40 V (SHE), the anodic activity of the Mponeng 6C type pyrrhotite was higher than that of the 4C type pyrrhotites. The same behaviour was observed in the absence of xanthate (see *Figure 42*).

In this section, the effect of chemical composition and crystal structure on the electrochemical behaviour of pyrrhotite in the absence and presence of xanthate was investigated. It was found that magnetic 4C pyrrhotite is more reactive than the non-magnetic 6C pyrrhotite under all conditions studied. The results also showed that different types of pyrrhotite behave differently in the presence of xanthate, suggesting that the flotation response of these pyrrhotite types could be different. Contact angle measurements would have been useful in determining the extent of hydrophobicity on the different pyrrhotites in the presence of xanthate.

5.4.2. The influence of galvanic interactions on pyrrhotite reactivity

Galvanic interaction occurs when minerals are in electrical contact and are present in a medium that facilitates charge transfer. The rates of the anodic and cathodic half-reactions that occur at the surface of each mineral type change due to galvanic interactions. In the case of mineral-mineral interactions, sulfide minerals with more positive (higher) rest potentials (i.e. noble minerals) act as cathodes in a galvanic couple, while minerals with more negative (lower) rest potentials (i.e. active minerals) act as anodes (Ekmekçi and Demirel, 1997).

The Sudbury Gertrude and Phoenix pyrrhotites were characterised with XRD and electron microprobe analyses. These samples were found to be 4C type pyrrhotites, with variations in trace metal contents (i.e. Ni, Cu and Co). Pyrrhotites with different crystal structures were previously shown (in *Section 5.4.1*) to react differently under similar conditions. A summary of the Qemscan results for the mixed samples was shown earlier in *Table 25*.

The aim of using only the 4C type pyrrhotite samples (Gertrude and Phoenix samples) was to investigate the influence of the amount of pentlandite in contact with pyrrhotite on the electrochemical behaviour of pyrrhotite. The pure Russia_2 4C type pyrrhotite was used in comparison with the mixed samples. The Russian pyrrhotite was referred to as a pure pyrrhotite; Sudbury Gertrude pyrrhotite was referred to as a medium-pentlandite-pyrrhotite; and Phoenix pyrrhotite was referred to as a high-pentlandite-pyrrhotite.

5.4.2.1. Rest potential measurements

The open circuit potentials of pure and mixed 4C type pyrrhotites are compared in *Figure 54*. The measurements are not very repeatable (*Appendix 2B*). The open circuit potential refers to the mixed potential between the active mineral (i.e. pyrrhotite) oxidation and oxygen reduction at the noble mineral (i.e. pentlandite) surface.

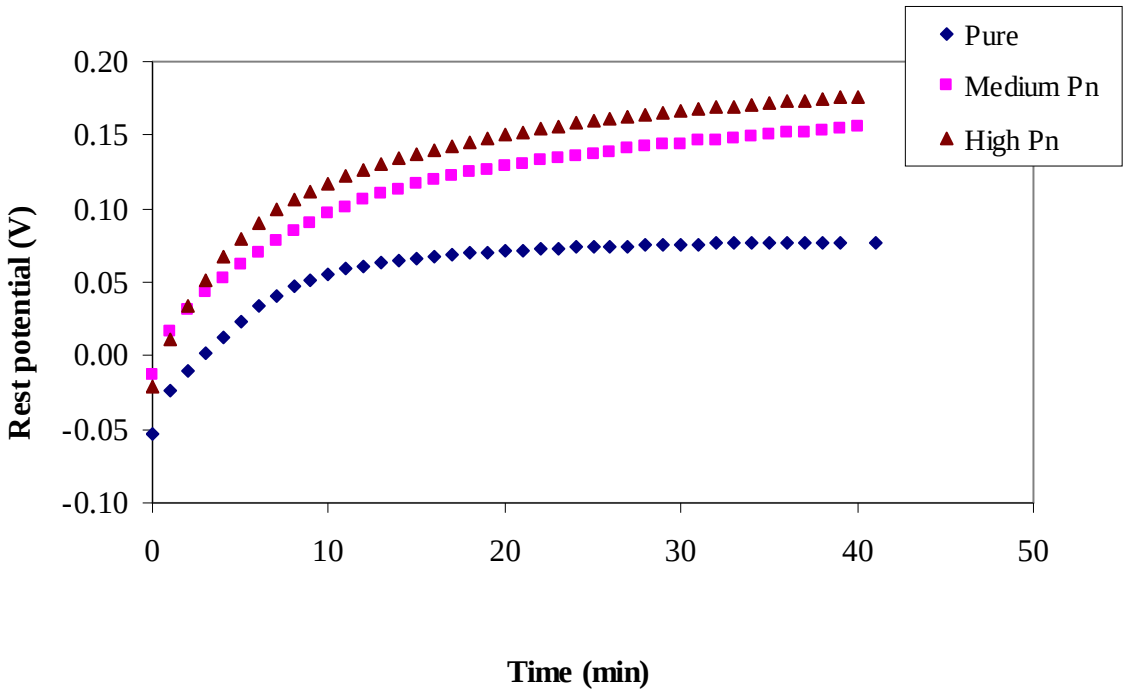

Figure 54: Rest potential of pure and mixed massive pyrrhotites in an oxygen-saturated 0.05 M borate solution at a pH of 9.3. Potential sweeps were carried out at 10 mV/s. (Pure: pure Russia_2 pyrrhotite; Medium Pn: medium-pentlandite Sudbury Gertrude pyrrhotite; High Pn: high-pentlandite Phoenix pyrrhotite).

The presence of pentlandite increased the rest potential: the higher the pentlandite content, the higher the rest potential. These results are supported by a number of authors (Rand, 1977; McIntosh and Groat, 1997; Ruonala *et al.*, 1997; Lu *et al.*, 2000; Mason and Rice, 2002; Khan and Kelebek, 2004; Cruz *et al.*, 2005; Santos *et al.*, 2006; Lin-lin *et al.*, 2009), who reported that pentlandite has a higher rest potential than pyrrhotite and that it is more noble and less susceptible to oxidation than pyrrhotite. *Figure 54* shows that the reactivity (i.e. oxidation) increases with a decreasing amount of pentlandite. As mentioned earlier (see

Section 5.4.1.1), the lower the rest potential, the higher the reactivity of the mineral towards the solution. In the mixed-mineral system, pentlandite acts as a cathode and pyrrhotite as an anode.

5.4.2.2. Cathodic polarisation diagrams

Cathodic scans of pure and mixed samples are presented in *Figure 55*. The repeatability of measurements is shown in *Appendix 2C.*

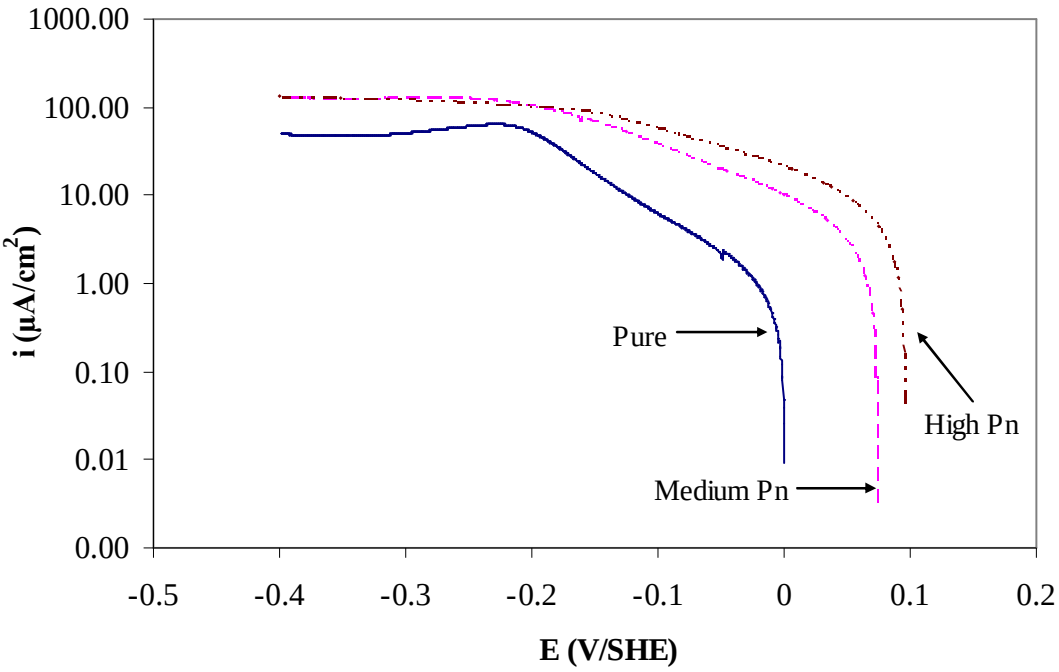

Figure 55: The cathodic polarisation diagrams of pure and mixed massive pyrrhotite samples in an oxygen-saturated 0.05 M borate solution at pH 9.3. Potential sweeps were carried out at 10 mV/s. (Pure: pure Russia_2 pyrrhotite; Medium Pn: medium-pentlandite Sudbury Gertrude pyrrhotite; High Pn: high-pentlandite Phoenix pyrrhotite).

In the region of activation control, pyrrhotite with a higher pentlandite content was found to have a higher oxygen reduction activity than a pure pyrrhotite (i.e. pentlandite has a higher rest potential and higher cathodic currents than pyrrhotite). These results agree with the rest potential measurement results of this present work and the work by Rand (1977), i.e. that

pentlandite behaves as a cathode (more noble) and pyrrhotite as an anode due to its lower rest potential. As a result, pyrrhotite is more susceptible to oxidation and pentlandite is galvanically protected when the two sulfide minerals are in electrical contact (Rand, 1977; McIntosh and Groat, 1997; Ruonala *et al.*, 1997; Lu *et al.*, 2000; Mason and Rice, 2002; Khan and Kelebek, 2004; Cruz *et al.*, 2005; Santos *et al.*, 2006; Lin-lin *et al.*, 2009). Current densities of mixed pyrrhotites are similar and higher than those of the pure pyrrhotite in the region of diffusion control. In this region, catalytic activity plays no role, because oxygen is reduced at its diffusion limited rate due to its low concentration and ease of reduction.

5.4.2.3. Polarisation resistance measurements

The polarisation resistance as a function of time for the pure and mixed pyrrhotite samples is presented in *Figure 56*. The repeatability of the measurements is presented in *Appendix 2D*.

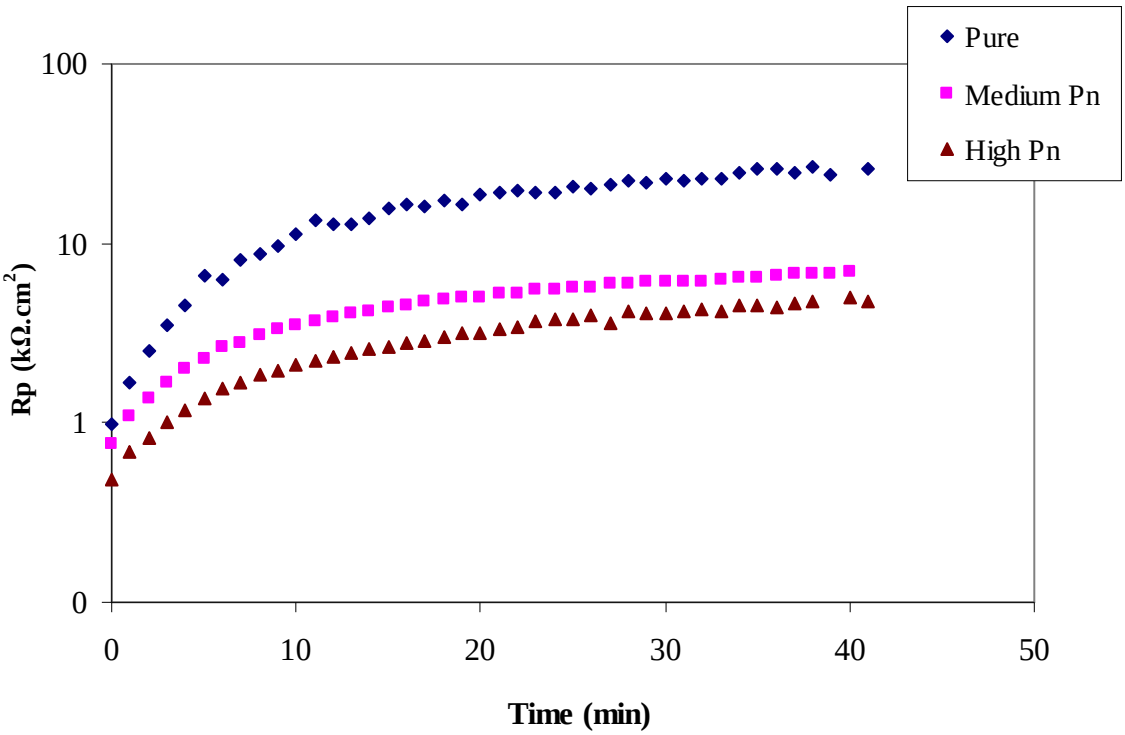

Figure 56: Comparison of the polarisation resistance of pure and mixed massive pyrrhotite samples in an oxygen-saturated 0.05 M borate solution at pH 9.3. Potential sweeps were carried out at 10 mV/s. (Pure: pure Russia_2 pyrrhotite; Medium Pn: medium-pentlandite Sudbury Gertrude pyrrhotite; High Pn: high-pentlandite Phoenix pyrrhotite).

The Rp values decreased with the increasing amount of pentlandite in the sample (*Figure 56*). This can be attributed to the presence of a large amount of Ni in pentlandite. Ni is more noble than Fe. The Fe to Ni ratio in pure pyrrhotite is higher than in pentlandite. In addition, while pyrrhotite grains are being oxidised, any pentlandite in electrical contact with them would be galvanically protected due to its higher open circuit potential. Thus, pyrrhotite oxidation will preferentially provide electrons for the reduction of the oxidant i.e. any reduction reaction occurring on the surface of pentlandite would consume electrons produced by pyrrhotite dissolution (McIntosh and Groat, 1997; Lu *et al.*, 2000; Mason and Rice, 2002; Cruz *et al.*, 2005; Santos *et al.*, 2006; Lin-lin *et al.*, 2009). The rest of the mixed minerals surfaces (where there is no pyrrhotite) are not covered by oxidation products, hence the low Rp values that suggest that there is still current flowing, which allows reactions to take place on the surface. The high Rp values of the pure mineral are due to the formation of large amounts of oxidation products on the surface (Hamilton and Woods, 1981; Buckley and Woods, 1985a; Buckley and Woods, 1985b; Hodgson and Agar, 1989; Mikhlin, 2000; Buswell and Nicol, 2002; Khan and Kelebek, 2004; Cruz *et al*., 2005).

These results indicate that the anodic reactivity increased with decreasing pentlandite content and correlate well with the rest potential measurements. Rest potential measurements showed that the sample with a higher pentlandite content (equivalent to higher nickel content) had a higher rest potential indicating lower anodic reactivity towards the solution.

The initial change in Rp was determined for the first 5 minutes and is presented in *Figure 57* for the pure and mixed 4C type pyrrhotites.

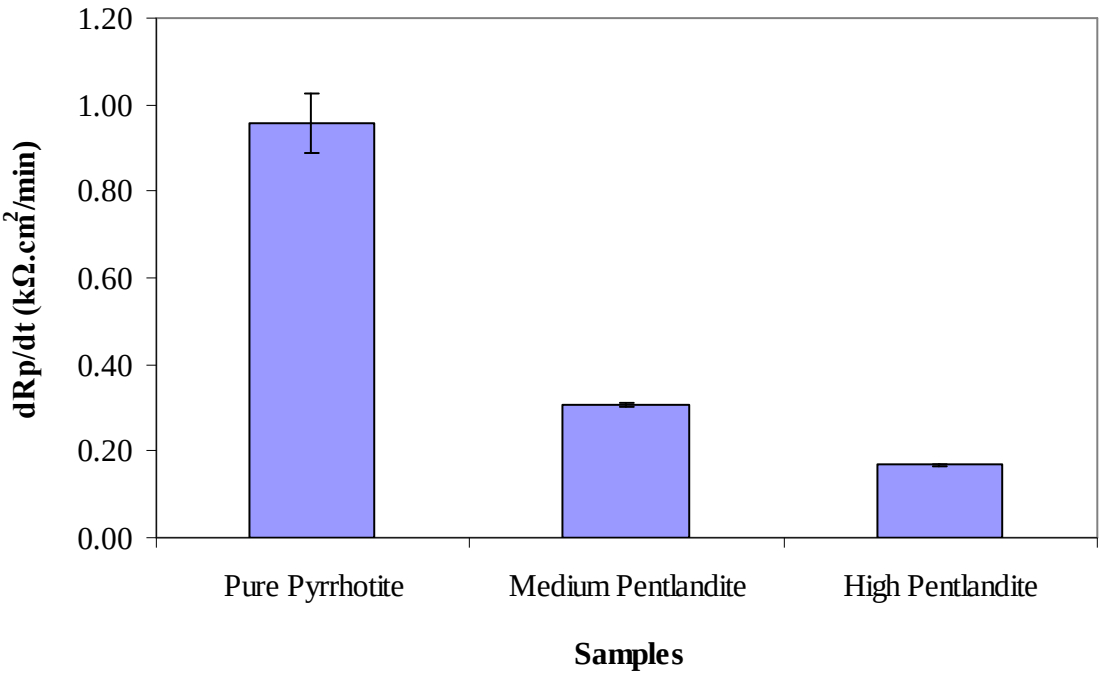

Figure 57: Comparison of the initial change in Rp of pure and mixed samples in an oxygen-saturated 0.05 M borate solution at pH 9.3. Potential sweeps were carried out at 10 mV/s. (Pure: pure Russia_2 pyrrhotite; Medium Pn: medium-pentlandite Sudbury Gertrude pyrrhotite; High Pn: high-pentlandite Phoenix pyrrhotite).

The change in Rp increased in the order: high-pentlandite < medium-pentlandite < pure; the anodic reactivity increased in a similar order.

5.4.2.4. Anodic polarisation diagrams in the absence of xanthate

Galvanic interactions do not apply in oxygen-deficient conditions because oxygen is required for the oxygen reduction reaction. In anodic scans, a potential is applied and the only reactions that take place are oxidation of the mineral in the absence of xanthate and oxidation of xanthate in the presence of xanthate. As pentlandite usually has high rest potentials, while pyrrhotite shows lower values, in those ores containing only pyrrhotite and pentlandite, the rest potential indicates that the former dissolves faster than the latter, given a certain set of conditions (Lu *et al.*, 2000). Due to its higher open circuit potential, pentlandite is oxidised at higher potentials than pyrrhotite. Therefore, at low potentials, the reactivity of pyrrhotite is

not influenced by pentlandite. As a result, the influence of trace metal content on reactivities of 4C type pyrrhotites was investigated. Trace metal content refers to the Co, Cu and Ni contents in solid solution with pyrrhotite, not in separate phases. It was shown in *Table 23* that the Phoenix pyrrhotite has a large quantity of trace metal content, particularly nickel. Nickel content increased in the order: Russia_2 < Sudbury Gertrude < Phoenix. The anodic polarisation diagrams were constructed to evaluate the anodic behaviour of pyrrhotite in contact with pentlandite (*Figure 58*). The measurements were repeatable (*Appendix 2E*).

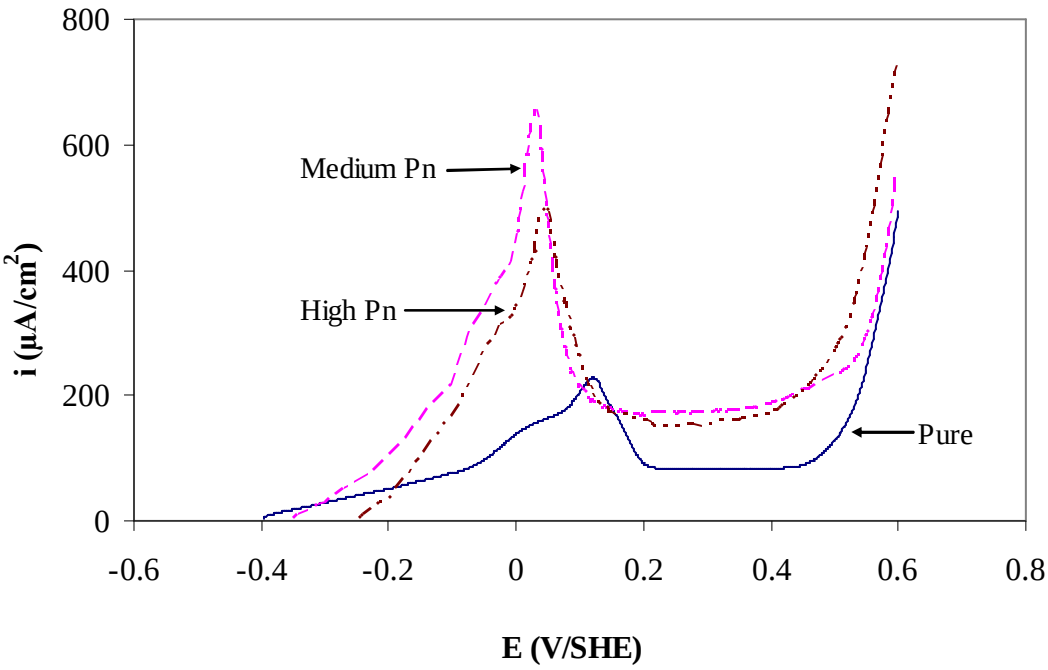

Figure 58: The anodic behaviour of pure and mixed pyrrhotite samples in a de-oxygenated 0.05 M $Na_2B_4O_7$ solution at pH 9.3 in the absence of potassium ethyl xanthate (KEX). Potential sweeps were carried out at 10 mV/s. (Pure: pure Russia_2 pyrrhotite; Medium Pn: medium-pentlandite Sudbury Gertrude pyrrhotite; High Pn: high-pentlandite Phoenix pyrrhotite).

The anodic currents of pyrrhotites started at negative potentials in the following order: pure pyrrhotite (Russia_2) < medium-pentlandite-pyrrhotite (Sudbury Gertrude) < high-pentlandite-pyrrhotite (Phoenix). The initial reactivities of these minerals increased in the order: high-pentlandite (Phoenix) < medium-pentlandite (Sudbury Gertrude) < pure pyrrhotite (Russia_2). These results compare well with the rest potential and polarisation resistance measurements (see *Figures 54*, *56* and *57*).

In the low potential region, < 0.10 V (SHE) and in mixed samples, pentlandite is inert and oxidation takes place only on pyrrhotite. In the case of mixed pyrrhotites, the anodic peaks occur at more negative potentials than with the pure pyrrhotite and the anodic currents are higher. Higher anodic currents of mixed samples indicate that the 4C type pyrrhotites in the mixed samples are much more reactive than the pure 4C type pyrrhotite. The reactivity decreased in the order: Sudbury Gertrude pyrrhotite > Phoenix pyrrhotite > Russia_2 pyrrhotite. Becker (2009) showed in cyclic voltammograms that the magnetic Sudbury Gertrude West pyrrhotite had higher anodic current densities than the magnetic Phoenix pyrrhotite in the potential range [-0.80 to 0.70 V (SHE)] investigated. No correlation could be found between the trace metal content and the reactivities of the 4C type pyrrhotites.

At intermediate potentials in the region 0.20 to 0.40 V (SHE), the mixed samples showed high passive currents, suggesting that the mixed samples are passivated to a lesser extent compared to the pure pyrrhotite. At oxidising potentials above 0.40 V (SHE), pentlandite also reacts, i.e. both minerals react, thus there are higher currents. As pentlandite has a large oxidation potential, it would be necessary to have high potentials for its complete dissolution (Santos *et al.*, 2006). The reactivity increases in the order: pure pyrrhotite (Russia_2) < medium-pentlandite (Sudbury Gertrude) < high-pentlandite (Phoenix). The enhanced anodic activity of the mixed samples could also be attributed to less passivation of the mineral surface.

5.4.2.5. Capacitance measurements

Capacitance measurements were conducted to investigate the possible formation of surface layers to validate the polarisation resistance measurements (see *Figure 56*). In the present work, a decrease in the capacitance values with time was observed and the relationship shown in *equation 31* (i.e. capacitance is inversely proportional to polarisation resistance) was found to hold in the case of pure and mixed samples [see *Figure 56* (Rp) and *Figure 59* (Cp)]. These results indicate an increased thickness of a layer on the surface when the amount of pentlandite decreases; this is shown by a reduction in the capacitance values with decreasing pentlandite content. The dielectric constant of the oxide film also changes, depending on the composition of the film (Craig, 1991).

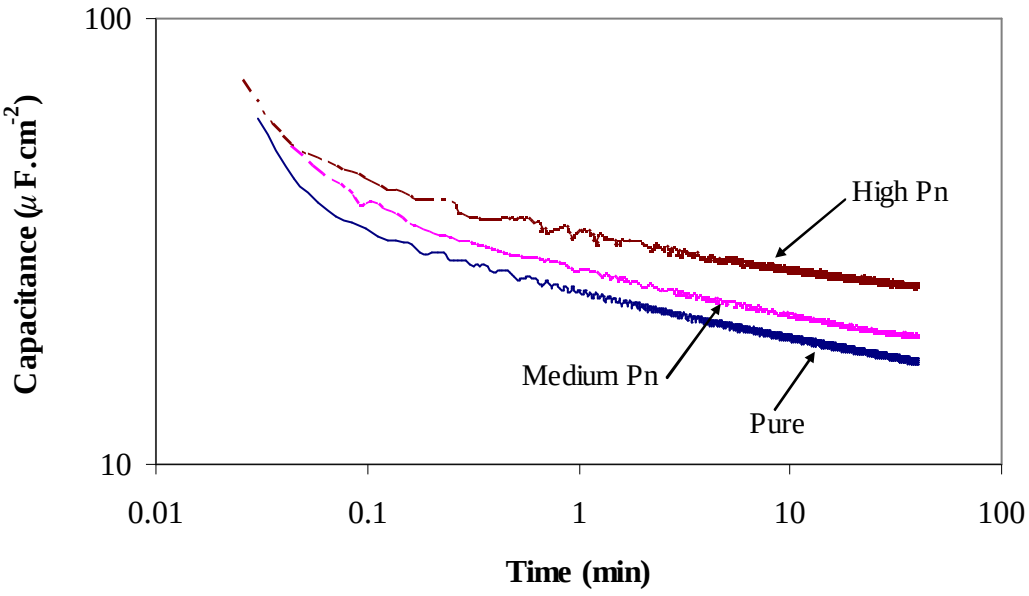

Figure 59: Capacitance measurements of pure and mixed samples in an oxygen-saturated 0.05 M borate solution at pH 9.3 in the absence of xanthate (KEX). (Pure: pure Russia_2 pyrrhotite; Medium Pn: medium-pentlandite Sudbury Gertrude pyrrhotite; High Pn: high- pentlandite Phoenix pyrrhotite).

Pure pyrrhotite is easily oxidised and forms more of the hydroxides on the surface. In the presence of pentlandite, the amount of hydroxides formed on the surface is reduced since pentlandite is more noble than pyrrhotite.

5.4.2.6. Anodic polarisation diagrams in the presence of xanthate

In anodic polarisation diagrams, galvanic interactions do not influence pyrrhotite reactivity in the low potential region since the only reaction taking place is oxidation of xanthate in the presence of xanthate. Pentlandite is more inert and does not affect the oxidation behaviour of pyrrhotite at low potentials. Anodic scans of the mixed samples were obtained in the presence of xanthate in a 0.05 M borate solution at pH 9.3. This was done to investigate the behaviour of the 4C type pyrrhotites in contact with pentlandite in the presence of xanthate; the aim was to determine the influence of trace metal content on pyrrhotite flotation response. The measurements were repeatable (see *Appendix 2G*).

Comparison of the reactivities of the mixed samples in the absence and presence of xanthate is shown in *Figures 60* and *61*. The anodic response and the starting potential of Sudbury Gertrude 4C type pyrrhotite at lower potentials shifted slightly to higher potentials [by ~ 0.05 V (SHE)] and the maximum oxidation peak currents coincide. The xanthate does not seem to have a significant influence on the anodic behaviour of pyrrhotite in this sample. At higher potentials, above 0.45 V (SHE), the anodic currents were higher due to the presence of xanthate.

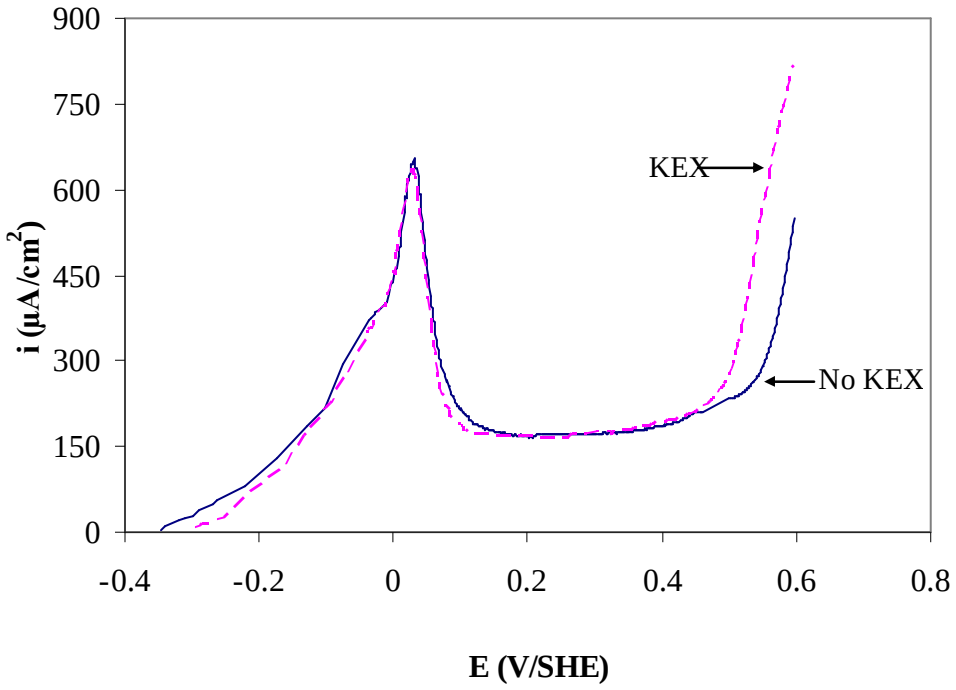

Figure 60: The anodic polarisation diagram of the Sudbury Gertrude 4C pyrrhotite in a 0.05 M borate solution at pH 9.3 in the absence and presence (1.0×10^{-3} M) of potassium ethyl xanthate (KEX). Potential sweeps were carried out at 10 mV/s.

With regard to the Phoenix 4C type pyrrhotite, the curve shifted slightly to lower potentials, the starting potential shifted by [~0.05 V (SHE)] and the maximum peak current was slightly higher. The increased anodic peak suggests that oxidation of xanthate was favoured on the Phoenix pyrrhotite. The anodic peaks moved to the region 0.13 – 0.15 V (SHE), representing only a small shift to lower potentials. These results suggest that, in the presence of xanthate, initial reactivity of the mixed sample is altered.

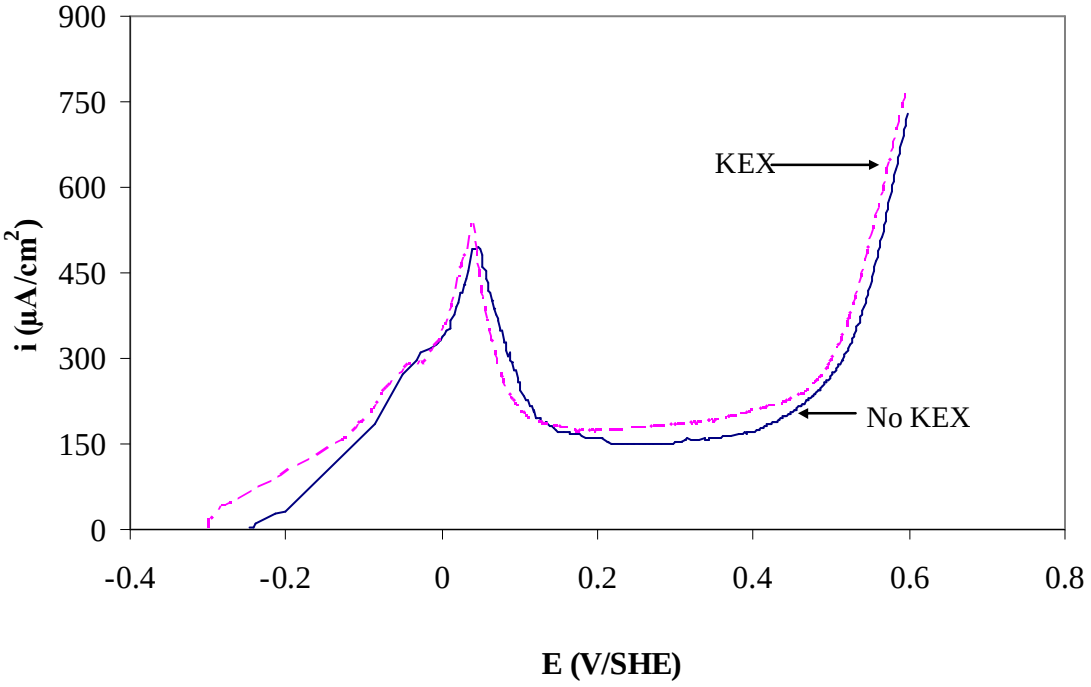

Figure 61: The anodic polarisation diagram of the Phoenix 4C pyrrhotite in a 0.05 M borate solution at pH 9.3 in the absence and presence (1.0 x 10^{-3} M) of potassium ethyl xanthate (KEX). Potential sweeps were carried out at 10 mV/s.

The anodic behaviour of pure and mixed pyrrhotite samples are shown in *Figure 62*.

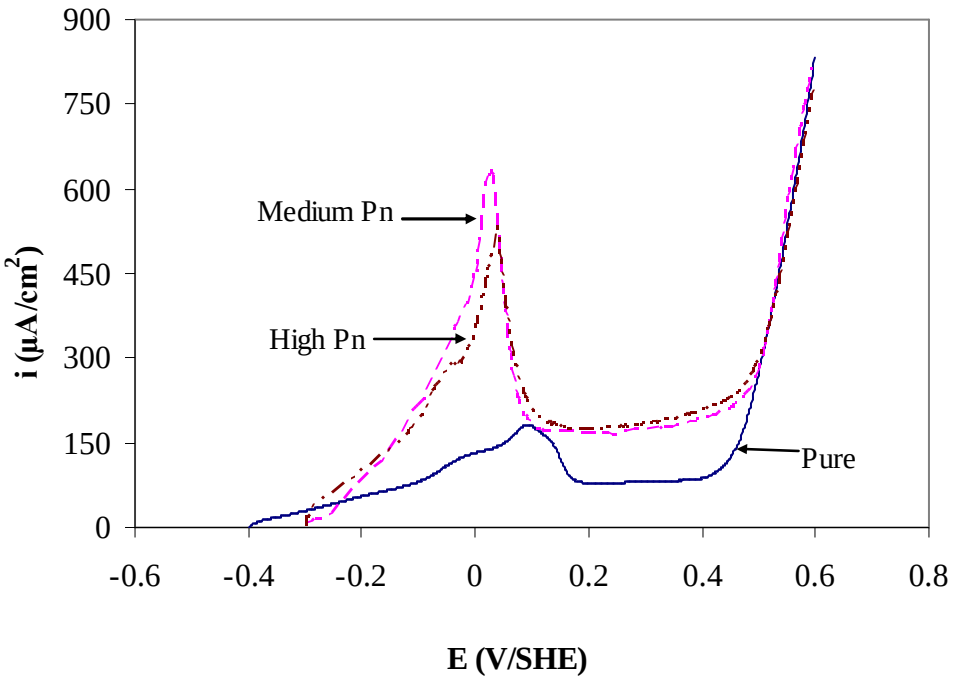

Figure 62: The anodic behaviour of pure and mixed pyrrhotite samples in a de-oxygenated 0.05 M $Na_2B_4O_7$ solution at pH 9.3 in the presence (1.0 x 10^{-3} M) of potassium ethyl xanthate (KEX). Potential sweeps were carried out at 10 mV/s.

Initially, the pure sample was more reactive than the mixed samples, whereas the mixed samples started showing anodic activity at the same potential, suggesting that the samples have the same initial reactivity. The current densities at the anodic peaks of the mixed samples were still higher than in the pure sample as in the case where there was no xanthate and the order remained the same. Again, the Gertrude pyrrhotite showed higher anodic currents than the Phoenix pyrrhotite, but the difference is not as pronounced as it is in the absence of xanthate.

These results show that xanthate interaction with the magnetic pyrrhotites could be different. Pure pyrrhotite is more covered with oxidation products than mixed samples and this layer impedes xanthate reactions, hence the low anodic peak currents. No correlation was found between trace metal content and pyrrhotite anodic reactivity in the presence of xanthate. Similar to measurements taken in the absence of xanthate, at intermediate potentials in the region 0.20 to 0.40 V (SHE), the mixed samples showed high passive currents, indicating less

passivation. In the high potential range, above 0.40 V (SHE), no differences in electrochemical behaviour were observed, unlike in the absence of xanthate.

These results show that when processing minerals, galvanic interactions and their influence on the electrochemical behaviour of minerals should be considered. No mineral should be considered in isolation.

The open circuit potential measurements, polarisation resistance measurements, cathodic polarisation diagrams and capacitance measurements show the influence of galvanic interaction on pyrrhotite in electrical contact with pyrrhotite. In the presence of pentlandite, oxygen reduction on the mixed mineral is enhanced. Anodic polarisation diagrams assisted in comparing the reactivity of the three magnetic pyrrhotites with variations in trace metal content in the low potential region. No correlation was observed between trace metal content and pyrrhotite reactivity. The Gertrude pyrrhotite with intermediate trace metal content was more reactive than the Phoenix pyrrhotite with the highest trace metal content. Mixed pyrrhotites were more reactive than the pure Russia_2 pyrrhotite with a very low (almost negligible) trace metal content. This shows that 4C type pyrrhotites from various locations vary in reactivity. At higher potentials, higher anodic currents were observed for mixed pyrrhotites. This is because both pyrrhotite and pentlandite in mixed samples were oxidised.

5.5. Gaseous carbon dioxide cleaning of oxidised pyrrhotite

Mineral oxidation decreases the number of surface sites available for the reaction with xanthate, resulting in poor mineral flotation. Pyrrhotite is known to be easily oxidised and as a result, its recovery and the subsequent recovery of any PGEs associated with it are reduced. Miller and Misra (1987) developed a process for froth flotation of coal using gaseous carbon dioxide and including a conditioning treatment of the coal with gaseous carbon dioxide followed by froth flotation. The time for the conditioning step was expected to be five to fifteen minutes, but this time period can be refined by experiment with the particular type of coal. The treatment resulted in improved results in that less reagent promoter and frother were required and the flotation time reduced.

In the next section, the influence of gaseous carbon dioxide on the electrochemical and flotation response of oxidised pyrrhotite using electrochemical measurements and microflotation tests is investigated. This was done to help understand and address the slow flotatiom response of pyrrhotite due to its rapid oxidation during flotation. The aim was to establish whether gaseous carbon dioxide had the same cleaning effect on oxidised pyrrhotite as was reported by Miller and Misra (1987) with oxidised coal. Cleaning of oxidised pyrrhotite is expected to improve pyrrhotite's interaction with flotation reagents, particularly xanthate, and improve its flotation recovery.

Carbon dioxide is soluble in water, in which it spontaneously interconverts between CO_2 and H_2CO_3 (carbonic acid). The relative concentrations of CO_2, H_2CO_3 and the deprotonated forms HCO^{3-} (bicarbonate) and CO_3^{2-} (carbonate) depend on the pH (Sayilgan and Aron, 2004; http://en.wikipedia.org/wiki/Carbon dioxide). Almost all carbonic species exist as HCO^{3-} between pH = 6.3 and 10.25, and as CO_3^{2-} above pH = 10.25 (Stumm and Morgan, 1981). In neutral or slightly alkaline water (pH > 6.5), the bicarbonate form predominates (> 50 %), becoming most prevalent (> 95 %) at the pH of seawater; in very alkaline water (pH > 10.4), the predominant form (> 50 %) form is carbonate. The bicarbonate and carbonate forms are very soluble, such that air-equilibrated ocean water (mildly alkaline with typical pH = 8.2 – 8.5) contains about 120 mg of bicarbonate per litre (http://en.wikipedia.org/wiki/Carbon dioxide).

Dissolved carbon dioxide gas in water forms a weak acidic mixture (Sayilgan and Aron, 2004; http://en.wikipedia.org/wiki/Carbon dioxide). In this study, the pH was reduced to values between 6.60 and 6.80. It should be noted that the pH could not be reduced any further due to the buffering effect of the borate solution at pH 9.3. The carbon dioxide treated surface refers to the pyrrhotite surface that was oxidised for an hour in the solution and then treated in a gaseous carbon dioxide saturated solution.

The electrochemical and microflotation measurements showing the influence of gaseous carbon dioxide on the electrochemical response of CO_2 treated pyrrrhotite surface are presented in this section. Two types of pyrrhotites (magnetic [4C] and non-magnetic [6C]) were used so as to determine whether CO_2 treatment will have the same influence on both pyrrhotites or not.

5.5.1. Electrochemical measurements

Rest potential and polarisation resistance measurements were taken for a freshly polished surface and after one hour of oxidation. Following oxidation, the electrode was kept in a solution and gaseous carbon dioxide was sparged into the solution for an hour, after which the electrochemical measurements were taken.

5.5.1.1. Rest potential measurements

Figures 63 and *64* compare rest potentials of polished and carbon dioxide treated pyrrhotite surfaces for the pure 4C and 6C pyrrhotites.

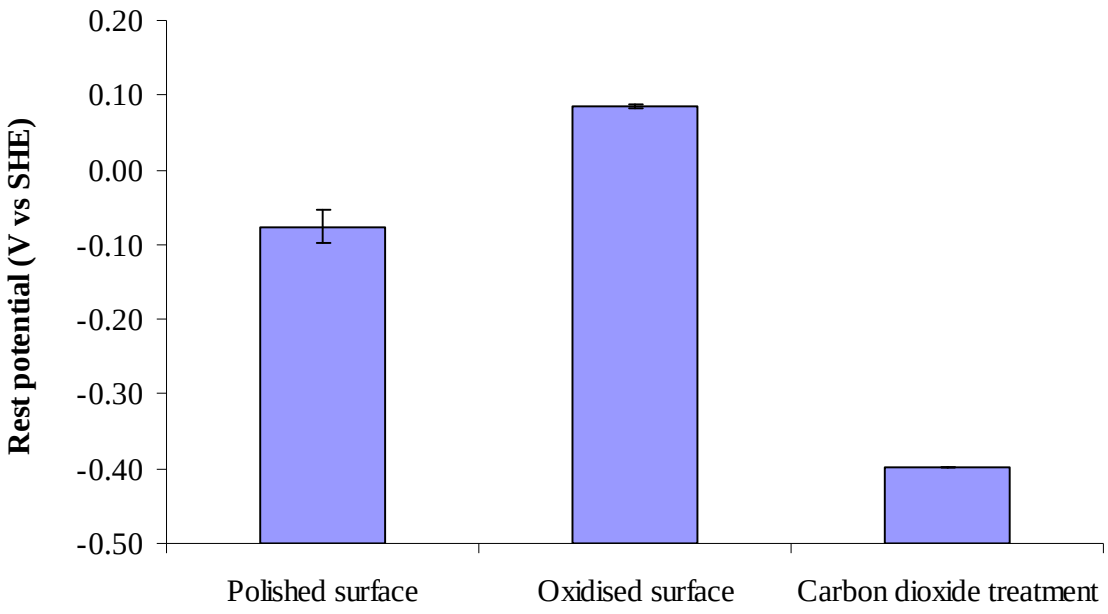

Figure 63: The influence of carbon dioxide treatment on the rest potentials of the Russian 4C type pyrrhotite in a 0.05 M borate solution at pH 9.3. Potential sweeps were carried out at 10 mV/s. One hour of CO_2 treatment.

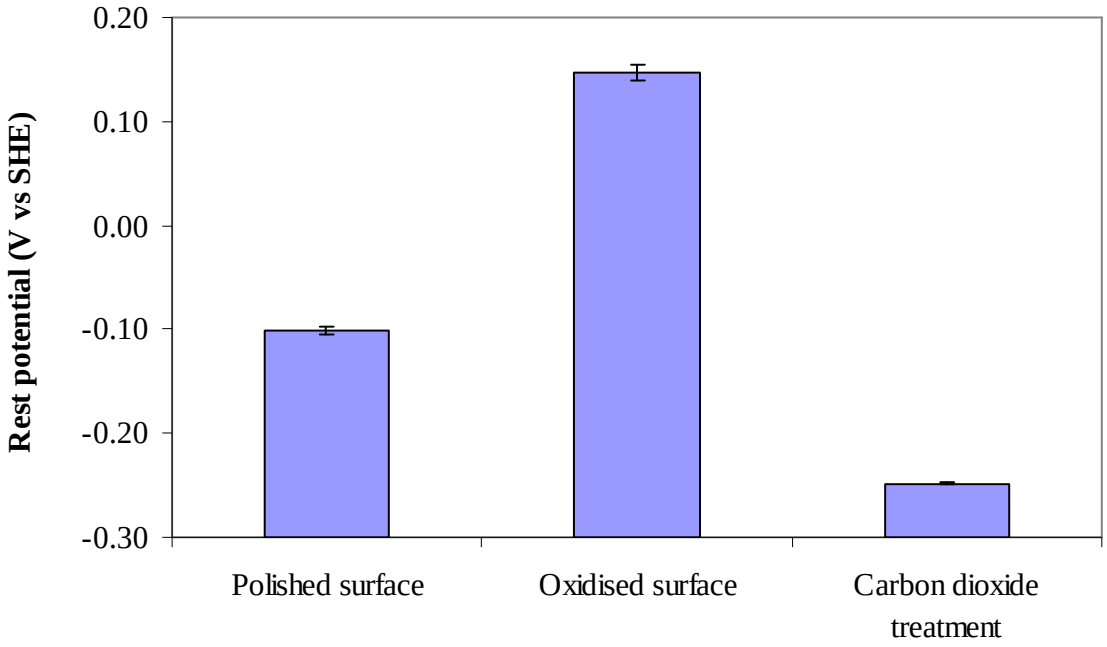

Figure 64: The influence of carbon dioxide treatment on the rest potentials of the Mponeng 6C type pyrrhotite in a 0.05 M borate solution at pH 9.3. Potential sweeps were carried out at 10 mV/s. One hour of CO_2 treatment.

In both the 4C and 6C type pyrrhotites, oxidation resulted in higher rest potentials; sparging of gaseous carbon dioxide into the solution reduced the rest potentials to values lower than those of the oxidised surfaces. These results show that carbon dioxide cleans the oxidised surfaces. According to Tolley *et al.* (1996) and Rand (1977), a decrease in open circuit rest potentials indicates increased reactivity of the mineral toward the solution.

5.5.1.2. Polarisation resistance measurements

The polarisation resistance measurements of the freshly polished, oxidised and carbon dioxide treated pyrrhotite surfaces are demonstrated in *Figures 65* and *66*, for both the 4C and 6C type pyrrhotites.

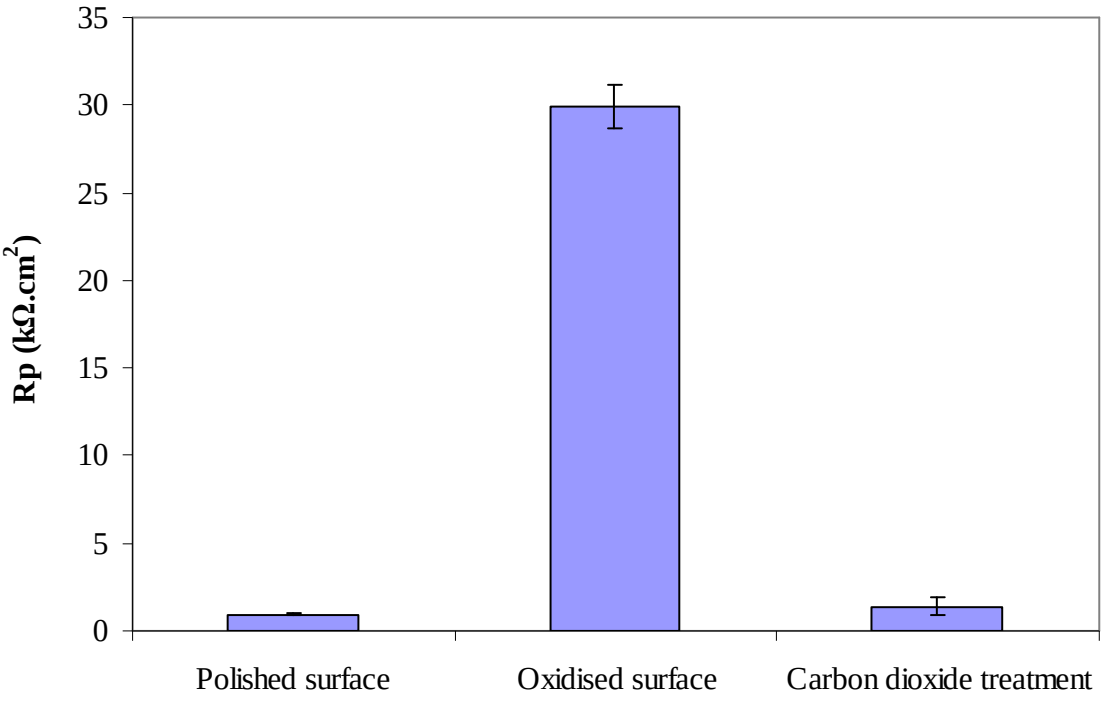

Figure 65: The influence of carbon dioxide treatment on the polarisation resistance measurements of the Russian 4C type pyrrhotite in a 0.05 M borate solution at pH 9.3. Potential sweeps were carried out at 10 mV/s. One hour of CO_2 treatment.

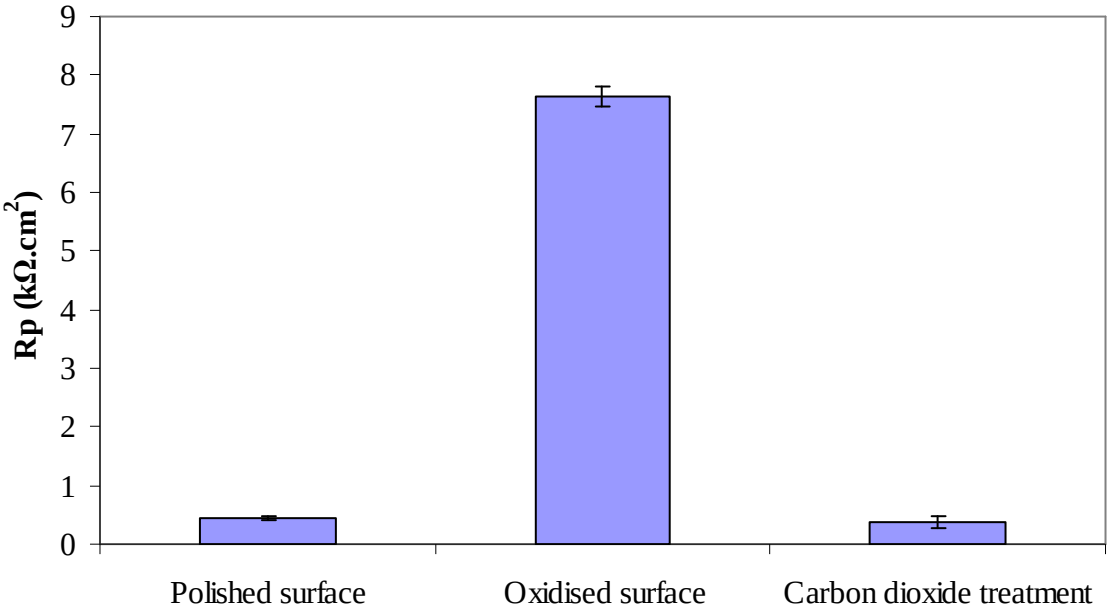

Figure 66: The influence of carbon dioxide treatment on the polarisation resistance measurements of the Mponeng 6C type pyrrhotite in a 0.05 M borate solution at pH 9.3. Potential sweeps were carried out at 10 mV/s. One hour of CO_2 treatment.

Similar to the rest potential measurement results, gaseous carbon dioxide resulted in depassivation of the oxidised pyrrhotite surfaces (i.e. lowering of the Rp values to values similar to those of the polished surfaces). Linter and Burstein (1999) observed that the dissolved carbon dioxide gas reacts with the iron component of the oxidised pipeline steel in such a way as to contribute to the steel's depassivation. It was shown that the dissolved gas enhances the anodic dissolution of Fe. Worth noting is that the acceleration of metal dissolution reaction by CO_2 was not a result of pH modification by CO_2. This is shown in *Figure 19*, where attempts to modify the behaviour of the metal, by small changes in pH, in order to render the solution more aggressive, did not simulate the effect of CO_2.

Carbon dioxide thus has a unique chemical effect on the reaction. It was reported that dissolved carbon dioxide accelerates the dissolution of low alloy steels in aqueous solutions by destabilising the oxide films that form. Destabilisation occurs by reaction of the oxide to produce ferrous carbonate and a dissolved complex of Fe, designated as biscarbonate-Fe(II),

$Fe(CO_3)_2^{2-}$. Formation of the complex enhances the metal dissolution rate. Reactions are depicted in *Figure 18, Section 2.3.7*. In the earlier work, carried out at pH 8.8, the rate of dissolution of the metal was shown to be controlled by mass transport of the complex away from the metal surface (Linter and Burstein, 1999).

From this, it can be postulated that the depassivation of the oxidised pyrrhotite surface by gaseous carbon dioxide occurs in such a way that dissolved CO_2 gas reacts with the iron component within the hydroxide film to form both ferrous carbonate and a dissolved complex.

5.5.1.3. Anodic polarisation diagrams in the absence of xanthate

The anodic behaviour of carbon dioxide treated pyrrhotite surfaces is presented in *Figures 67* and *68* for the 4C and 6C type pyrrhotites, respectively. The repeatability of measurements is illustrated in *Appendix 3A*.

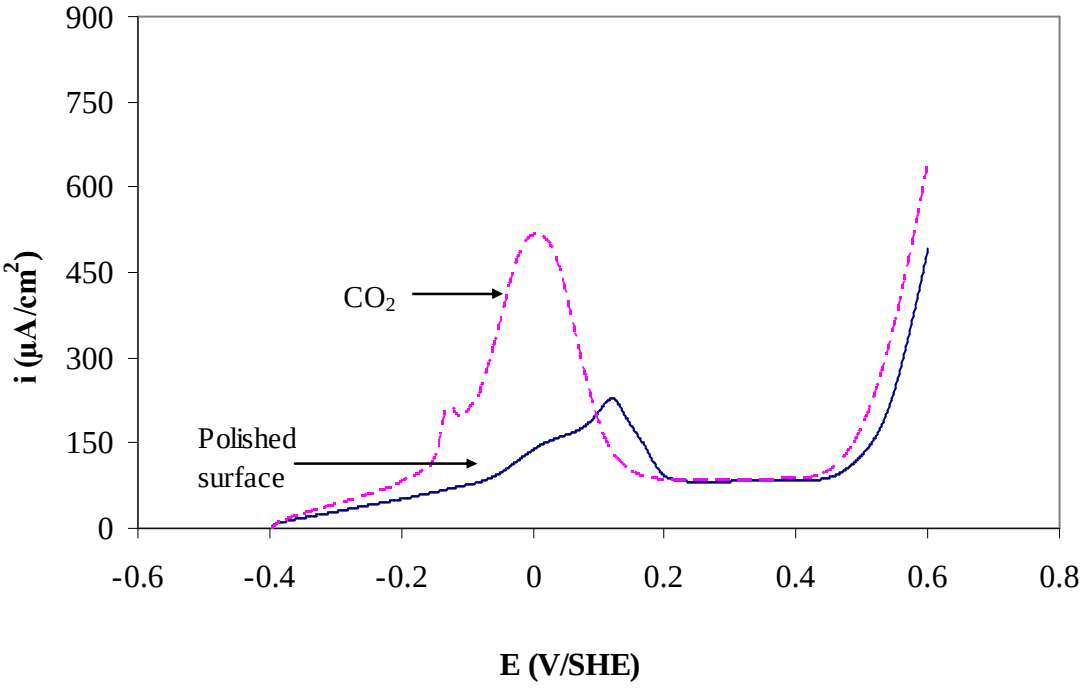

Figure 67: The anodic polarisation diagram of a polished and carbon dioxide treated Russian 4C pyrrhotite in a de-oxygenated 0.05 M borate solution in the absence of potassium ethyl xanthate (KEX). Potential sweeps were carried out at 10 mV/s. One hour of CO_2 treatment.

In the case of the 4C type pyrrhotite, the starting potentials of the polished and CO_2 treated surfaces were similar. The anodic peak of the CO_2 treated surface shifted to cathodic potentials and showed higher anodic current densities, suggesting that the surface became more reactive. In the intermediate potential range, the passive currents were similar. At higher potentials, the CO_2 treated surface had higher anodic currents.

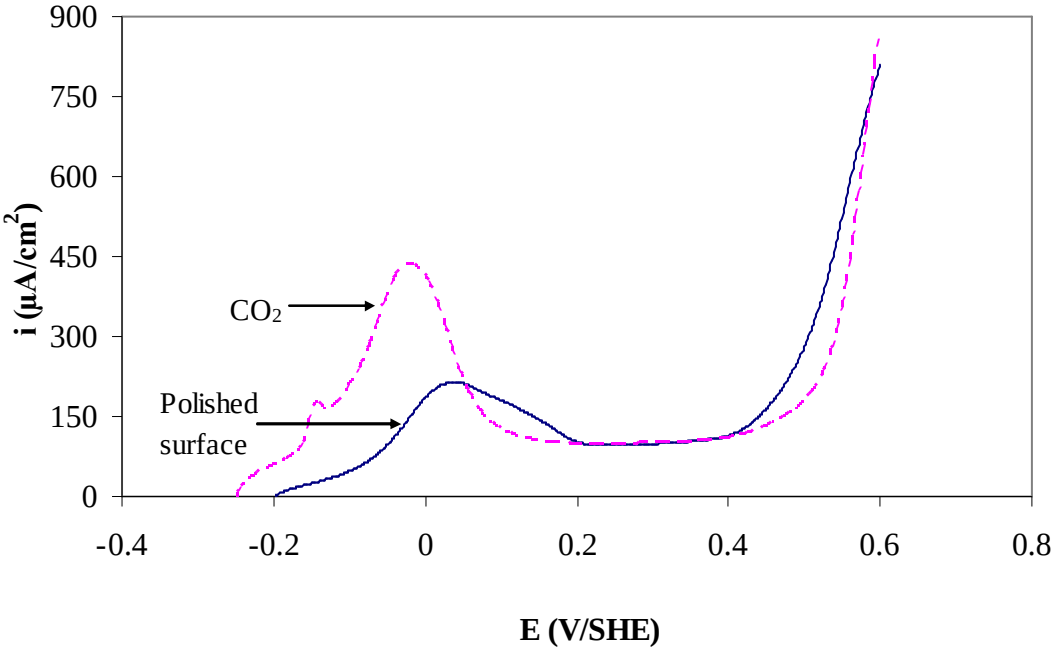

Figure 68: The anodic polarisation diagram of a polished and carbon dioxide treated Mponeng 6C pyrrhotite in a 0.05 M borate solution in the absence of potassium ethyl xanthate (KEX). Potential sweeps were carried out at 10 mV/s. One hour of CO_2 treatment.

For the 6C type pyrrhotite, the use of carbon dioxide resulted in the shifting of the starting potential and the curve to lower potentials, rendering the surface more reactive. The region where oxidation products were observed for polished surfaces [-0.10 to 0.25 V (SHE)] shifted to lower potentials [-0.17 to 0.19 V (SHE)]. The passive currents for the polished and CO_2 treated surface were also similar to the 4C type pyrrhotite.

The observations in this study cannot be expected to be exactly the same as the study done by Linter and Burstein (1999), in which anodic curves were measured on steel in a CO_2 saturated solution. In the present work, after treating the oxidised sample in CO_2, the samples were quickly transferred to a nitrogen de-oxygenated solution. This was done to investigate the response of a CO_2 treated surface under conditions similar to those of a polished surface. The CO_2 saturated solution was not completely removed or dried when transferring the sample to the cell containing the fresh de-oxygenated tetraborate solution. The enhanced anodic currents showed that the surfaces were clean and were allowed to react easily. On the anodic curves of the CO_2 treated surface, there is a small peak to the left of the major anodic peak.

The adsorbed CO_2 and ferrous carbonate species that it was proposed would form on the surface might have been responsible for the high anodic currents and the small peak when the electrode is transferred to the de-oxygenated solution. Linter and Burstein (1999) reported that the dissolved gas enhances the anodic dissolution of Fe.

Results show that the CO_2 treated surface is more reactive than the wet-polished surface. The same behaviour was observed for both the 4C and 6C type pyrrhotites. The reason for the low anodic currents in the wet-polished surface was investigated by comparing: a wet-polished surface, a wet-polished surface that was treated in carbon dioxide for an hour prior to measurement; and a surface oxidised in O_2-rich tetraborate solution for an hour and which was also treated in carbon dioxide. The 4C type pyrrhotite was used. *Figure 69* reveals the low anodic currents associated with the oxidation of a wet-polished surface in a de-oxygenated borate solution. This suggests that the adsorbed water and interaction of the surface with oxygen or moisture in the atmosphere after polishing partially inhibits the anodic reaction, possibly due to the formation of a surface layer prior to the electrochemical measurement.

This result shows the rapid oxidation of pyrrhotite in air and in contact with water. Oxidation of pyrrhotite is inhibited significantly in alkaline solution, suggesting that iron oxide on the surface retards further reaction (Hamilton and Woods, 1981). It is evident that carbon dioxide removed the oxidation product layer and the measurements are close to those of an oxidised surface treated in carbon dioxide. This shows that whether there is a thick or a thin oxide layer on the pyrrhotite surface, carbon dioxide removes the layer in a similar manner. This also shows that sample polishing affects the rate of oxidation and new polishing techniques that minimise oxidation are essential.

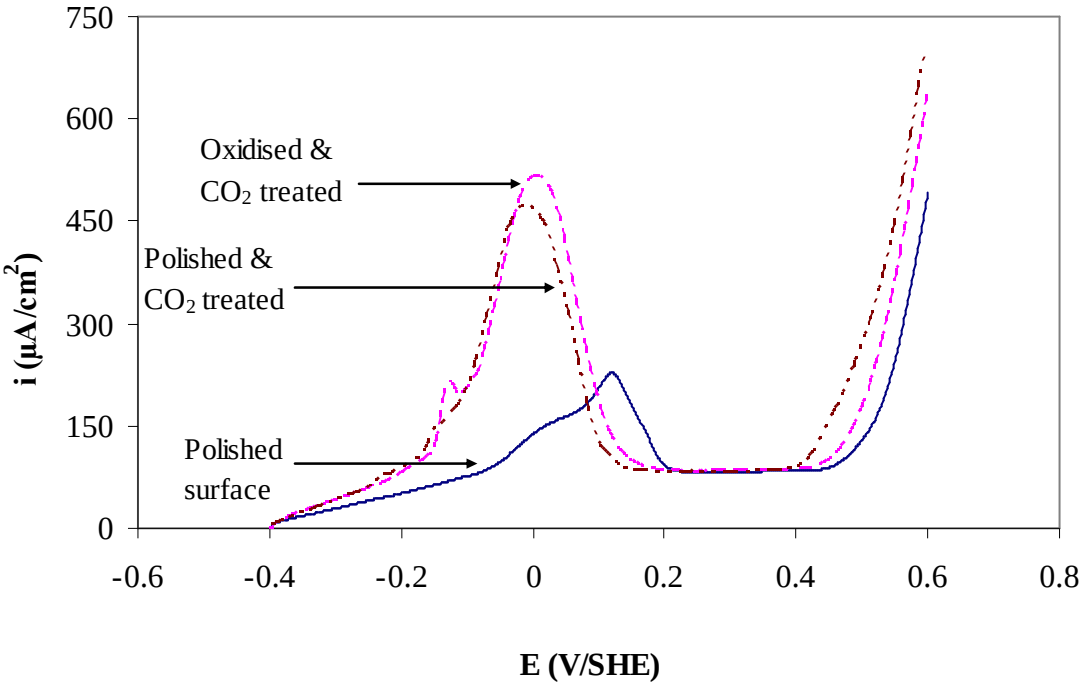

Figure 69: Comparison of the anodic polarisation diagram of a polished, polished and carbon dioxide treated, and oxidised carbon dioxide treated Russian 4C pyrrhotite in a 0.05 M borate solution in the absence of potassium ethyl xanthate (KEX). Potential sweeps were carried out at 10 mV/s. One hour of CO_2 treatment.

A comparison of the carbon dioxide treated 4C and 6C type pyrrhotites (*Figure 70*) illustrates that the anodic activity of the 4C type pyrrhotite started at a lower potential and had higher anodic peak currents than the 6C type pyrrhotite. This suggests that the order in the reactivity of these pyrrhotites was not altered (i.e. magnetic 4C type pyrrhotite is more reactive than the non-magnetic 6C type pyrrhotite). Both samples showed a small anodic peak before the major anodic peak after CO_2 treatment. The small peak could be attributed to the adsorbed CO_2 or other species forming on the surface due to the presence of adsorbed CO_2.

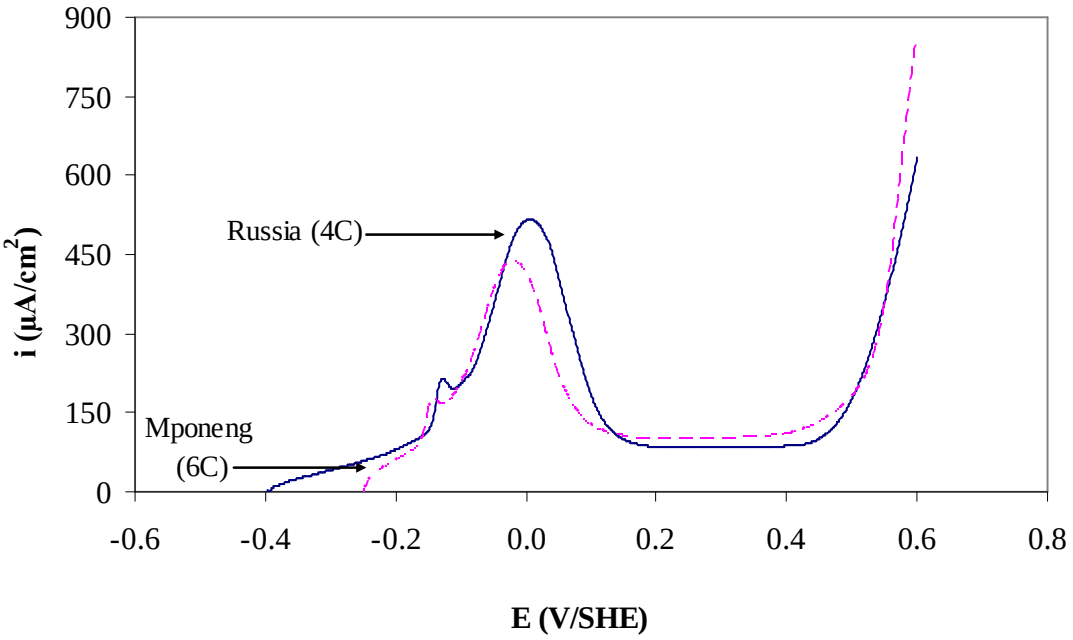

Figure 70: The anodic behaviour of the carbon dioxide treated Russian 4C and Mponeng 6C pyrrhotite samples in a de-oxygenated 0.05 M $Na_2B_4O_7$ solution in the absence of potassium ethyl xanthate (KEX). Potential sweeps were carried out at 10 mV/s. One hour of CO_2 treatment.

In the region where passivation is expected (between 0 and 0.45 V [SHE]) the 6C type pyrrhotite has slightly higher anodic currents, indicating that its surface does not passivate to the same extent as the 4C type pyrrhotite. The low current flow on the 4C type pyrrhotite surface suggests that it is more passivated. These results correlate well with the polarisation resistance measurements shown earlier in *Figures 65* and *66* (where Rp for the 4C and 6C type pyrrhotites is 1.41 and 0.38 $k\Omega.cm^2$, respectively after treatment with carbon dioxide). In the higher potential region, the 6C pyrrhotite showed higher anodic current densities than the 4C pyrrhotite.

5.5.1.4. ToF-SIMS

ToF-SIMS was employed to investigate the changes on the surface of the polished pyrrhotite surface treated in an oxygen-saturated 0.05 M borate solution for an hour and after a one-hour treatment of an oxidised surface with gaseous carbon dioxide - for both the Russian (4C type)

and Mponeng (6C type) pyrrhotites. Images of an oxidised and gaseous carbon dioxide treated surface are shown in *Figures 71* and *72*.

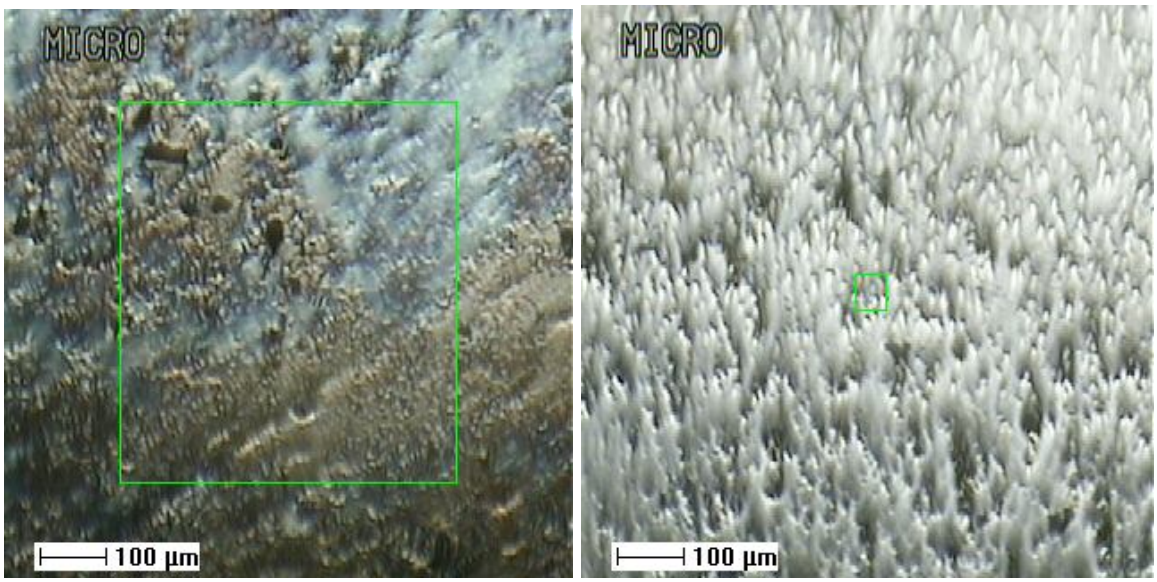

(a) (b)

Figure 71: The ToF-SIMS Russian pyrrhotite surface images: (a) one-hour oxidised surface in an oxygen-saturated 0.05 M borate solution and; (b) one-hour gaseous carbon dioxide treated surface.

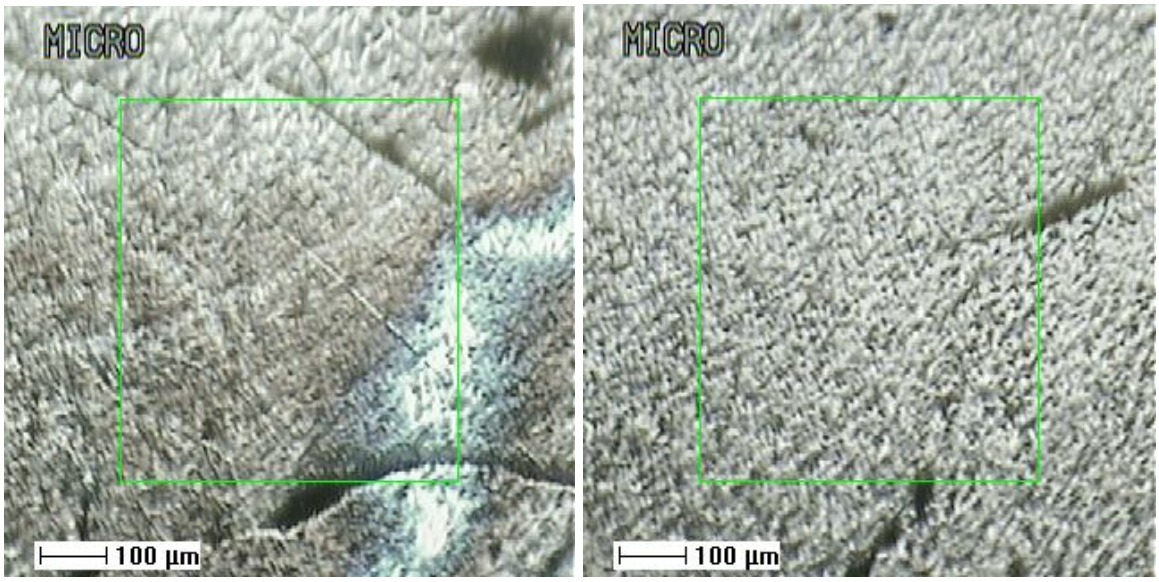

(a) (b)

Figure 72: The ToF-SIMS Mponeng pyrrhotite surface images: (a) one-hour oxidised surface in an oxygen-saturated 0.05 M borate solution and; (b) one-hour gaseous carbon dioxide treated surface.

The change in surface texture and colour in the images indicate that the oxide layers on the surfaces were removed. The CO_2 treated samples' images are similar to those of polished surfaces shown earlier in *Figures 44* and *45*, *Section 5.4.1.6*. Polished samples were also not smooth and had pores.

Depth profiles of the above-mentioned surfaces were obtained and are presented in *Figures 73* to *74*.

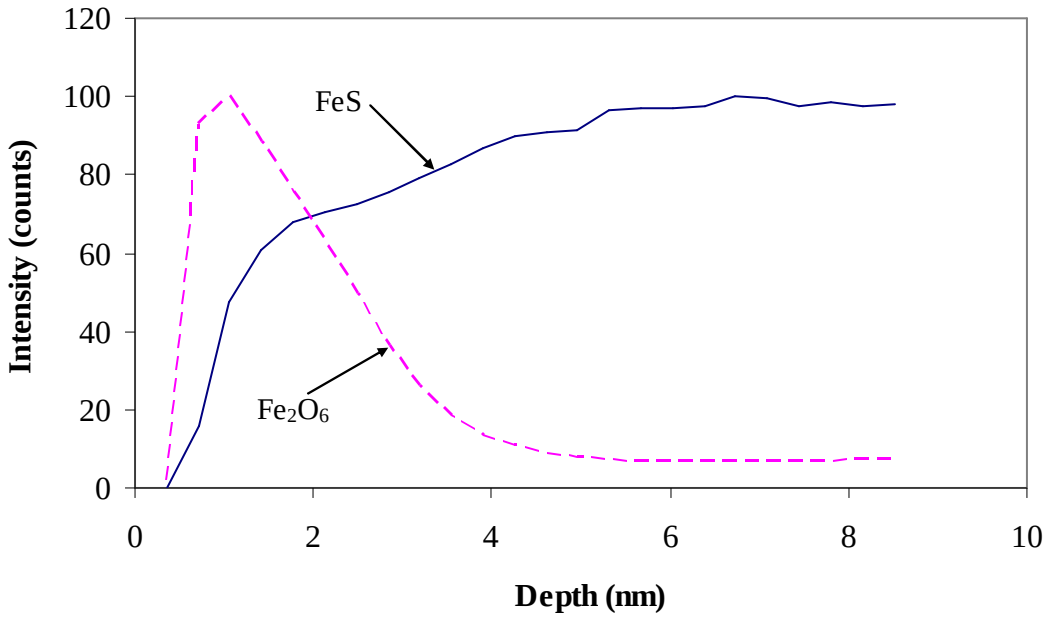

Figure 73: ToF-SIMS depth profile of an oxidised and one hour gaseous carbon dioxide treated 4C type pyrrhotite in a 0.05 M borate solution.

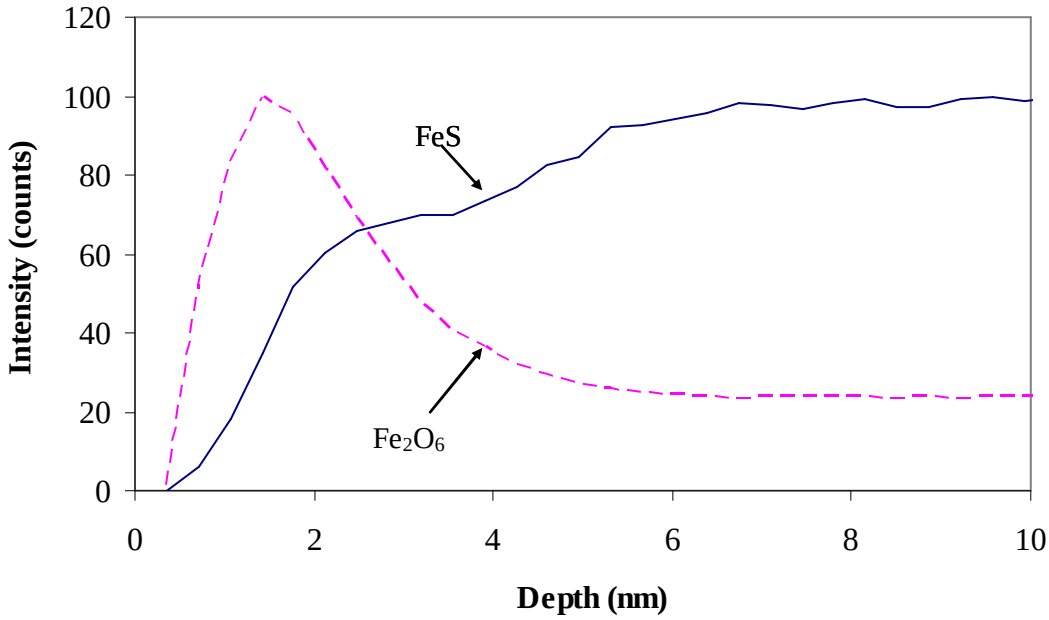

Figure 74: ToF-SIMS depth profile of an oxidised and one hour gaseous carbon dioxide treated 6C type pyrrhotite in a 0.05 M borate solution.

Depth profiles shown earlier in *Figures 48* and *49* indicated that an oxide product was formed on the surface after oxidation. Fe(III)-oxyhydroxide was found and reported to be the major oxidation product on the pyrrhotite surface (Buckley and Woods, 1985a; Pratt *et al.*, 1994). On the depth profile graph, FeS and Fe_2O_6 refer to the pyrrhotite surface and oxidation product, respectively. As mentioned earlier in *Section 5.4.1.6*, the point where the two curves intersect does not indicate the thickness of the oxide layer on the surface. When determining the oxide layer thickness, a 20 % error has to be taken into account because of uneven sputtering. As indicated in *Figures 71* and *72*, the surfaces are not flat, therefore uneven sputtering is expected. If there were no error, the thickness would be taken as the depth corresponding to where height 'h' starts becoming constant (see *Figure 46*). Taking into account the 20 % error on the oxide depth profile, the thickness is the depth corresponding to 80 % of height 'h'.

The depth profiles show that the oxide layer was reduced to values close to those of the polished surface after treatment with carbon dioxide, i.e. from 11.56 to 3.22 nm and 10.46 to 3.69 nm for the 4C and 6C type pyrrhotites, respectively. The observed electrochemical measurements in the presence of gaseous carbon dioxide are supported by ToF-SIMS images

[*Figures 71* and *72*] and depth profiles [*Figures 73* and *74*]. It is evident from the images and depth profiles that the oxide layer observed on the oxidised surface was removed by dissolved gaseous carbon dioxide.

As mentioned earlier, ToF-SIMS results cannot be directly correlated with the electrochemical measurements due to sample preparation that was done prior to transferring the sample to the equipment. However, the results can be used to show the presence of oxidation products on the surface and the cleaning effect of gaseous carbon dioxide on the oxidised pyrrhotite surface.

5.5.1.5. Anodic polarisation diagrams in the presence of xanthate

The anodic response of carbon dioxide treated surfaces was also studied in the presence of ethyl xanthate, so as to relate the influence of carbon dioxide on the measurements with collector adsorption. The repeats are not very good. The results are presented in *Figures 75* and *76*.

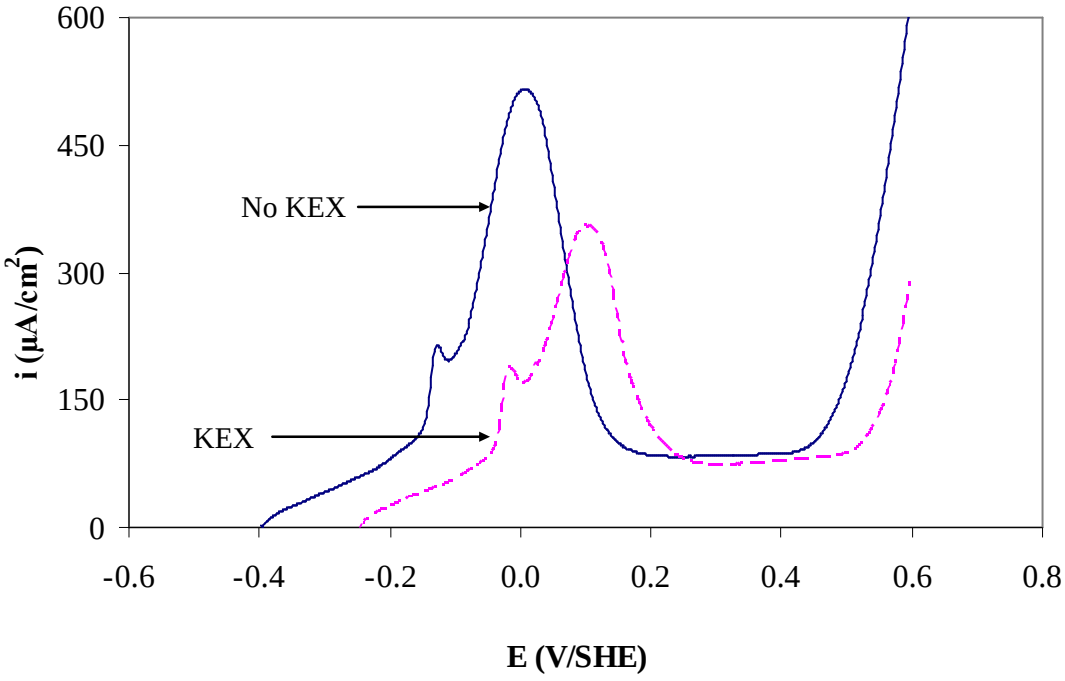

Figure 75: The anodic polarisation diagram of the Russian 4C pyrrhotite in a 0.05 M borate solution in the absence and presence of potassium ethyl xanthate (KEX). Potential sweeps were carried out at 10 mV/s. One hour of CO_2 treatment.

Figure 75 shows that for the Russian 4C type pyrrhotite, in the presence of xanthate, the starting potential and the curve shifted to positive potentials. However, in the presence of xanthate (as indicated in *Figures 50* to *52*) the curve normally shifts to the negative potentials. Xanthate alters the reactivity of the mineral. The maximum anodic peaks shifted to the potential region between -0.04 and 0.28 V (SHE). It was mentioned earlier (in *Section 5.4.1.7*) that the equilibrium potential for the transformation of xanthate to dixanthogen at an ethyl concentration of 1.0 x 10^{-3} M is 0.118 V (SHE) lies within the -0.04 to 0.28 V (SHE) range. The maximum anodic peak current is also reduced, signifying the reduction in the mineral oxidation due to xanthate adsorption on the surface. The small anodic peak is again present when xanthate is used; it might be due to the adsorbed CO_2 and ferrous carbonate species that formed after CO_2 treatment. At higher potentials, the anodic currents in the presence of xanthate are lower than in the absence of xanthate, indicating a passivation layer of xanthate species on the surface.

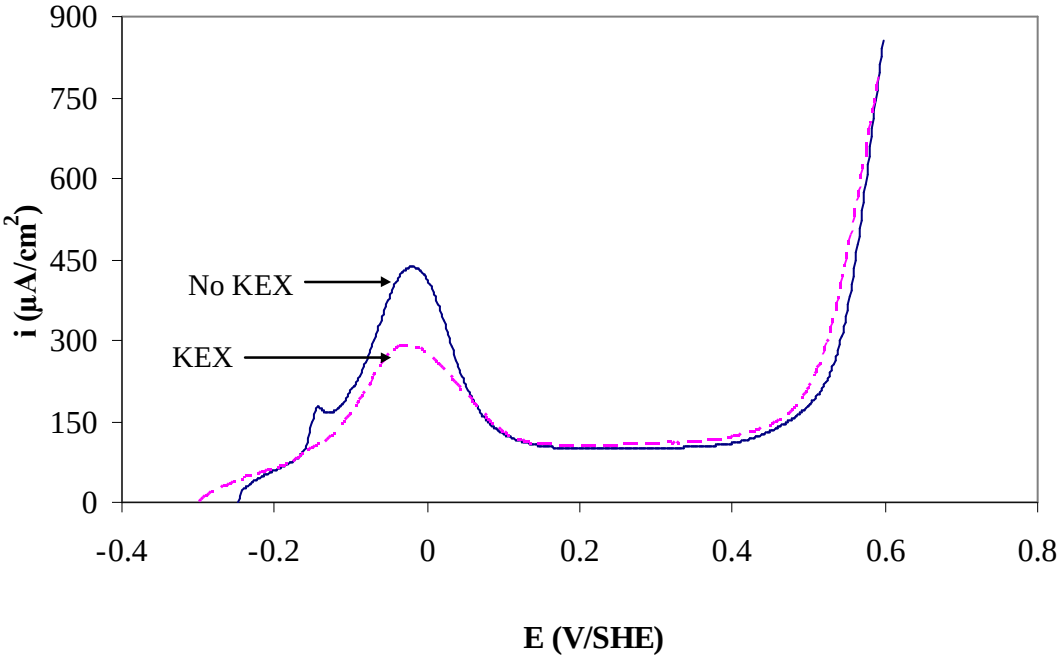

Figure 76: The anodic polarisation diagram of the Mponeng 6C pyrrhotite in a 0.05 M borate solution in the absence and presence of potassium ethyl xanthate (KEX). Potential sweeps were carried out at 10 mV/s. One hour of CO_2 treatment.

In contrast to the 4C type pyrrhotite, in the presence of xanthate, the anodic activity of the 6C type pyrrhotite started at a slightly lower potential and the maximum anodic peak did not shift. The anodic peak is in the -0.17 to 0.15 V (SHE) range and includes 0.118 V (SHE). The anodic peak current is reduced, indicating the presence of xanthate on the surface. The small anodic peak that appeared prior to the major anodic peak disappeared in the presence of xanthate. The repeats of the measurements shown in *Appendix 3A* indicate that the appearance of the small peak was not consistent in the anodic curves of the 6C type pyrrhotite, even in the absence of xanthate. The current densities in the passive region and at higher potentials are similar.

A comparison of the anodic response of the 4C and 6C type pyrrhotites treated in carbon dioxide saturated tetraborate solution in the presence of potassium ethyl xanthate is shown in *Figure 77*.

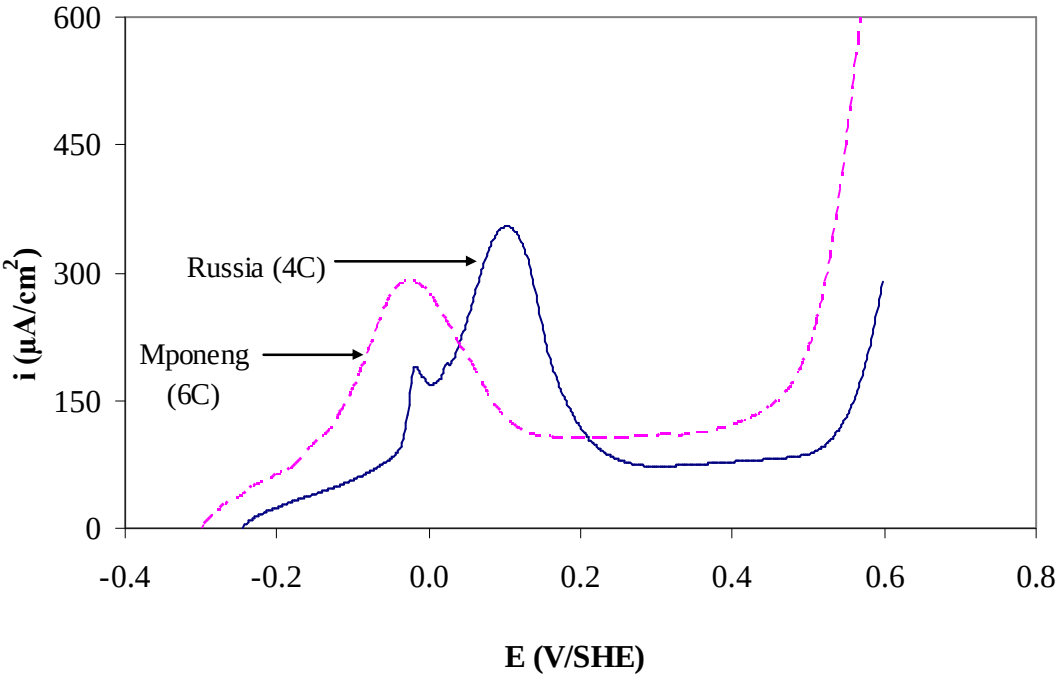

Figure 77: Anodic behaviour of pure pyrrhotite samples in a de-oxygenated 0.05 M $Na_2B_4O_7$ solution in the presence of xanthate (KEX). Potential sweeps were carried out at 10 mV/s. One hour of CO_2 treatment.

In the presence of xanthate, the anodic curve of the 6C type pyrrhotite shifted to negative currents, suggesting that the initial anodic reactivity of the 6C type pyrrhotite is higher than that of the 4C type pyrrhotite. The lower potential at which anodic processes occur on the Mponeng pyrrhotite, as compared to the Russian pyrrhotite, mean that the Russian pyrrhotite is slightly oxidised thus reducing the capacity to adsorb xanthate. This behaviour is different to what was observed when the two minerals were compared in the absence and presence of xanthate for polished surfaces (see *Figure 42* and *Figure 53*, respectively) and CO_2 treated surfaces (see *Figure 70*). However, the maximum anodic peak current of the 4C type pyrrhotite is higher, suggesting that as the potential is increased in the intermediate range, it is more reactive. As the potential is increased to higher potentials, the 6C type pyrrhotite is more reactive than the 4C type pyrrhotite, suggesting that oxidation of the adsorbed xanthate (possibly the formation of dixanthogen) on the 6C pyrrhotite is higher than on the 4C pyrrhotite.

As in the absence of xanthate, the wet-polished and carbon dioxide treated surfaces are compared in the presence of xanthate (*Figures 78* and *79*). *Figure 78* demonstrates that for the 4C type pyrrhotite, the polished surface was initially more reactive; at intermediate potentials, its anodic currents were low due to the possible formation of surface layers preventing the interaction of xanthate with the surface. At higher potentials, the anodic currents of the CO_2 treated surface were lower than that of the polished surface, indicating a thicker passivation layer of xanthate species on the CO_2 treated surface. These results suggest that the mechanism through which xanthate interacts with a polished surface and a CO_2 treated surface is likely to be different. This might be due to different surface species.

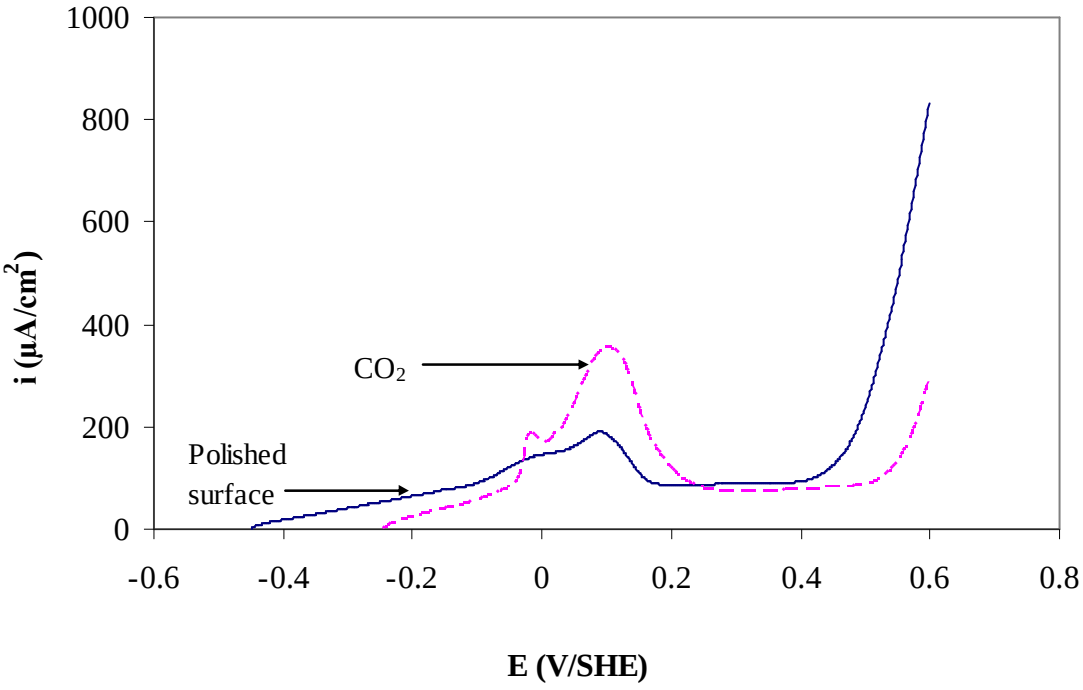

Figure 78: The anodic polarisation diagram of a polished and carbon dioxide treated Russian 4C pyrrhotite in a 0.05 M borate solution in the presence of potassium ethyl xanthate (KEX). Potential sweeps were carried out at 10 mV/s. One hour of CO_2 treatment.

The starting potential of the 6C type pyrrhotite treated in carbon dioxide is lower (*Figure 79*). Similar to in the absence of xanthate, the curve shifted to lower potentials and anodic peak currents were higher than those of the polished pyrrhotite surface. These results show an improved reactivity of the CO_2 treated 6C type pyrrhotite in the presence of xanthate. At

higher potentials, the polished surface had higher anodic currents, indicating a thicker passivation layer of xanthate species on the CO_2 treated surface.

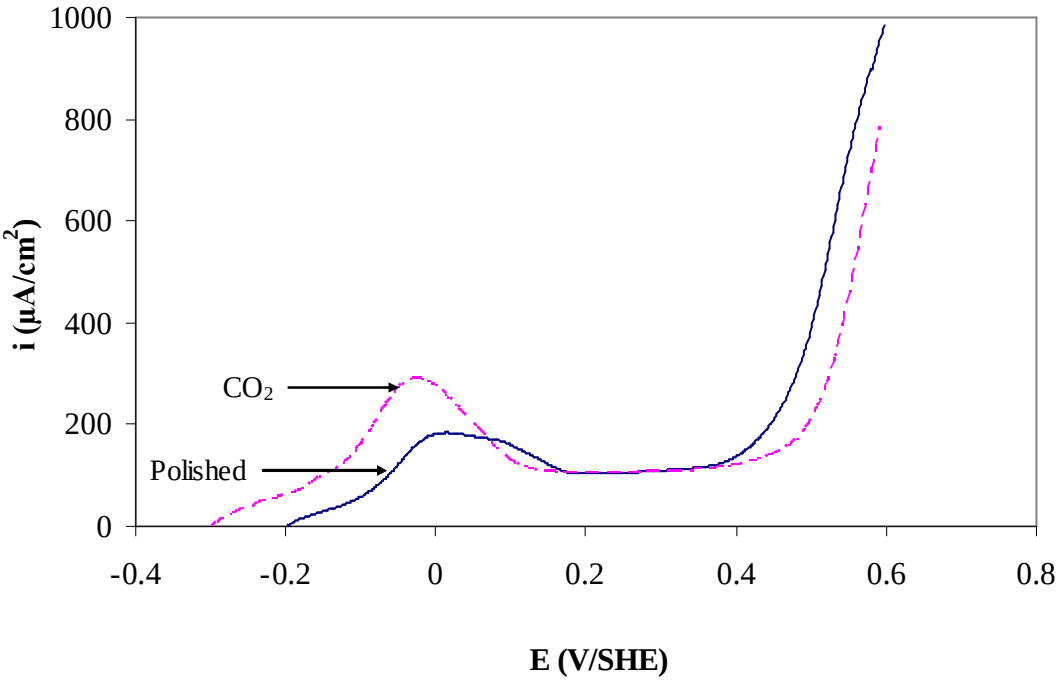

Figure 79: The anodic polarisation diagram of a polished and carbon dioxide treated Mponeng 6C pyrrhotite in a 0.05 M borate solution in the presence of potassium ethyl xanthate (KEX). Potential sweeps were carried out at 10 mV/s. One hour of CO_2 treatment.

Overall, in the presence of xanthate, the maximum anodic peak currents for both the 4C and 6C pyrrhotites are increased on the CO_2 treated surface than the polished surface. In the higher potential region, the CO_2 treated surface showed lower anodic reactivity, indicating a thicker passivation layer of xanthate species on the CO_2 treated surface. These results suggest that xanthate interacts better with a CO_2 treated surface.

In this section, it was shown that the order in the reactivity of the minerals (4C and 6C pyrrhotites) is altered under different operating conditions, i.e. polished versus CO_2 treated surface and in the absence and presence of potassium ethyl xanthate. Surface characterisation studies would have been useful in identifying the surface species and in describing the mechanism through which gaseous carbon dioxide interacts with the surface in the absence

and presence of xanthate. Contact angle measurements would have been ideal in determining the extent of hydrophobicity on both the 4C and 6C type pyrrhotites in the presence of xanthate.

5.5.2. Microflotation measurements

Major flotation variables are divided into three interactive groups, viz. the equipment, operation and chemical components (Klimpel, 1980). The interactive nature of the variables makes it difficult to analyse the effect of any particular component, thus careful planning and a set of experiments are necessary to investigate the effects of a particular parameter on performance. Some of the physical (operational) factors influencing the flotation process are bubble-particle and particle-particle interactions in aqueous suspension in slurry or an aqueous solution. The mechanical factors include the manner in which gas bubbles are generated and particles are dispersed (Du Plessis, 2004). The chemical factors, including the addition of surface active reagents, determine the extent of mineral particle wettability and the characteristics of the froth that is generated.

In the case of sulfide mineral flotation, chemical factors have a larger influence on the flotation process. Thiocarbonates, particularly xanthates, are widely used as collectors for selective and bulk flotation of sulfide minerals from PGM ores. Pyrrhotite is easily oxidised and this results in slow and poor flotation of pyrrhotite (Miller *et al.*, 2005). Surface oxidation of sulfide minerals, such as that found in the regions of a sulfide ore body near the water table, can have a significant impact upon flotation because the oxidation products inhibit efficient interaction and adsorption of xanthate on the surface.

Gaseous carbon dioxide conditioning of oxidised pyrrhotite surfaces was shown by electrochemical measurements and ToF-SIMS to clean the surface and enhance the anodic reactivity of the minerals in the absence and presence of xanthate. It is important to determine the influence and significance of CO_2 conditioning on the flotation behaviour of an oxidised ore. Pyrrhotite is a mineral of interest in this study, hence a pure pyrrhotite sample was sourced and used in the microflotation measurements in order to investigate the influence of CO_2 conditioning on its flotation behaviour. Unfortunately, a large quantity of the 6C type pyrrhotite sample could not be obtained and the only pyrrhotite sample used was that of the

4C type pyrrhotite from Russia, which was purchased from Ward's Natural Science Establishment. It is anticipated that these microflotation measurements will help address the slow flotation response of pyrrhotite due to oxidation.

The same particle size distribution selected for the measurements was 38 – 106 µm. Due to a lack of enough sample to repeat the measurements, the reproducibility in flotation tests could not be shown. The conditions were kept the same throughout so as to minimise error in the measurements.

Flotation results of the freshly ground pyrrhotite sample using sodium isobutyl xanthate (SIBX) are illustrated in *Figure 80*. Microflotation tests were performed in synthetic plant water. The air flow rate was increased from 6 ml/min to 58 ml/min due to the low flotation recoveries observed even after Cu activation. Recovery increased from 2.02 to 3.22 % after copper activation. In the absence of copper activation, increasing the air flow rate resulted in an overall flotation recovery increase from 2.02 % to 17.13 %.

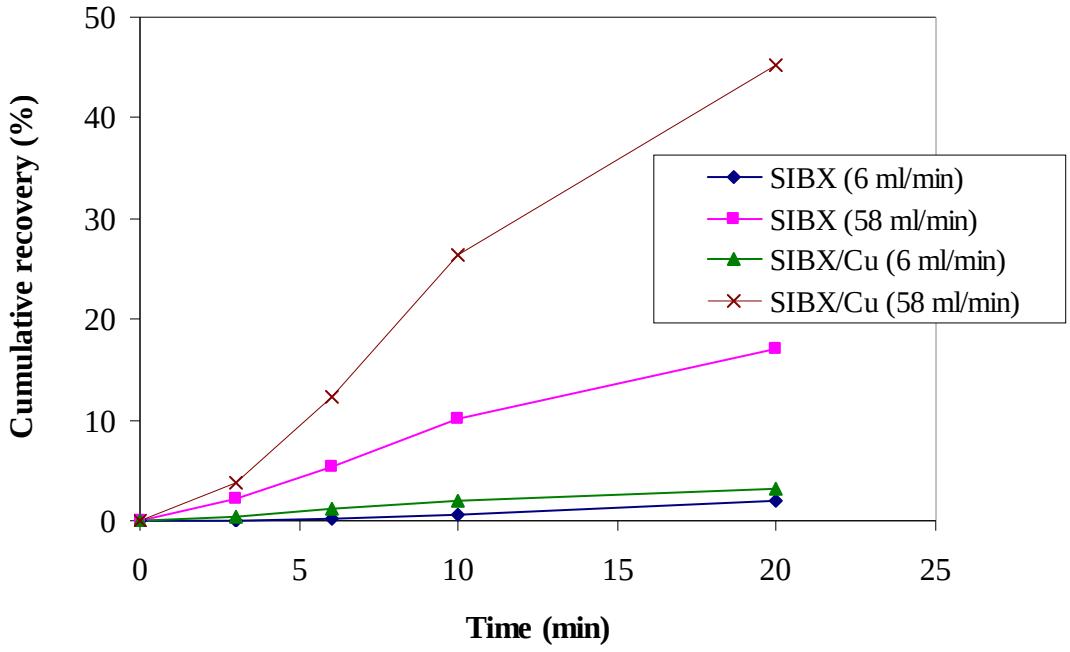

Figure 80: Recovery-time curves during microflotation of the freshly ground magnetic 4C type pyrrhotite in a synthetic solution containing 5 x 10^{-5} M sodium isobutyl xanthate at pH 9.3. SIBX: in the presence of sodium isobutyl xanthate only (SIBX for two different flow rates); SIBX/Cu: Copper sulfate conditioning at 0.4 x 10^{-4} M before sodium isobutyl xanthate addition (SIBX/Cu for two different flow rates). The particle size range was 38 – 106 µm.

It was the aim of this study to investigate the influence of CO_2 conditioning without any copper activation and it was observed that copper activation was required to improve the flotation response of freshly ground pyrrhotite. With copper activation, the final flotation recovery, at an air flow rate of 58 ml/min, increased from 17.13 to 45.19 %.

The influence of gaseous carbon dioxide conditioning on the flotation response of oxidised pyrrhotite sample was investigated (*Figure 81*). The sample was oxidised in distilled water for 24 hours and transferred to fresh distilled water. Then gaseous carbon dioxide was bubbled continuously for 30 and 45 minutes. The sample was then filtered, rinsed with fresh synthetic water and conditioned with copper sulfate before xanthate addition in the microflotation cell.

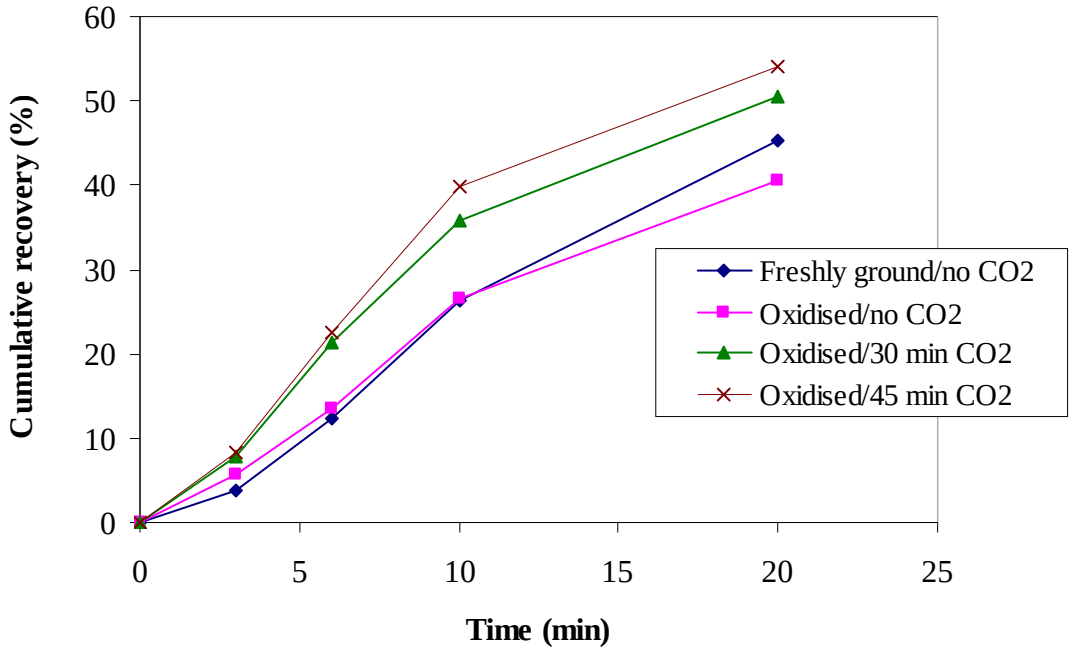

Figure 81: Recovery-time curves during microflotation of the freshly ground and pre-oxidised magnetic 4C type pyrrhotite in a synthetic solution containing 5 x 10^{-5} M sodium isobutyl xanthate and 0.4 x 10^{-4} M copper sulfate at pH 9.3. The particle size range was 38 – 106 µm.

The air flow rate was kept constant, at 58 ml/min; copper sulfate concentration was at 0.4 x 10^{-4} M; sodium isobutyl xanthate was at 5 x 10^{-5} M. When comparing the freshly ground and oxidised pyrrhotite sample without carbon dioxide treatment, the recovery was initially slightly higher for the oxidised sample. The recovery was the same after 10 minutes, but the final overall recovery of the freshly ground sample was higher by 4.58 %. This shows the negative influence of oxidation on the flotation response of pyrrhotite. However, this response was expected to be more negative.

After 30 minutes of gaseous carbon dioxide pre-conditioning, there was an increase in the final recovery by 9.83 %, i.e. from 40.61 to 50.44 %. With an extra 15 minutes of treatment (increased from 30 to 45 minutes), the increase in flotation recovery after 10 minutes was not that significant, with the final recovery increasing from 50.44 to 54.10 %.

Copper activation and higher air flow rate were found to improve pyrrhotite flotation response. Other studies have shown that pyrrhotite flotation recovery is significantly

improved with the addition of copper sulfate in alkaline solutions (Leppinen, 1990; Senior *et al*., 1995; Kelebek *et al*., 1996). The oxidation of pyrrhotite impaired pyrrhotite flotation only marginally. Gaseous carbon dioxide treatment of oxidised pyrrhotite resulted in the cleaning and improved interaction of xanthate with the pyrrhotite surface, shown by the improved flotation response of pyrrhotite. It is anticipated that CO_2 pre-conditioning would have the same influence on the flotation response of pre-oxidised base-metal sulfide ore deposits.

6. CONCLUSIONS

The electrochemical behaviour of pyrrhotites varying in chemical composition, crystal structure and amount of pentlandite, in the absence and presence of potassium ethyl xanthate, was investigated. It was observed that the influence of galvanic interaction between pentlandite and pyrrhotite on the reactivity of pyrrhotite applies only in oxygen-saturated conditions, where pentlandite acts as a cathode and pyrrhotite as an anode. Under oxygen-deficient conditions (such as in anodic polarisation diagrams), pentlandite acts as an inert material in the low potential region; it does not have an influence on the reactivity of pyrrhotite. At higher potentials, both pyrrhotite and pentlandite are oxidised. The influence of gaseous carbon dioxide on the electrochemical and microflotation response of CO_2 treated oxidised pyrrhotite was also studied.

The reactivity of the 4C and 6C type pyrrhotites were studied using rest potential, polarisation resistance and anodic and cathodic polarisation diagrams in a 0.05 M tetraborate solution at pH 9.3 in the absence and presence of xanthate. In the absence of xanthate, the rest potential, polarisation resistance measurements and anodic scans showed that the magnetic 4C pyrrhotite is more reactive (i.e. easily oxidised) and passivated to a larger extent than the non-magnetic 6C type pyrrhotite. The magnetic 4C type pyrrhotite samples obtained from Russia had no major differences in their electrochemical behaviour. The cathodic polarisation diagrams showed that the non-magnetic 6C type pyrrhotite is a good substrate for oxygen reduction and is less susceptible to oxidation. Anodic polarisation diagrams were used to study the interaction of xanthate with the pyrrhotite surface; these indicated that the maximum anodic current density was reduced on the 4C and 6C type pyrrhotites due to the presence of xanthate on the surface inhibiting mineral oxidation. The order in the anodic reactivity was not affected by the presence of xanthate (i.e. magnetic 4C pyrrhotite is more reactive than the 6C type pyrrhotite). Current density-time transients showed that the magnetic 4C pyrrhotite is anodically more reactive than the 6C type pyrrhotite. ToF-SIMS measurements showed that an oxide layer forms on the pyrrhotite surface after oxidation and 4C pyrrhotite has a slightly thicker layer than the 6C pyrrhotite.

In oxygen-saturated solutions, the rest potential and polarisation resistance measurements demonstrated that the amount of pentlandite in contact with pyrrhotite results in galvanic interaction and reduces the anodic reactivity of the mixed pyrrhotite sample. The reactivity

decreased in the order: pure pyrrhotite (Russian sample) > medium-pentlandite- pyrrhotite (Sudbury Gertrude sample) > high-pentlandite-pyrrhotite (Phoenix sample).

The polarisation resistance values were also lowered in the same order due to different mineral phases and uneven surface film forming on the surface (since pyrrhotite is oxidised and pentlandite is galvanically protected). Cathodic polarisation diagrams indicated that pentlandite enhances the oxygen reduction activity of the mixed mineral samples. Anodic polarisation diagrams showed that under oxygen-deficient conditions, pentlandite does not have an influence on the reactivity of pyrrhotite since it acts as an inert material at low potentials. As a result, the reactivities of the magnetic 4C type pyrrhotites from various deposits (i.e. Russia, Sudbury Gertrude and Phoenix) were compared. Anodic polarisation diagrams in the absence and presence of xanthate showed that the anodic reactivity increased in the order: Russian pyrrhotite < Phoenix pyrrhotite < Sudbury Gertrude pyrrhotite. No correlation was observed between the different oxidation behaviour of the magnetic 4C type pyrrhotites and the trace metal content. In the higher potential region, higher anodic currents were observed due to the oxidation of both pyrrhotite and pentlandite. The reactivity increased in the order: pure pyrrhotite (Russian sample) < medium-pentlandite-pyrrhotite (Sudbury Gertrude sample) < high-pentlandite-pyrrhotite (Phoenix sample).

Oxidised pyrrhotite electrodes were treated by continuously bubbling gaseous carbon dioxide in a tetraborate solution for an hour, prior to electrochemical measurements. The pH was reduced from 9.30 to between 6.60 and 6.80. The rest potential and polarisation resistance values decreased after CO_2 treatment, showing that CO_2 treatment results in cleaning and depassivation of the mineral surface. The depassivation occurs by reaction of dissolved gaseous carbon dioxide and the oxidation products to produce ferrous carbonate and a dissolved complex of Fe. The formation of the complex enhances the metal dissolution rate.
It was shown in anodic polarisation diagrams that the CO_2 treated surface becomes more reactive than an oxidised and wet-polished surface. The low anodic currents of the wet-polished surface indicated that there was an oxidation product layer passivating the surface. Following CO_2 treatment, higher anodic currents were observed, suggesting that the oxidation product layer was removed. ToF-SIMS results showed that the mineral surface was clean following CO_2 treatment. Gaseous carbon dioxide conditioning of oxidised pyrrhotite surfaces was shown (by electrochemical measurements and ToF-SIMS) to clean the pyrrhotite surfaces and enhance anodic reactivity of both the 4C and 6C type pyrrhotites in

the absence and presence of xanthate. In the presence of xanthate and at higher potentials, the anodic currents of the CO_2 treated surface were lower than the polished surface, indicating a thicker passivation layer of xanthate species on the CO_2 treated surface. The order in the anodic reactivity of the 4C and 6C type pyrrhotites was not consistent when using CO_2 in the absence and presence of xanthate.

The influence of gaseous carbon dioxide conditioning on the flotation response of oxidised pyrrhotite was investigated by microflotation measurements, using the pure magnetic 4C type pyrrhotite sample. The flotation response of pyrrhotite was improved by copper activation and higher air flow rate. Oxidation of pyrrhotite was observed to reduce the flotation recovery of pyrrhotite. Gaseous carbon dioxide conditioning of oxidised pyrrhotite resulted in the cleaning and improved interaction of xanthate with the pyrrhotite surface, shown by the improved flotation response of pyrrhotite.

7. RECOMMENDATIONS FOR FUTURE RESEARCH

The following recommendations are made for future research:

- A study of the electrochemical behaviour of a 5C type pyrrhotite under the same conditions used in this study to compare its electrochemical response to that of the 4C and 6C type pyrrhotites.
- Ethylene diamine tetra-acetate (EDTA) extraction of oxidised species to determine and compare the level of oxidation of pyrrhotite samples treated using different techniques.
- FTIR and Raman studies of the different pyrrhotite surfaces to determine the xanthate species forming on the surface in the presence of xanthate.
- Contact angle measurements to determine the extent of hydrophobicity of the pure polished and CO_2 treated pyrrhotite surfaces as well as of mixed pyrrhotite samples.
- XPS studies of the polished, oxidised and CO_2 treated surfaces to establish the products that form on the surface under various conditions.
- Laboratory scale batch flotation tests on pyrrhotite samples in order to confirm the microflotation results of gaseous carbon dioxide conditioning on the flotation response of oxidised pyrrhotite observed in this study and to determine the influence of the presence of a froth phase and other minerals (i.e. galvanic interaction) on pyrrhotite flotation (i.e. grade and recovery).
- Impurities were not found to have an impact on the anodic reactivity of the Phoenix, Sudbury Gertrude and Russian magnetic pyrrhotites. Measurements of the conductivities of these samples might assist in determining if the differences in the anodic reactivity might be due to the difference in conductivities.

8. REFERENCES

Adam, K., Natarajan, K.A. and Iwasaki, I. 1984. *Grinding media wear and its effect on the flotation of sulfide minerals.* International Journal of Minerals Processing, vol 12, Issues 1-3, pp. 39-54.

Agar, G.E. 1991. *Flotation of chalcopyrite, pentlandite, pyrrhotite ores.* International Journal of Minerals Processing, vol 33, pp.1–19.

Ahn, J.H. and Gebhardt, J.E. 1991. *Effect of grinding media-chalcopyrite interaction on the self-induced flotation of chalcopyrite.* International Journal of Minerals Processing, vol 33, Issues 1-4, pp. 243-262.

Ahonen, L. and Tuovinen, O.H. 1994. *Solid-phase alteration and iron transformation in column bioleaching of a complex sulfide ore. In Environmental Geochemistry of Sulfide Oxidation* Edited by C.N., Alpers and D.W. Blowes. ACS Symposium Series 550, American Chemical Society, Washington D.C., pp. 78-79.

Alekseeva, R.K. 1965. *Causes of the differing floatability for pyrrhotite modifications.* Tsvetnaya Metallurgiya, vol 6, no. 3, pp. 19-22.

Allison, S.A., Goold, L.A., Nicol, M.J. and Granville, A. 1972. *A determination of the products of reaction between various sulfide minerals and aqueous xanthate solution, and a correlation of the products with electrode rest potentials.* Metallurgical Transactions, vol 3, pp. 2513-2618.

Baltrusaitis, J. and Grassian, V.H. 2005. *Surface reactions of carbon dioxide at the adsorbed water-iron oxide interface*. Journal of Physical Chemistry B, vol 109, pp. 12227-12230.

Becker, M. 2005. *Mineralogy of Pyrrhotite in the Nkomati and Tati Sulfide Deposits.* MPRU Report, University of Cape Town, Cape Town.

Becker, M. 2006. *An investigation into the crystallography, mineralogy and processing characteristics of pyrrhotite from selected nickeliferous and platinum group element (PGM) deposits.* PhD Proposal, University of Cape Town and University of Pretoria, RSA.

Becker, M. 2009. *The mineralogy and crystallography of pyrrhotite from selected nickel and PGE ore deposits and its effect on flotation performance.* PhD Dissertation, University of Pretoria, Pretoria.

Belzile, N., Goldsack, D., Maki, S. and McDonald, A. 1997a. *Acid mine drainage in the Sudbury area, Ontario.* In *Environmental Geology of Urban Areas.* Edited by N., Eyles. Geological Association of Canada, pp. 223-226.

Belzile, N., Chen, Y., Cai, M. and Li, Y. 2004. *A review on pyrrhotite oxidation.* Journal of Geochemical Exploration, vol 84, pp. 65-76.

BGMN® is a registered trademark of Dr. Jöhn Bergmann, Dresden, Germany.

Bierens de Haan, S. 1991. *A review of the rate of pyrite oxidation in aqueous systems at low temperatures.* Earth-Science Review, vol 31, pp. 1-10.

Bozkurt, V., Xu, Z. and Finch, J.A. 1998. *Pentlandite/pyrrhotite interaction and xanthate adsorption.* International Journal of Minerals Processing, vol 52, pp. 203-214.

Bozkurt, V., Xu, Z. and Finch, J.A. 1999. *Effect of depressants on xanthate adsorption on pentlandite and pyrrhotite: single vs mixed minerals.* Canadian Metallurgical Quarterly, vol 38, no. 2, pp. 105-112.

Bradshaw, D.J. and O'Connor, C.T. 1996. *Measurement of the sub-process of bubble loading in flotation.* Minerals Engineering, vol 9, no. 4, pp. 443-448.

Bradshaw, D.J., Buswell, A.M., Harris, P.J. and Ekmecki, Z. 2006. *Interactive effects of the type of milling media and copper sulfate addition on the flotation performance of sulfide minerals from Merensky ore Part I: Pulp chemistry.* International Journal of Mineral Processing, vol 78, pp. 153-163.

Brynard, H.J., De Villiers, J.P.R. and Viljoen, E.A. 1976. *A mineralogical investigation of the Merensky reef at the Western Platinum mine near Marikana, South Africa.* Economic Geology, vol 71, pp. 1299-1307.

Buchanan, D.L., 1979. *Platinum-group metal production from the Bushveld Complex and its relationship to world markets.* Bureau for Mineral Studies, University of Witwatersrand, pp. 325.

Buckley, A.N., Hamilton, I.C. and Woods, R. 1985. *Investigation of the surface oxidation of sulfide minerals by linear sweep voltammetry and X-ray photoelectron spectroscopy. In Flotation of Sulfide Minerals.* Edited by K.S.E. Forssberg. Elsevier, pp. 41-59.

Buckley, A.N., Hope, G. and Woods, R. 2003. *Metals from sulfide minerals: the role of adsorption of organic reagents in processing technologies. In Solid-Liquid Interfaces: Macroscopic Phenomena-Microscopic Understanding*, Edited by K., Wandelt and S., Thurgate. Springer, Heidelberg, pp. 61-96.

Buckley, A.N. and Woods, R. 1985a. *X-ray photoelectron spectroscopy of oxidised pyrrhotite surfaces.* Applied Surface Science, vol 22/23, pp. 280-287.

Buckley, A.N. and Woods, R. 1985b. *X-ray photoelectron spectroscopy of oxidised pyrrhotite surfaces.* Applied Surface Science, vol 20, pp. 472-480.

Buckley, A.N. and Woods, R. 1997. *Chemisorption – the thermodynamically favoured process in the interaction of thiol collectors with sulfide minerals.* International Journal of Mineral Processing, vol 51, Issues 1-4, pp. 15-26.

Buswell, A.M., Bradshaw, D.J., Harris, P.J. and Ekmekci, Z. 2002. *The use of electrochemical measurements in the flotation of a platinum group minerals (PGM) bearing ore.* Minerals Engineering, vol 15, pp. 394-404.

Buswell, A.M., Bradshaw, D.J., Harris, P.J. and Harris, M. 1988. *The use of electrochemical measurements in the characterisation of flotation pulp chemistry on laboratory and plant*

scale. Unpublished report, Mineral Processing Research Unit, University of Cape Town, pp. 132.

Buswell, A.M. and Nicol, M.J. 2002. *Some aspects of the electrochemistry of the flotation of pyrrhotite*. Journal of Applied Electrochemistry, vol 32, pp. 1321-1329.

Cabri, L.J. 1988. *New developments in determination of the distribution of precious metals in ore deposits.* Proceedings of the Seventh Quadrennial IAGOD Symposium, pp. 149-154.

Caldeira, C.L., Ciminelli, V.S.T, Dias, A. and Osseo-Asare, K. 2003. *Pyrite oxidation in alkaline solutions: nature of the product layer.* International Journal of Mineral Processing, vol 72, pp. 373-386.

Chang, C.S., Cooke, S.R.B. and Iwasaki, I. 1954. *Flotation characteristics of pyrrhotite with xanthate.* Trans. AIME 199, 209.

Chander, S. 1991. *Electrochemistry of sulfide flotation: Growth characteristics of surface coatings and their properties, with special reference to chalcopyrite and pyrite.* International Journal of Minerals Processing, vol 33, pp. 121-134.

Cheng, X. and Iwasaki, I. 1992. *Effect of chalcopyrite and pyrrhotite interaction on flotation separation.* Minerals and Metallurgical Processing, vol 9, no. 2, pp. 73-79.

Cheng, X., Iwasaki, I. and Smith, K.A. 1999. *Electrochemical study of multielectrode systems and their relevance to the differential flotation of complex sulfide ores.* Minerals and Metallurgical Processing, vol 16, no. 1, pp. 69-71.

Clarke, P. 1995. *The Interaction of Metal Ions and their Hydrolysis Products with Sulfide Mineral Surfaces.* Ph.D. Thesis, University of South Australia.

Clarke, P., Fornasiero, D., Ralston, J. and Smart, R.St.C. 1995. *A study of the removal of oxidation products from sulfide mineral surfaces.* Minerals Engineering, vol 8, Issue 11, pp. 1347-1357

Craig, B.D. 1991 *Fundamental aspects of corrosion films in corrosion science.* New York: Plenum.

Cruz, R., Luna-Sa´nchez, R.M., Lapidus, G.T., Gonza´lez, I. and Monroy, M. 2005. *An experimental strategy to determine galvanic interactions affecting the reactivity of sulfide mineral concentrates.* Hydrometallurgy, vol 78, pp. 198–208.

Debnath, N.C. and Anderson, A.B. 1982. *Optical spectra of ferrous and ferric oxides and the passive film: A molecular orbital study*. Journal of Electrochemical Society, vol 129, pp. 2169-2174.

Desborough, G.A. and Carpenter, R.H. 1965. *Phase relations in pyrrhotite*. Economic Geology, vol 60, pp. 1431-1450.

De Villiers, J.P.R., Brynard, H.J. and Viviers, L. 1980. *A mineralogical investigation of ores from the Merensky reef and their flotation products.* National Institute for Metallurgy, Randburg.

De Villiers, J.P.R. and Liles, D.C. 2010. *The crystal structure and vacancy distribution in 6C pyrrhotite*. American Mineralogist, vol 95, pp. 148-152.

De Wet, J.R., Pistorius, P.C. and Sandenbergh, R.F. 1997. *The influence of cyanide on pyrite flotation from gold leach residues with sodium isobutyl xanthate.* International Journal of Minerals Processing, vol 49, pp. 149-169.

Du Plessis, R. 2004. *The thiocarbonate flotation chemistry of auriferous pyrite.* PhD Dissertation, University of Utah, Salt Lake City, Utah.

Dunn, J.G., Hollbach, D.J. and Ibrado, A.S. 1995. *The dissolution of pyrrhotite in cyanide solution.* Proc. Randol. Gold Forum, pp. 145–148.

Dunne, R.C. 2007. *Flotation of platinum-group metals, In Froth Flotation: A Century of Innovation.* Edited by M.C., Fuerstenau, G.J., Jameson, Yoon, R-H., Little, Colo: Society for Mining, Metallurgy and Exploration.

Ekmekçi, Z. and Demirel, H. 1997. *Effects of galvanic interaction on collectorless flotation behaviour of chalcopyrite and pyrite.* International Journal of Minerals Processing, vol 52, pp. 31-48.

Fairthorne, G. 1995. *The Interaction of Thionocarbamate Collectors with Sulfide Mineral Surfaces.* PhD Thesis, University of South Australia.

Feng, D. and Aldrich, C. 2000. *A comparison of the flotation of ore from the Merensky Reef after wet and dry grinding.* International Journal of Minerals Processing, vol 60, pp. 115–129.

Finkelstein, N.P. and Allison, S.A. 1976. *Flotation. In A.M. Gaudin Memorial Volume.* Edited by M.C. Fuerstenau. American Institute of Mining, Metallurgy and Petroleum Engineering Inc., New York, N.Y., vol 1, pp. 414-457.

Finkelstein, N.P. and Poling, G.W. 1977. *The role of dithiolates in the flotation of sulfide minerals.* Minerals Science Engineering, vol 9, no. 4, pp. 177-197.

Fornasiero, D., Montalti, M. and Ralston, J. 1995. *Kinetics of adsorption of ethyl xanthate on pyrrhotite. In situ UV and infrared spectroscopic studies.* Journal of Colloid and Interface Science. vol 172, pp. 467- 478.

Fornasiero, D., Li, F., Ralston, J. and Smart, R. St. 1994. *Oxidation of Galena Surfaces: I. X-Ray Photoelectron Spectroscopic and Dissolution Kinetics Studies.* Journal of Colloid and Interface Science, vol 164, pp. 333-344.

Freeman, W.A., Newell, R. and Quast, K.B. 2000. *Effect of grinding media and NaHS on copper recovery at NorthParkes Mines.* Minerals Engineering, vol 13, no. 13, pp. 1395-1403.

Fuerstenau, D.W. 1982 *The Principles of Flotation.* South African Institute of Mining and Metallurgy, Johannesburg, pp. 183-198.

Fuerstenau, M.C. 1982. *Chemistry of Collectors in Solution. In Principles of Flotation.* Edited by R.P. King, South African Institute of Mining and Metallurgy, Johannesburg, pp. 1–16.

Gain, S.B. 1984. *Distribution and origin of the platinum-group elements in the UG-2 chromititelayer on Maandagshoek, Eastern Bushveld complex.* University of Pretoria, Pretoria.

Gauert, C.D.K., De Waal, S.A. and Wallmach, T. 1995. *Geology of the ultrabasic to basic Uitkomst complex, eastern Transvaal, South Africa: an overview.* Journal of African Earth Sciences, vol. 21, no. 4, pp. 553-570.

Godel, B., Barnes, S and Maier, W.D. 2007. *Platinum-group elements in sulfide minerals, Platinum-group minerals, and whole-rocks of the Merensky reef (Bushveld Complex, South Africa): Implications for the formation of the reef.* Journal of Petrology, vol 48, no. 8, pp. 1569-1604.

Hamilton, I. C. and Woods, R. 1981. *An investigation of surface oxidation of pyrite and pyrrhotite by linear potential sweep voltammetry.* Journal of Electroanalytical Chemistry, vol 18, pp. 327-343.

Hamilton, I., C. and Woods, R. 1983. *An investigation of the deposition of sulfur on the gold electrode.* Journal of Electrochemistry, vol 13, pp. 783.

Healy, T.W. 1984. *Pulp chemistry, surface chemistry and flotation. In Principles of Mineral Flotation.* Edited by M.H. Jones and J.T. Woodcock. Wark Symposium, pp. 43-56.

Heyes, G.W. and Trahar, W.J. 1984. *The flotation of pyrite and pyrrhotite in the absence of conventional collectors.* In Edition by Richardson, P.R., Srinivasan, S.S. and Woods, R. Proceedings of the International Symposium of Electrochemical Society. Pennington, NJ, vol 84, no.10, pp. 189.

Hodgson, M. and Agar, G.E. 1984. *An electrochemical investigation into the natural floatability of pyrrhotite.* In Edition by Richardson, P.R., Srinivasan, S.S. and Woods, R.

Proceedings of the International Symposium of Electrochemical Society. Pennington, NJ, vol 84, no.10, pp. 189.

Hodgson, M. and Agar, G.E. 1989. *Electrochemical investigation into the flotation chemistry of pentlandite and pyrrhotite: process water and xanthate interactions.* Canadian Metallurgical Quarterly, vol 28, no. 3, pp. 189-198.

Iwasaki, I. 1988. *Flotation behaviour of pyrrhotite in the processing of copper-nickel ores.* In Edition by Tyrolor, G.P. and Landdolt, C.A. Extractive Metallurgy of Nickel and Cobalt. The Metallurgical Society.

Jambor, J.L. 1986. *Detailed mineralogical examination of alteration products in core WA-20 from Waite Amulet tailings.* CANMET Division Report MSL 86-137(IR). Department of Energy Mines Resources Canada.

Janzen, M.P. 1996. *Role of ferric iron, trace metal content, and crystal structure on pyrrhotite oxidation.* M.Sc. Thesis, University of Waterloo, Waterloo, Ontario.

Janzen, M.P., Nicholson, R.V. and Scharer, J.M. 2000. *Pyrrhotite reaction kinetics: Reaction rates for oxidation by oxygen, ferric iron, and for nonoxidative dissolution.* Geochim. Cosmochim. Acta, vol 64, no. 9, pp. 1151-1522.

Johnson, R.S. 1986. *The Phoenix and Selkirk nickel-copper sulfide ore deposits, Tati greenstone belt, Eastern Botswana. In Mineral Deposits of Southern Africa* Edited by Anhaeusser, C.R. and Maske, S. Johannesburg, vol. 1, pp. 243-248.

Jones, C.F., Lecount, S., Smart, R.St.C. and White, T. 1992. *Compositional and structural alteration of pyrrhotite surfaces in solution: XPS and XRD studies.* Applied Surface Science, vol 55, pp. 65-85.

Jones, D.A. 1996. *Principles and prevention of corrosion.* 2nd edition, New Jersey: Prentice-Hall.

Jones, M.H. and Woodcock, J.T. 1986. *Dixanthogen determination in flotation liquors by solvent extraction and Ultraviolet Spectrometry*. Analytical Chemistry, vol 58, pp. 588-591.

Jones, R.T. 1999. *Platinum smelting in South Africa.* South African Journal of Science, vol. 95, pp. 525-534.

Kaiser, H. and Specker, H. 1955. Bewurtung und Vergleich von Analysenverfahren. Zeitchrift für Analytische chemie, vol 149, pp. 44-46.

Kelebek, S., Wells, P.F. and Fekete, S.O. 1996. *Differential flotation of chalcopyrite, pentlandite and pyrrhotite in Ni-Cu sulfide ores.* Canadian Metallurgical Quarterly, vol 35, no. 4, pp. 329-336.

Khan, A. and Kelebek, S. 2004. *Electrochemical aspects of pyrrhotite and pentlandite in relation to their flotation with xanthate. Part-I: Cyclic voltammetry and rest potential measurements.* Journal of Applied Electrochemistry, vol 34, pp. 849-856.

Klein, C. and Hurlburt, C.S. 1993. *Manual of Mineralogy.* John Wiley & Sons, New York, 21st edition, pp. 681.

Klimpel, R.R. 1980. *Selection of chemical reagents for flotation.* Mineral Processing Plant Design, AIME, vol 45, 907-934.

Knipe, S.W., Mycroft, J.R., Pratt, A.R., Nesbitt, H.W. and Bancroft, G.M. 1995. X-*ray photoelectron spectroscopic study of water adsorption on iron sulfide minerals* Geochim. Cosmochim. Acta, vol 59, pp. 1079-1090.

Koto, K., Morimoto, N., and Gyobu, A. 1975. *The superstructure of the intermediate pyrrhotite. I. Partially disordered distribution of metal vacancy in the 6C type, Fe_nS_{n+1}.* Acta Crystallographica, vol B31, pp. 2759–2764.

Kwong, E.C.M. 1995. *Abiotic and biotic pyrrhotite dissolution.* M.A.Sc. Thesis, University of Waterloo, Waterloo, Ontario.

Laskowski, J.S. 2004. *Activation in flotation circuits. Challenges and Opportunities.* Proceedings of the 10th International Mineral Processing Symposium. Edited by A. Akar *et al*., Cesme-Izmir, pp. 377–394.

Laskowski, J.S., Liu, Q. and Zhan, Y. 1997. *Sphalerite activation: Flotation and electrokinetic studies.* Minerals Engineering, vol 10, Issue 8, pp. 787-802

Lehmann, M. N., Kaur, P., Pennifold, R.M. and Dunn, J.G. 2000. *A comparative study of the dissolution of hexagonal and monoclinic pyrrhotites in cyanide solution.* Hydrometallurgy, vol 55, pp. 255 – 273.

Leppinen, J.O. 1990. *FTIR and flotation investigation of the adsorption of ethyl xanthate on activated and non-activated sulfide minerals.* International Journal of Minerals Processing, vol 30, Issues 3-4, pp. 245–263.

Leppinen, J.O., Basilio, C.I. and Yoon, R.H. 1989. *In-situ FTIR study of ethyl xanthate adsorption on sulfide minerals under conditions of controlled potential.* International Journal of Minerals Processing, vol 26, Issues 3-4, pp. 259–274.

Liebenberg, L. 1970. *The sulfides of the layered sequence of the Bushveld Igneous Complex. In: Symposium on the Bushveld Igneous Complex and other Layered Intrusions.* Geological Society of South Africa, Special Publication, vol 1, pp. 108-207.

Linge, H.G. 1995. *Anodic oxidation of pyrrhotite in simulated CIP liquors.* Minerals Engineering, vol 8, no. 7, pp. 795-806.

Lin-lin, T., Mao-fa, J., Hong-ying, Y., Juan, Y, You-jing, F. and Yao, Z. 2009. *Dynamic corrosion of copper-nickel sulfide by Acidithiobacillus ferrooxidans.* Transaction of Nonferrous Metal Society China, vol 19, pp. 438 – 445.

Linter, B.R. and Burstein, G.T. 1999. *Reactions of pipeline steels in carbon dioxide solutions. Corrosion Science,* vol 41, pp. 117-139.

Lovell, V.M. 1982. *Industrial Flotation Reagents. In Principles of Flotation*. Edited by R.P. King. South African Institute of Mining and Metallurgy, Johannesburg, pp. 73-89.

Lowson, R.T. 1982. *Aqueous oxidation of pyrite by molecular oxygen.* Chemical Rev., vol 5, pp. 461-497.

Lu, Z.Y., Jeffrey, M.I., Zhu, Y. and Lawson, F. 2000. *Studies of pentlandite leaching in mixed oxygenated acidic chloride–sulfate solutions.* Hydrometallurgy, vol 56, pp. 63–74.

Maier, W.D., Gomwe, T., Barnes, S.J., Li, C. and Theart, H. 2003. *Platinum Group Elements in the Uitkomst Complex, South Africa.* South African Journal of Geology, vol 104, pp. 287-300.

Majima, H. and Peters, E. 1966. *Oxidation rates of sulfide minerals by aqueous oxidation at elevated temperatures.* Trans. Metall. Soc. AIME, vol 236, pp. 1409-1413.

Manyeruke, T.D. 2003. *The petrography and geochemistry of the Platreef on the farm Townlands, near Potgietersrus, northern Bushveld Complex.* MSc Thesis, University of Pretoria, Pretoria.

Mason, L.J. and Rice, N.M. 2002. *The adaptation of thiobacillus ferrooxidans for the treatment of nickel–iron sulfide concentrates.* Minerals Engineering, vol 15, pp. 795–808.

McIntosh, J.M. and Groat, L.A. 1997. *Biological–mineralogical interactions.* Short course series, Mineralogical association of Canada, Ottawa.

Merkle, R.K.W. and Von Gruenewaldt, G. 1986. *Compositional variation of Co-rich pentlandite: relation to the evolution of the upper zone of the Western Bushveld Complex.* South Africa, Canadian Mineralogist, pp. 529-546.

Mikhlin, Y. 2000. *Reactivity of pyrrhotite surfaces: An electrochemical study*. Phys. Chem. Chem. Phys., vol 2, pp. 5672-5677.

Mikhlin, Y.L., Kuklinskii, A.V., Pavlenko, N.I., Varnek, V.A., Asonov, I.P., Okotrub, A.V., Selyutin, G.E. and Solovyey, L.A. 2002. *Spectroscopic and XRD studies of the air degradation of acid-reacted pyrrhotite.* Geochim. Cosmochim. Acta, vol 66, pp. 4057-4067.

Miller, J.D., Du Plessis, R., Simmons, G.I. and Kotlyar, D.G. 2002. *The effect of activation on the low potential hydrophobic state of pyrite amyl xanthate flotation with nitrogen*. SME Annual Meeting, pp. 1-5.

Miller, J.D., Li, J., Davidtz, J.C. and Vos, F. 2005. *A review of pyrrhotite flotation chemistry in the processing of PGM ores.* Minerals Engineering, vol 18, pp. 855-865.

Miller, J.D. and Misra, M. 1987. *Coal cleaning by gaseous carbon dioxide conditioning and froth flotation.* United States patent 4676804.

Moignard, M.S., Dixon, D.R. and Healy, T.W. 1977. *Electrokinetic Properties of the Zinc Sulfide-Water and Nickel Sulfide-Water Interfaces.* Proceedings of the Australian Institute of Mining and Metallurgy, vol 263, pp. 31-38.

Morimoto, N., Gyobu, A., Mukaiyama, H. and Izawa, E. 1975. *Crystallography and stability of pyrrhotites.* Economic Geology, vol 70, pp. 824-833.

Mostert, A.B. 1982. *A mineralogical and petrological investigation of the Platreef on Drenthe 778 LR, Northwest of Potgietersrus.* MSc Thesis, University of Pretoria, Pretoria.

Nakazawa, H. and Iwasaki, I. 1985. *Effect of pyrite-pyrrhotite contact on their floatabilities.* Minerals and Metallurgical Processing, vol 2, no. 4, pp. 203-220.

Nakazawa, H. and Iwasaki, I. 1986. *Galvanic contact between nickel arsenide and pyrrhotite and its effect on pyrrhotite.* International Journal of Minerals Processing, vol 18, Issues 3-4, pp. 203-215.

Nakazawa, H. and Morimoto, N. 1971. *Phase relations and superstructures of pyrrhotite, $Fe_{1-x}S$.* Mat. Res. Bull., vol 6, pp. 345–358.

Nanthakumar, B., Kelebek, S. and Katsabanis, P.D. 2007. *Impact of oxidation on flotation of Ni-Cu sulfide ore with respect to grinding.* Mineral Processing and Extractive Metallurgy, vol 116, no. 3, pp. 197-206.

Newell, A.J.H., Bradshaw, D.J. and Harris, P.J. 2005. *The effect of heavy oxidation upon flotation and potential remedies for Merensky type sulfides*. Minerals Engineering, pp. 1-11.

Nicholson, R.V. and Scharer, J.M. 1994. *Laboratory studies of pyrrhotite oxidation kinetics. In Environmental Geochemistry of Sulfide Oxidation.* Edited by C.N. Alpers and D.W. Blowes, American Chemistry Society, Washington DC, pp. 14-30.

Nicol, M.J. 1984. In Edition by Richarson, P.E., Srinivasan, S. and Woods, R. International Symposium on Electrochemistry Mineral and Metal Processing. Electrochemical Society, pp. 152–168.

Nguyen, A.V. and Schulze, H.J.2004. *Colloidal science of flotation*. Marcel Dekker, New York.

Nordstrom, D.K. and Alpers, C.N. 1999. *Geochemistry of acid mine waters. In The Environmental Geochemistry of Mineral Deposits: Part A. Processes, Methods, and Health Issues.* Edited by Plumlee, G.S. and Longston, M.D. Society of Economic Geologists, Littleton, CO. Reviews in Economic Geology, vol 6A, pp. 133-160.

Oberthür, T., Kojoken, K. and Weiser, T.W. 2002. *Local variations and regional trends in PGE geochemistry and mineralogy in the main sulfide zone of the Great Dyke, Zimbabwe.* Proceedings: 9th International Platinum Symposium, Billings, Montana, USA, 21-25 July, 2002.

Orlova, T.A., Stupnikov, V.M. and Krestan, A.L. 1989. *Mechanism of oxidative dissolution of sulfides.* Zhurnal Prikladnoi Khimii, vol 61, pp. 2172-2177.

Orwe, D., Grano, S.R. and Lauder, D.W., 1997. *Chalcocite oxidation and its influence on fine copper recovery at the Ok Tedi concentrator*. Proceedings, Sixth Mill Operators Conference, Australian Institute of Mining and Metallurgy, pp. 85-95.

Orwe, D., Grano, S.R. and Lauder, D.W. 1998 *Increasing fine copper recovery at the Ok Tedi concentrator, Papua New Guinea.* Minerals Engineering, vol 11, no. 2, pp. 171-187.

Penberthy, C.J. 2001. *The effect of mineralogical variation in the UG-2 chromitite on recovery of platinum-group elements.* PhD Dissertation, University of Pretoria, Pretoria.

Persson, I. 1993. *Adsorption of ions and molecules to solid surfaces in connection with flotation of sulfide minerals.* Journal of Co-ordination Chemistry, vol 32, no. 4, pp. 261-341.

Peters, E. 1977. *In Trends in Electrochemistry*. Edited by Rand, D.A.J and Welsh, B.J. Plenum Press, New York, pp. 267.

Plaskin, I.N. and Bessonov, S.V. 1957 Proceedings of the 2nd International Congress of Surface Activ., vol 3, pp. 361.

Plysunin, A.M., Mironov, A.G., Belomestrova, N.V. and Chernigova, S.Y. 1990. *Laboratory studies on gold-bearing sulfide oxidation*. Geokhimiya, vol 1, pp. 51-60.

Pofsai, M. and Dodonay, L. 1990. *Pyrrhotite superstructures: Part I. Fundamentals structures of the NC (N = 2, 3, 4 and 5) type*. Eur. J. Mineral, vol 2, pp. 525-528.

Pratt, A.R., Muir, I.J. and Nesbitt, H.W. 1994. *X-ray photoelectron and Auger electron spectroscopic studies of pyrrhotite and mechanism of air oxidation.* Geochim. Cosmochim. Acta, vol 58, no. 2, pp. 827 – 841.

Pratt, A.R., Nesbitt, H.W. and Mycroft, J.R. 1996. *The increased reactivity of pyrrhotite and magnetite phases in sulfide mine tailings*. Journal of Geochemical Exploration, vol 56, Issue 1, pp. 1-11.

Ralston, J. 1991. *E_h and its consequences in sulfide mineral flotation*. Minerals Engineering, vol 4, Issues 7-11, pp. 859-878.

Ralston, J., Alabaster, P. and Healy, T.W. 1981. *Activation of zinc sulfide with Cu(II), Cd(lI), Pb(II):IlL The mass-spectrometric determination of elemental sulfur.* International Journal of Mineral Processing, vol 7, pp. 279-310

Ralston, J. and Healy, T.W. 1980a. *Activation of zinc sulfide with Cu^{2+}, Cd^{2+} and Pb^{2+}. Part II*. International Journal of Mineral Processing, vol 7, pp. 203–217.

Ralston, J. and Healy, T.W. 1980b. *Activation of zinc sulfide with Cu(II), Cd(II), Pb(II): Part I-II*. International Journal of Mineral Processing, vol 7, pp. 175-201 and 203-217.

Rand, D.A.J. 1977. *Oxygen reduction on sulfide minerals Part III. Comparison of activities of various copper, iron, lead and nickel mineral electrodes* Journal Electroanalytical Chemistry, vol 83, pp. 19-32.

Rao, S.R. 2004. *Surface Chemistry of Froth Flotation*. 2nd edition, vol 2, Kluwer Academic/Plenum Publishers.

Rao, S.R. and Finch, J.A. 1988. *Galvanic interactions studies on sulfide minerals.* Canadian Metallurgical Quarterly, vol 27, no. 4, pp. 253-259.

Ribbe, P.H. 1984. *Average structures of alkali and plagioclase feldspars: systematics and applications. In: Feldspars and feldspathoids: structures, properties and occurrences.* Edited by W.L. Brown, D. Reidel Publishing Co, Dordrecht, pp. 1-54.

Ritchie, I.M., Bailey, S. and Woods, R. 1999. *The metal-solution interface*. Advances in Colloid and Interface Science, vol 80, pp. 183-231.

Ruonala, M., Heimala, S. and Jounela, S. 1997. *Different aspects of using electrochemical potential measurements in mineral processing.* International Journal of Mineral Processing, vol 51, pp. 97 – 110.

Russell, P., Batchelor, D. and Thornton, J. 2004. *SEM and AFM: Complementary techniques for high resolution surface investigations*. Digital Instruments, Veeco Metrology Group.

Santos, L.R.G., Barbosa, A.F., Souza, A.D. and Leão, V.A. 2006. *Bioleaching of a complex nickel–iron concentrate by mesophile bacteria.* Minerals Engineering, vol 19, pp. 1251 – 1258.

Sayilgan, A. and Arol, A.I. 2004. *Effect of carbonate alkalinity on flotation behaviour of quartz.* International Journal of Mineral Processing, vol 74, pp. 233 – 238.

Senior, G.D., Shannon, L.K. and Trahar, W.J. 1994. *The flotation of pentlandite from pyrrhotite with particular reference to the effects of particle size.* International Journal of Mineral Processing, vol 7, pp. 203–217, vol 42, pp. 169-190.

Senior, G.D., Trahar, W.J. and Guy, P.J. 1995. *The selective flotation of pentlandite from a nickel ore*. International Journal of Mineral Processing, vol 43, pp. 209-234.

Simmons, G.L., Gathje, J.C., de Beer, W. and Moritz, R. 2003. *Inert Gas Flotation Technologies.* XXII International Mineral Processing Congress Proceedings, The University of Cape Town, South Africa, 29 September to 3 October.

Steger, H.F. 1982. *Oxidation of sulfide minerals, VII, Effect of temperature and relative humidity on the oxidation of pyrrhotite.* Chemical Geology, vol 35, pp. 281-295.

Steger, H.F. and Desjardins, L.S. 1977. *Oxidation of sulfide minerals: 3. Determination of sulfate and thiosulfate in oxidised sulfide minerals.* Talanta, vol 24, pp. 675-679.

Steger, H.F. and Desjardins, L.S. 1978. *Oxidation of sulfide minerals: 4. Pyrite, chalcopyrite and pyrrhotite.* Chemical Geology, vol 23, pp. 225-237.

Stumm, W. and Morgan, J.J. 1981. *Aquatic Chemistry.* Wiley-Interscience, New York.

Suter, T., Peter, T. and Böhni, H. 1995. *Microelectrochemical investigations of MnS inclusions.* Materials Science Forum, vol 192 – 194, pp. 25-40.

Theart, H.F.J. and De Nooy, C.D. 2001. *The Platinum-group minerals in two parts of the massive sulfide body of the Uitkomst Complex, Mpumalanga, South Africa*. South African Journal of Geology, vol 104, pp. 287–300.

Thomas, J.E., Smart, R.St.C. and Skinner, W.M. 2000. *Kinetics factors for oxidative and non-oxidative dissolution of iron sulfides.* Minerals Engineering, vol 10 – 11, pp. 1149-1159.

Thomas, J.E., Skinner, W.M. and Smart, R.St.C. 2001. *A mechanism to explain sudden changes in rates and products for pyrrhotite dissolution in acid solution.* Geochim. Cosmochim. Acta, vol 65, pp. 1-12.

Tolley, W., Kotlyar, D. and Van Wagoner, R. 1996. *Fundamental electrochemical studies of sulfide mineral flotation.* Engineering, vol 9, no. 6, pp. 603-637.

Valli, M. and Persson, I. 1994. *Interactions between sulfide minerals and alkylxanthates.* Colloids Surfaces A: Physicochemical Engineering Aspects, vol 83, pp. 207-217.

Van Wouw, K. 2003. *Internal report: Mineralogical investigation of the platinum-group minerals in flotation products from Mimosa Platinum mine.*

Van Zyl, A.M. 1996. *The sulfides of the Uitkomst Complex, Badplaas, South Africa*. MSc thesis, University of Pretoria, pp. 121.

Vaughan, D.J. and Craig, J.R. 1978. *Mineral chemistry of metal sulfides* Cambridge University Press, Cambridge, UK, pp. 493.

Vaughan, D.J., England, K.E.R., Kelsall, G.H. and Yin, Q. 1995. *Electrochemical oxidation of chalcopyrite ($CuFeS_2$) and the related metal-enriched derivatives $Cu_4Fe_5S_8$, $Cu_9Fe_9S_{16}$, and $Cu_9Fe_8S_{16}$.* American Mineralogist, vol 80, pp. 725-731.

Vermaak, C.F. and Hendriks, L.P. 1976. *A review of the mineralogy of the Merensky reef, with specific reference to new data on the precious metal mineralogy*. Economic Geology, vol 71, pp. 1244-1269.

Vermaak, M.K.G. 2005. *Fundamentals of the flotation behaviour of palladium bismuth telluride*. PhD Dissertation, University of Pretoria, Pretoria.

Vermaak, M.K.G., Miller, J.D. and Li, J. 2006. *Electrochemical interactions of industrially important platinum-containing minerals.* Unpublished article.

Vermaak, M.K.G., Miller, J.D. and Moats, M.S. 2005. *Single particle microelectrodes for electrochemical analysis of flotation processes.* Unpublished article.

Vermaak, M.K.G, Venter, J.A. and Pistorius, P.C. 2004. *Electrochemical studies of the interaction of ethyl xanthate with Pd-Bi-Te.* International Platinum Conference 'Platinum Adding Value', South African Institute of Mining and Metallurgy.

Viljoen, M.J., Theron, J., Underwood, B., Walters, B.M., Weaver, J. and Peyerl, W. 1986. *The Amandebult Section of Rustenburg Platinum Mines Limited. In Mineral Deposits of Southern Africa.* Edited by Anhaeusser, C.R. and Maske, S. Johannesburg, vol 2, pp. 1041-1060.

Wagner, P.A. 1929. *The platinum deposits and mines of South Africa*. Oliver and Boyd, Edinburgh, pp. 362.

Wang, X., Forssberg, K.S.E. and Bolin, N.J. 1989. *The Aqueous and Surface Chemistry of Activation in the Flotation of Sulfide Minerals - A Review. Part I: An Electrochemical Model.* Minerals Processing and Extractive Metallurgy Review, vol 4, pp.135-165.

Weisener, C. and Gerson, A. 2000. *An investigation of the Cu (II) adsorption mechanism on pyrite by ARXPS and SIMS.* Minerals Engineering, vol 13, pp. 1329–1340.

Wesseldijk, Q.I., Reuter, M.A., Bradshaw, D.J. and Harris, P.J. 1999. *The flotation behaviour of chromite with respect to the beneficiation of UG-2 ore*. Minerals Engineering, vol 12, no. 10, pp. 1177–1184.

Wiese, J., Harris, P. and Bradshaw, D. 2005. *Investigation of the role and interactions of a dithiophosphate collector in the flotation of sulfides from the Merensky reef*. Minerals Engineering, vol 18, pp. 791-800.

Winter, G. and Woods, R. 1973. *The relation of collector redox potential to flotation efficiency: monothiocarbonates.* Separation Science, vol 8, pp. 261-267.

Woods, R. 1984. *Electrochemistry of sulfide flotation. Principles of Mineral Flotation.* Edited by M.H. Jones and J.T. Woodcock. Wark Symposium, pp. 91-115.

Xiao, Z. and Laplante, A.R. 2004. *Characterising and recovering the platinum group minerals - a review.* Minerals Engineering, vol 17, pp. 961-979.

Yakhontova, L.K., Nesterovich, L.G. and Grudev, A.P. 1983. *New data on natural oxidation of pyrrhotite.* Vestnik Moskovskogo Universiteta Geologiya, vol 38, pp. 41-44.

Yoon, R.H., Basilio, C.I., Marticorena, M.A., Kerr, A.N. and Stratton-Crawley, R. 1995. *A study of the pyrrhotite depression mechanism by diethylenetriamine.* Minerals Engineering, vol 8, Issue 7, pp. 807-816.

Yuehua, H., Qin, Z. and Guohua, G. 2005. *FTIR investigation of electrochemical flotation in the ethyl xanthate-pyrrhotite system*. Proceedings of the Jan D. Miller symposium, pp. 169 - 178.

http://www.bullion.org.za/MiningEducation/PDF%20and%20Word%20Docs/Platinum%20group%20metals%20in%20SA.pdf Viewed: 01 February 2007.

http://www.miningweekly.com/article/tati-nickel-2007-05-18 Viewed: 18 March 2009.

http://arkisto.gtk.fi/ej/ej49_backups/ej49_pages_258_260.pdf Viewed: 15 June 2009.

http://products.narishige-group.com/group1/MN-153/injection/english.html Viewed: 06 August 2009.

http://serc.carleton.edu/research_education/geochemsheets/techniques/ToFSIMS.html Viewed: 06 August 2009.

http://www.phi.com/surface-analysis-techniques/TOFSIMS.html Viewed: 06 August 2009.

http://en.wikipedia.org/wiki/Carbon dioxide Viewed: 18 March 2009.

9. APPENDICES

APPENDIX 1: Pure samples

APPENDIX 1A: Rest potential

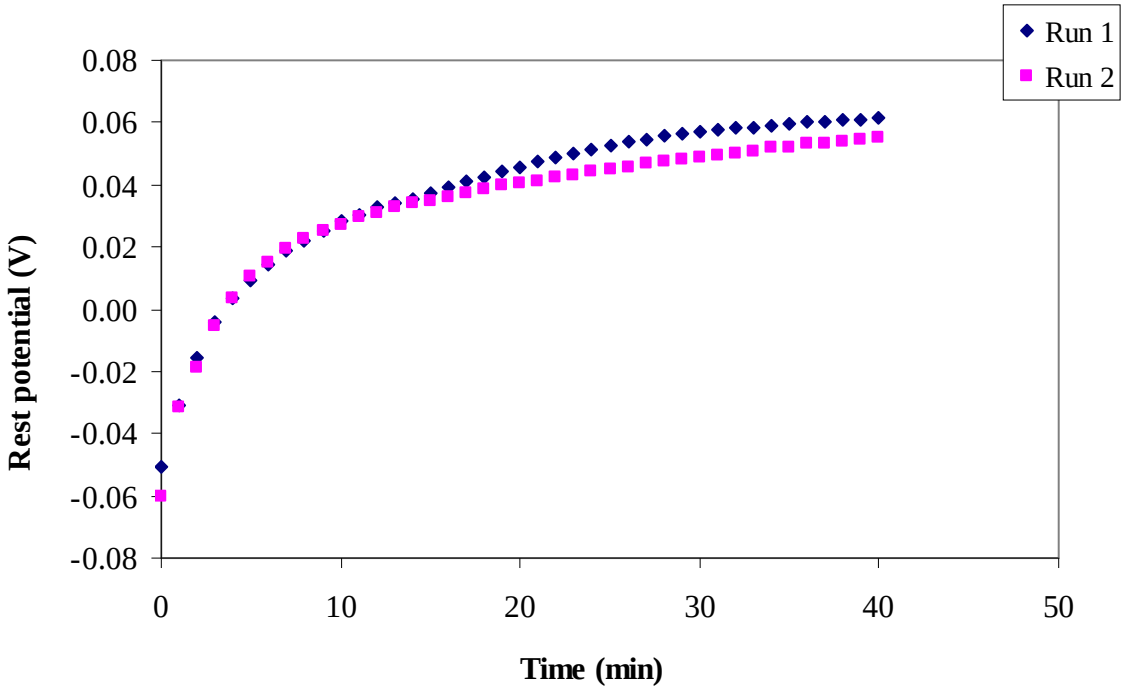

Figure 1A1: Rest potential measurements of the Russia_1 4C type pyrrhotite in an oxygen-saturated 0.05 M borate solution at pH 9.3. Potential sweeps were carried out at 10 mV/s.

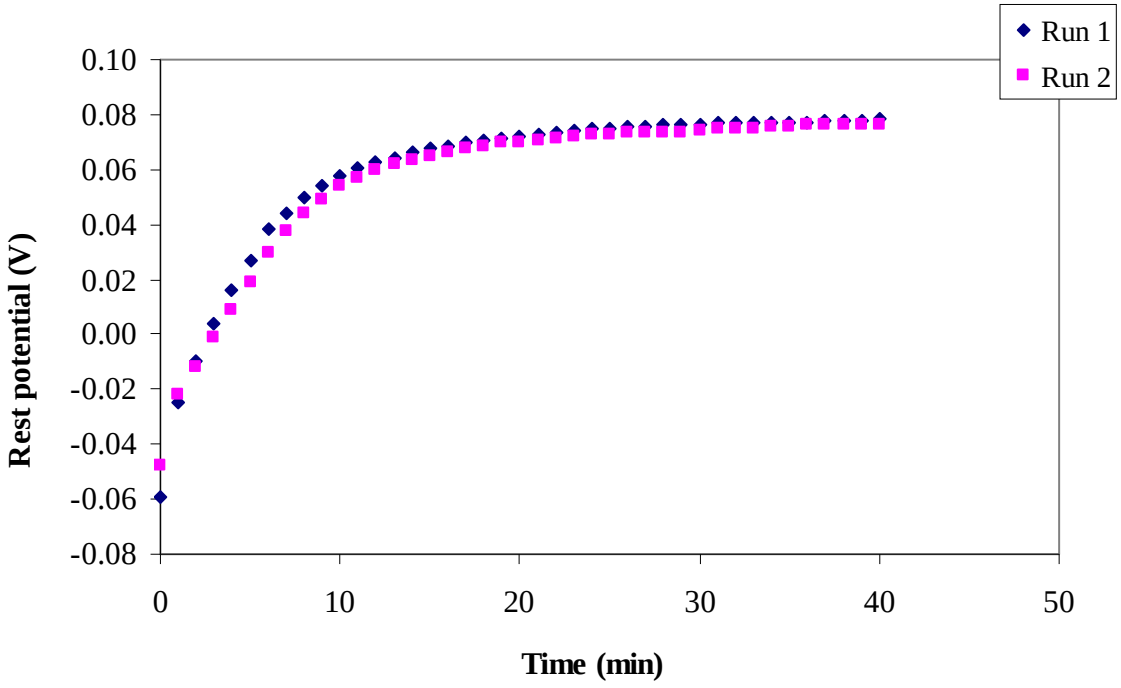

Figure 1A2: Rest potential measurements of the Russia_2 4C type pyrrhotite in an oxygen-saturated 0.05 M borate solution at pH 9.3. Potential sweeps were carried out at 10 mV/s.

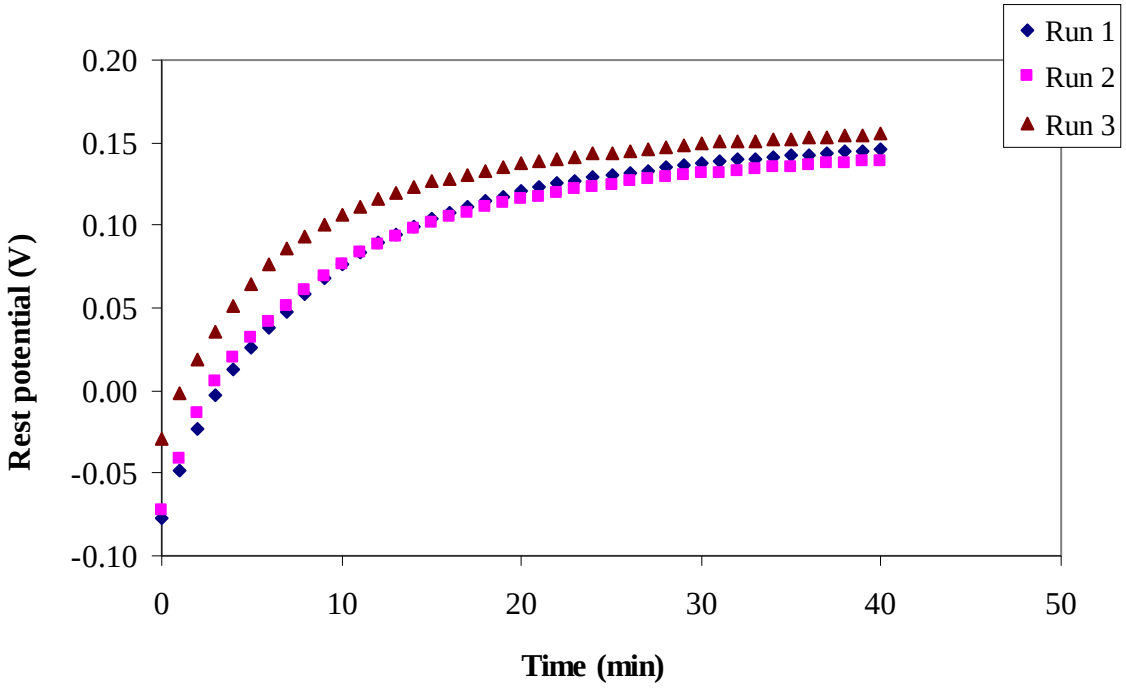

Figure 1A3: Rest potential measurements of the Mponeng 6C type pyrrhotite in an oxygen-saturated 0.05 M borate solution at pH 9.3. Potential sweeps were carried out at 10 mV/s.

APPENDIX 1B: Cathodic scans

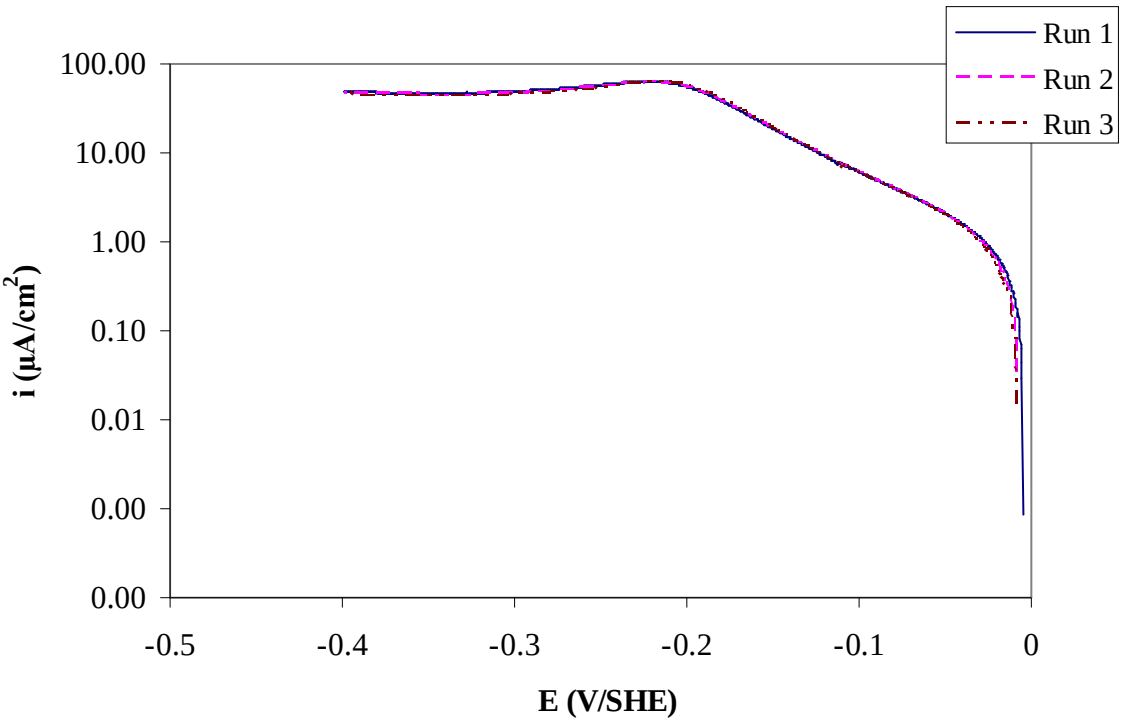

Figure 1B1: Cathodic scans of the Russia_1 4C type pyrrhotite in an oxygen-saturated 0.05 M borate solution at pH 9.3. Potential sweeps were carried out at 1 mV/s.

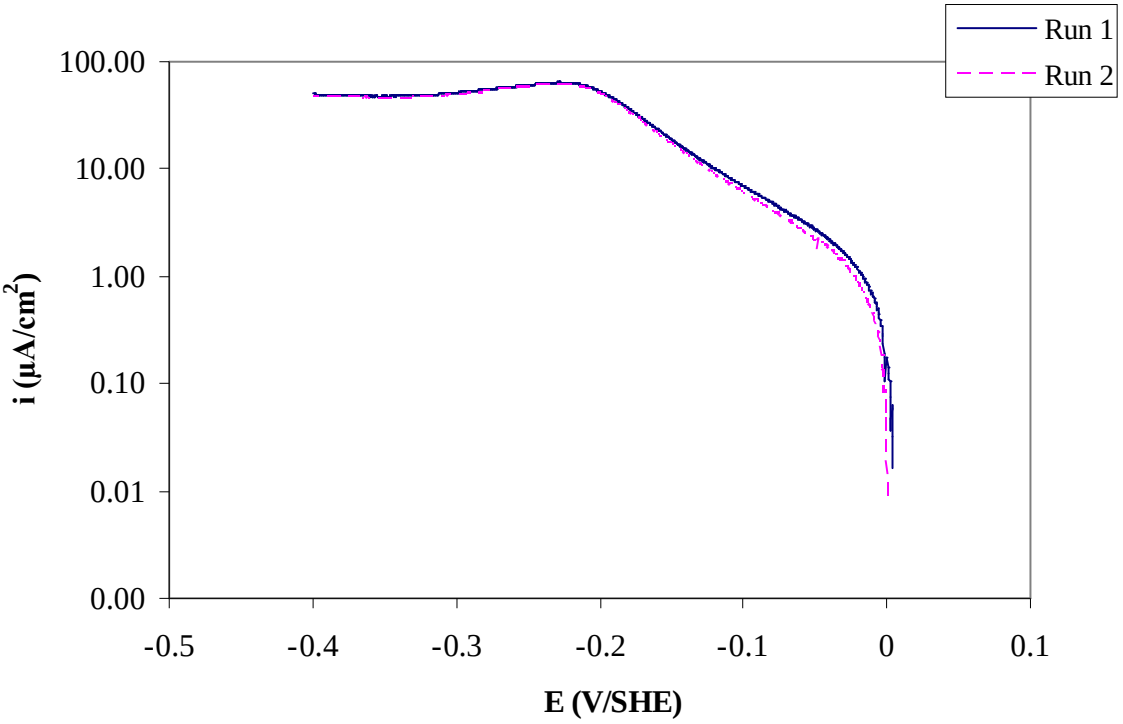

Figure 1B2: Cathodic scans of the Russia_2 4C type pyrrhotite in an oxygen-saturated 0.05 M borate solution at pH 9.3. Potential sweeps were carried out at 1 mV/s.

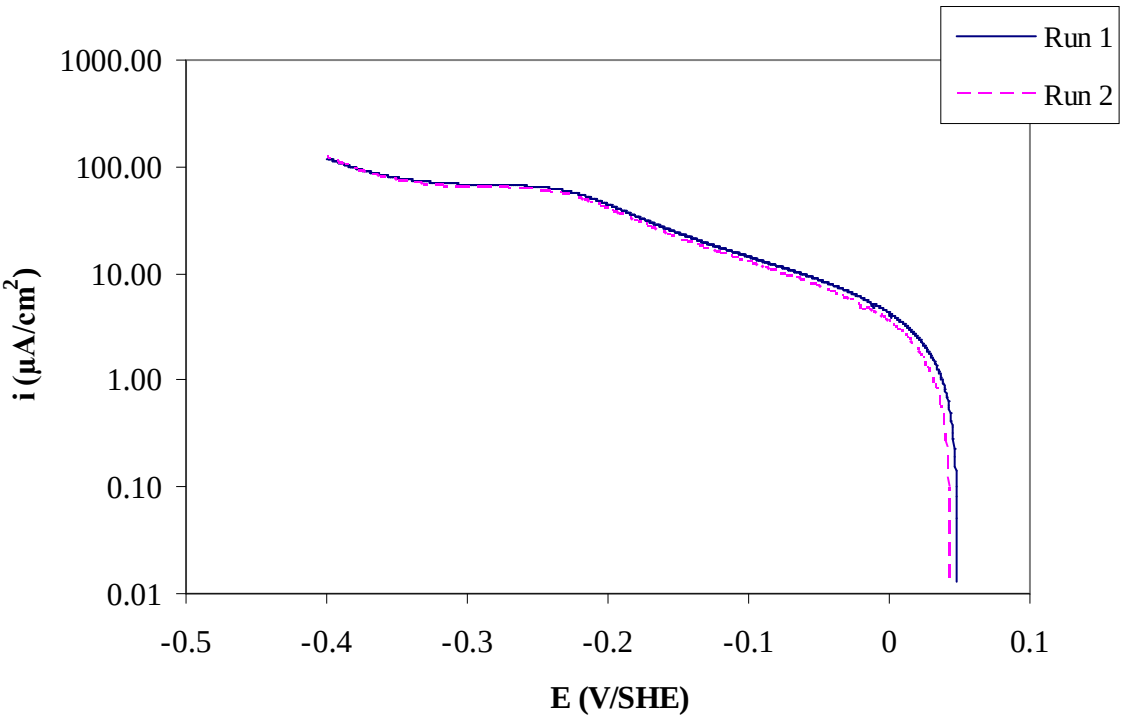

Figure 1B3: Cathodic scans of the Mponeng 6C type pyrrhotite in an oxygen-saturated 0.05 M borate solution at pH 9.3. Potential sweeps were carried out at 1 mV/s.

APPENDIX 1C: Polarisation resistance

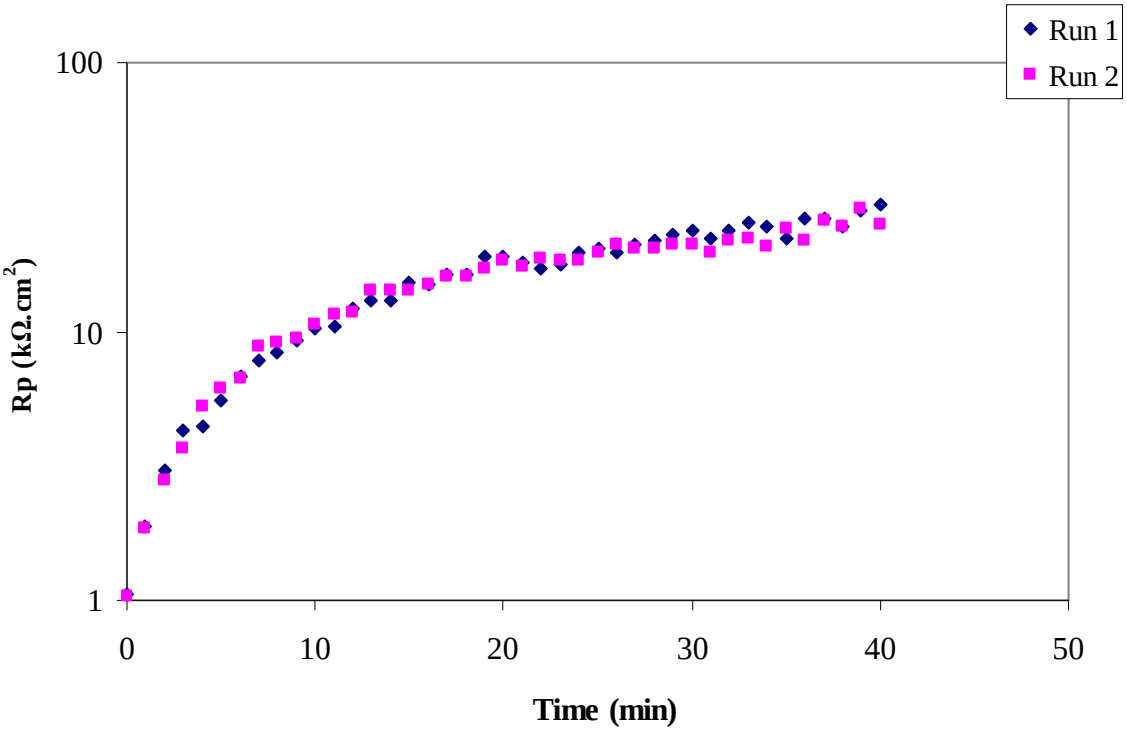

Figure 1C1: Polarisation resistance measurement of the Russia_1 4C type pyrrhotite in an oxygen-saturated 0.05 M borate solution at pH 9.3. Potential sweeps were carried out at 10 mV/s.

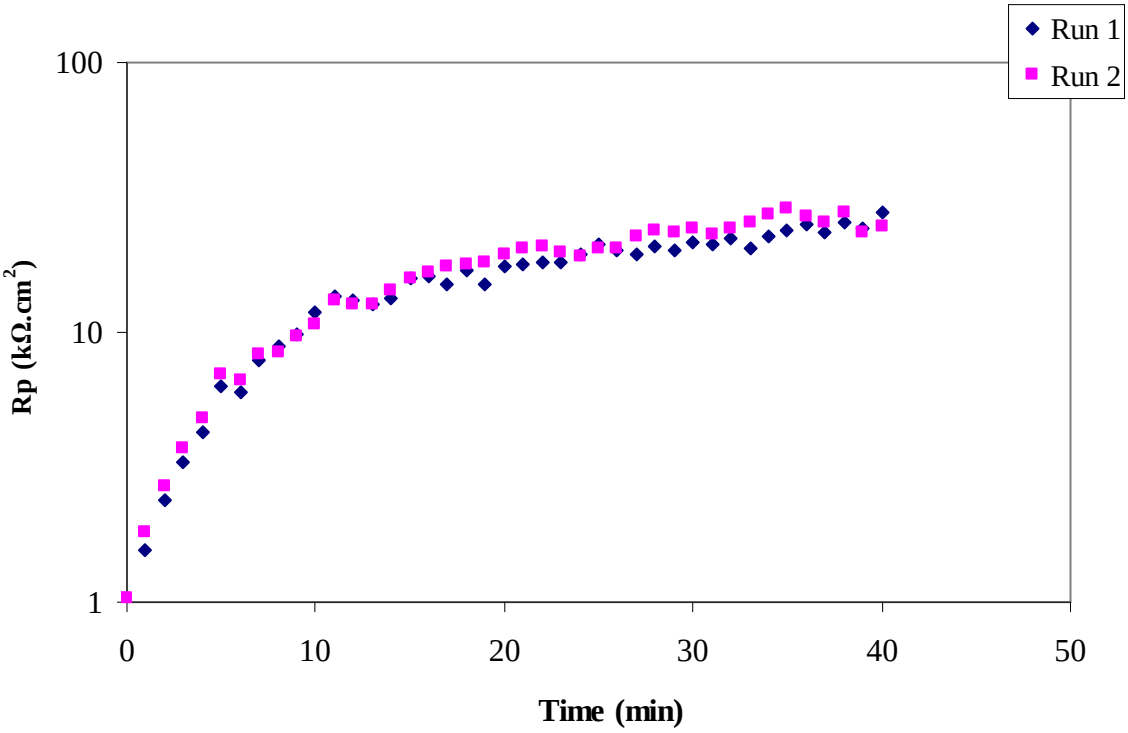

Figure 1C2: Polarisation resistance measurement of the Russia_2 4C type pyrrhotite in an oxygen-saturated 0.05 M borate solution at pH 9.3. Potential sweeps were carried out at 10 mV/s.

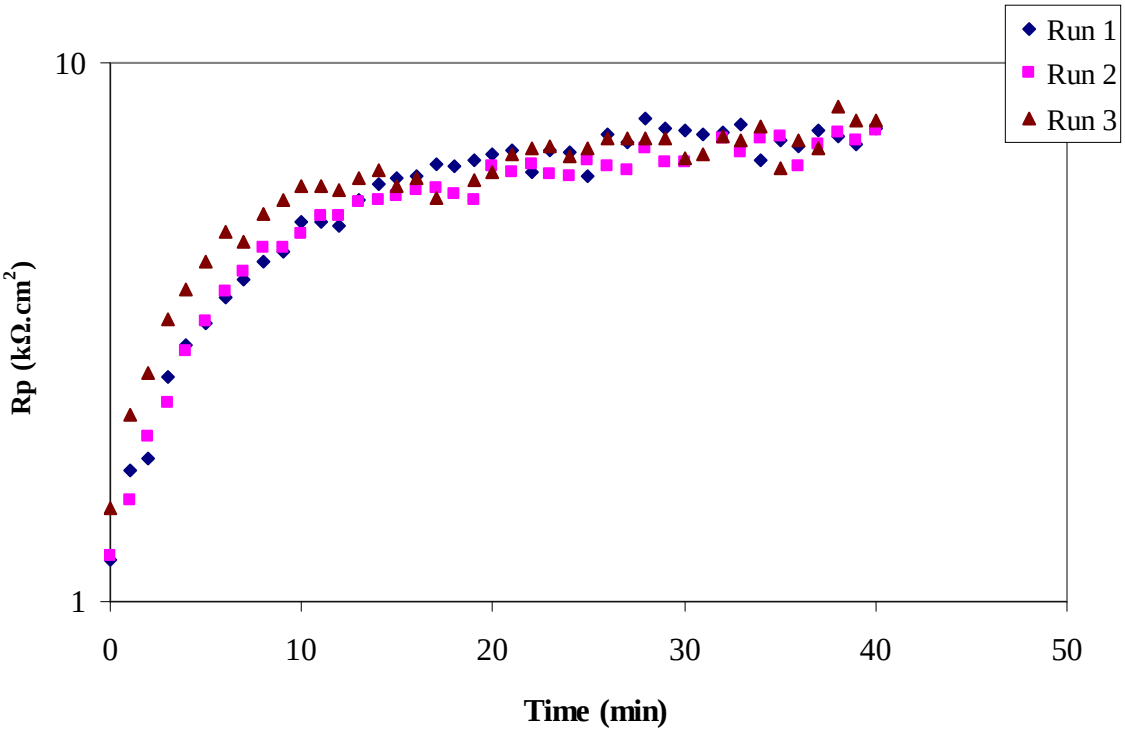

Figure 1C3: Polarisation resistance measurement of the Mponeng 6C type pyrrhotite in an oxygen-saturated 0.05 M borate solution at pH 9.3. Potential sweeps were carried out at 10 mV/s.

APPENDIX 1D: Anodic scans in the absence of xanthate

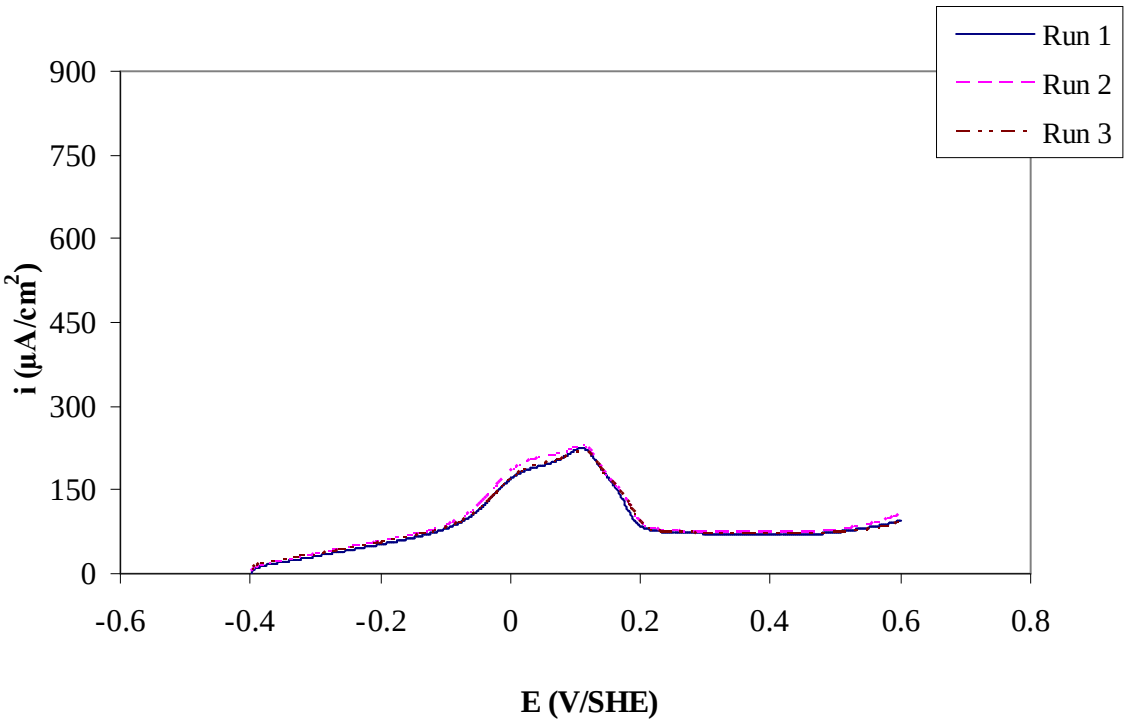

Figure 1D1: Anodic scans of the Russia_1 4C type pyrrhotite in a de-oxygenated 0.05 M borate solution at pH 9.3 in the absence of xanthate. Potential sweeps were carried out at 10 mV/s.

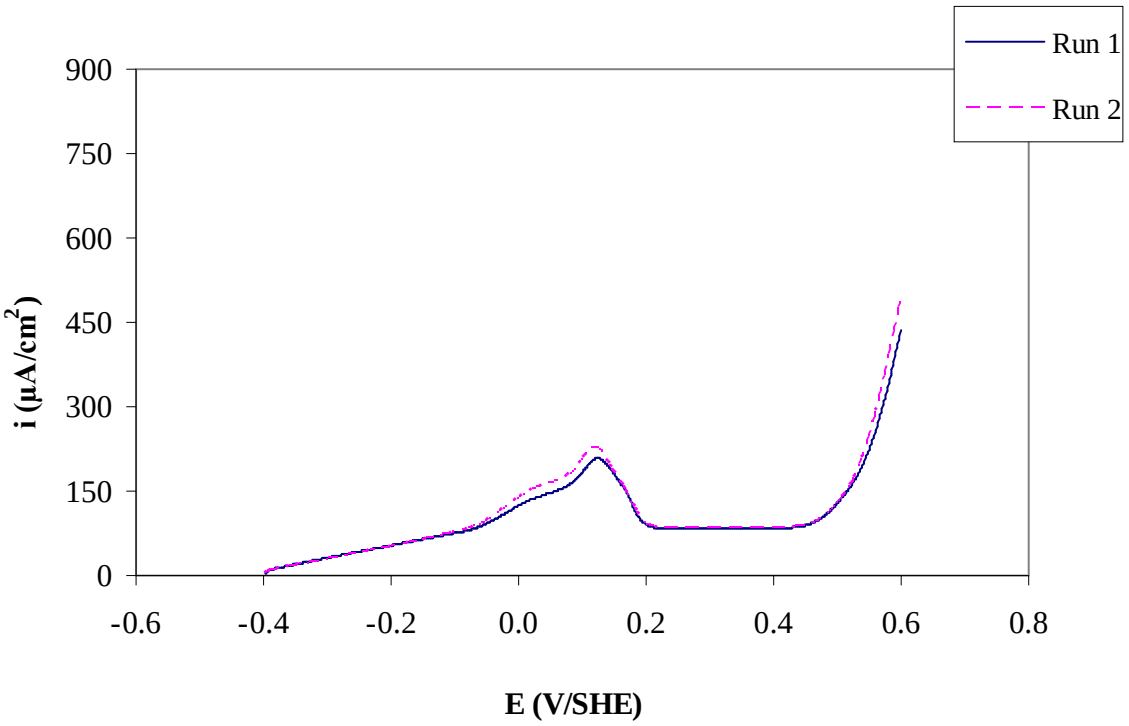

Figure 1D2: Anodic scans of the Russia_2 4C type pyrrhotite in a de-oxygenated 0.05 M borate solution at pH 9.3 in the absence of xanthate. Potential sweeps were carried out at 10 mV/s.

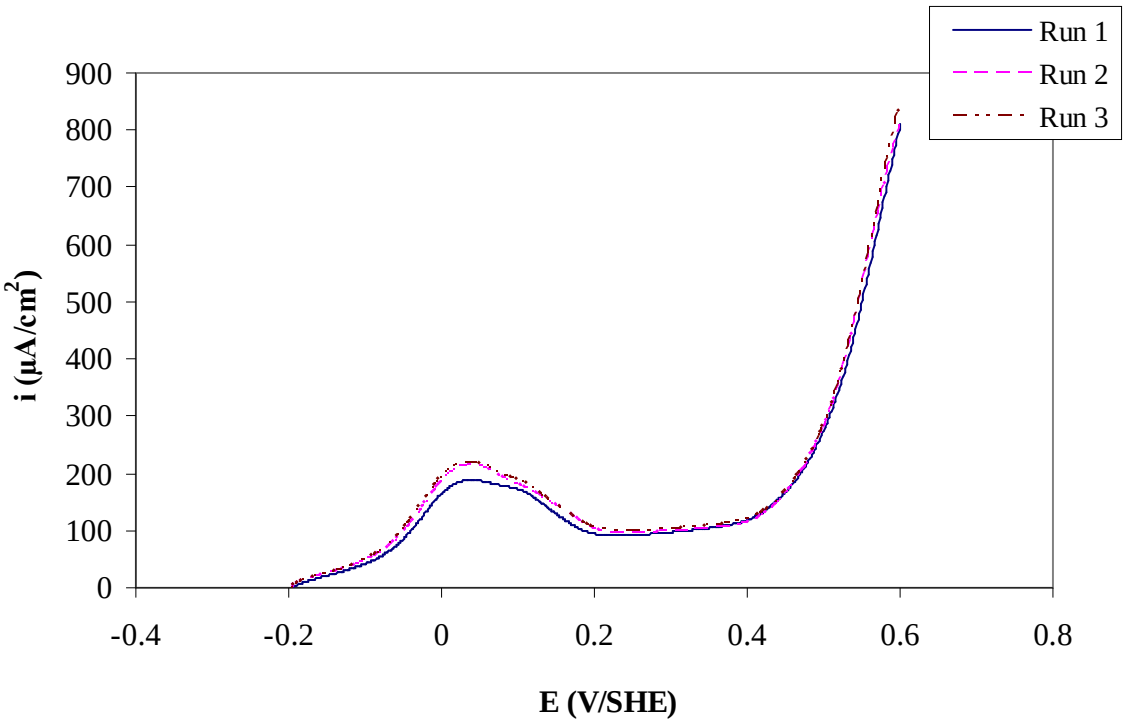

Figure 1D3: Anodic scans of the Mponeng 6C type pyrrhotite in a de-oxygenated 0.05 M borate solution at pH 9.3 in the absence of xanthate. Potential sweeps were carried out at 10 mV/s.

APPENDIX 1E: Current density-time transients

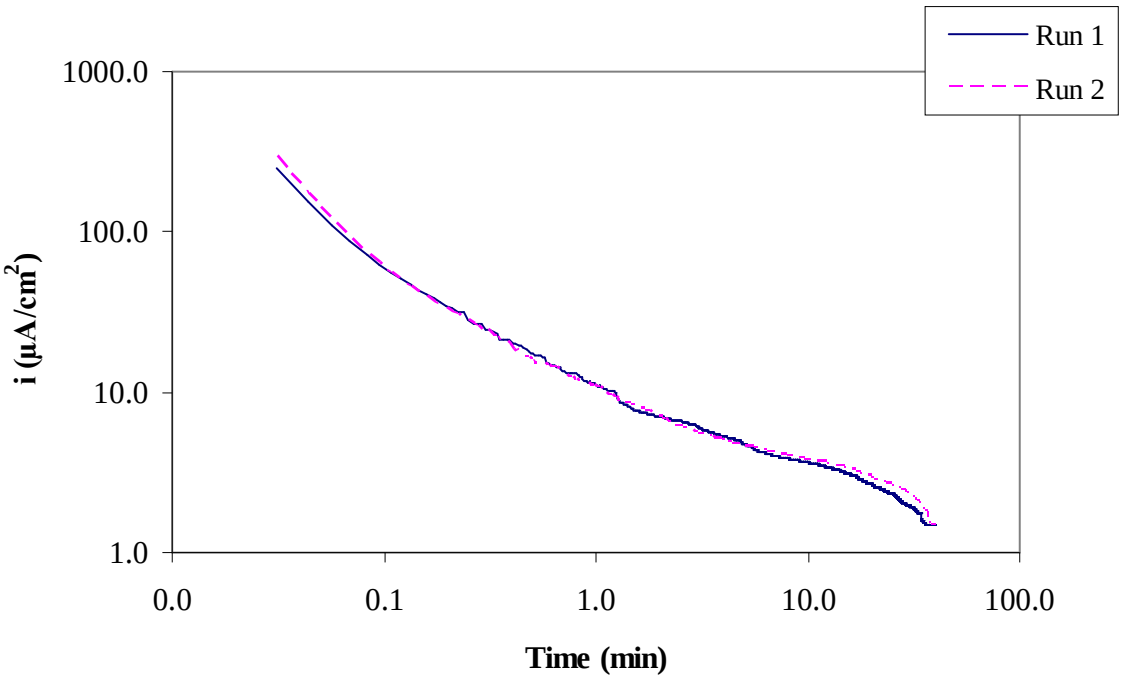

Figure 1E1: Current density-time transients in response to a step in electrode potential from rest potential to 0.25 V (SHE) in a de-oxygenated 0.05 M borate solution at pH 9.3 of the Russian 4C type pyrrhotite. Potential sweeps were carried out at 10 mV/s.

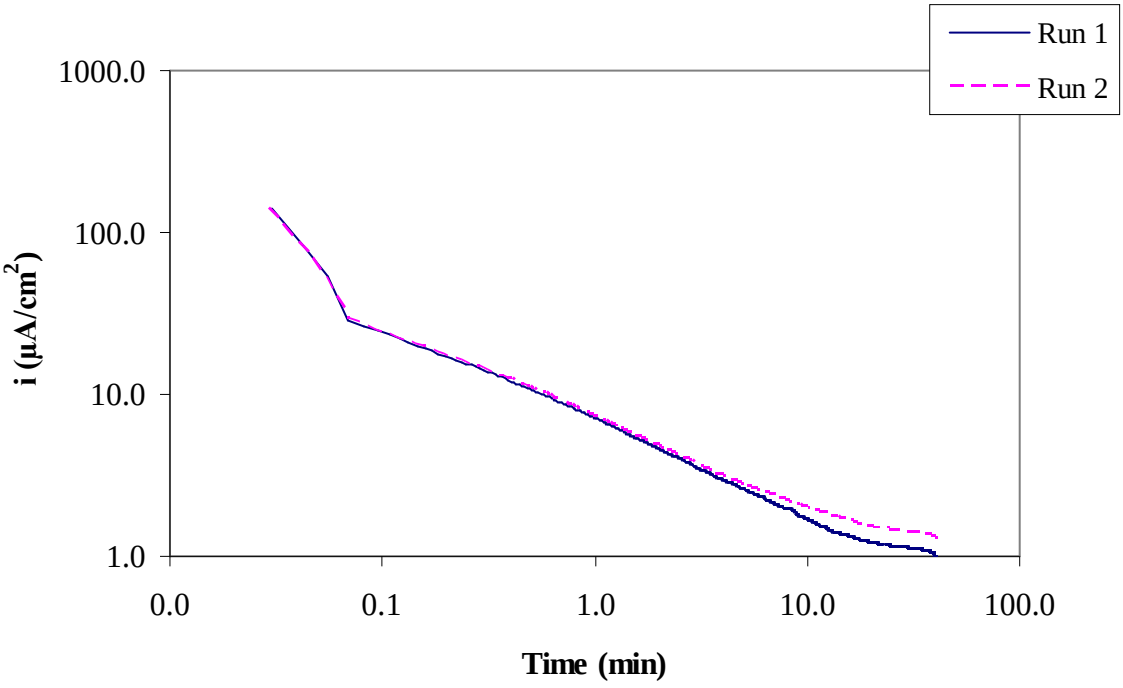

Figure 1E2: Current density-time transients in response to a step in electrode potential from rest potential to 0.25 V (SHE) in a de-oxygenated 0.05 M borate solution at pH 9.3 of the Mponeng 6C type pyrrhotite. Potential sweeps were carried out at 10 mV/s.

APPENDIX 1F: Anodic scans in the presence of xanthate

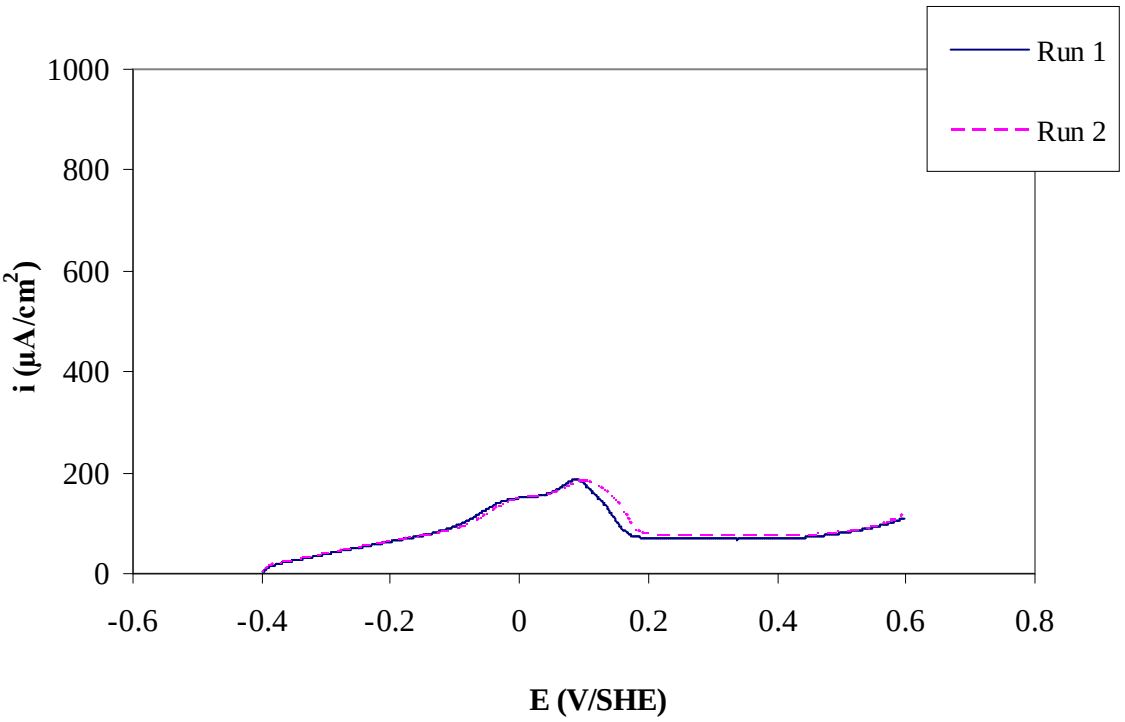

Figure 1F1: Anodic scans of the Russia_1 4C type pyrrhotite in a de-oxygenated 0.05 M borate solution at pH 9.3 in the presence of potassium ethyl xanthate. Potential sweeps were carried out at 10 mV/s.

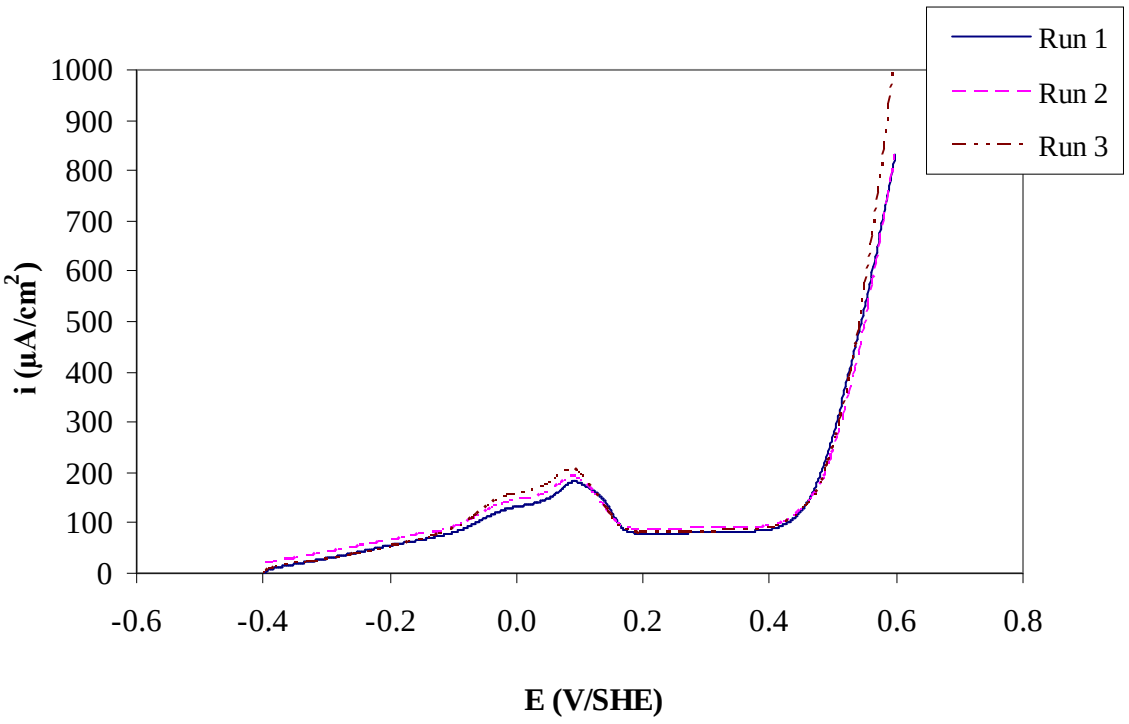

Figure 1F2: Anodic scans of the Russia_2 4C type pyrrhotite in a de-oxygenated 0.05 M borate solution at pH 9.3 in the presence of potassium ethyl xanthate. Potential sweeps were carried out at 10 mV/s.

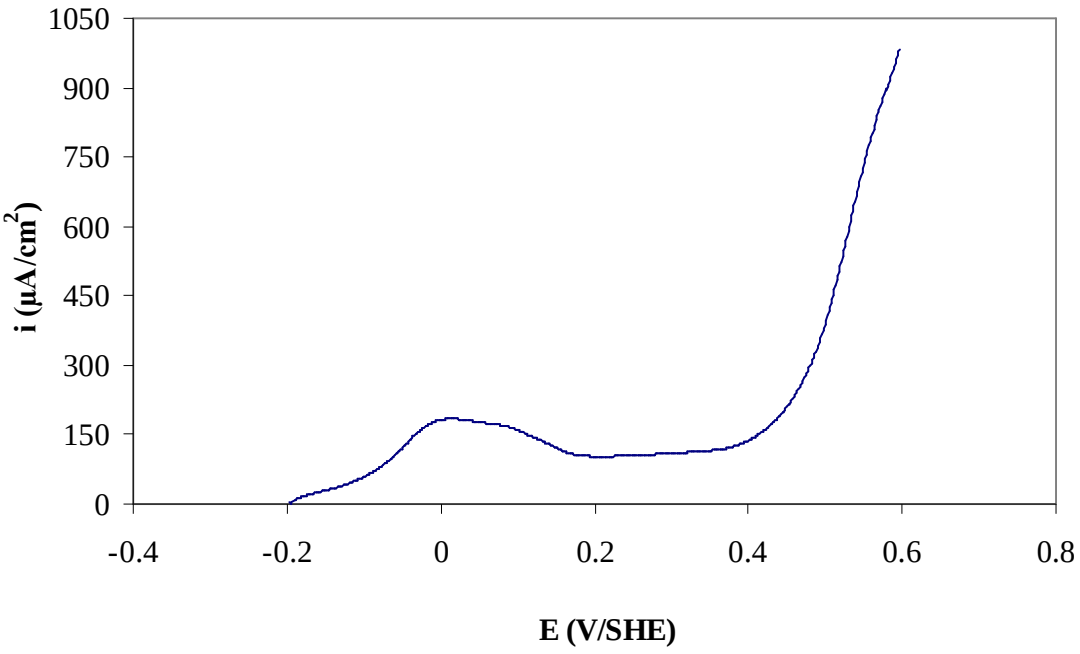

Figure 1F3: Anodic scans of the Mponeng 6C type pyrrhotite in a de-oxygenated 0.05 M borate solution at pH 9.3 in the presence of potassium ethyl xanthate. Potential sweeps were carried out at 10 mV/s.

APPENDIX 2: Mixed samples

APPENDIX 2A: Qemscan quantification

Table 2A1: Concentration (mass %) of various sulfides, minerals and gangue material in mixed massive electrodes.

	Phoenix	**Gertrude**
Mineral		
Pentlandite	17.635	5.657
Millerite	0.000	0.000
Pyrite	1.040	0.559
Pyrrhotite	80.436	87.213
Chalcopyrite	0.059	0.133
Bornite	0.000	0.036
Other Sulfides	0.055	0.022
Orthopyroxene	0.291	1.141
Clinopyroxene	0.018	0.057
Olivine	0.000	0.000
Feldspar	0.129	0.753
Talc	0.062	0.012
Serpentine	0.000	0.023
Actinolite	0.000	0.153
Amphibole	0.000	0.056
Chlorite	0.008	0.680
Mica	0.008	0.781
Quartz	0.000	1.018
Fe Oxides	0.086	0.299
Chromite	0.025	0.000
Carbonates	0.064	0.617
Other silicates	0.042	0.275
Other Minerals	0.041	0.515
Total	100.000	100.000

APPENDIX 2B: Rest potential

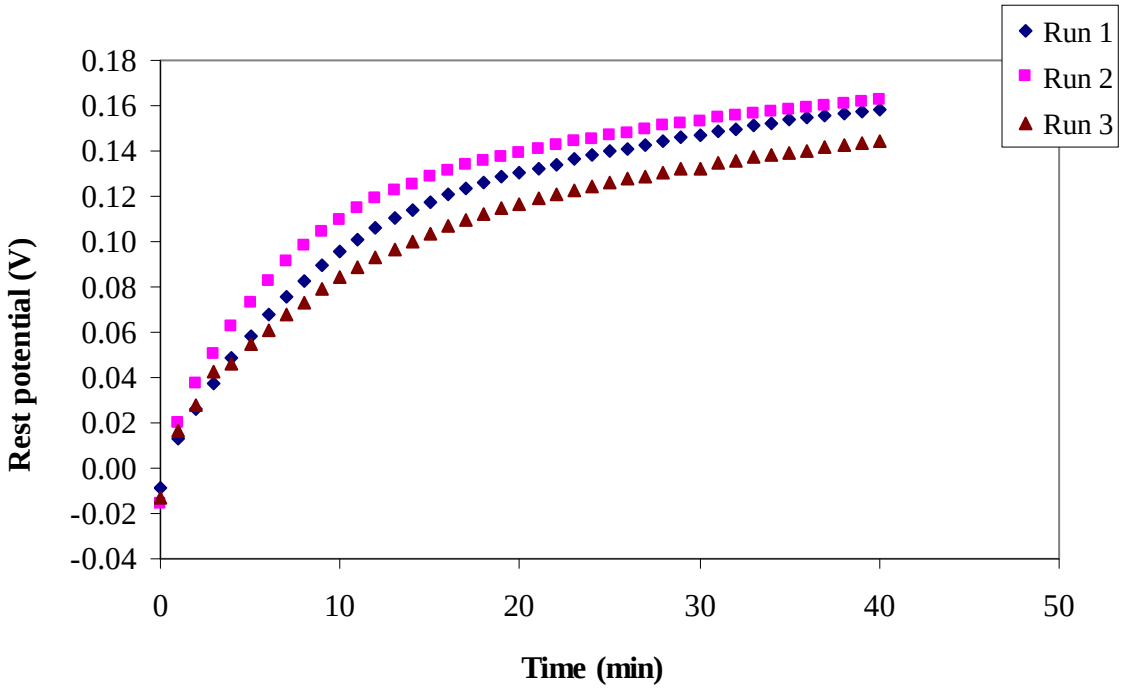

Figure 2B1: Rest potential measurements of the Sudbury Gertrude 4C type pyrrhotite in an oxygen-saturated 0.05 M borate solution at pH 9.3. Potential sweeps were carried out at 10 mV/s.

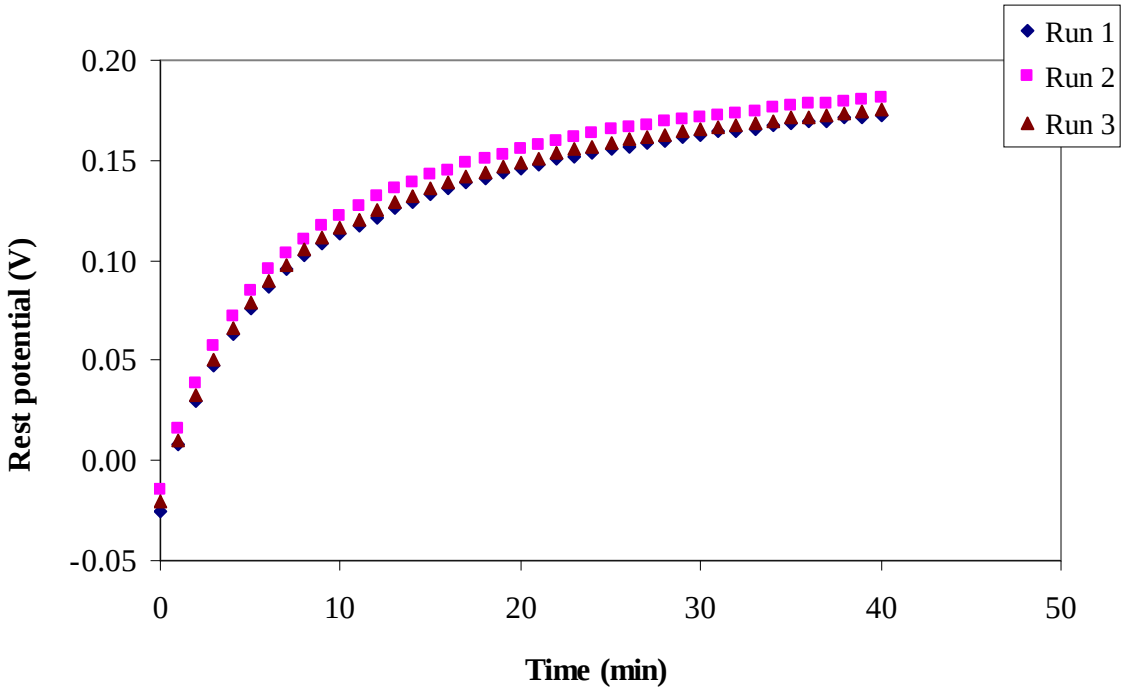

Figure 2B2: Rest potential measurements of the Phoenix 4C type pyrrhotite in an oxygen-saturated 0.05 M borate solution at pH 9.3. Potential sweeps were carried out at 10 mV/s.

APPENDIX 2C: Cathodic scans

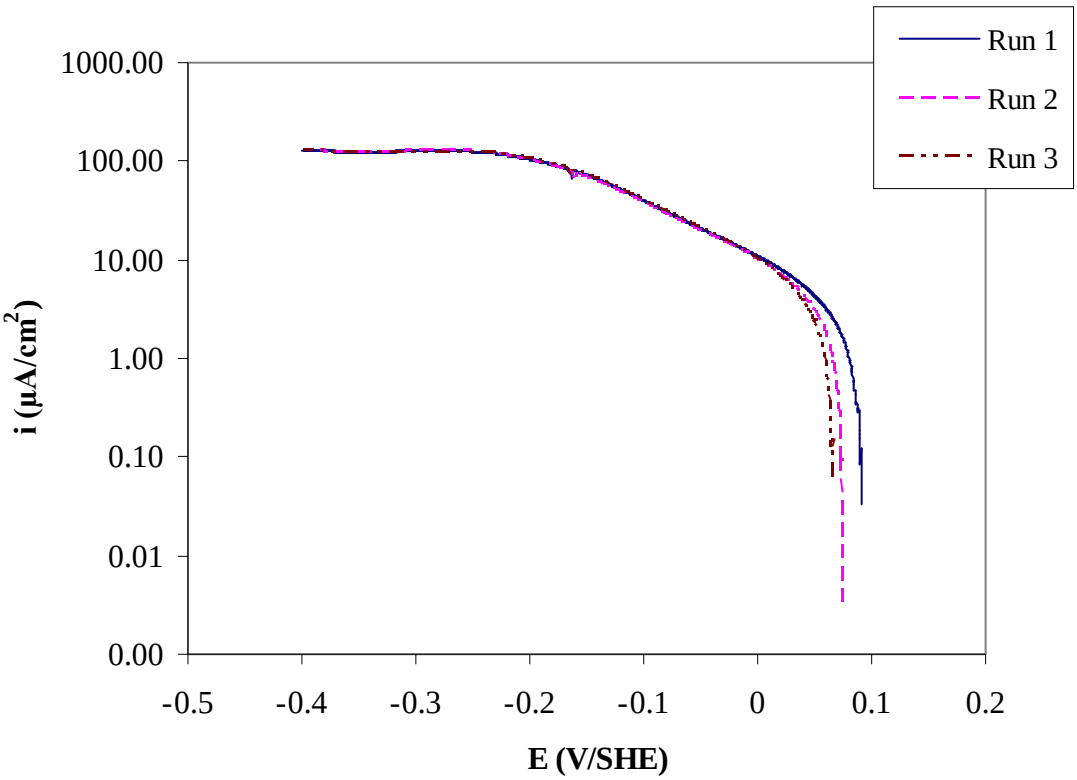

Figure 2C1: Cathodic scans of the Sudbury Gertrude 4C type pyrrhotite in an oxygen-saturated 0.05 M borate solution at pH 9.3. Potential sweeps were carried out at 1 mV/s.

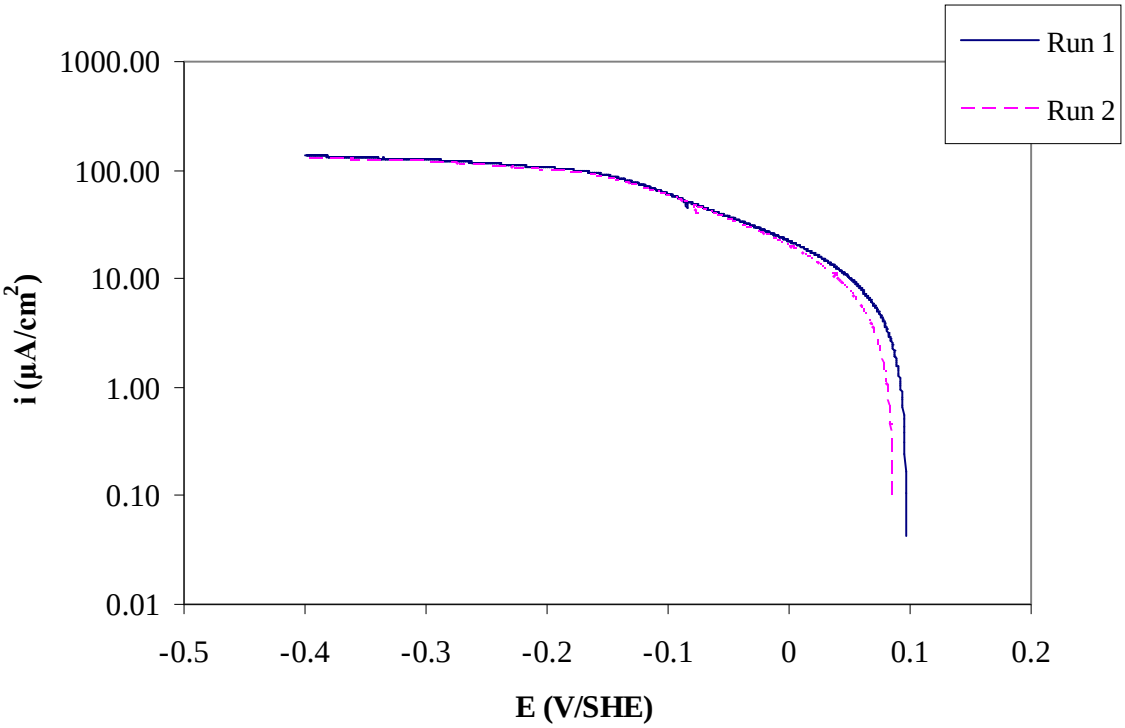

Figure 2C2: Cathodic scans of the Phoenix 4C type pyrrhotite in an oxygen-saturated 0.05 M borate solution at pH 9.3. Potential sweeps were carried out at 1 mV/s.

APPENDIX 2D: Polarisation resistance

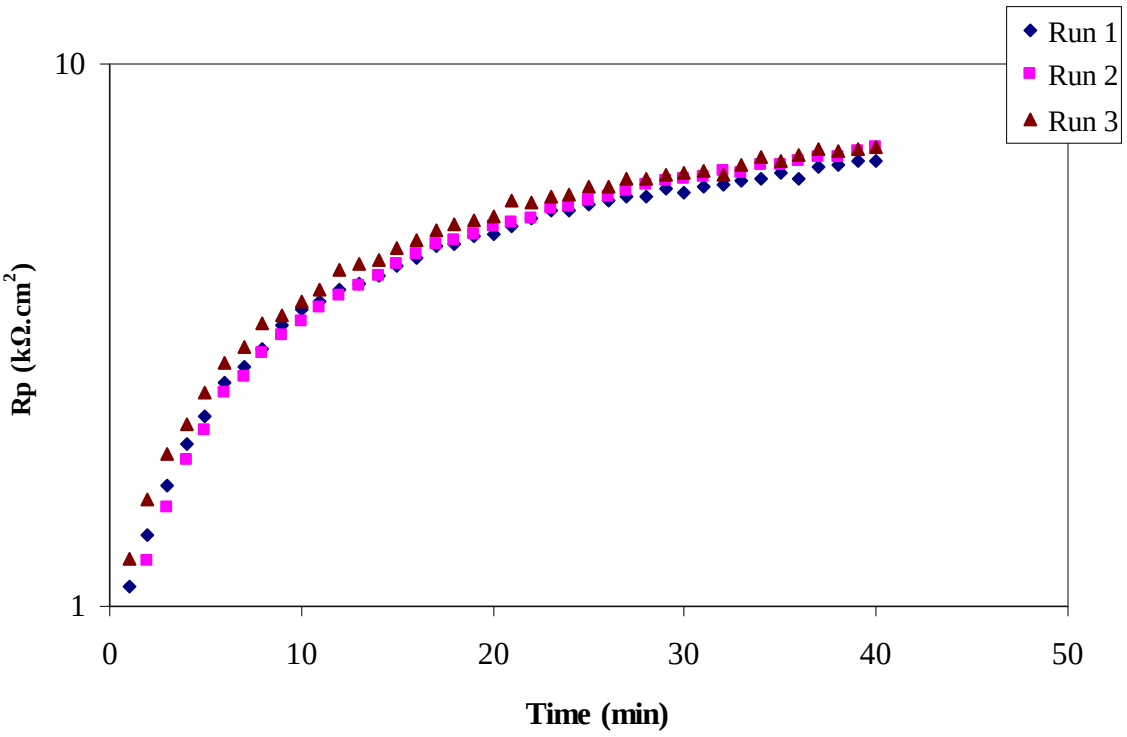

Figure 2D1: Polarisation resistance measurement of the Sudbury Gertrude 4C type pyrrhotite in an oxygen-saturated 0.05 M borate solution at pH 9.3. Potential sweeps were carried out at 10 mV/s.

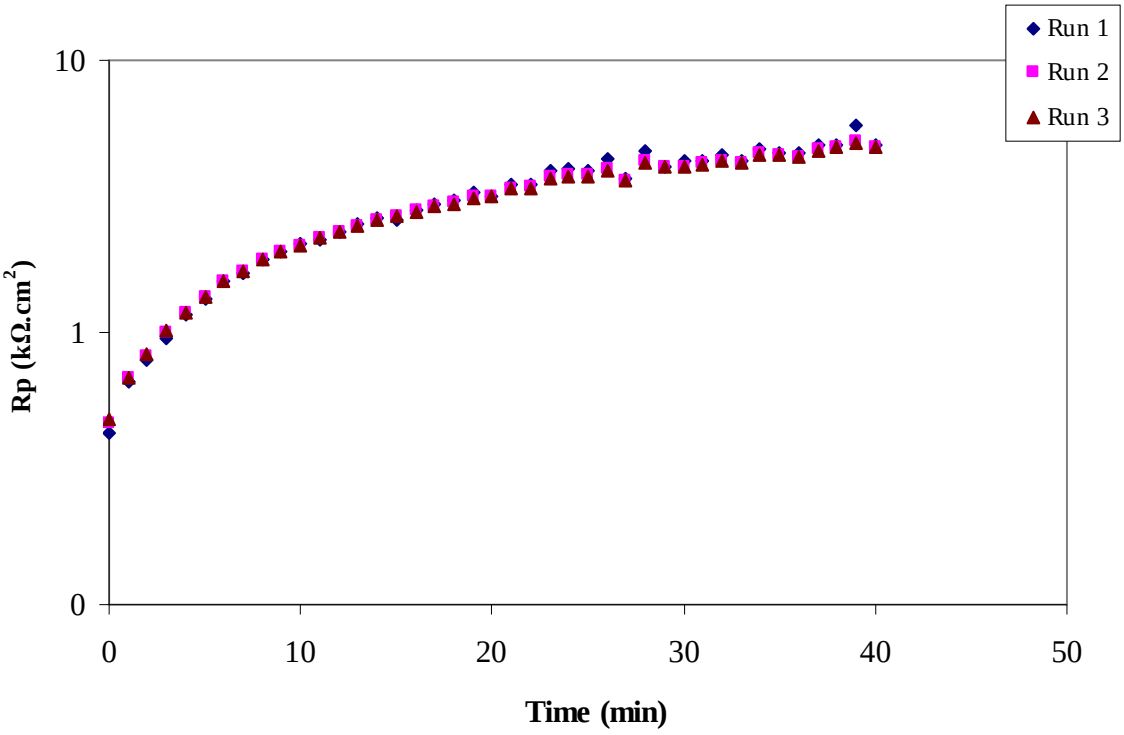

Figure 2D2: Polarisation resistance measurement of the Phoenix 4C type pyrrhotite in an oxygen-saturated 0.05 M borate solution at pH 9.3. Potential sweeps were carried out at 10 mV/s.

APPENDIX 2E: Anodic scans

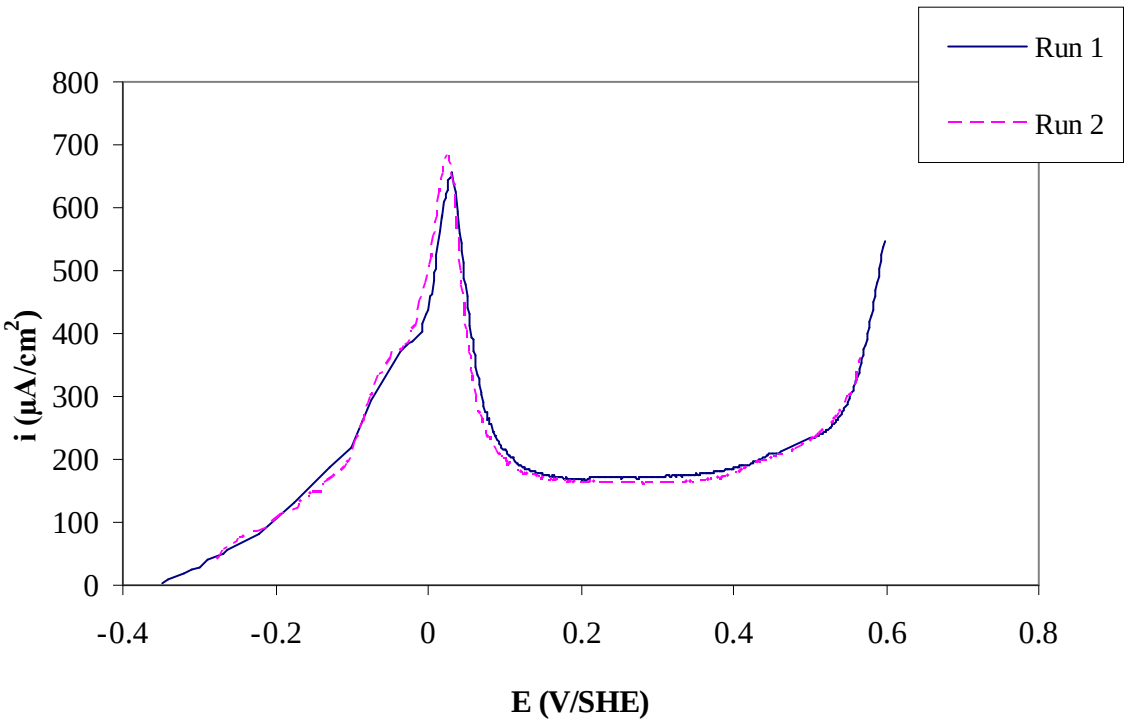

Figure 2E1: Anodic scans of the Sudbury Gertrude 4C type pyrrhotite in a de-oxygenated 0.05 M borate solution at pH 9.3 in the absence of xanthate. Potential sweeps were carried out at 10 mV/s.

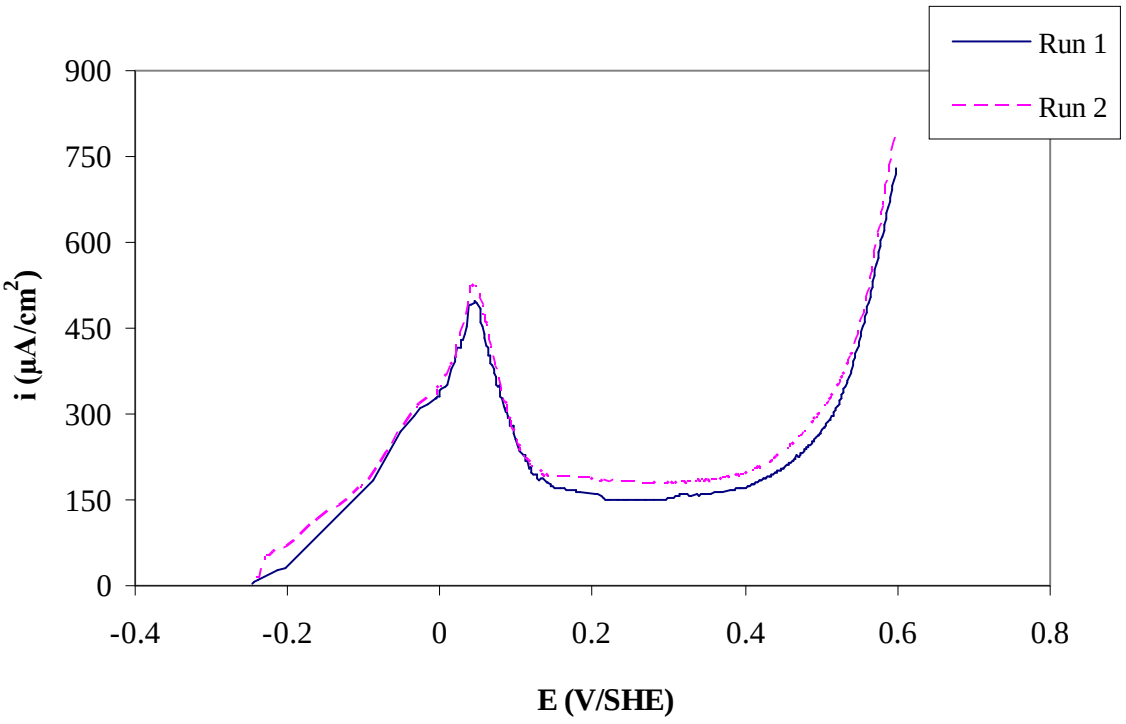

Figure 2E2: Anodic scans of the Phoenix 4C type pyrrhotite in a de-oxygenated 0.05 M borate solution at pH 9.3 in the absence of xanthate. Potential sweeps were carried out at 10 mV/s.

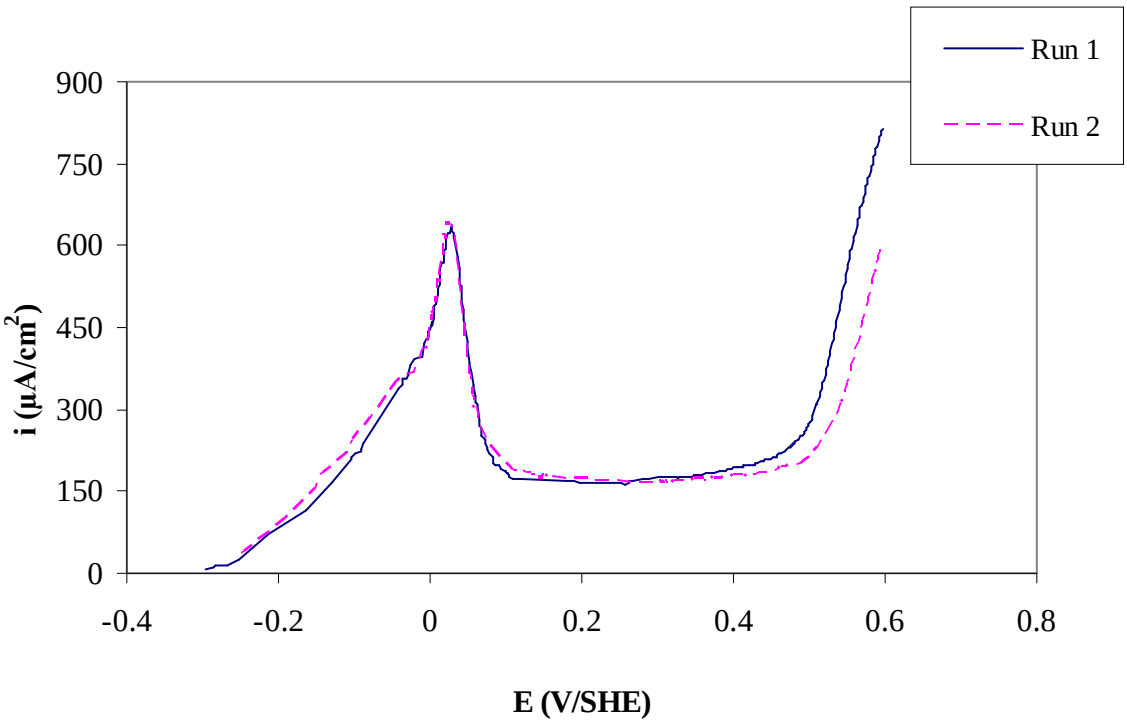

Figure 1: Anodic scans of the Sudbury Gertrude 4C type pyrrhotite in a de-oxygenated 0.05 M borate solution at pH 9.3 in the presence of xanthate. Potential sweeps were carried out at 10 mV/s.

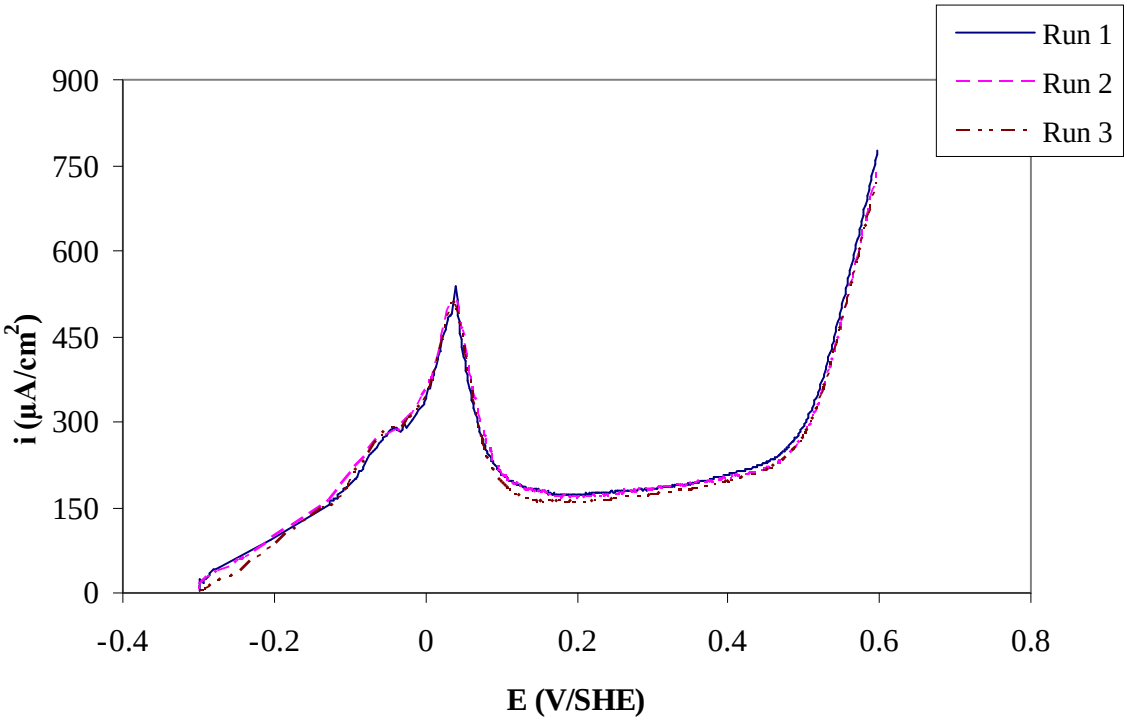

Figure 2E4: Anodic scans of the Phoenix 4C type pyrrhotite in a de-oxygenated 0.05 M borate solution at pH 9.3 in the presence of xanthate. Potential sweeps were carried out at 10 mV/s.

APPENDIX 2F: Capacitance

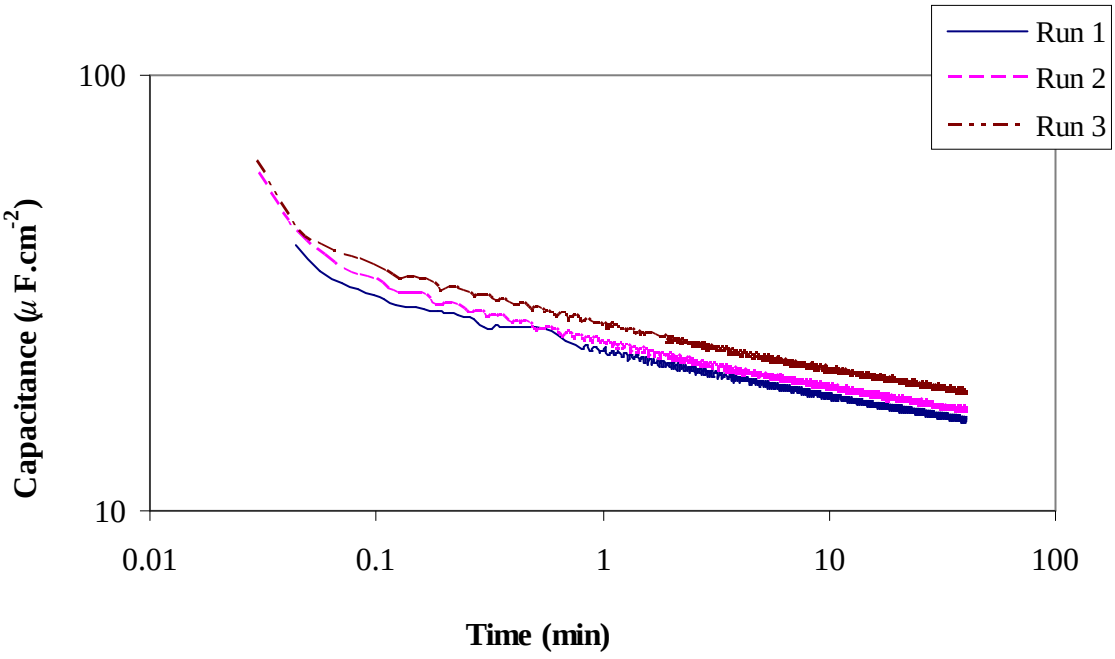

Figure 2F1: Capacitance measurements of a Russian 4C type pyrrhotite in an oxygen-saturated 0.05 M borate solution at pH 9.3 in the absence of xanthate.

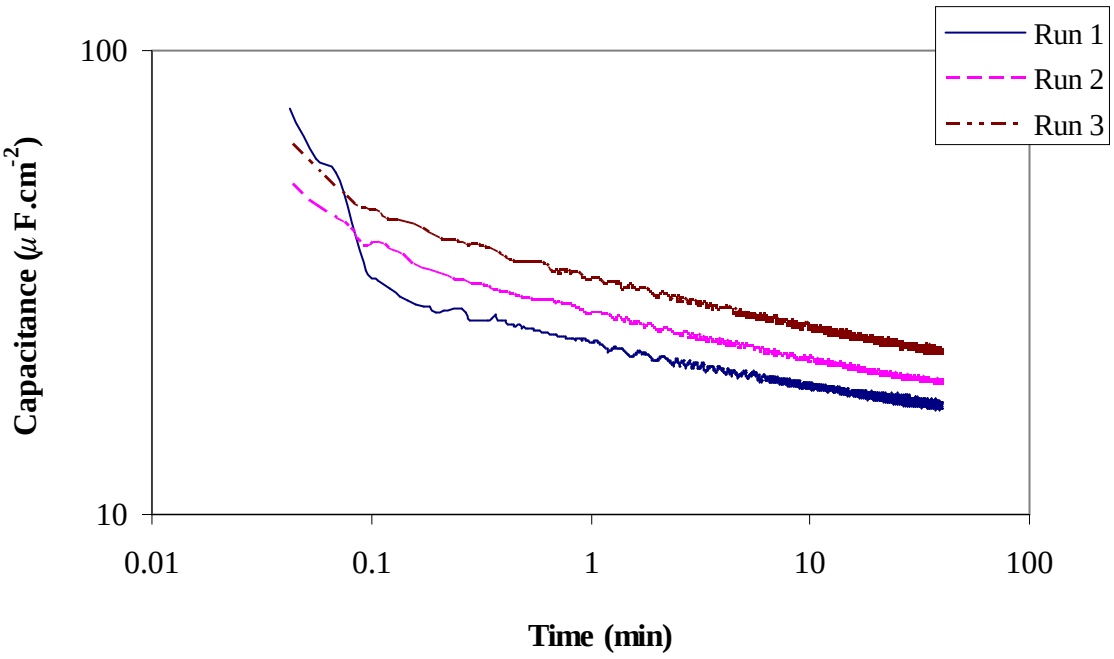

Figure 2F2: Capacitance measurements of a Sudbury Gertrude 4C type pyrrhotite in an oxygen-saturated 0.05 M borate solution at pH 9.3 in the absence of xanthate.

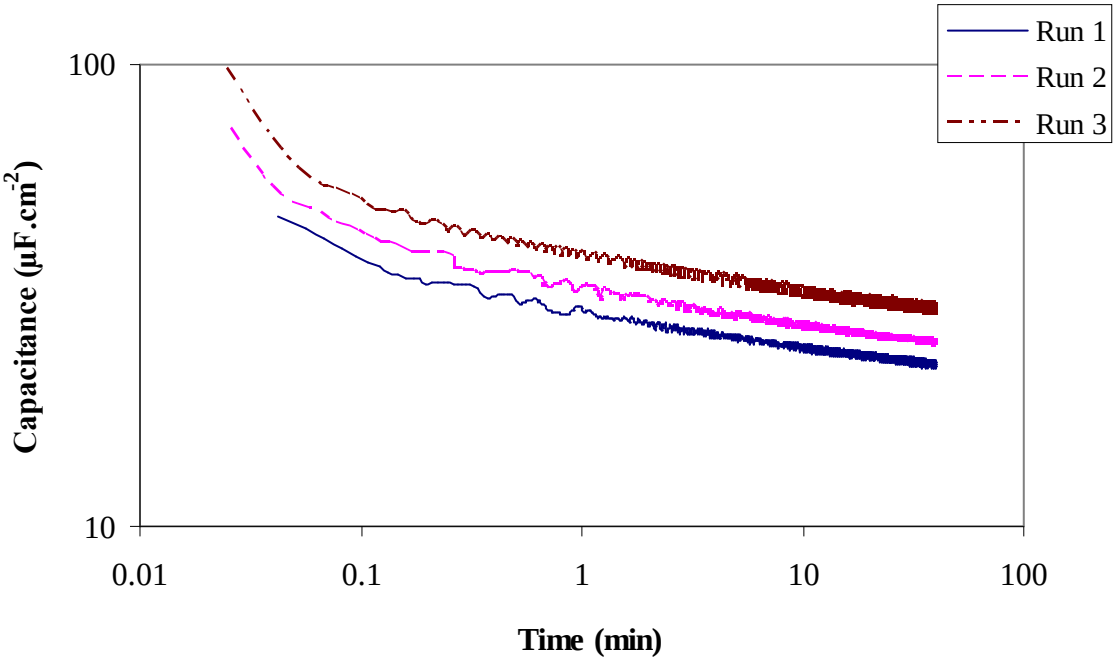

Figure 2F3: Capacitance measurements of a Phoenix 4C type pyrrhotite in an oxygen-saturated 0.05 M borate solution at pH 9.3 in the absence of xanthate.

APPENDIX 3: Gaseous carbon dioxide pre-treatment

APPENDIX 3A: Anodic scans

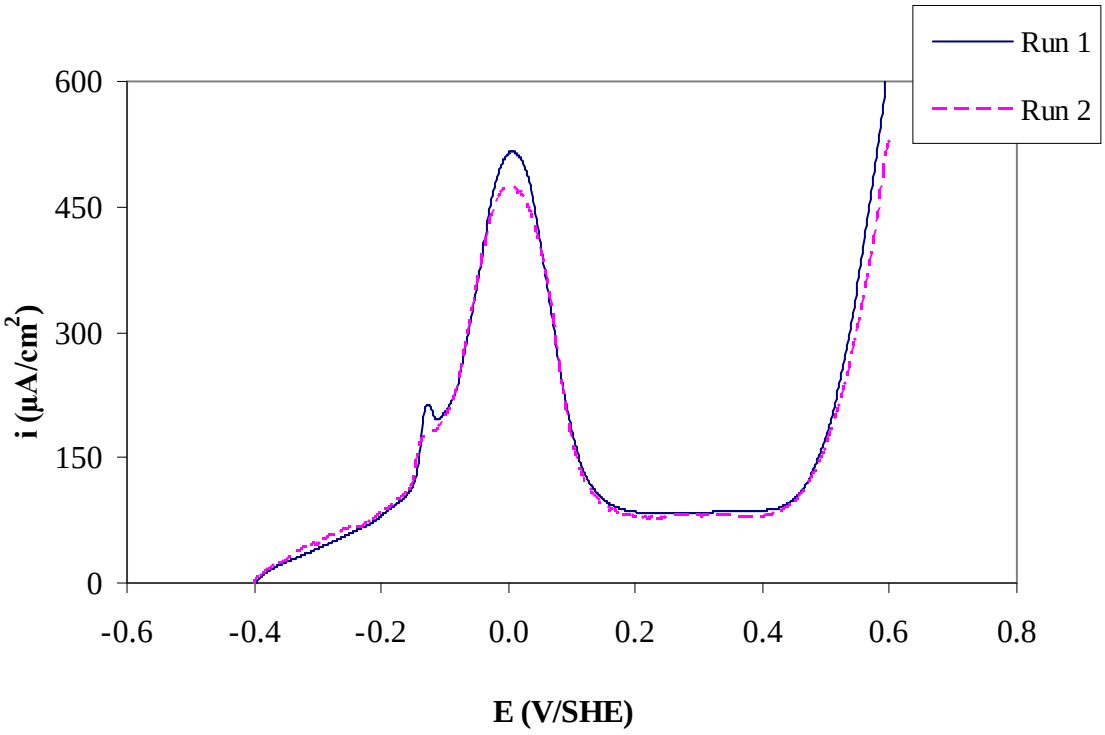

Figure 3A1: Anodic scans of the oxidised and CO_2 pre-treated Russian 4C type pyrrhotite in a de-oxygenated 0.05 M borate solution at pH 9.3 in the absence of xanthate. Potential sweeps were carried out at 10 mV/s. One hour of CO_2 treatment.

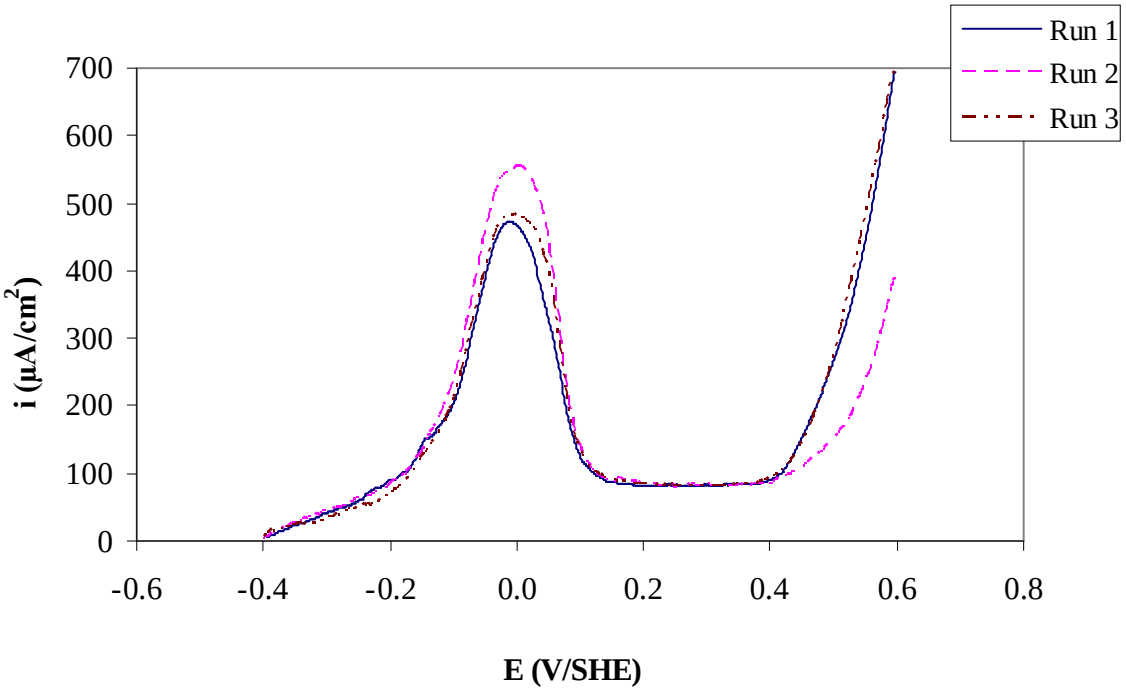

Figure 3A2: Anodic scans of the wet-polished and CO_2 pre-treated Russian 4C type pyrrhotite in a de-oxygenated 0.05 M borate solution at pH 9.3 in the absence of xanthate. Potential sweeps were carried out at 10 mV/s. One hour of CO_2 treatment.

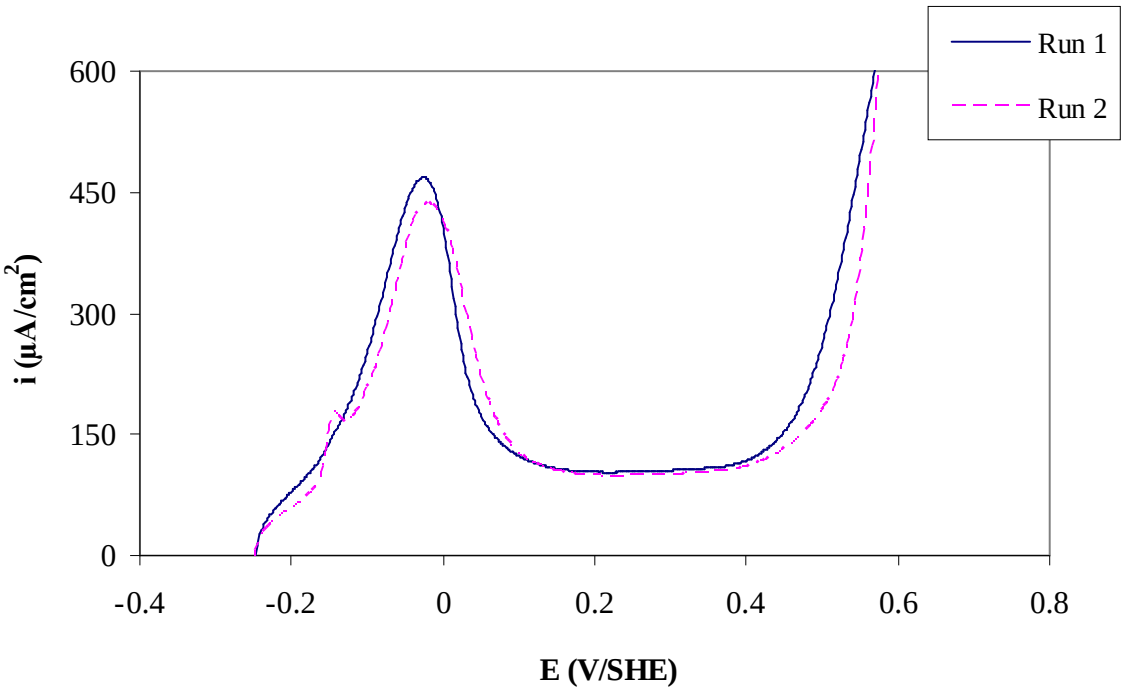

Figure 3A3: Anodic scans of the oxidised and CO_2 pre-treated Mponeng 6C type pyrrhotite in a de-oxygenated 0.05 M borate solution at pH 9.3 in the absence of xanthate. Potential sweeps were carried out at 10 mV/s. One hour of CO_2 treatment.

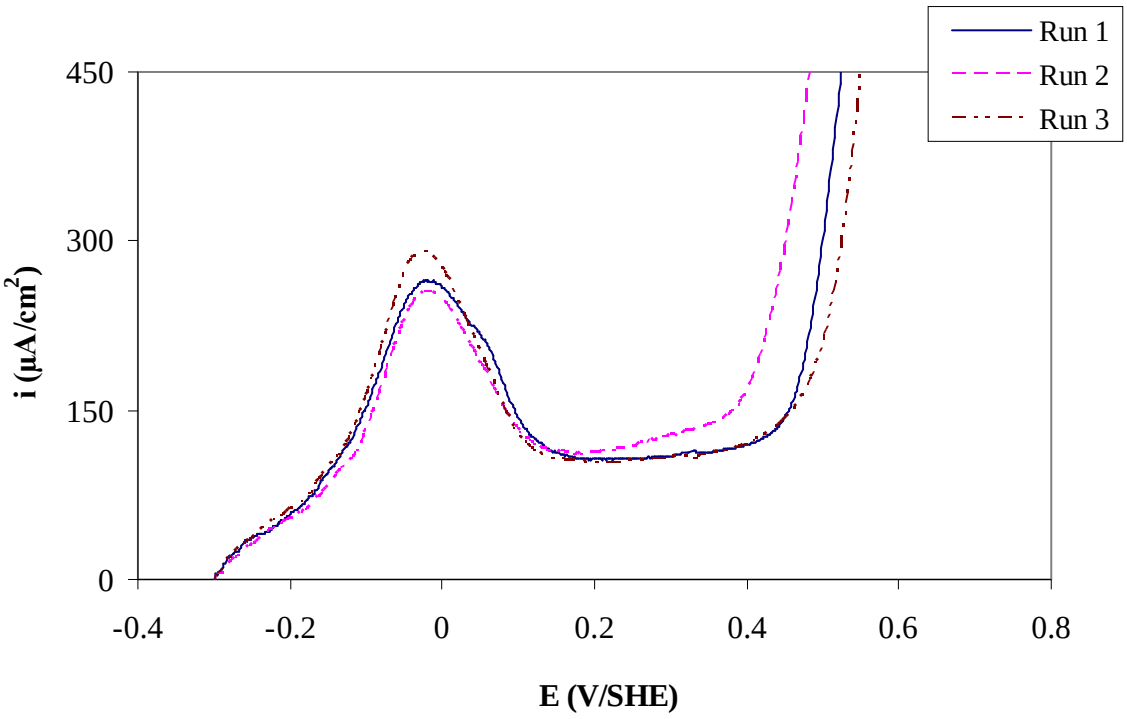

Figure 3A4: Anodic scans of the oxidised and CO_2 pre-treated Mponeng 6C type pyrrhotite in a de-oxygenated 0.05 M borate solution at pH 9.3 in the presence of xanthate. Potential sweeps were carried out at 10 mV/s. One hour of CO_2 treatment.